

Nonlinear Flow in Porous Media

Numerical Solution of the Navier-Stokes System with Two Pressures and Application to Paper Making

Stefan Rief

Vom Fachbereich Mathematik der Universität
Kaiserslautern zur Verleihung des akademischen
Grades Doktor der Naturwissenschaften (Doctor rerum
naturalium, Dr. rer. nat.) genehmigte Dissertation.

1. Gutachter: Prof. Dr. H. Neunzert
2. Gutachter: Prof. Dr. R. Helmig

Vollzug der Promotion: 15. September 2005

D 386

To me it seems that those Sciences are vain and full of error which are not born of experience, mother of all certainty, first hand experience which in its origin, or means, or end has passed through one of the five senses.

Leonardo da Vinci (1452-1519)

Es ist nicht das Wissen, sondern das Lernen, nicht das Besitzen, sondern das Erwerben, nicht das Dasein, sondern das Hinkommen, was den größten Genuß gewährt. Wenn ich eine Sache ganz ins Klare gebracht und erschöpft habe, so wende ich mich davon weg, um wieder ins Dunkle zu gehen, so sonderbar ist der nimmersatte Mensch, hat er ein Gebäude vollendet, so ist es nicht, um ruhig darin zu wohnen, sondern um ein anderes anzufangen.

Carl Friedrich Gauß (1777-1855)

I want to express my gratitude to Prof. Dr. Helmut Neunzert for suggesting the interesting problem, for helpful and encouraging discussions and for his patience. Moreover, I thank Prof. Dr. Kai Velten, Dr. Konrad Steiner and all the members of the SKS and HPC departments of the Fraunhofer Institut für Techno- und Wirtschaftsmathematik for their motivating and never-ending encouragement. Prof. Dr. Andro Mikelić's advice in theoretical questions is highly appreciated. My thanks also go to Prof. Dr. Michael Junk who carefully read the manuscript and gave helpful comments. For the financial support of my studies I thank the Deutsche Forschungsgemeinschaft.

Contents

Chapter 1. Introduction	1
1.1. Filtration laws and upscaling	2
1.2. Thesis outline	5
1.3. Terminology and mathematical fundamentals	6
Chapter 2. The Navier-Stokes system with two pressures	13
2.1. The Navier-Stokes problem on periodic porous media	13
2.2. Formal asymptotic analysis	18
2.3. Existence, uniqueness and regularity of the solution	20
2.4. Convergence of the homogenization process	24
2.5. Extension of Darcy's law	27
Chapter 3. Numerical solution of the two pressure system by scale splitting	33
3.1. Micro and macro problems	34
3.2. Numerical solution algorithms	40
3.3. Numerical results	67
Chapter 4. Numerical solution of the full two pressure system	87
4.1. Numerical solution algorithm	88
4.2. Numerical results	96
Chapter 5. Modeling and simulation of the pressing section of a paper machine	103
5.1. Model of a press nip	105
5.2. Numerical solution algorithms	113
5.3. General model parameters	119
5.4. Numerical results and discussion	125
Conclusion	143
Bibliography	145

CHAPTER 1

Introduction

Flow phenomena in porous media are of great practical interest. This is due to the fact, that porous media appear quite often in nature and have a brought range of technical applicability. We find porous media in fields such as ground water hydrology, civil engineering, petroleum production, ceramic and textile engineering and in the automotive industry. They appear as sand, soil, ceramic and metal foams, wipes, diapers, paper machine clothings, activated-carbon filters, air filters, oil filters and diesel particulate filters.

Porous media are characterized by having at least two distinct length scales, where the second scale is introduced by a porous micro structure. Typically, both scales differ by orders of magnitude. For example, in ground water research, flows are modeled and predicted which extend to some square kilometers, whereas pore sizes of soil are less than $1mm$. Another example of a porous medium is shown in Figure 1.

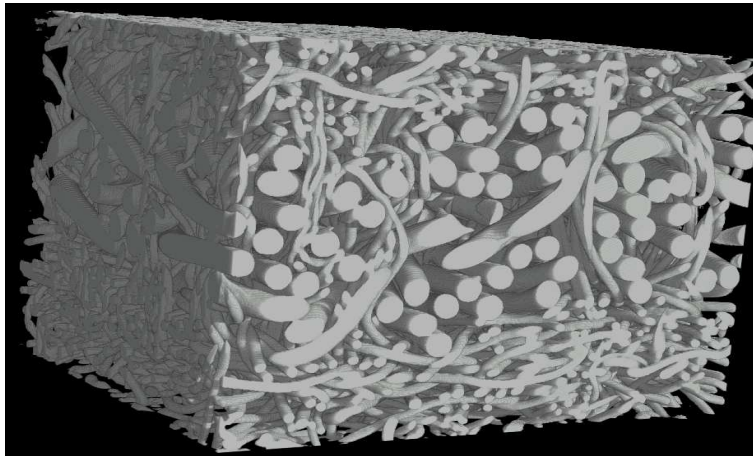


FIGURE 1. Dewatering felt used in paper machines

We see the micro structure of a dewatering felt, which is a technical textile used in paper machines. The cross-section of the sample is approximately $1mm^2$ and the characteristic length of the pores may reach a few microns. In contrast, the macroscopic dimensions are in the range of some meters.

The fact, that we have to consider two largely varying length scales, renders the

direct numerical simulation of porous media flows in many cases impossible. The required resolution to resolve the micro structure leads to huge problems, which can not be handled by existing computer architectures. Therefore, engineers, physicists and mathematicians try to find macroscopic descriptions of the phenomena in porous media, which will often be sufficient for the desired application. One way to derive a macroscopic description is to start from first principles, i.e. from equations which are valid at the pore scale. Then, one applies some kind of upscaling method. Once the upscaled model is available, one would like to have an estimate in which sense the macroscopic description is related to the micro problem. This is somehow the ideal way, but sometimes hard to accomplish. The purely experimental approach denotes the other extreme leading to phenomenological laws whose range of applicability is very often quite uncertain in a strict sense. Nevertheless, the point is, that the experimental approach sometimes gives answers, where the rigorous mathematical derivation has not been successful up to now.

There exists a vast literature on flow in porous media and upscaling methods. For reference purposes, we want to mention the classical textbooks on porous media theory by Allen ([3]), Bear ([6], [7], [8], [9]), Bensoussan, Lions, Papanicolaou ([10]), Dullien ([22]), Greenkorn ([38]), Hornung ([43]), Jikov, Kozlov, Oleinik ([45]), Karviany ([46]), Lions ([49]), Sanchez-Palencia ([65]) and Scheidegger ([66], [67]).

1.1. Filtration laws and upscaling

In this thesis, we will mainly be concerned with saturated, stationary, incompressible Newtonian flow in porous media and its upscaling by homogenization. Therefore, we give a short historical overview on the achieved scientific results. In 1856, it was Henry Darcy, who published his famous filtration law ([18]). He investigated saturated water flow through sand columns as illustrated by Figure 2 on the next page.

He found that the volumetric flow rate Q is proportional to the cross-section $A = \frac{\pi D^2}{4}$ of the column, inversely proportional to the length l of the column and proportional to the hydrodynamic head $h_1 - h_2$, i.e.

$$Q = \frac{KA(h_1 - h_2)}{l},$$

where K is the proportionality factor. The hydrodynamic head is measured by water manometers and corresponds to the pressure drop.

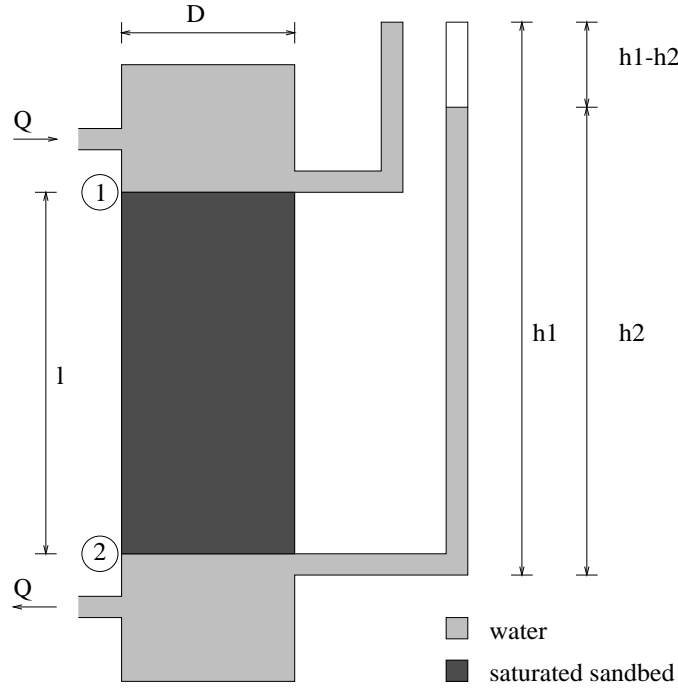


FIGURE 2. Darcy's experiment ([38])

Darcy's law in differential form and extended to multi-dimensions reads:

$$(1.1) \quad v = -\frac{\mathcal{K}}{\mu} \cdot \nabla p,$$

where v and p denote the *effective* velocity and pressure, respectively. μ is the dynamic viscosity of the fluid and \mathcal{K} is the permeability tensor.

In 1863, J. Dupuit ([21]) found that the pressure drops predicted by Darcy's law are smaller than his measured pressure drops, especially when flow rates become large. In 1901, Forchheimer ([27]) proposed the following quadratic extension of Darcy's law, which accounts for higher pressure drops:

$$(1.2) \quad v + b\|v\|v = -\frac{\mathcal{K}}{\mu} \cdot \nabla p.$$

In (1.2), the constant $b > 0$ is often referred to as *Forchheimer coefficient*.

Motivated by the empirical laws (1.1), (1.2), a lot of research has been going on to theoretically derive macroscopic descriptions of porous media flows. There exists a variety of different approaches, which are discussed in detail in the aforementioned textbooks (e.g. [6], pp. 161-184). For instance, capillary tube models consider Hagen-Poiseuille flow in a certain arrangement of tubes representing the porous medium. Due to the analytic solution of the Navier-Stokes equation in this case, a linear relationship between velocity and pressure drop is obtained. Another possibility is the concept of overlapping continua

(see [3] and Chapter 5), where fluid and solid phase are considered to be defined *everywhere*. From a general momentum balance equation, it is possible to obtain Darcy's law under the assumptions that inertia is negligible and that the interaction of fluid and solid phase obeys Stokes' law. The third method we want to mention is the volume averaging approach which integrates the Navier-Stokes equations over a sufficiently large representative volume element of the porous medium. With certain assumptions on the averaged flow field, it is again possible to obtain Darcy's law. The volume averaging method can also be employed to derive nonlinear extensions of Darcy's law. The drawback of these methods is the lack of an approximation result which relates the macroscopic equations to the Navier-Stokes equations on the micro scale.

A major breakthrough was achieved in the late seventies of the last century, when the multi-scale homogenization method evolved ([10], [49], [65]). To derive Darcy's law, the Stokes equations in a periodic porous medium are considered. Using two-scale expansions of the velocity and pressure, i.e.

$$\begin{aligned} u(x) &= u_0(x, y) + \varepsilon u_1(x, y) + \cdots, \\ p(x) &= p_0(x, y) + \varepsilon p_1(x, y) + \cdots, \end{aligned}$$

where $y = \frac{x}{\varepsilon}$ and ε is the size of the periodicity cell of the porous medium, yields a Stokes system with two pressures for u_0 , p_0 and p_1 . Due to linearity of the system, it is possible to separate the scales and it becomes obvious, that u_0 and p_0 are in some sense related by Darcy's law. Moreover, the permeability tensor \mathcal{K} is determined by the solution of some Stokes problems on the periodicity cell. We will come back to this point in Chapter 2. Convergence results as ε tends to zero are given by Tartar ([68]) and Allaire ([2]) in two and three dimensions, respectively.

Considering the Navier-Stokes equations in a periodic porous medium, the structure of the homogenized system depends on the scaling of the Reynolds number Re . Following [50], we assume $Re = Re_\varepsilon = \frac{1}{\mu} \varepsilon^{-\gamma}$. Then, three cases have to be distinguished:

- $\gamma < 1$: The zeroth order equations form a Stokes system with two pressures.
- $\gamma = 1$: A Navier-Stokes system with two pressures is obtained in zeroth order.
- $\gamma > 1$: The homogenization process leads to ill-posed problems.

In [76], [52], [62], nonlinear extensions of Darcy's law are formally derived for $\gamma < 1$, by taking into account higher order problems. In contrast to (1.2), they obtain an additional cubic term. Convergence results are presented in [53].

The rigorous justification of their filtration laws can be found in [13]. Although, the case $\gamma = 1$ is formally derived in the early books on homogenization by Lions [49] and Sanchez-Palencia [65], it took over fifteen years for the first theoretical results. In 1995, Mikelić [54] proved unique solvability of the nonlinear two pressure system for a porous medium with periodic outer boundary with respect to one space direction. The Navier-Stokes system with two pressures does not allow to separate the scales explicitly due to the persistent nonlinear convective term. Therefore, in [12] and [14], still for a special, essentially one-dimensional case unique existence of a solution is proved and the filtration law is made explicit by means of a Taylor expansion of the nonlinear function relating u_0 and p_0 . In [50], [55], the restrictions on the geometry are overcome and the existing results are generalized to multi-dimensional porous media with impervious and periodic outer boundaries. Considering isotropic porous media and using symmetry of the Navier-Stokes equations on the periodicity cell, the authors theoretically obtain a cubic extension of Darcy's law.

1.2. Thesis outline

The aim of the thesis is the numerical investigation of saturated, stationary, incompressible Newtonian flow in porous media when inertia is not negligible. We focus our attention to the Navier-Stokes system with two pressures derived by two-scale homogenization.

The thesis is subdivided into five Chapters. After the introductory remarks on porous media, filtration laws and upscaling methods, the first chapter is closed by stating the basic terminology and mathematical fundamentals.

In Chapter 2, we start by formulating the Navier-Stokes equations on a periodic porous medium. By two-scale expansions of the velocity and pressure, we formally derive the Navier-Stokes system with two pressures. For the sake of completeness, known existence and uniqueness results are repeated and a convergence proof is given. Finally, we consider Stokes and Navier-Stokes systems with two pressures with respect to their relation to Darcy's law.

Chapter 3 and Chapter 4 are devoted to the numerical solution of the nonlinear two pressure system. Therefore, we follow two approaches. The first approach which is developed in Chapter 3 is based on a splitting of the Navier-Stokes system with two pressures into micro and macro problems. The splitting is achieved by Taylor expanding the permeability function or by discretely computing the permeability function. The problems to be solved are a series of Stokes and Navier-Stokes problems on the periodicity cell. The Stokes problems are solved by an Uzawa conjugate gradient method. The Navier-Stokes

equations are linearized by a least-squares conjugate gradient method, which leads to the solution of a sequence of Stokes problems. The macro problem consists of solving a nonlinear uniformly elliptic equation of second order. The least-squares linearization is applied to the macro problem leading to a sequence of Poisson problems. All equations will be discretized by finite elements. Numerical results are presented at the end of Chapter 3.

The second approach presented in Chapter 4 relies on the variational formulation in a certain Hilbert space setting of the Navier-Stokes system with two pressures. The nonlinear problem is again linearized by the least-squares conjugate gradient method. We obtain a sequence of Stokes systems with two pressures. For the latter systems, we propose a fast solution method which relies on pre-computing Stokes systems on the periodicity cell for finite element basis functions acting as right hand sides. Finally, numerical results are discussed.

In Chapter 5 we are concerned with modeling and simulation of the pressing section of a paper machine. We state a two-dimensional model of a press nip which takes into account elasticity and flow phenomena. Nonlinear filtration laws are incorporated into the flow model. We present a numerical solution algorithm and the chapter is closed by a numerical investigation of the model with special focus on inertia effects.

1.3. Terminology and mathematical fundamentals

In this section, we want to give a short exposition on basic notation and mathematical concepts, which are needed in the subsequent chapters. They are taken from the books [1], [24], [29], [30] and [31].

Numbers, vectors and matrices. The sets of natural, integer and real numbers are denoted by \mathbb{N} , \mathbb{Z} and \mathbb{R} , respectively. \mathbb{N}_0 is the set of natural numbers including zero. \mathbb{R}^+ is the set of all strictly positive real number. All positive real numbers including zero are abbreviated by \mathbb{R}_0^+ . \mathbb{R}^- is defined as $\mathbb{R} \setminus (\mathbb{R}^+ \cup \{0\})$. The absolute value of a number is given by $|\cdot|$. Open intervals are denoted $]a, b[$, where $a, b \in \mathbb{R}$. Half-closed intervals, i.e. $[a, b[$ and $]a, b]$, and the closed interval $[a, b]$ use enclosing brackets indicating that endpoints are included. Let $n \in \mathbb{N}$. Then, \mathbb{Z}^n is the set of integer n -tuples. The canonical basis vectors e_i , $i \in \{1, \dots, n\}$ of the real vector space \mathbb{R}^n are defined by

$$(e_i)_k = \begin{cases} 1, & \text{if } i = k, \\ 0, & \text{else.} \end{cases}$$

Let $v \in \mathbb{R}^n$ be a vector. Identifying \mathbb{R}^n by the space of one-column matrices $\mathbb{R}^{n \times 1}$, the transpose of v is denoted by $v^T \in \mathbb{R}^{1 \times n}$. Let $A \in \mathbb{R}^{n \times m}$ and $B \in \mathbb{R}^{m \times o}$, $m, o \in \mathbb{N}$, then the usual matrix product is defined by

$$(A \cdot B)_{ij} := \sum_{k=1}^m (A)_{ik} (B)_{kj}.$$

Let \mathbb{R}^n be equipped with the usual topology induced by the scalar product

$$(1.3) \quad (x, y) := x^T \cdot y = \sum_{i=1}^n x_i y_i, \quad x, y \in \mathbb{R}^n$$

and norm

$$\|x\| := \sqrt{(x, x)}, \quad x \in \mathbb{R}^n.$$

To simplify notation, the transpose symbol in (1.3) is often omitted.

Differential operators. Let $f : \mathbb{R}^n \rightarrow \mathbb{R}$ be a real-valued function. The *nabla* operator and the *Laplacian* are defined by

$$\nabla f := \left(\frac{\partial f}{\partial x_1}, \dots, \frac{\partial f}{\partial x_n} \right)^T \quad \text{and} \quad \Delta f := \sum_{i=1}^n \frac{\partial^2 f}{\partial x_i^2},$$

respectively. For vector-valued functions $f : \mathbb{R}^n \rightarrow \mathbb{R}^n$, the *divergence* operator and Laplacian read

$$\operatorname{div} f := \nabla \cdot f = \sum_{i=1}^n \frac{\partial f_i}{\partial x_i} \quad \text{and} \quad \Delta f := (\Delta f_1, \dots, \Delta f_n)^T,$$

respectively. Let $f : \mathbb{R}^n \rightarrow \mathbb{R}^m$ be a differentiable function. Then $Df(x) \in \mathbb{R}^{m \times n}$ is defined by

$$(Df(x))_{ij} = \frac{\partial f_i}{\partial x_j}(x), \quad \forall i, j \in \{1, \dots, m\}.$$

Let $f, g : \mathbb{R}^n \rightarrow \mathbb{R}^n$. Then we set

$$\nabla f : \nabla g = \sum_{i=1}^n \sum_{j=1}^n \frac{\partial f_i}{\partial x_j} \frac{\partial g_i}{\partial x_j}$$

and

$$((f \cdot \nabla)g)_i = \sum_{j=1}^n f_j \frac{\partial g_i}{\partial x_j}, \quad \forall i \in \{1, \dots, n\}.$$

Multi-indices. A multi-index $\alpha = (\alpha_1, \dots, \alpha_n)$ of length n is a n -tuple of numbers in \mathbb{N}_0 , i.e. $\alpha \in \mathbb{N}_0^n$. The order of a multi-index is defined by

$$|\alpha| := \alpha_1 + \dots + \alpha_n.$$

Multi-indices will appear to simplify notation. Let $\alpha, \beta \in \mathbb{N}_0^n$ be multi-indices with $\alpha_i \leq \beta_i$, $\forall i \in \{0, \dots, n\}$ and let $x \in \mathbb{R}^n$. Then, we define sums, products and binomial coefficients as

$$\sum_{\alpha=0}^{\beta} := \sum_{\alpha_1=0}^{\beta_1} \cdots \sum_{\alpha_n=0}^{\beta_n}, \quad x^\alpha = x_1^{\alpha_1} \dots x_n^{\alpha_n} \quad \text{and}$$

$$\binom{\beta}{\alpha} = \binom{\beta_1}{\alpha_1} \cdots \binom{\beta_n}{\alpha_n} = \frac{\beta_1!}{(\beta_1 - \alpha_1)! \alpha_1!} \cdots \frac{\beta_n!}{(\beta_n - \alpha_n)! \alpha_n!},$$

respectively. The differential operator D^α is to be understood in the following way:

$$D^\alpha := \left(\frac{\partial}{\partial x_1}\right)^{\alpha_1} \cdots \left(\frac{\partial}{\partial x_n}\right)^{\alpha_n}.$$

Topology. For the basic definitions of open, closed, bounded, compact and connected sets in \mathbb{R}^n we refer to the Appendix of [24] for instance. Now, let Ω be an open subset of \mathbb{R}^n . If Ω is additionally connected, it is called a domain. $\bar{\Omega}$ denotes the closure of Ω and $\partial\Omega$ is its boundary.

Lebesgue spaces. Let Ω be a domain in \mathbb{R}^n . For $q \in [1, \infty[$, let $L^q = L^q(\Omega)$ denote the Banach space of all real Lebesgue-measurable functions u defined in Ω , such that

$$\|u\|_{L^q(\Omega)} := \left(\int_{\Omega} |u|^q dx \right)^{\frac{1}{q}} < \infty.$$

As usual, we identify functions in $L^q(\Omega)$, which are equal up to a set of measure zero on Ω . The characteristic function of Ω is defined by

$$\mathbf{1}_{\Omega}(x) := \begin{cases} 1, & \text{if } x \in \Omega, \\ 0, & \text{else.} \end{cases}$$

Then, the volume or measure of Ω is given by

$$|\Omega| = \int_{\Omega} \mathbf{1}_{\Omega}(x) dx.$$

For $q = 2$, $L^q(\Omega)$ is a Hilbert space under the scalar product

$$(u, v)_{L^2(\Omega)} := \int_{\Omega} uv dx, \quad u, v \in L^2(\Omega).$$

In view of appropriate function spaces for pressure solutions of Stokes and Navier-Stokes systems, we set

$$L_0^2(\Omega) := \{u \in L^2(\Omega) \mid \int_{\Omega} u \, dx = 0\}.$$

The definition of product spaces of L^2 is straight forward:

$$(1.4) \quad L^2(\Omega)^n := \{u = (u_1, \dots, u_n) \mid u_i \in L^2(\Omega); i = 1, \dots, n\}.$$

For $u, v \in L^2(\Omega)^n$, the scalar product and norm are introduced by

$$(1.5) \quad (u, v)_{L^2(\Omega)^n} := \sum_{i=1}^n (u_i, v_i)_{L^2(\Omega)} \quad \text{and} \quad \|u\|_{L^2(\Omega)^n} := \sqrt{(u, u)_{L^2(\Omega)^n}},$$

respectively.

Lipschitz continuity of boundaries. Following [24], we recall the definition of a Lipschitz continuous boundary. First, a function $f : \mathbb{R}^m \supset M \rightarrow \mathbb{R}^n$ is Lipschitz continuous, if there exists a constant L such that

$$|f(x) - f(y)| \leq L|x - y|, \quad \forall x, y \in M.$$

Let Ω be a bounded domain in \mathbb{R}^n . $\partial\Omega$ is called *Lipschitz continuous*, if there exist $0 < \alpha \in \mathbb{R}$, a number $R \in \mathbb{N}$, and a finite number of local Cartesian coordinate systems x_1^i, \dots, x_n^i and Lipschitz continuous functions $a_i : \mathcal{M}_i = \{\hat{x}^i = (x_2^i, \dots, x_n^i) \in \mathbb{R}^{n-1}; |\hat{x}^i| \leq \alpha\} \rightarrow \mathbb{R}, i = 1, \dots, R$, such that

$$\partial\Omega = \bigcup_{i=1}^R \Lambda_i, \quad \text{with} \quad \Lambda_i = \{(x_1^i, \hat{x}^i) \mid x_1^i = a_i(\hat{x}^i), |\hat{x}^i| < \alpha\}.$$

If there exists $0 < \beta \in \mathbb{R}$, such that $\forall i \in \{1, \dots, R\}$

$$\begin{aligned} & \{(x_1^i, \hat{x}^i) \mid a_i(\hat{x}^i) < x_1^i < a_i(\hat{x}^i) + \beta, |\hat{x}^i| < \alpha\} \subset \Omega \\ \text{and} \quad & \{(x_1^i, \hat{x}^i) \mid a_i(\hat{x}^i) - \beta < x_1^i < a_i(\hat{x}^i), |\hat{x}^i| < \alpha\} \subset \mathbb{R}^n \setminus \overline{\Omega}, \end{aligned}$$

we say that Ω is locally located on one side of its boundary. On Lipschitz continuous boundaries, there exists a measure and the outer normal ν is defined up to a set of measure zero.

Sobolev spaces. Let Ω be a domain in \mathbb{R}^n . $C^k(\Omega)$ is the space of all real valued functions with continuous derivatives up to order k in Ω . The set of functions in $C^k(\Omega)$, whose derivatives up to order k are continuously extendable onto $\overline{\Omega}$ is denoted by $C^k(\overline{\Omega})$. Setting $C^\infty(\overline{\Omega}) := \bigcap_{k=1}^\infty C^k(\overline{\Omega})$, we define the space

$$\mathcal{D}(\Omega) = C_0^\infty(\Omega) := \{u \in C^\infty(\overline{\Omega}) \mid \text{supp}(u) \subset \Omega \text{ is compact}\},$$

where the support of a function is given by $\text{supp}(u) = \overline{\{x \mid u(x) \neq 0\}}$. Equipped with the topology of locally uniform convergence (see [24] for details), the dual space of \mathcal{D} is denoted by \mathcal{D}' . The elements of \mathcal{D}' are called distributions. A distribution $f_\alpha \in \mathcal{D}'$ is called the α -th order distributional derivative of a distribution $f \in \mathcal{D}'$, if

$$(1.6) \quad \langle f_\alpha, v \rangle = (-1)^{|\alpha|} \langle f, D^\alpha v \rangle, \quad \forall v \in \mathcal{D},$$

where $\langle f, v \rangle$ denotes the value of f applied to v . Green's theorem implies that for functions $f \in C^k(\overline{\Omega})$ the definition (1.6) reduces to the classical derivative of f . Therefore, we use the classical notation $D^\alpha f := f_\alpha$.

Note, that any function $u \in L^p(\Omega)$ is a distribution by setting

$$(1.7) \quad \langle u, v \rangle = \int_{\Omega} uv \, dx, \quad \forall v \in \mathcal{D}.$$

The integral in (1.7) is defined, because $\mathcal{D} \subset L^p(\Omega)'$ for $p \in [1, \infty[$.

Now, let $k \in \mathbb{N}_0$ and $p \in [1, \infty[$. We define the function space

$$W^{k,p}(\Omega) := \{u, D^\alpha u \in L^p(\Omega); \forall \alpha \in \mathbb{N}_0^n \text{ with } |\alpha| = 0, \dots, k\}$$

equipped with the norm

$$\|u\|_{W^{k,p}(\Omega)} := \left(\sum_{|\alpha|=0}^k \|D^\alpha u\|_{L^p(\Omega)}^p \right)^{\frac{1}{p}}.$$

The spaces $W^{k,p}$ are called *Sobolev spaces* and our main interest is the case $k = 1$ and $p = 2$. We will use the common notation

$$H^1(\Omega) := W^{1,2}(\Omega).$$

$H^1(\Omega)$ is a Hilbert space when equipped with the scalar product

$$(u, v)_{H^1(\Omega)} := \int_{\Omega} uv \, dx + \int_{\Omega} \nabla u \cdot \nabla v \, dx, \quad \forall u, v \in H^1(\Omega).$$

The construction of the product space $H^1(\Omega)^n$ is in complete analogy to the definition of the space $L^2(\Omega)^n$ in (1.4), (1.5).

If Ω is a bounded and Lipschitz continuous domain, there exists a uniquely determined continuous linear operator $\theta : W^{1,p}(\Omega) \rightarrow L^p(\partial\Omega)$, such that

$$\theta u = u|_{\partial\Omega}, \quad \forall u \in C^\infty(\overline{\Omega}),$$

where $u|_{\partial\Omega}$ denotes the restriction of the function u to the boundary of Ω . $\theta u \in L^p(\partial\Omega)$ is called the trace of the function $u \in W^{1,p}(\Omega)$ on the boundary $\partial\Omega$. The following inequality is an immediate consequence of the continuity of the trace operator θ . We have

$$(1.8) \quad \|\theta u\|_{L^p(\partial\Omega)} \leq C \|u\|_{W^{1,p}(\Omega)}, \quad \forall u \in W^{1,p}(\Omega),$$

with some constant C . Hence, it makes sense to speak of boundary values of functions in $W^{1,p}(\Omega)$. Finally, we define the space

$$H_0^1(\Omega) := \{u \in W^{1,2}(\Omega) \mid u = 0 \text{ on } \partial\Omega\}.$$

Due to the Poincaré inequality, $H_0^1(\Omega)$ is a Hilbert space when equipped with the following scalar product

$$(u, v)_{H_0^1(\Omega)} := \int_{\Omega} \nabla u \cdot \nabla v \, dx, \quad \forall u, v \in H_0^1(\Omega).$$

Hölder spaces. Following [31], let $x_0 \in D \subset \mathbb{R}^n$, $0 < \gamma < 1$, D bounded and $f : D \rightarrow \mathbb{R}$ a function. f is called *Hölder continuous with exponent γ at x_0* , if

$$[f]_{\gamma, x_0} := \sup_{x \in D \setminus \{x_0\}} \frac{|f(x) - f(x_0)|}{|x - x_0|^\gamma} < \infty.$$

f is *Hölder continuous with exponent γ in D* , if

$$[f]_{\gamma, D} := \sup_{x, y \in D; x \neq y} \frac{|f(x) - f(y)|}{|x - y|^\gamma} < \infty.$$

Let Ω be an open set in \mathbb{R}^n and $k \in \mathbb{N}_0$. The Hölder space $C^{k,\gamma}(\overline{\Omega})$ is defined as the subspaces of $C^k(\overline{\Omega})$ consisting of functions whose k -th order partial derivatives are Hölder continuous in Ω . $C^{k,\gamma}(\overline{\Omega})$ becomes a Banach space by introducing the following norm:

$$\begin{aligned} \|u\|_{C^{k,\gamma}(\overline{\Omega})} &:= \sum_{|\alpha|=0}^k \max_{x \in \Omega} \max_{|\alpha|} |D^\alpha u(x)| \\ &\quad + \sum_{|\alpha|=k} \sup_{x, y \in \Omega; x \neq y} \frac{|D^\alpha u(x) - D^\alpha u(y)|}{|x - y|^\alpha}. \end{aligned}$$

Note, that $C^{k,\gamma}(\overline{\Omega})$ is also a Banach algebra. Again, product spaces of Hölder continuous functions are constructed in complete analogy to (1.4), (1.5).

Special Lebesgue and Hölder spaces. Let $\Omega, Y \subset \mathbb{R}^n$ and \mathbf{Y} be a function space over Y equipped with the norm $\|\cdot\|_{\mathbf{Y}}$. Then the space $L^2(\Omega, \mathbf{Y})$ consists of all functions $u : \Omega \times Y \rightarrow \mathbb{R}$, such that

$$\begin{aligned} u(x, \cdot) &\in \mathbf{Y}, \quad \forall x \in \Omega, \\ u(\cdot, y) &\text{ is Lebesgue-measurable for all } y \in \mathbf{Y} \text{ and} \\ \int_{\Omega} \|u(x, \cdot)\|_{\mathbf{Y}}^2 \, dx &< \infty. \end{aligned}$$

Analogously, we will use the space $C^{k,\gamma}(\overline{\Omega}, Y)$.

Landau symbols. We specify the order of convergence by using the Landau symbols o and O . Let (a_i) and (b_i) be sequences of positive real numbers, where $b_i > 0$. If there is a constant C , such that $a_i \leq Cb_i, \forall i \in \mathbb{N}$, one writes $a_i = O(b_i)$. If $\lim_{i \rightarrow \infty} \frac{a_i}{b_i} = 0$, we say $a_i = o(b_i)$.

Periodicity. Let $\Omega \subset \mathbb{R}^n$ be a domain which can be periodically repeated by suitable translations in at least one direction. If $\Gamma \subset \partial\Omega$ is periodic with respect to the same translations, we call Γ Ω -periodic. Let f be a function defined on Ω . If f has equal values on an Ω -periodic boundary Γ , we say f is Γ -periodic. If the values of f periodically change in sign, we call f Γ -antiperiodic.

CHAPTER 2

The Navier-Stokes system with two pressures

The Navier-Stokes system with two pressures is first mentioned in the books by Sanchez-Palencia [65] and J.L. Lions [49]. They formally derive the system by a two-scale asymptotic expansion of the solution of the Navier-Stokes system on a periodic porous medium. Its derivation is formal, done in the same way as for the Stokes system with two pressures. In contrast to the latter system whose solvability, convergence and equivalence to Darcy's law is well understood in that time, no theoretical results were available for the Navier-Stokes system with two pressures. A. Mikelić gives the first answers concerning existence, uniqueness and regularity of the solution of a special two-dimensional case of the Navier-Stokes system with two pressures in [54]. Additionally, he proves convergence of the homogenization process. In [12], [14], [50] and [55], the results are generalized and the system is interpreted as a nonlinear extension of Darcy's law.

In this chapter, we repeat the results known for the Navier-Stokes system with two pressures, thereby, adapting the macroscopic boundary conditions to our needs in the subsequent chapters. Starting with the definition of a periodic porous medium, we formulate the Navier-Stokes system in dimensional and non-dimensional form and repeat important properties of its solution. Performing a formal two-scale analysis, we derive the homogenized two pressure system. After recalling existence, uniqueness and regularity results, we give a convergence result of the homogenization process. Some remarks on how the Navier-Stokes system with two pressures extends Darcy's law are made in the final section of this chapter.

2.1. The Navier-Stokes problem on periodic porous media

2.1.1. Definition of a porous medium. Following [2] and [55], we define a periodic structure in \mathbb{R}^n starting with the unit cell $Y =]0, 1[^n$. Let Y_s be a closed subset of \bar{Y} and $Y_f = Y \setminus Y_s$. Y_s and Y_f are called *solid part* and *fluid part*, respectively. We will frequently refer to this basic construction as *periodicity cell*. Since we want to consider flow phenomena in porous media, Y_s will sometimes be called *obstacle*.

Now, we make the periodic repetition of Y_s all over \mathbb{R}^n and set $Y_s^k = Y_s + k$, $k \in \mathbb{Z}^n$. Obviously, the set $E_s = \bigcup_{k \in \mathbb{Z}^n} Y_s^k$ is a closed subset of \mathbb{R}^n and $E_f = \mathbb{R}^n \setminus E_s$ is an open set in \mathbb{R}^n . We need this basic periodic structure to have certain properties. Therefore, we claim three hypotheses made in [2]:

- Y_f and Y_s have strictly positive measures in \bar{Y} ,
- E_f and the interior of E_s are open sets with the boundary fulfilling a Lipschitz condition, and are locally located on one side of their boundary. Moreover, E_f is connected.
- Y_f is an open connected set whose boundary fulfills a local Lipschitz condition.

Finally, we explicitly assume that ∂Y_f is Y -periodic.

REMARK 2.1. The above assumptions provide a first *regularity setup*, which is needed (and modified, if necessary) for the theoretical considerations in this thesis. On the other hand, some configurations are excluded. For instance, due to the connectivity of E_f , impermeable media in certain space directions are forbidden. This condition will guarantee positive definiteness of Darcy's permeability tensor. An example of a two-dimensional periodicity cell fulfilling all the assumptions is shown in Figure 1. For a more detailed discussion on these assumptions, we refer to [2].

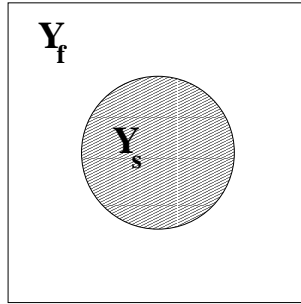


FIGURE 1. Example of a periodicity cell

Using the periodic structure from above, we define the periodic porous medium: Let $\Omega \subset \mathbb{R}^n$ be a bounded and connected open set with a Lipschitz boundary. Let $0 < \varepsilon \in \mathbb{R}^+$. The set Ω is covered with a regular mesh of size ε , each cell being a cube Y_i^ε with $1 \leq i \leq N(\varepsilon) = |\Omega| \varepsilon^{-n} [1 + o(1)]$. Each cube Y_i^ε is homeomorphic to Y , by a linear homeomorphism Π_i^ε , being composed of a translation and an homothety of ratio $\frac{1}{\varepsilon}$:

$$\Pi_i^\varepsilon : Y_i^\varepsilon \rightarrow Y, \quad x \mapsto y = \frac{x}{\varepsilon} + \text{translation}.$$

Now, we define

$$Y_{s_i}^\varepsilon := (\Pi_i^\varepsilon)^{-1}(Y_s), \quad Y_{f_i}^\varepsilon := (\Pi_i^\varepsilon)^{-1}(Y_f).$$

We construct Ω^ε by picking out from Ω the solid parts $Y_{s_i}^\varepsilon$:

$$\Omega^\varepsilon := \Omega \setminus \bigcup_{i=1}^{N(\varepsilon)} Y_{s_i}^\varepsilon.$$

Ω^ε denotes the part of Ω occupied by the fluid. For simplicity, we suppose that Ω^ε is connected possibly suppressing fluid part components near the boundary. Finally, we set

$$S^\varepsilon := \partial \bigcup_{i=1}^{N(\varepsilon)} Y_{s_i}^\varepsilon$$

and claim that the boundary of Ω^ε is partitioned into two parts, i.e.

$$\partial\Omega^\varepsilon = \partial\Omega \cup S^\varepsilon, \quad \partial\Omega \cap S^\varepsilon = \emptyset.$$

We call $\partial\Omega$ *outer boundary* and S^ε *inner boundary*.

An example of a periodic porous medium can be seen in the following figure, where Ω is simply the unit square and $\varepsilon = \frac{1}{4}$:

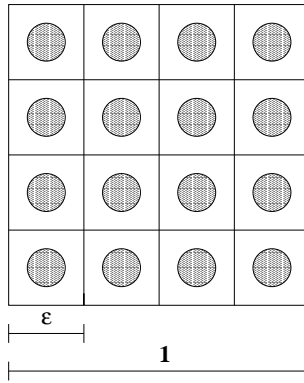


FIGURE 2. Example of a porous medium

Clearly, the parameter ε is intended to create a *micro structure* in the porous medium and, therefore, can be thought to be small, i.e. $\varepsilon \ll 1$.

2.1.2. The Navier-Stokes problem. Stationary incompressible flow of a Newtonian fluid is described by the following Navier–Stokes system:

$$(2.1) \quad \begin{aligned} -\nu\Delta u + (u \cdot \nabla) u + \frac{1}{\rho}\nabla p &= f, \\ \operatorname{div} u &= 0. \end{aligned}$$

For the time being, let the Navier-Stokes system be formulated on an arbitrary open set \mathcal{S} in \mathbb{R}^n . The velocity $u : \mathcal{S} \rightarrow \mathbb{R}^n$ and the pressure $p : \mathcal{S} \rightarrow \mathbb{R}$ are the unknowns. $\nu \in \mathbb{R}^+$ is the kinematic viscosity of the fluid (not to be mixed up with the outer normal) and $\rho \in \mathbb{R}^+$ denotes the fluid density. $f : \mathcal{S} \rightarrow \mathbb{R}^n$ represents the given density of external volume forces. The first line of (2.1) is often referred to as momentum balance equations or Navier-Stokes equations. The second line of (2.1) shows the mass balance equation or continuity equation.

In view of the asymptotic analysis in the subsequent paragraph, we derive (2.1) in dimensionless form. By doing so, some characteristic numbers, namely the Reynolds number and the Froude number will enter the Navier-Stokes equations. Thereby, it is possible to see which terms are dominant and which will *survive* the homogenization process.

Introducing the characteristic length L_0 , the characteristic velocity U_0 and the characteristic volume force F_0 , we define the dimensionless quantities

$$(2.2) \quad x' = \frac{x}{L_0}, \quad u' = \frac{u}{U_0}, \quad p' = \frac{p}{\rho U_0^2}, \quad f' = \frac{f}{F_0}.$$

The Reynolds number and Froude number are defined by

$$(2.3) \quad Re := \frac{L_0 U_0}{\nu} = \frac{\rho L_0 U_0}{\mu} \quad \text{and} \quad Fr := \frac{U_0^2}{F_0 L_0},$$

respectively. For later use, we introduce the dynamic viscosity $\mu \in \mathbb{R}^+$ in (2.3). It is related to the kinematic viscosity by $\nu = \frac{\mu}{\rho}$.

Using (2.2) and (2.3) in (2.1) yields

$$(2.4) \quad \begin{aligned} -\frac{1}{Re} \Delta u' + (u' \cdot \nabla) u' + \nabla p' &= \frac{1}{Fr} f', \\ \operatorname{div} u' &= 0, \end{aligned}$$

the dimensionless form of the stationary incompressible Navier–Stokes system. Now, let Ω^ε be the fluid part of a porous medium being defined as in the preceding paragraph. After applying transformation (2.2) the macroscopic length scale of Ω^ε is 1 and its microscopic length scale is assumed to be ε . We suppose that the Reynolds number and the Froude number depend on ε in the following way:

$$(2.5) \quad Re_\varepsilon = \frac{1}{\mu} \varepsilon^{-1} \quad \text{and} \quad Fr_\varepsilon = \varepsilon.$$

We explicitly keep the dynamic viscosity in (2.5). In this way, it enters the homogenized system derived in section 2.2 and, besides geometry, boundary conditions and forces, it will be an important parameter influencing the flow characteristics of the limit equations.

To be able to prescribe two kinds of boundary conditions, we assume that the outer boundary $\partial\Omega$ is partitioned into two subsets Γ_1 and $\Gamma_2 = \partial\Omega \setminus \Gamma_1$ fulfilling a local Lipschitz condition, respectively. Moreover, Γ_1 has to be Ω -periodic. Note, that we did not exclude the case that Γ_1 or Γ_2 is empty. Supplemented by periodic boundary conditions for the velocity and the pressure on Γ_1 and by no-slip boundary conditions for the velocity on Γ_2 , we can finally formulate our Navier-Stokes system. It reads:

$$(2.6) \quad \begin{aligned} -(\mu\varepsilon)\Delta u^\varepsilon + (u^\varepsilon \cdot \nabla) u^\varepsilon + \nabla p^\varepsilon &= \varepsilon^{-1} f && \text{in } \Omega^\varepsilon, \\ \operatorname{div} u^\varepsilon &= 0 && \text{in } \Omega^\varepsilon, \\ \{u^\varepsilon, p^\varepsilon\} &&& \text{is } \Gamma_1 \text{- periodic,} \\ u^\varepsilon &= 0 && \text{on } S^\varepsilon \cup \Gamma_2. \end{aligned}$$

To point out the dependence on the small parameter, we use ε as superfix of the velocity and the pressure in (2.6). The function f is assumed to be defined on Ω and can be thought of as being restricted to Ω^ε . Therefore, we skip the superfix of f .

REMARK 2.2. Without further notice, we assume f to be Γ_1 - periodic throughout this thesis.

Now, to fix ideas, Figure 3 illustrates an example of the domain Ω and its outer boundaries $\Gamma_1 = \Gamma_{11} \cup \Gamma_{12}$ and $\Gamma_2 = \Gamma_{21} \cup \Gamma_{22}$. Considering the unit force in x-direction as excitation of the system (2.6), one can interpret the periodic boundaries Γ_{11} and Γ_{12} as inlet and outlet, respectively. The zero velocities on Γ_2 act like an impervious wall.

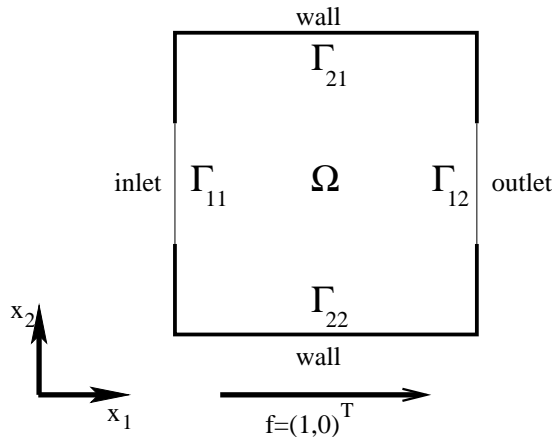


FIGURE 3. Example of a force driven flow and interpretation of the outer boundaries

2.1.3. Existence, uniqueness and regularity of the solution. After having stated the Navier-Stokes problem on a periodic porous medium in the preceding paragraph, we are interested in theoretical results on existence, uniqueness and regularity of the solution. There exists a vast literature on the Navier-Stokes equations and we refer here only to the books by Feistauer ([24]), Galdi ([29], [30]), Ladyženskaja ([48]) and Temam ([71], [72]). Due to the possible appearance of periodic and homogeneous Dirichlet boundary conditions in (2.6), we have to modify the classical solution spaces for the velocity and the pressure. We define

$$V(\Omega^\varepsilon) := \{v \in H^1(\Omega^\varepsilon)^n \mid \operatorname{div} v = 0 \text{ in } \Omega^\varepsilon, \\ v \text{ is } \Gamma_1\text{-periodic, } v = 0 \text{ on } \Gamma_2 \cup S^\varepsilon\}$$

and

$$Q(\Omega^\varepsilon) := \{q \in L_0^2(\Omega^\varepsilon) \mid q \text{ is } \Gamma_1\text{-periodic}\}.$$

Now, we have the following result:

Theorem 2.3. *Let Ω^ε be the fluid part of a porous medium. If $f \in L^2(\Omega)^n$ is sufficiently small, the Navier-Stokes problem (2.6) has a unique weak solution $(u^\varepsilon, p^\varepsilon) \in V(\Omega^\varepsilon) \times Q(\Omega^\varepsilon)$.*

Proof: If $\Gamma_1 = \emptyset$, the result is classical and can be found in [24], chapter 8 for example. If $\Gamma_1 \neq \emptyset$, we have (at least) homogeneous Dirichlet boundary conditions on S^ε . Use the modified solution spaces $V(\Omega^\varepsilon)$ and $Q(\Omega^\varepsilon)$ in the proofs of [24], chapter 8, and find that, they do not change any essential statement there. ■

2.2. Formal asymptotic analysis

Since ε is assumed to be a small parameter, we are interested to find an asymptotic description of the Navier-Stokes system on a periodic porous medium as $\varepsilon \rightarrow 0$. The problem (2.6) contains two scales: the macroscopic scale of the domain Ω and the microscopic scale of the periodicity cell Y . Therefore, it is somehow *natural* to make this separation of scales explicit. The two-scale Ansatz, first introduced in [10], expands the solutions in powers of ε and separates the scales by means of an additional variable $y = \frac{x}{\varepsilon}$:

$$(2.7) \quad \begin{aligned} u^\varepsilon &= u_0(x, y) + \varepsilon u_1(x, y) + \varepsilon^2 u_2(x, y) + \cdots, \\ p^\varepsilon &= \frac{1}{\varepsilon} (p_0(x, y) + \varepsilon p_1(x, y) + \varepsilon^2 p_2(x, y) + \cdots), \end{aligned}$$

where u_i and p_i are defined in $\Omega \times Y_f$. Additionally, we suppose Y -periodicity in the second argument and want $u_i(x, y) = 0$ if $y \in Y_s$.

In [65] and [49] the structure of the Ansatz (2.7), i.e. the choice of the leading power of ε and of the sequence of powers, is not motivated. In [50] the leading power is concluded from a priori estimates of the velocity and the pressure. The structure of the powers of ε can be found by investigating equations (2.6) and observing that, for example, functions associated with $\varepsilon^{\frac{j}{2}}$, $j \in \mathbb{N}$ lack the dependence on the excitation of the system and, therefore, would be zero anyway.

Now, we proceed with the asymptotic analysis. Recalling the definition of the variable y , we find the differential operators ∇ , div and Δ expanded by means of the chain rule. When applied to functions depending on x and y , they read:

$$(2.8) \quad \begin{aligned} \nabla &= \nabla_x + \frac{1}{\varepsilon} \nabla_y, \\ \operatorname{div} &= \operatorname{div}_x + \frac{1}{\varepsilon} \operatorname{div}_y, \\ \Delta &= \Delta_x + \frac{2}{\varepsilon} \operatorname{div}_x \nabla_y + \frac{1}{\varepsilon^2} \Delta_y, \end{aligned}$$

where the indices indicate differentiation with respect to x or y .

Substituting (2.7) and (2.8) in the Navier-Stokes system (2.6) and collecting equal powers of ε , we obtain:

$$\begin{aligned} \varepsilon^{-2} : \quad & \nabla_y p_0(x, y) = 0 \quad \text{in } \Omega \times Y_f, \\ \varepsilon^{-1} : \quad & -\mu \Delta_y u_0(x, y) + (u_0(x, y) \cdot \nabla_y) u_0(x, y) + \nabla_y p_1(x, y) \\ & = f(x) - \nabla_x p_0(x, y) \quad \text{in } \Omega \times Y_f, \\ & \operatorname{div}_y u_0(x, y) = 0 \quad \text{in } \Omega \times Y_f, \\ \varepsilon^0 : \quad & -\mu \Delta_y u_1(x, y) - 2\mu \operatorname{div}_x \nabla_y u_0(x, y) + (u_0(x, y) \cdot \nabla_x) u_0(x, y) \\ & + (u_0(x, y) \cdot \nabla_y) u_1(x, y) + (u_1(x, y) \cdot \nabla_y) u_0(x, y) \\ & + \nabla_x p_1(x, y) + \nabla_y p_2(x, y) = 0 \quad \text{in } \Omega \times Y_f, \\ & \operatorname{div}_x u_0(x, y) + \operatorname{div}_y u_1(x, y) = 0 \quad \text{in } \Omega \times Y_f. \end{aligned}$$

Since we are only interested in equations for the leading coefficient functions in (2.7), we can stop at the order of ε^0 . Let's have a closer look at the five equations. Clearly, from the first equation it follows that

$$p_0(x, y) = p_0(x)$$

does not depend on y . Therefore, the second equation is a Navier-Stokes equation for u_0 and p_1 in the variable y with right hand side $f(x) - \nabla_x p_0(x)$ only

depending on the macroscopic variable x . Of course, p_0 is still an unknown. The third equation is a continuity equation for u_0 completing the Navier-Stokes system on the periodicity cell. The fourth equation turns out to be superfluous. Integrating the last equation over the fluid part of the periodicity cell, yields

$$(2.9) \quad \begin{aligned} \operatorname{div}_x \int_{Y_f} u_0(x, y) dy &= - \int_{Y_f} \operatorname{div}_y u_1(x, y) dy \\ &= - \int_{\partial Y_f} \nu(y) \cdot u_1(x, y) d\Gamma(y) = 0. \end{aligned}$$

The boundary integral in (2.9) vanishes due to the homogeneous Dirichlet conditions of u_1 on ∂Y_s and due to periodicity and anti-periodicity of u_1 and the outer normal ν , respectively.

The formal considerations and assumptions on the Ansatz functions give a complete Navier-Stokes system comprising all necessary boundary conditions. From a macroscopic point of view, we only have a first order partial differential equation (2.9). As already mentioned in [49], we can not suppose to have no-slip boundary conditions on Γ_2 as stated in (2.6). Nevertheless, there exists a slightly weaker assumption, which will turn out to be the correct choice. Summing up the results of this paragraph including the macroscopic boundary conditions, the Navier-Stokes system with two pressures reads

$$(2.10) \quad \left\{ \begin{array}{l} -\mu \Delta_y u_0(x, y) + (u_0(x, y) \cdot \nabla_y) u_0(x, y) \\ \quad + \nabla_y p_1(x, y) = f(x) - \nabla_x p_0(x) \quad \text{in } \Omega \times Y_f, \\ \operatorname{div}_y u_0(x, y) = 0 \quad \text{in } \Omega \times Y_f, \\ u_0(x, y) = 0 \quad \text{on } \Omega \times \partial Y_s, \\ \{u_0, p_1\} \text{ is } Y\text{-periodic,} \end{array} \right.$$

$$(2.11) \quad \left\{ \begin{array}{l} \operatorname{div}_x \int_{Y_f} u_0(x, y) dy = 0 \quad \text{in } \Omega, \\ \nu(x) \cdot \int_{Y_f} u_0(x, y) dy \text{ is } \Gamma_1\text{-antiperiodic,} \\ p_0 \text{ is } \Gamma_1\text{-periodic,} \\ \nu(x) \cdot \int_{Y_f} u_0(x, y) dy = 0 \quad \text{on } \Gamma_2. \end{array} \right.$$

(2.10) will frequently be referred to as *microscopic problem*. Analogously, (2.11) is called *macroscopic problem*. Both problems are coupled by the right hand side $f - \nabla_x p_0$.

2.3. Existence, uniqueness and regularity of the solution

Before considering existence, uniqueness and regularity of the solution of the Navier-Stokes system with two pressures (2.10), (2.11), we show corresponding

properties of the solution of its linear counterpart, the *Stokes system with two pressures*. It reads

$$(2.12) \quad \left\{ \begin{array}{l} -\mu\Delta_y u_0(x, y) + \nabla_y p_1(x, y) \\ \quad = f(x) - \nabla_x p_0(x) \quad \text{in } \Omega \times Y_f, \\ \quad \operatorname{div}_y u_0(x, y) = 0 \quad \text{in } \Omega \times Y_f, \\ \quad u_0(x, y) = 0 \quad \text{on } \Omega \times \partial Y_s, \\ \quad \{u_0, p_1\} \quad \text{is } Y\text{-periodic,} \end{array} \right.$$

$$(2.13) \quad \left\{ \begin{array}{l} \operatorname{div}_x \int_{Y_f} u_0(x, y) dy = 0 \quad \text{in } \Omega, \\ \nu(x) \cdot \int_{Y_f} u_0(x, y) dy \quad \text{is } \Gamma_1\text{-antiperiodic,} \\ \quad p_0 \quad \text{is } \Gamma_1\text{-periodic,} \\ \nu(x) \cdot \int_{Y_f} u_0(x, y) dy = 0 \quad \text{on } \Gamma_2. \end{array} \right.$$

The system has the same structure as the Navier-Stokes system with two pressures, i.e. it consists of a micro problem (2.12) and a macro problem (2.13). The difference lies in the missing convective term in the micro problem, which is a Stokes problem, hence giving the system its name. Following [49], we introduce several Hilbert spaces. Let

$$\mathcal{W} := \{w \in H^1(Y_f)^n \mid \operatorname{div}_y w = 0 \text{ in } Y_f, w = 0 \text{ on } \partial Y_s, w \text{ is } Y\text{-periodic}\}.$$

Then \mathcal{W} is a Hilbert space equipped with the scalar product of $H_0^1(Y_f)^n$. Using \mathcal{W} , we define another Hilbert space

$$\mathcal{V} := \left\{ v \in L^2(\Omega; \mathcal{W}) \mid \begin{array}{l} \operatorname{div}_x \int_{Y_f} v(x, y) dy = 0 \text{ in } \Omega, \\ \nu(x) \cdot \int_{Y_f} v(x, y) dy \text{ is } \Gamma_1\text{-antiperiodic,} \\ \nu(x) \cdot \int_{Y_f} v(x, y) dy = 0 \text{ on } \Gamma_2 \end{array} \right\}$$

provided with the scalar product

$$(u, v)_{\mathcal{V}} := \mu \int_{\Omega} \int_{Y_f} \nabla_y u(x, y) : \nabla_y v(x, y) dy dx.$$

Clearly, \mathcal{W} and \mathcal{V} are function spaces designed for velocities defined on the periodicity cell and on the product space $\Omega \times Y_f$, respectively. It will turn out that the following space \mathcal{Q}^0 is appropriate for the pressure p_0 :

$$\mathcal{Q}^0 := \{q \in H^1(\Omega) \mid q \text{ is } \Gamma_1\text{-periodic, } \int_{\Omega} q(x) dx = 0\}.$$

In a similar way as for the velocity, one constructs the pressure space for p_1 . We set

$$\mathcal{R} := \{r \in L_0^2(Y_f) \mid r \text{ is } Y\text{-periodic}\}$$

and

$$\mathcal{Q}^1 := \{q \in L^2(\Omega; \mathcal{R}) \mid q \text{ is } \Gamma_1\text{-periodic}\}.$$

Let us define a scalar product for the space \mathcal{Q}^1 by

$$(q, r)_{\mathcal{Q}^1} := \int_{\Omega} \int_{Y_f} q(x, y) r(x, y) dy dx.$$

Now, the next theorem states a solvability result of the Stokes system with two pressures.

Theorem 2.4. *If $f \in L^2(\Omega)^n$, the problem*

$$(2.14) \quad \text{Find } u_0 \in \mathcal{V}, \text{ such that}$$

$$\mu \int_{\Omega} \int_{Y_f} \nabla_y u_0(x, y) : \nabla_y v(x, y) dy dx = \int_{\Omega} \int_{Y_f} f(x) \cdot v(x, y) dy dx, \quad \forall v \in \mathcal{V}$$

is uniquely solvable. Moreover, it is equivalent in the weak sense to the Stokes system with two pressures (2.12), (2.13) implying the unique existence of the pressures $(p_0, p_1) \in \mathcal{Q}^0 \times \mathcal{Q}^1$.

Proof: We will only present the ideas to prove this theorem. For a detailed proof, we refer to [49].

The unique solvability of the variational formulation (2.14) is provided by the Lax-Milgram lemma. Its assumptions are immediately fulfilled since the bilinear form is the scalar product of the Hilbert space \mathcal{V} .

Now, if (u_0, p_0, p_1) is a solution of (2.12), (2.13), one has to show that

$$(2.15) \quad \int_{\Omega} \int_{Y_f} (\nabla_x p_0(x) + \nabla_y p_1(x, y)) \cdot v(x, y) dy dx = 0, \quad \forall v \in \mathcal{V}.$$

Applying partial integration, taking into account the boundary conditions of the pressures and test functions and using the divergence property of the test functions, yields the result. The opposite insertion is proved by constructing the two pressures. In [49] a penalty method is used. In [55] special test functions for the variational problem are constructed to get rid of the micro scale. Then, they apply a result essentially due to DeRahm, i.e. the fact that any vector function orthogonal to divergence free vector functions is a gradient. Therefore, they obtain p_0 . Repeating the argument, the unique existence of the microscopic pressure p_1 is obtained. ■

REMARK 2.5. In Theorem 2.4 the pressures p_0 and p_1 are eliminated. An alternative way of proving unique existence and regularity is shown in the last section of the chapter (see Theorem 2.14).

In order to proof unique solvability of the nonlinear problem and in view of the convergence result in the next section, the regularity with respect to x has to be increased. Following [50], we introduce the following Hölder spaces

$$\begin{aligned} \tilde{\mathcal{V}} := \{v \in C^{1,\gamma}(\bar{\Omega}; \mathcal{W}) \mid & \operatorname{div}_x \int_{Y_f} v(x, y) dy = 0 \text{ in } \Omega, \\ & \nu(x) \cdot \int_{Y_f} v(x, y) dy \text{ is } \Gamma_1 \text{-antiperiodic,} \\ & \nu(x) \cdot \int_{Y_f} v(x, y) dy = 0 \text{ on } \Gamma_2\}, \end{aligned}$$

$$\tilde{\mathcal{Q}}^0 := \{q \in C^{2,\gamma}(\bar{\Omega}) \mid q \text{ is } \Gamma_1 \text{-periodic, } \int_{\Omega} q(x) dx = 0\}$$

and

$$\tilde{\mathcal{Q}}^1 := \{q \in C^{1,\gamma}(\bar{\Omega}; \mathcal{R}) \mid q \text{ is } \Gamma_1\text{-periodic}\}.$$

Additionally, we assume $\partial\Omega$ to be of class $C^{2,\gamma}$. The definition of the regularity of the boundaries goes along the same construction as given for Lipschitz continuous boundaries in Chapter 1 with adapted regularity of the functions a_i . Now, we have

Theorem 2.6. *There exists a neighborhood $\mathcal{N} \subset C^{1,\gamma}(\bar{\Omega})^n$ of zero, such that the problem (2.10), (2.11) is uniquely solvable with $(u_0, p_0, p_1) \in \tilde{\mathcal{V}} \times \tilde{\mathcal{Q}}^0 \times \tilde{\mathcal{Q}}^1$ for all $f \in \mathcal{N}$.*

Proof: We will only point out the ideas of the proof. In [50] the implicit function theorem (see [77]) is used to prove the assertion. Therefore, a function $G : \tilde{\mathcal{V}} \times \tilde{\mathcal{Q}}^0 \times \tilde{\mathcal{Q}}^1 \times C^{1,\gamma}(\bar{\Omega})^n \rightarrow C^{1,\gamma}(\bar{\Omega}, \mathcal{W}')$ is defined by

$$\begin{aligned} G(v, q_1, q_0, g) := & -\mu \Delta_y v(x, y) + (v(x, y) \cdot \nabla_y) v(x, y) \\ & + \nabla_y q_1(x, y) + \nabla_x q_0(x) - g(x). \end{aligned}$$

Here, \mathcal{W}' denotes the dual space of \mathcal{W} . Now, they show that G is continuously differentiable at $(0, 0, 0, 0)$ and that its partial Fréchet derivative with respect to (v, q_1, q_0) is invertible. The latter claim leads to the question of unique solvability of a problem quite similar to the Stokes system with two pressures, but with higher regularity. It can be answered in complete analogy like in the proof of Theorem 2.4. ■

2.4. Convergence of the homogenization process

In this section we will prove a convergence result which shows how the solution of the homogenized system (2.10), (2.11) approximates the solution of the Navier-Stokes system (2.6). In [50] the cases of periodic and impervious boundaries are considered separately. Due to our setup where both types of boundaries may appear, we have to follow the arguments of the impervious case. Only minor formal changes are necessary due to the presence of Γ_1 . The convergence result is restricted to the case $n = 2$. Additionally, more regularity is needed. Therefore, we suppose that $\partial\Omega$ is of class C^4 and ∂Y_s is of class C^2 . By defining

$$\begin{aligned} \tilde{\mathcal{V}} := \{v \in C^{2,\gamma}(\bar{\Omega}; C_{\text{per}}^{2,\gamma}(Y_f)^2) \mid & \operatorname{div}_x \int_{Y_f} v(x, y) dy = 0 \text{ in } \Omega, \\ & \nu(x) \cdot \int_{Y_f} v(x, y) dy \text{ is } \Gamma_1 \text{-antiperiodic,} \\ & \nu(x) \cdot \int_{Y_f} v(x, y) dy = 0 \text{ on } \Gamma_2\}, \end{aligned}$$

$$\tilde{\mathcal{Q}}^0 := \{q \in C^{3,\gamma}(\bar{\Omega}) \mid q \text{ is } \Gamma_1 \text{-periodic, } \int_{\Omega} q(x) dx = 0\}$$

and

$$\begin{aligned} \tilde{\mathcal{Q}}^1 := \{q \in C^{2,\gamma}(\bar{\Omega}; C_{\text{per}}^{1,\gamma}(Y_f)) \mid & q \text{ is } \Gamma_1\text{-periodic,} \\ & \int_{Y_f} q(x, y) dy = 0, \quad \forall x \in \Omega\}, \end{aligned}$$

we have the following variant of Theorem 2.6:

Theorem 2.7. *There exists a neighborhood $\mathcal{N} \subset C^{2,\gamma}(\bar{\Omega})^2$ of zero, such that the problem (2.10), (2.11) is uniquely solvable with $(u_0, p_0, p_1) \in \tilde{\mathcal{V}} \times \tilde{\mathcal{Q}}^0 \times \tilde{\mathcal{Q}}^1$ for all $f \in \mathcal{N}$.*

Proof: To prove the theorem, one can copy the proof of Theorem 2.6 and replace the corresponding function spaces. ■

REMARK 2.8. The subscript *per* in the definition of the function spaces $\tilde{\mathcal{V}}$, $\tilde{\mathcal{Q}}^0$ and $\tilde{\mathcal{Q}}^1$ indicates full periodic boundary conditions on ∂Y .

Setting

$$u_0^\varepsilon(x) := u_0(x, \frac{x}{\varepsilon}) \quad \text{and} \quad p_1^\varepsilon(x) := p_1(x, \frac{x}{\varepsilon}),$$

we have

Theorem 2.9. *Let $f \in C^{2,\gamma}(\overline{\Omega})^2$. Then there exists a constant d , such that for $\|f\|_{C^{1,\gamma}(\overline{\Omega})^2} < d$ we have*

$$\|u^\varepsilon - u_0^\varepsilon\|_{L^2(\Omega)^2} \leq C\varepsilon^l, \quad 0 < l < \frac{1}{6}.$$

Furthermore, there exists an extension $\tilde{\Pi}^\varepsilon$ of $\Pi^\varepsilon := \varepsilon p^\varepsilon - p_0 - \varepsilon p_1^\varepsilon$ and

$$\|\tilde{\Pi}^\varepsilon\|_{L_0^q(\Omega)} \leq C\varepsilon^l, \quad 0 < l < \frac{1}{6}, \quad \forall q \in]1, 2[.$$

Proof: The proof is very technical and can be found in detail in [50]. Nevertheless, we repeat the essential ideas.

The observation, that u_0^ε does not vanish on Γ_2 makes the construction of a suitable boundary layer necessary. According to [51], there exists $\delta_0 > 0$ and a function $s^\delta \in C^3(\overline{\Omega})^2$, $0 < \delta \leq \delta_0$ fulfilling

$$\begin{aligned} \operatorname{div} s^\delta &= 0 && \text{in } \Omega, \\ s^\delta(x) &= \int_{Y_f} u_0(x, y) dy && \text{on } \Gamma_2, \\ \|D^m s^\delta\|_{L^q(\Omega)} &\leq C\delta^{\frac{1}{q}-|m|}, && |m| \leq 3, \quad q \in [1, \infty[, \end{aligned}$$

where m is a multi-index.

Let $\alpha \in \mathbb{R}^2$ be the right hand side of the micro problem (2.10). The corresponding velocity and pressure solutions are denoted by $w(\alpha)$ and $\pi(\alpha)$, respectively. The permeability function $\mathcal{F} : \mathbb{R}^2 \rightarrow \mathbb{R}^2$ is defined by

$$(2.16) \quad \mathcal{F}(\alpha) := \int_{Y_f} w(\alpha) dy.$$

Taking the microscopic mean value of u_0 yields the averaged velocity \bar{u}_0 , i.e.

$$(2.17) \quad \bar{u}_0(x) := \int_{Y_f} u_0(x, y) dy.$$

Now, by choosing f small enough, i.e. $\|f\|_{C^{1,\gamma}(\overline{\Omega})^2} < d$, the following definitions are well-posed:

$$\begin{aligned} (2.18) \quad v^\delta(x, y) &:= w(\mathcal{F}^{-1}(\mathcal{F}(f(x) - \nabla_x p_0(x)) - s^\delta(x)))(y) \\ &= w(\mathcal{F}^{-1}(\bar{u}_0(x) - s^\delta(x)))(y), \\ q^\delta(x, y) &:= \pi(\mathcal{F}^{-1}(\mathcal{F}(f(x) - \nabla_x p_0(x)) - s^\delta(x)))(y) \\ &= \pi(\mathcal{F}^{-1}(\bar{u}_0(x) - s^\delta(x)))(y). \end{aligned}$$

For details on the constant d , we refer to [50], where d is computed explicitly. Clearly, the computations involve bounds on ∇p_0 in terms of an appropriate norm of f .

The second observation is the fact, that $\operatorname{div} v^\delta(x, \frac{x}{\varepsilon}) = \operatorname{div}_x v^\delta(x, \frac{x}{\varepsilon}) \neq 0$. Therefore, a divergence corrector is found by considering the following problem, which has at least one solution:

$$\begin{aligned} \text{Find } Q^\delta \in C^2(\Omega; C_{\text{per}}^2(Y_f))^2, \quad & \text{such that} \\ \operatorname{div}_y Q^\delta = -\operatorname{div}_x v^\delta \quad & \text{in } \overline{\Omega} \times Y_f, \\ Q^\delta = 0 \quad & \text{on } \overline{\Omega} \times \partial Y_s. \end{aligned}$$

Since Q^δ does not vanish on $\partial\Omega$, a cut-off function $\xi^\delta \in C^2(\overline{\Omega})$ has to be used with $\xi^\delta = 1$ on $\partial\Omega$. Its support is restricted to points, whose distance to $\partial\Omega$ is less than ε , and, for $0 \leq |m| \leq 2$, its m th order derivatives are of order $O(\varepsilon^{-|m|})$. Now, we set

$$(2.19) \quad v^{\delta, \varepsilon}(x) := \begin{cases} v^\delta(x, \frac{x}{\varepsilon}), & \text{if } x \in \Omega^\varepsilon, \\ 0, & \text{if } x \in \Omega \setminus \Omega^\varepsilon \end{cases}$$

and

$$(2.20) \quad Q^{\delta, \varepsilon}(x) := \begin{cases} \varepsilon Q^\delta(x, \frac{x}{\varepsilon}), & \text{if } x \in \Omega^\varepsilon, \\ 0, & \text{if } x \in \Omega \setminus \Omega^\varepsilon. \end{cases}$$

Observe, that in view of a convergence results in $L^2(\Omega)^2$ the definitions (2.19), (2.20) include an zero extension to Ω . In the same way, u^ε is extended without change in notation. The extension of the pressures p_ε and q^δ is more complicated and we refer to [53].

We define the differences

$$(2.21) \quad \begin{aligned} w^\varepsilon(x) &:= u^\varepsilon(x) - (v^{\delta, \varepsilon}(x) + (1 - \xi^\varepsilon(x))Q^{\delta, \varepsilon}(x)), \\ \tilde{\Pi}^\varepsilon(x) &:= \varepsilon p^\varepsilon(x) - (p_0(x) + \varepsilon q^\delta(x, \frac{x}{\varepsilon})), \end{aligned}$$

where the pressures are extended to Ω without change in notation. Then, plugging (2.21) in (2.6), yields

$$(2.22) \quad -\mu\varepsilon^2 \Delta w^\varepsilon + \nabla \tilde{\Pi}^\varepsilon + \varepsilon(u^\varepsilon \cdot \nabla)w^\varepsilon + \varepsilon(w^\varepsilon \cdot \nabla)v^{\delta, \varepsilon} = \Psi^{\delta, \varepsilon},$$

where $\Psi^{\delta, \varepsilon}$ collects all terms which are not explicitly written in (2.22). When w^ε is taken as a test function in (2.22), various estimates on the appearing functions and their derivatives, a divergence estimate of the approximating velocity $v^{\delta, \varepsilon}(x) + (1 - \xi^\varepsilon(x))Q^{\delta, \varepsilon}(x)$ and a bound on the pressure extension $\tilde{\Pi}^\varepsilon$ give the assertion of the theorem. \blacksquare

REMARK 2.10. In [50] an alternative convergence result is stated for the case when $\Gamma_2 = \emptyset$. Due to the absence of boundary layers, convergence is improved to the order of ε .

2.5. Extension of Darcy's law

We repeat the well-known equivalence of the Stokes system with two pressures (2.12), (2.13) and Darcy's law. Based on this result, we explain the nonlinear extension of Darcy's law by the Navier-Stokes system with two pressures.

2.5.1. Derivation of Darcy's law from the Stokes system with two pressures. The first auxiliary step in the derivation of Darcy's law is the formulation of Stokes problems on the periodicity cell. The canonical basis vectors in \mathbb{R}^n are used as right hand sides of the Stokes equations. Hence, the i th cell problem is defined by

$$(2.23) \quad \begin{aligned} -\Delta_y w_i + \nabla_y \pi_i &= e_i && \text{in } Y_f, \\ \operatorname{div}_y w_i &= 0 && \text{in } Y_f, \\ w_i &= 0 && \text{on } \partial Y_s, \\ \{w_i, \pi_i\} &&& \text{is } Y\text{-periodic.} \end{aligned}$$

The variational formulation of (2.23) reads

$$(2.24) \quad \begin{aligned} &\text{Find } w_i \in \mathcal{W}, \text{ such that} \\ \int_{Y_f} \nabla_y w_i : \nabla_y v \, dy &= \int_{Y_f} e_i \cdot v \, dy, \quad \forall v \in \mathcal{W}. \end{aligned}$$

Clearly, (2.23) (resp. (2.24)) has unique solutions $(w_i, \pi_i) \in \mathcal{W} \times \mathcal{R}$. Due to linearity with respect to the right hand side, the micro problem (2.12) of the Stokes system with two pressures can be rewritten as

$$(2.25) \quad u_0(x, y) = \frac{1}{\mu} \sum_{i=1}^n w_i(y) \left(f_i(x) - \frac{\partial p_0(x)}{\partial x_i} \right),$$

where the microscopic pressure p_1 has been eliminated. Observe, that due to the definition of w_i the continuity equation with respect to y and the microscopic boundary conditions are fulfilled by u_0 . Taking the mean in (2.25) and using the notation (2.17), we obtain the well-known linear relationship of the macroscopic velocity and the difference of outer forces and the pressure:

$$(2.26) \quad \bar{u}_0(x) = \frac{\mathcal{K}}{\mu} \cdot (f(x) - \nabla_x p_0(x)),$$

where the permeability tensor \mathcal{K} is defined as

$$(2.27) \quad (\mathcal{K})_{ij} = k_{ij} = \int_{Y_f} w_{ji} dy,$$

where w_{ji} is the i -th component of w_j . Equation (2.26) expresses Darcy's law in differential form.

Definition 2.11. A matrix $A \in \mathbb{R}^{n \times n}$ is called positive, if $x^T \cdot A \cdot x \geq 0$, $\forall x \in \mathbb{R}^n$. If, additionally, the equivalence $x^T \cdot A \cdot x = 0 \Leftrightarrow x = 0$ holds, A is called positive definite.

In the subsequent chapters, we will need the following classical property of the permeability tensor.

Lemma 2.12. \mathcal{K} is symmetric and positive definite.

Proof: Following [65], symmetry of \mathcal{K} is shown by using the variational formulation (2.24) of the cell problems:

$$\begin{aligned} k_{ij} &= \int_{Y_f} w_{ji} dy = \int_{Y_f} w_j \cdot e_i dy = \int_{Y_f} \nabla_y w_j : \nabla_y w_i dy \\ &= \int_{Y_f} \nabla_y w_i : \nabla_y w_j dy = \int_{Y_f} w_i \cdot e_j dy = \int_{Y_f} w_{ij} = k_{ji}. \end{aligned}$$

Let $\alpha = (\alpha_1, \dots, \alpha_n)^T \in \mathbb{R}^n$. Then, \mathcal{K} is positive, since

$$\begin{aligned} \alpha \cdot \mathcal{K} \cdot \alpha^T &= \sum_{i,j=1}^n \alpha_i \alpha_j k_{ij} = \sum_{i,j=1}^n \alpha_i \alpha_j \int_{Y_f} w_j \cdot e_i dy \\ &= \sum_{i,j=1}^n \alpha_i \alpha_j \int_{Y_f} \nabla_y w_j : \nabla_y w_i dy = \left\| \sum_{i=1}^n \alpha_i w_i \right\|_{Y_f}^2 \geq 0. \end{aligned}$$

To complete the proof, it remains to show the equivalence

$$(2.28) \quad \sum_{i=1}^n \alpha_i w_i = 0 \quad \Leftrightarrow \quad \alpha_i = 0 \quad \forall i \in \{1, \dots, n\}.$$

Let's assume $\sum_{i=1}^n \alpha_i w_i = 0$. Since Y_f is Y -periodic and connected, we can construct test functions $v_i \in \mathcal{W}$, that fulfill

$$\int_{Y_f} v_i dy = \alpha_i e_i.$$

Using $\sum_{i=1}^n v_i$ as test function in the variational formulation of the cell problems, yields

$$\begin{aligned} 0 &= \int_{Y_f} (\nabla_y \sum_{i=1}^n \alpha_i w_i) : (\nabla_y \sum_{i=1}^n v_i) dy = \int_{Y_f} \sum_{i=1}^n \alpha_i e_i \cdot \sum_{i=1}^n v_i dy \\ &= \int_{Y_f} (\sum_{i=1}^n \alpha_i e_i)^2 dy = \sum_{i=1}^n \alpha_i^2. \end{aligned}$$

Therefore, we have $\alpha_i = 0$. The other inclusion of (2.28) is obvious. \blacksquare

REMARK 2.13. The construction of the test functions in the proof of Lemma 2.12 can be done by considering solutions of modified cell problems. For instance, let $i = 1$ and replace the periodic boundary conditions on the upper and lower boundaries of the periodicity cell by no-slip conditions. The solution of this problem is denoted by v_1^* . From a physical point of view, it is clear that the integral over the left boundary of the normal component of v_1^* is strictly positive, since the obstacle does not block the flow completely. Due to mass conservation, the integral over every cross section in y direction takes the same strictly positive value. By using similar arguments, one can conclude that the integrals over cross sections in x direction are zero. Therefore, we have $\int_{Y_f} v_1^* dy = \alpha_1^* e_1$. By scaling of v_1^* , we obtain the desired test function.

The properties of the permeability tensor \mathcal{K} can be employed to prove a result similar to Theorem 2.4. Let $\partial\Omega$ be Lipschitz continuous, then we have

Theorem 2.14. *The Stokes system with two pressures has a unique solution $(u_0, p_0, p_1) \in \mathcal{V} \times \mathcal{Q}^0 \times \mathcal{Q}^1$.*

Proof: Following [49], the macroscopic continuity equation and boundary conditions read in terms of the average velocity \bar{u}_0 :

$$(2.29) \quad \begin{aligned} \operatorname{div}_x \bar{u}_0(x) &= 0 && \text{in } \Omega, \\ \nu(x) \cdot \bar{u}_0(x) &&& \Gamma_1\text{-antiperiodic,} \\ \nu(x) \cdot \bar{u}_0(x) &= 0 && \text{on } \Gamma_2. \end{aligned}$$

Substituting (2.26) in (2.29), the averaged velocity is eliminated. Via (2.26), the impervious boundary conditions on \bar{u}_0 induce Neumann boundary conditions on the pressure p_0 on Γ_2 . Hence, we have the following linear elliptic

problem with constant coefficients:

$$(2.30) \quad \begin{aligned} -\operatorname{div}_x \left(\frac{\mathcal{K}}{\mu} \cdot \nabla_x p_0(x) \right) &= -\operatorname{div}_x \left(\frac{\mathcal{K}}{\mu} \cdot f(x) \right) && \text{in } \Omega, \\ p_0 &&& \text{is } \Gamma_1\text{-periodic,} \\ \nu(x) \cdot \left(\frac{\mathcal{K}}{\mu} \cdot \nabla_x p_0(x) \right) &= \nu(x) \cdot \left(\frac{\mathcal{K}}{\mu} \cdot f(x) \right) && \text{on } \Gamma_2 \end{aligned}$$

Clearly, (2.30) admits a unique solution in \mathcal{Q}^0 . The velocity $u_0 \in \mathcal{V}$ is given by formula (2.26). For the second pressure p_1 , there exists an analogous formula:

$$(2.31) \quad p_1(x, y) = \sum_{i=1}^n \pi_i(y) \left(f_i(x) - \frac{\partial p_0(x)}{\partial x_i} \right),$$

hence giving $p_1 \in \mathcal{Q}^1$. Uniqueness of u_0 and p_1 is induced by uniqueness of p_0 and uniqueness of the solutions of the cell problems. \blacksquare

REMARK 2.15. The analytic splitting of the Stokes system with two pressures into (2.23), (2.27) and (2.30) is possible due to linearity of the system. In the nonlinear case, where the convective term is still present on the micro scale, the situation is more complicated. In the next chapter, we will make use of the splitting into micro and macro problem to numerically solve the Navier-Stokes system with two pressures.

2.5.2. Connection of the Navier-Stokes system with two pressures and Darcy's law. In the previous section, it is shown that the Stokes system with two pressures is equivalent to Darcy's law. It is intuitively obvious, that for large viscosities the Stokes equations on the micro scale approximate the Navier-Stokes equations, since velocities become small and, therefore, the convective term becomes negligible. A mathematical proof for the (single pressure) Navier-Stokes problem is given in [30], where the difference of the Stokes and Navier-Stokes solution is bounded by C/μ for $\mu \rightarrow \infty$ and some constant C . This result is often referred to as *infinite viscosity limit of the Navier-Stokes equations*. Hence, it is reasonable to expect, that for large μ , the Navier-Stokes system with two pressures will approximately give Darcian-like flow. On the other hand, for decreasing μ , we expect deviations due to inertia.

In [50] and [55], these expectations are approved in a more general framework which starts from the scaling of the Navier-Stokes system on a periodic porous medium. Within this framework, the asymptotic behavior of the Reynolds number (2.5) used to derive the Navier-Stokes system with two pressures is

just a special case ($\gamma = 1$) of

$$Re_\varepsilon = \frac{1}{\mu} \varepsilon^{-\gamma},$$

where $0 \leq \gamma \leq 1$. In [65] and [2] the case $\gamma \ll 1$ is investigated. Due to the asymptotically low Reynolds number, they use the Stokes system instead of the Navier-Stokes system on the pore scale. Hence, the Stokes system with two pressures is obtained. Even if we keep the convective term, it is shown in [55], that the final result is Darcy's law when solely considering the leading order terms of the asymptotic expansions. By additionally taking into account the first lower order term, it is possible to derive a nonlinear extension of Darcy's law, whose nonlinearity becomes the more important the closer γ approaches 1. In the case $\gamma = 1$, one can derive a structurally similar law, which reads

$$(2.32) \quad \bar{u}_0 = \frac{\mathcal{K}}{\mu} (f - \nabla p_0) + \frac{1}{\mu^3} \sum_{i,j=1}^n T^{ij} \left(f_i - \frac{\partial p_0}{\partial x_i} \right) \left(f_j - \frac{\partial p_0}{\partial x_j} \right) + O(|f - \nabla p_0|^3).$$

We will repeat the derivation of (2.32) in the next chapter. The numerical results derived in Chapter 3 and 4 will confirm these theoretical results and will illustrate in detail how the Navier-Stokes system with two pressures extends Darcy's law.

CHAPTER 3

Numerical solution of the two pressure system by scale splitting

The aim of this chapter is to solve the Navier-Stokes system with two pressures numerically. In contrast to Chapter 4, where the system is solved as a whole, we want to make use of the splitting of (2.10), (2.11) into micro and macro problems.

Two ways of solving the micro problem are established. The theoretical background of the first approach is due to [50]. It is based on a Taylor expansion of the permeability function, which has already been introduced in Chapter 2. This approach requires the solution of a sequence of Stokes problems on the periodicity cell and, to the best of the author's knowledge, is numerically investigated for the first time. The second approach consists of the discrete computation of the permeability function by solving the Navier-Stokes system on the periodicity cell for several right hand sides. The discrete permeability function is then least-squares fitted in powers of $(f_i - \frac{\partial p_0}{\partial x_i})$, $i = 1, \dots, n$, giving the same structure of the permeability function as in the case of the Taylor expansion. The type of the macro problem depends on the properties of the permeability function. It is shown in [50], that for small f the macro problem is a quasilinear elliptic equation of second order for the pressure p_0 .

After having formulated the micro and macro problems in the first section of this chapter, the numerical solution algorithms are presented. We introduce a general augmented Lagrangian Uzawa conjugate gradient method due to [28], which can be applied to solve a certain class of saddle-point problems. Furthermore, we present a general least-squares conjugate gradient method due to [36]. It will serve as nonlinear solver. By means of these two basic solvers, we will derive discrete variants of our micro and macro problems: After discretizing the Stokes problems by finite elements, the Uzawa algorithm reduces the solution of the discrete Stokes systems to the solution of a sequence of linear elliptic equations of second order. The Navier-Stokes problems appearing during the discrete computation of the permeability function will first be linearized by the least-squares conjugate gradient method. Thereby, one obtains a sequence of Stokes problems to which the Uzawa method is again applied. Linearization of the quasilinear macro equations by the least-squares algorithm

yields a sequence of linear elliptic problems of second order. All equations are discretized in two dimensions by finite element methods.

An extensive numerical study of the Navier-Stokes system with two pressures closes this chapter. The numerical study focuses on geometric variations of the periodicity cell and the macro domain Ω . Moreover, variations of the viscosity μ as control parameter of inertia are performed. The study illustrates how inertia effects act on the micro scale and macro scale and how the filtration laws gradually deviate from Darcy's law when inertia becomes more and more important. Thereby, it can easily be observed, that the well-known Forchheimer law is in general not able to approximate the complex filtration laws obtained by the Navier-Stokes system with two pressures.

3.1. Micro and macro problems

The Navier-Stokes system with two pressures comprises a set of partial differential equations and appropriate boundary conditions. The equations related to the micro scale are grouped in (2.10) and form a Navier-Stokes system on the periodicity cell with periodic and no-slip boundary conditions on the outer boundary and on the boundary of the obstacle, respectively. It reads

$$(3.1) \quad \begin{aligned} -\mu \Delta_y w(\alpha) + (w(\alpha) \cdot \nabla_y) w(\alpha) + \nabla_y \pi(\alpha) &= \alpha && \text{in } Y_f, \\ \operatorname{div}_y w(\alpha) &= 0 && \text{in } Y_f, \\ w(\alpha) &= 0 && \text{on } \partial Y_s, \\ \{w(\alpha), \pi(\alpha)\} &&& \text{is } Y\text{-periodic,} \end{aligned}$$

where $w(\alpha)$, $\pi(\alpha)$ and $\alpha = (\alpha_1, \dots, \alpha_n)^T \in \mathbb{R}^n$ replace u_0 , p_1 and $f - \nabla p_0$, respectively, in (2.10). The variational formulation of (3.1) reads

$$(3.2) \quad \begin{aligned} &\text{Find } w(\alpha) \in \mathcal{W}, \text{ such that} \\ \mu \int_{Y_f} \nabla_y w(\alpha) : \nabla_y v \, dy + \int_{Y_f} (w(\alpha) \cdot \nabla_y) w(\alpha) \cdot v \, dy \\ &= \int_{Y_f} \alpha \cdot v \, dy, \quad \forall v \in \mathcal{W}. \end{aligned}$$

The macroscopic mass balance equation and corresponding boundary conditions are grouped in (2.11). In the Proof of Theorem 2.9, we introduced the permeability function $\mathcal{F} : \alpha \mapsto \mathcal{F}(\alpha) := \int_{Y_f} w(\alpha) \, dy$. Clearly, it is only well-defined, if the corresponding Navier-Stokes system admits a unique solution, i.e. when α is small. To fix ideas, let $\alpha \in \mathcal{N}_0$, where $\mathcal{N}_0 \in \mathbb{R}^n$ is a sufficiently small neighborhood of zero. The existence of \mathcal{N}_0 is guaranteed by classical uniqueness results for the Navier-Stokes system, where smallness of the right hand side assures controllability of the convective term by the viscous term

(see Chapter 2 and references therein). In [50], \mathcal{N}_0 is explicitly computed. Now, by means of the permeability function (2.11) can be rewritten as

$$(3.3) \quad \begin{aligned} \operatorname{div}_x \mathcal{F}(f - \nabla_x p_0) &= 0 && \text{in } \Omega, \\ p_0 & && \text{is } \Gamma_1\text{-periodic,} \\ \nu(x) \cdot \mathcal{F}(f - \nabla_x p_0) &= 0 && \text{on } \Gamma_2. \end{aligned}$$

The type of problem (3.3) depends on the properties of the permeability function \mathcal{F} . In [50], a detailed analysis is developed. We will shortly summarize the main ideas and results.

By formally taking the derivatives with respect to α in (3.1), the following system of partial differential equations is obtained:

$$(3.4) \quad \begin{aligned} -\mu \Delta_y \frac{\partial w(\alpha)}{\partial \alpha_j} + \left(\frac{\partial w(\alpha)}{\partial \alpha_j} \cdot \nabla_y \right) w(\alpha) \\ + (w(\alpha) \cdot \nabla_y) \frac{\partial w(\alpha)}{\partial \alpha_j} + \nabla_y \frac{\partial \pi(\alpha)}{\partial \alpha_j} &= e_j && \text{in } Y_f \\ \operatorname{div}_y \frac{\partial w(\alpha)}{\partial \alpha_j} &= 0 && \text{in } Y_f, \\ \frac{\partial w(\alpha)}{\partial \alpha_j} &= 0 && \text{on } \partial Y_s, \\ \left\{ \frac{\partial w(\alpha)}{\partial \alpha_j}, \frac{\partial \pi(\alpha)}{\partial \alpha_j} \right\} & && \text{is } Y\text{-periodic.} \end{aligned}$$

We remark, that letting $\alpha = 0$ in (3.4) and since $w(0) = 0$, leads to slightly modified linear cell problems (2.23) which are known from the homogenization process in the linear case. The difference comes only from the viscosity μ . More explicitly, setting $w_j := \frac{\partial w(0)}{\partial \alpha_j}$ and $\pi_j := \frac{\partial \pi(0)}{\partial \alpha_j}$, we find

$$(3.5) \quad \begin{aligned} -\mu \Delta_y w_j + \nabla_y \pi_j &= e_j && \text{in } Y_f, \\ \operatorname{div} w_j &= 0 && \text{in } Y_f, \\ w_j &= 0 && \text{on } \partial Y_s, \\ \{w_j, \pi_j\} & && \text{is } Y\text{-periodic.} \end{aligned}$$

The positive and symmetric permeability tensor introduced in the previous chapter in the context of Darcy's law is then given by

$$(3.5) \quad \frac{1}{\mu} (\mathcal{K})_{ij} = \frac{1}{\mu} k_{ij} = \int_{Y_f} w_{ji} dy = \int_{Y_f} \frac{\partial w(0)}{\partial \alpha_j} dy = \frac{\partial \mathcal{F}_i(0)}{\partial \alpha_j}.$$

In (3.5), the permeability tensor does not include the viscosity of the fluid, reflecting the fact, that we think of permeability as being an intrinsic property

of the porous medium and that permeability does not include fluid properties. Now, we summarize essential properties of the permeability function.

Lemma 3.1. *There exists a neighborhood \mathcal{N}_1 of zero fulfilling the inclusion $\overline{\mathcal{N}}_1 \subset \mathcal{N}_0 \subset \mathbb{R}^n$ and constants $C_1, C_2 > 0$, such that*

$$(3.6) \quad (\mathcal{F}(\alpha) - \mathcal{F}(\beta)) \cdot (\alpha - \beta) > 0, \quad \alpha \neq \beta, \quad \forall \alpha, \beta \in \mathcal{N}_0,$$

$$(3.7) \quad \mathcal{F} \in C^1(\mathcal{N}_0)^n$$

and

$$(3.8) \quad C_1 \|\xi\|^2 \leq \sum_{i,j=1}^n \xi_i \xi_j \frac{\partial \mathcal{F}_i(\alpha)}{\partial \alpha_j} \leq C_2 \|\xi\|^2, \quad \forall \alpha \in \overline{\mathcal{N}}_1, \quad \forall \xi \in \mathbb{R}^n.$$

Proof: For details, we refer to [50]. The idea to prove monotonicity is as follows. Considering the variational formulations of (3.1) for $\alpha, \beta \in \mathcal{N}_0$ and using $w(\alpha) - w(\beta)$ as test function, leads to

$$(3.9) \quad (\mathcal{F}(\alpha) - \mathcal{F}(\beta)) \cdot (\alpha - \beta) = \mu \int_{Y_f} |\nabla_y (w(\alpha) - w(\beta))|^2 dy \\ + \int_{Y_f} ((w(\alpha) - w(\beta)) \cdot \nabla_y) w(\beta) \cdot (w(\alpha) - w(\beta)) dy.$$

Controlling the convective term in (3.9) by the viscous term, requires the same restrictions to the left hand side as used to get unique solvability. Therefore, we have (3.6).

Continuous differentiability (3.7) is due to the above considerations in combination with continuity properties of the linear, bilinear and trilinear forms appearing in the variational formulation of the Navier-Stokes systems (3.1) and (3.4).

To prove the upper bound in (3.8), $\xi_i \xi_j \frac{\partial w(\alpha)}{\partial \alpha_i}$ is used as test function in the variational formulation of (3.4). Again, bounding the convective term and using Sobolev embedding theory, yields the results. To obtain the lower bound, the permeability tensor \mathcal{K} is employed. Due to its positive definiteness and since $\frac{\partial \mathcal{F}_i(0)}{\partial \alpha_j} = \frac{1}{\mu} k_{ij}$, it is possible to extend the positive definiteness of \mathcal{K} to a neighborhood $\mathcal{N}_1 \subset \mathcal{N}_0$ of zero. \blacksquare

To be able to apply standard theory for quasilinear partial differential equations of second order, \mathcal{F} has to be extended in an appropriate way, such that (3.8) holds for all $\alpha \in \mathbb{R}^n$.

Lemma 3.2. *There exists a neighborhood $\mathcal{N}_2 \subset \mathcal{N}_1$ of zero, an extension $\tilde{\mathcal{F}} : \mathbb{R}^n \rightarrow \mathbb{R}^n$ of the permeability function \mathcal{F} and constants $\tilde{C}_0, \tilde{C}_1, \tilde{C}_2 > 0$,*

such that

$$(3.10) \quad \tilde{\mathcal{F}} \in C^1(\mathbb{R}^n)^n,$$

$$(3.11) \quad \|\tilde{\mathcal{F}}(\alpha)\| \leq \tilde{C}_0 \|\alpha\|, \quad \forall \alpha \in \mathbb{R}^n,$$

$$(3.12) \quad \tilde{C}_1 \|\xi\|^2 \leq \sum_{i,j=1}^n \xi_i \xi_j \frac{\partial \tilde{\mathcal{F}}_i(\alpha)}{\partial \alpha_j} \leq \tilde{C}_2 \|\xi\|^2, \quad \forall \alpha, \xi \in \mathbb{R}^n$$

and

$$(3.13) \quad \tilde{\mathcal{F}}(\alpha) = \mathcal{F}(\alpha), \quad \forall \alpha \in \mathcal{N}_2.$$

Proof: The main ideas to prove the Lemma go along the following lines. In [50], the neighborhoods \mathcal{N}_0 and \mathcal{N}_1 , which insure well-posedness and ellipticity of \mathcal{F} , respectively, are explicitly computed as balls around zero with certain radii

$$(3.14) \quad \sigma_0 = \mu \frac{(1 - |Y_f|)^3}{C(n)|Y_f|^{1/2}} \quad \text{and} \quad \sigma_1 = \frac{\lambda_1(\mathcal{K})\sigma_0}{\lambda_1(\mathcal{K}) + 2\tilde{C}_0},$$

respectively. In (3.14), $\lambda_1(\mathcal{K})$ denotes the smallest eigenvalue of the permeability tensor (3.5). Let ω_n be the volume of the unit ball in \mathbb{R}^n , then the constants in (3.14) are defined by

$$\tilde{C}_0 := \frac{|Y_f|}{(1 - |Y_f|)^2} n^n \omega_n^{2-2/n}$$

and

$$C(n) := n^{3n/2-2} \omega_n^{3-3/n} (3n/(4-n))^{3/2}.$$

Set

$$(3.15) \quad \sigma_2 = \frac{\lambda_1(\mathcal{K})\sigma_0}{\lambda_1(\mathcal{K}) + 6\tilde{C}_0}$$

and choose $\sigma \in \mathbb{R}$, such that $0 < \sigma < \sigma_2 (< \sigma_1 < \sigma_0)$. In [50], the authors define a positive and monotonely decreasing function Ψ by

$$\Psi(t) := \begin{cases} 1, & t < 1, \\ 1 - \frac{2(t-1)^2\sigma^2}{(\sigma_0-\sigma)^2}, & 1 \leq t < \frac{\sigma_0+\sigma}{2\sigma}, \\ 1 - \frac{2(t-1)\sigma(\sigma_0-\sigma t)}{(\sigma_0-\sigma)^2} - \frac{2t\sigma-\sigma_0-\sigma}{\sigma_0-\sigma}, & \frac{\sigma_0+\sigma}{2\sigma} \leq t < \frac{\sigma_0}{\sigma}, \\ 0, & t \geq \frac{\sigma_0}{\sigma}. \end{cases}$$

Ψ is continuously differentiable on \mathbb{R}^+ . Then, the extension of \mathcal{F} is defined by

$$\tilde{\mathcal{F}}(\alpha) := \Psi\left(\frac{\|\alpha\|^2}{\sigma^2}\right)\mathcal{F}(\alpha) + \tilde{C}_0\left(1 - \Psi\left(\frac{\|\alpha\|^2}{\sigma^2}\right)\right)\alpha.$$

By means of the extension and the above defined constants, the properties (3.10) - (3.13) follow. \blacksquare

Now, we are able to state two theorems on unique solvability of the macro problem.

Theorem 3.3. *Let $\partial\Omega$ be of class $C^{2,\gamma}$. Then, there exists a neighborhood $\mathcal{N} \subset C^{1,\gamma}(\bar{\Omega})^n$ of zero, such that the problem (3.3) is uniquely solvable with $p_0 \in \tilde{\mathcal{Q}}^0$ for all $f \in \mathcal{N}$.*

Proof: Using Lemma 3.2, the proof follows for the extension $\tilde{\mathcal{F}}$ from results of the book by Ladyženskaja and Ural'ceva ([47]). By choosing f sufficiently small, $\|f - \nabla_x p_0\|_{C^{1,\gamma}(\bar{\Omega})^n} < \sigma_2$ can be achieved, and, therefore, problem (3.3) is solved due to (3.13). ■

REMARK 3.4. Note, that Theorem 3.3 is the basis of an alternative way to prove solvability of the Navier-Stokes system with two pressures. Once the macroscopic pressure p_0 is known, the unique existence of $(u_0, p_1) \in \tilde{\mathcal{V}} \times \tilde{\mathcal{Q}}^1$ is immediate.

In view of the numerical solution of the macro problem, we formulate

Theorem 3.5. *Let $\partial\Omega$ be Lipschitz continuous and $f \in H^1(\Omega)^n$. Then, problem (3.3) with \mathcal{F} being substituted by $\tilde{\mathcal{F}}$ is uniquely solvable with $p_0 \in \mathcal{Q}^0$.*

Proof: See [78] for example. ■

REMARK 3.6. Clearly, after having computed solutions of the modified equation of Theorem 3.5, one will have to check a posteriori, whether the solution stays in the *range* of \mathcal{F} or not.

Theoretical considerations of properties of the permeability function give solvability of the macro problem. Nevertheless, to solve the macro problem numerically, one has to compute \mathcal{F} . In [50], it is shown, that the permeability function can be expanded in a Taylor series around zero. Therefore, the differential calculus from above is extended. Let m be a multi-index. Then, derivatives of the Navier-Stokes system with respect to the right hand side α

are defined by

$$(3.16) \quad -\mu \Delta_y (D_\alpha^m w(\alpha)) + \nabla_y (D_\alpha^m \pi(\alpha)) = \delta(m) \\ - \sum_{j=0}^m \binom{m}{j} ((D_\alpha^m w(\alpha)) \cdot \nabla_y) D_\alpha^{m-j} w(\alpha) \quad \text{in } Y_f, \\ \operatorname{div}_y (D_\alpha^m w(\alpha)) = 0 \quad \text{in } Y_f, \\ D_\alpha^m w(\alpha) = 0 \quad \text{on } \partial Y_s, \\ \{D_\alpha^m w(\alpha), D_\alpha^m \pi(\alpha)\} \quad \text{is } Y\text{-periodic,}$$

where the Kronecker-like symbol δ is given by

$$\delta(m) := \begin{cases} \alpha, & \text{if } |m| = 0, \\ e_{m_i}, & \text{if } |m| = 1 \text{ and } m_i = 1, \\ 0, & \text{else.} \end{cases}$$

Setting

$$(3.17) \quad D_\alpha^m \mathcal{F}(\alpha) = \int_{Y_f} D_\alpha^m w(\alpha) dy,$$

we can formulate a theorem on the Taylor expandability of the permeability function \mathcal{F} . It reads

Theorem 3.7. *There exists a neighborhood $\mathcal{N}_3 \subset \mathcal{N}_0$ of zero, such that*

$$(3.18) \quad \mathcal{F}(\alpha) = \sum_{m \in \mathbb{N}^n} \frac{1}{m!} (D_\alpha^m \mathcal{F})(0) \alpha^m, \quad \forall \alpha \in \mathcal{N}_2,$$

i.e. \mathcal{F} is real analytic and coincides with its Taylor expansion in \mathcal{N}_2 .

Proof: In [50], bounds on $\|D_\alpha^m \mathcal{F}(\alpha)\|$ are established by an induction proof. The root test yields the radius of convergence of the Taylor series to be

$$\sigma_3 = \sigma_0 (2 \cdot 3^n + \mu - 4 - 2\sqrt{(3^n - 2) \cdot (3^n + \mu - 2)}).$$

■

REMARK 3.8. The Taylor coefficients $D_\alpha^m \mathcal{F}(0)$ can be computed recursively for $|m| = 0, 1, 2, \dots$ by linear Stokes problems. This is due to $\alpha = 0$ and $w(0) = 0$. In this case, the right hand side of the momentum balance equation in (3.16) depends only on previously calculated solutions $D_\alpha^j w(0)$, $|j| < |m|$.

Besides the computation of \mathcal{F} in terms of its Taylor expansion, one can directly solve (3.1) for various right hand sides α . This second approach leads to

a discrete description of the permeability function. We will make use of this possibility by discretizing the right hand side in a ball around zero as illustrated by Figure 1. Knowing the permeability function discretely, a least-squares fit in powers of $(f_i - \frac{\partial p_0}{\partial x_i})$ is performed, giving the same structure of \mathcal{F} as in the case of the Taylor expansion. This polynomial structure might be interesting by itself. This is due to the fact, that many publications on nonlinear extensions of Darcy's law try to find the *correct* power coming next to the linear term. Nevertheless, in view of an accurate description of \mathcal{F} when solving the macro problem, some kind of interpolation may be better. We will come back to this point in Section 3.2.4.

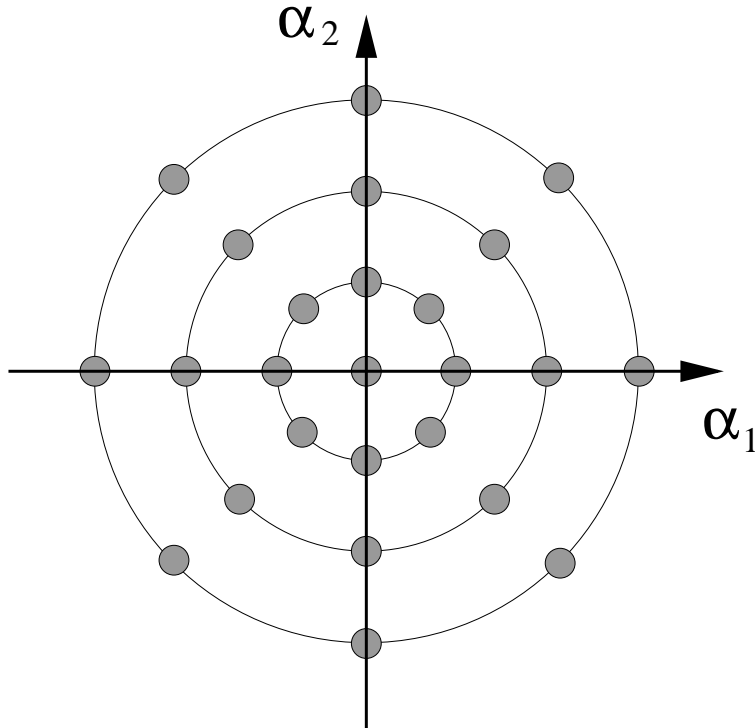


FIGURE 1. Discretization of the permeability function

3.2. Numerical solution algorithms

3.2.1. An augmented Lagrangian Uzawa conjugate gradient method. In view of solving the Stokes problems on the periodicity cell, we present a variant of Uzawa's algorithm. It is studied in full detail in [28] and, therefore, we only give the basic ideas. Many of the following statements are considered in a more general framework in [16].

Let $n, m \in \mathbb{N}$ and $A \in \mathbb{R}^{n \times n}$ be a symmetric and positive definite matrix,

$B \in \mathbb{R}^{n \times m}$ and $b \in \mathbb{R}^n$. Then, we define a quadratic functional $J : \mathbb{R}^n \rightarrow \mathbb{R}$ by

$$(3.19) \quad J(v) := \frac{1}{2}(Av, v) - (b, v), \quad v \in \mathbb{R}^n.$$

By means of (3.19), we formulate the following well-posed equality constrained minimization problem:

$$(3.20) \quad \begin{aligned} &\text{Find } u \in \mathbb{R}^n, \text{ such that} \\ &J(u) \leq J(v), \quad \forall v \in \text{Ker } B = \{v \in \mathbb{R}^n \mid Bv = 0\}, \\ &Bu = 0. \end{aligned}$$

By introducing a Lagrange multiplier $p \in \mathbb{R}^m$, the Lagrangian $\mathcal{L} : \mathbb{R}^n \times \mathbb{R}^m \rightarrow \mathbb{R}$ with respect to (3.20) reads

$$\mathcal{L}(v, q) := J(v) + (q, Bv).$$

$(u, p) \in \mathbb{R}^n \times \mathbb{R}^m$ is called a saddle-point of \mathcal{L} , if

$$\mathcal{L}(u, q) \leq \mathcal{L}(u, p) \leq \mathcal{L}(v, p), \quad \forall v \in \mathbb{R}^n, \forall q \in \mathbb{R}^m,$$

or, equivalently,

$$\text{Min}_{v \in \mathbb{R}^n} \text{Max}_{q \in \mathbb{R}^m} \mathcal{L}(v, q) = \mathcal{L}(u, p) = \text{Max}_{q \in \mathbb{R}^m} \text{Min}_{v \in \mathbb{R}^n} \mathcal{L}(v, q).$$

We summarize basic properties of saddle-points of \mathcal{L} and their connection to the minimization problem (3.20) in the following

Theorem 3.9. *\mathcal{L} has at least one saddle-point $(u, p) \in \mathbb{R}^n \times \mathbb{R}^m$, where u is the solution of (3.20) and common to all saddle-points of \mathcal{L} . Saddle-points of \mathcal{L} are characterized by the first order optimality conditions*

$$\begin{aligned} Au + B^T p &= b, \\ Bu &= 0. \end{aligned}$$

Interpreting B as a linear mapping from \mathbb{R}^n into \mathbb{R}^m , uniqueness of p is guaranteed by B being surjective.

Proof: See [28] and references therein. ■

First introduced by [41] and [60], the augmented Lagrangian \mathcal{L}_r , $0 < r \in \mathbb{R}$ is given by

$$(3.21) \quad \mathcal{L}_r(v, q) := J(v) + (q, Bv) + \frac{r}{2}\|Bv\|^2 = \mathcal{L}(v, q) + \frac{r}{2}\|Bv\|^2.$$

REMARK 3.10. Clearly, any saddle-point of \mathcal{L}_r is a saddle-point of \mathcal{L} and vice-versa. Adding the quadratic term $\frac{r}{2}\|Bv\|^2$ to the functional \mathcal{L} will improve convergence of the solution algorithm. Letting $q = 0$ in (3.21), we observe the

penalized functional with respect to the linear constraint $Bu = 0$. Nevertheless, the presence of the term (q, Bv) avoids making r tend to infinity to obtain the exact solution of (3.20). Hence, the condition number of the linear systems will not be deteriorated.

Now, we will consider Uzawa's algorithm ([5], [37]) to calculate a saddle-point of \mathcal{L}_r . The algorithm has the following iterative structure:

Step 0: Initialization

Let

$$(3.22) \quad p^0 \in \mathbb{R}^m$$

be given.

For $0 \leq j \in \mathbb{N}_0$, assuming p^j is known, compute $u^j \in \mathbb{R}^n$, p^{j+1} by

Step 1:

Solve

$$(3.23) \quad \begin{aligned} &\text{Find } u^j \in \mathbb{R}^n, \text{ such that} \\ &\mathcal{L}_r(u^j, p^j) \leq \mathcal{L}_r(v, p^j), \quad \forall v \in \mathbb{R}^n. \end{aligned}$$

Step 2:

Set

$$(3.24) \quad p^{j+1} = p^j + \rho^j B u^j, \quad 0 < \rho^j \in \mathbb{R}.$$

Set $j = j + 1$ and go to **Step 1**.

REMARK 3.11. Note, that (3.23) is equivalent to solving

$$(3.25) \quad (A + rB^T B)u^j + B^T p^j = b.$$

Uzawa's algorithm converges under the assumptions of the next theorem.

Theorem 3.12. *Let $0 < \alpha_0 \in \mathbb{R}$ and $\alpha_0 < 2r$. Then, for all $p^0 \in \mathbb{R}^m$ and $0 < \alpha_0 \leq \rho^j \leq 2r$ the sequence u^j converges to the solution of (3.20). Furthermore, p^j converges to $\hat{p} + \mathcal{P}_{\text{Ker } B^T}(p^0)$, where $\hat{p} \in \text{Im } B = \{q \in \mathbb{R}^m \mid \exists v \in \mathbb{R}^n, \text{ such that } Bv = q\}$ is uniquely determined and $\mathcal{P}_{\text{Ker } B^T}$ is the projector of \mathbb{R}^m onto $\text{Ker } B^T$.*

Proof: See [28]. ■

Now, setting $A_r := A + rB^T B$ and eliminating u^j , Uzawa's algorithm can be rewritten as

$$(3.26) \quad \begin{aligned} &\text{Let } p^0 \in \mathbb{R}^m \text{ be given. Compute for } 0 \leq j \in \mathbb{N}_0 \\ &p^{j+1} = p^j + \rho^j (BA_r^{-1} B^T p^j - BA_r^{-1} b). \end{aligned}$$

Introducing the (dual) functional $J_r^* : \mathbb{R}^m \rightarrow \mathbb{R}$ by

$$\begin{aligned} J_r^*(q) &:= -\operatorname{Min}_{v \in \mathbb{R}^n} \mathcal{L}_r(v, q) \\ &= \frac{1}{2}(BA_r^{-1}B^T q, q) - (BA_r^{-1}b, q) + \frac{1}{2}(A_r^{-1}b, b), \end{aligned}$$

we observe, that (3.26), hence (3.20), are in fact gradient type algorithms applied to the minimization of J_r^* . In [28] the *steepest descent method*, the *minimum residual method* and the *conjugate gradient method* are applied to the minimization process. Theoretical considerations and numerical experiments exhibit the conjugate gradient method to be the most efficient due to its second order convergence.

Before we formulate the conjugate gradient method, we perform some preliminary considerations. Using (3.25), the gradient g^j of the functional J_r^* is given by

$$\begin{aligned} g^j &= BA_r^{-1}B^T p^j - BA_r^{-1}b = BA_r^{-1}(B^T p^j - b) \\ &= -BA_r^{-1}A_r u^j = -Bu^j, \quad \forall j \in \mathbb{N}_0. \end{aligned}$$

In case of the conjugate gradient method, the descent directions w^j are chosen according to the following rules

$$\begin{aligned} (3.27) \quad w^0 &= g^0, \\ w^j &= g^j + \gamma^j w^{j-1}, \quad 0 < \gamma^j \in \mathbb{R}, \quad \text{such that} \\ &(BA_r^{-1}B^T w^j, w^{j-1}) = 0, \quad \forall j \in \mathbb{N}. \end{aligned}$$

Due to the the orthogonality condition in (3.27), γ^j is determined by

$$(3.28) \quad \gamma^j = -\frac{(BA_r^{-1}B^T g^j, w^{j-1})}{(BA_r^{-1}B^T w^{j-1}, w^{j-1})} = \frac{\|g^j\|^2}{\|g^{j-1}\|^2} = \frac{\|Bu^j\|^2}{\|Bu^{j-1}\|^2}.$$

In (3.28), the orthogonality relations

$$\begin{aligned} (3.29) \quad (BA_r^{-1}B^T w^i, w^j) &= 0, \quad i \neq j, \\ (g^i, g^j) &= 0, \quad i \neq j, \\ (g^i, w^j) &= 0, \quad i > j, \end{aligned}$$

are used, which are proved by induction in [59] or any other text book on conjugate gradient methods.

Now that the descent direction is known, ρ^j has to be computed as minimizer

of the functional J_r^* . More precisely,

$$(3.30) \quad \begin{aligned} \rho^j &= \underset{\rho \in \mathbb{R}_0^+}{\text{ArgMin}} J_r^*(p^j - \rho w^j) \\ &= \underset{\rho \in \mathbb{R}_0^+}{\text{ArgMin}} J_r^*(p^j) + \frac{1}{2} \rho^2 (BA_r^{-1} B^T w^j, w^j) - \rho(g^j, w^j). \end{aligned}$$

Neglecting the constant term in (3.30) and using (3.29), we obtain

$$(3.31) \quad \rho^j = \frac{(g^j, w^j)}{(BA_r^{-1} B^T w^j, w^j)} = \frac{\|g^j\|^2}{(g^j, BA_r^{-1} B^T w^j)}.$$

Introducing z^j as solution of the linear system $z^j = A_r^{-1} B^T w^j$, (3.31) reduces to

$$\rho^j = -\frac{\|g^j\|^2}{(Bw^j, Bz^j)}.$$

For u^{j+1} the following equality is immediate

$$A_r u^{j+1} = b - B^T p^{j+1} = b - B^T p^j + \rho^j B^T w^j = A_r u^j + \rho^j A_r z^j$$

and, therefore

$$u^{j+1} = u^j + \rho^j z^j.$$

Summarizing the considerations from above leads to the following conjugate gradient algorithm, which provides the solution of (3.26) and (3.20):

Step 0: Initialization

Let

$$(3.32) \quad p^0 \in \mathbb{R}^m$$

be given. Compute $u^0 \in \mathbb{R}^n$ as the solution of

$$(3.33) \quad A_r u^0 = b - B^T p^0$$

and set

$$(3.34) \quad g^0 = -Bu^0 \quad \text{and}$$

$$(3.35) \quad w^0 = g^0.$$

For $0 \leq j \in \mathbb{N}_0$, assuming that u^j, p^j, g^j, w^j are known, compute $u^{j+1}, p^{j+1}, g^{j+1}, w^{j+1}$ by

Step 1: Descent

Compute

$$(3.36) \quad A_r z^j = B^T w^j \quad \text{and}$$

$$(3.37) \quad \rho^j = -\frac{\|g^j\|^2}{(g^j, Bz^j)}.$$

Then, set

$$(3.38) \quad p^{j+1} = p^j - \rho^j w^j \quad \text{and}$$

$$(3.39) \quad u^{j+1} = u^j + \rho^j z^j.$$

Step 2: Construction of the new descent direction

Define $g^{j+1} \in \mathbb{R}^m$ as

$$(3.40) \quad g^{j+1} = -B u^{j+1}.$$

Compute γ^j by

$$(3.41) \quad \gamma^j = \frac{\|g^{j+1}\|^2}{\|g^j\|^2}$$

and set

$$(3.42) \quad w^{j+1} = g^{j+1} + \gamma^j w^j.$$

Set $j = j + 1$ and go to **Step 1**.

REMARK 3.13. The matrix $BA_r^{-1}B^T$ is not necessarily positive definite, but at least positive semi-definite. However, as mentioned in [28], the conjugate gradient algorithm converges in the quotient space $\mathbb{R}^m \setminus \text{Ker } B^T$.

3.2.2. A least-squares conjugate gradient method. The method is due to R. Glowinski. It was first introduced in the literature in the late seventies of the twentieth century as a method to solve a class of nonlinear problems. For the early publications we refer to [36] and the references therein. The method became very popular as a solver for the Navier-Stokes equations, because of its robustness and efficiency at least up to $Re \approx 1000$ (see [40]). Following [35] and [63], we introduce in this section the solution of a nonlinear problem, given in a quite general form, by least-squares and conjugate gradient methods. Therefore, we present the nonlinear problem, formulate a corresponding least-squares formulation and apply the Polak-Ribière conjugate gradient algorithm. The section is completed by a convergence analysis of the method based on [34].

3.2.2.1. Formulation of the abstract problem. Let V be a real Hilbert space equipped with the scalar product $(\cdot, \cdot)_V$ and induced norm $\|\cdot\|_V$. We denote by V' the dual space of V , by $\langle \cdot, \cdot \rangle$ the duality pairing between V' and V , and by $\|\cdot\|_{V'}$ the corresponding dual norm, i.e.

$$\|f\|_{V'} = \sup_{v \in V \setminus \{0\}} \frac{|\langle f, v \rangle|}{\|v\|_V}, \quad \forall f \in V'.$$

We want to consider the following problem:

$$(3.43) \quad \begin{aligned} &\text{Find } u \in V, \text{ such that} \\ &S(u) = 0, \end{aligned}$$

where S is a nonlinear operator from V to V' . We suppose that (3.43) has at least one solution to keep the discussion reasonable. Any further assumptions on problem (3.43) are postponed to the place where they are needed.

3.2.2.2. *Least-squares formulation.* A least-squares formulation of (3.43) is obtained by observing that any solution of (3.43) is also a minimizer over V of the functional $J : V \rightarrow \mathbb{R}$ defined by

$$(3.44) \quad J(v) = \frac{1}{2} \|S(v)\|_{V'}^2.$$

Clearly, J should vanish for the minimizing solution. Hence, a least-squares formulation of (3.43) is:

$$(3.45) \quad \begin{aligned} &\text{Find } u \in V, \text{ such that} \\ &J(u) \leq J(v), \quad \forall v \in V. \end{aligned}$$

Now, let A be the duality isomorphism corresponding to $(\cdot, \cdot)_V$ and $\langle \cdot, \cdot \rangle$, i.e. obeying

$$(3.46) \quad \begin{aligned} \langle A v, w \rangle &= (v, w)_V, \quad \forall v, w \in V, \\ \|v\|_V &= \|A v\|_{V'}, \quad \forall v \in V. \end{aligned}$$

Let us remark that A is uniquely defined by the Riesz Representation theorem. Using (3.46) in (3.44), we get

$$(3.47) \quad J(v) = \frac{1}{2} \langle A \xi(v), \xi(v) \rangle = \frac{1}{2} \|\xi(v)\|_V^2,$$

where ξ is a nonlinear function of v obtained via the solution of the well-posed linear problem

$$(3.48) \quad A \xi(v) = S(v).$$

3.2.2.3. *Solution of the least-squares problem.* We suppose from now on, that S is differentiable over V implying in turn the differentiability of J (see (3.58), (3.59)). We denote by S' and J' the Fréchet-derivatives of S and J , respectively.

From the differentiability of J it is quite natural to solve the minimization problem (3.45) by a conjugate gradient algorithm. Among the possible conjugate gradient algorithms we have selected the Polak-Ribière variant (cf. [58], [59]), whose very good performance (in general) has been discussed in [61].

The Polak-Ribière method applied to the solution of (3.45) provides the following algorithm:

Step 0: Initialization

Let

$$(3.49) \quad u^0 \in V$$

be given. Compute $g^0 \in V$ as the solution of

$$(3.50) \quad A g^0 = J'(u^0)$$

and set

$$(3.51) \quad w^0 = g^0.$$

For $0 \leq j \in \mathbb{N}_0$, assuming that u^j, g^j, w^j are known, compute $u^{j+1}, g^{j+1}, w^{j+1}$ by

Step 1: Descent

Compute

$$(3.52) \quad \rho^j = \underset{\rho \in \mathbb{R}_0^+}{\text{Arg Min}} J(u^j - \rho w^j).$$

Then, set

$$(3.53) \quad u^{j+1} = u^j - \rho^j w^j.$$

Step 2: Construction of the new descent direction

Define $g^{j+1} \in V$ as the solution of

$$(3.54) \quad A g^{j+1} = J'(u^{j+1}).$$

Compute γ^j by

$$(3.55) \quad \gamma^j = \frac{\langle A(g^{j+1} - g^j), g^{j+1} \rangle}{\langle A g^j, g^j \rangle} = \frac{(g^{j+1} - g^j, g^{j+1})_V}{\|g^j\|_V^2}$$

and set

$$(3.56) \quad w^{j+1} = g^{j+1} + \gamma^j w^j.$$

Set $j = j + 1$ and go to **Step 1**.

REMARK 3.14. The two non-trivial steps of algorithm (3.49)–(3.56) are:

- (i) The solution of the one-dimensional minimization problem (3.52) to obtain ρ^j ; in practice, one will have further information on the structure of problem (3.43), which is then used for the implementation of (3.52). We will return to this point when considering the problems to which the least-squares conjugate gradient algorithm will be applied to. The problems which we consider always require the solution of some linear problem associated to A .

- (ii) The calculation of g^{j+1} from u^{j+1} which requires the solution of two linear problems associated to A (namely (3.48) with $v = u^{j+1}$ and (3.54)).

Owing to the importance of Step 2, let us detail the calculation of $J'(u^j)$ and g^j . Let $v \in V$, then $J'(v)$ may be defined by

$$(3.57) \quad \langle J'(v), w \rangle = \lim_{t \rightarrow 0} \frac{J(v + tw) - J(v)}{t}, \quad \forall w \in V.$$

We obtain from (3.47), (3.48), (3.57) by applying the product rule of differentiation in Banach spaces (see [77]):

$$(3.58) \quad \langle J'(v), w \rangle = \langle A \xi(v), \eta(v, w) \rangle,$$

where ξ and η are the solutions of (3.48) and

$$(3.59) \quad A \eta(v, w) = S'(v) \cdot w,$$

respectively. Since A is self-adjoint (from (3.46)), we also have from (3.58), (3.59) that

$$(3.60) \quad \begin{aligned} \langle J'(v), w \rangle &= \langle A \xi(v), \eta(v, w) \rangle \\ &= \langle A \eta(v, w), \xi(v) \rangle = \langle S'(v) \cdot w, \xi(v) \rangle. \end{aligned}$$

Therefore, $J'(v) \in V'$ may be identified with the linear functional

$$(3.61) \quad w \mapsto \langle S'(v) \cdot w, \xi(v) \rangle.$$

It follows then from (3.54), (3.60) and (3.61), that g^j is the solution of the following linear variational problem:

$$\begin{aligned} &\text{Find } g^j \in V, \text{ such that} \\ &\langle A g^j, w \rangle = \langle S'(u^j) \cdot w, \xi^j(u^j) \rangle, \quad \forall w \in V, \end{aligned}$$

where ξ^j is the solution of (3.48) corresponding to $v = u^j$.

REMARK 3.15. It is clear from the above observations, that an efficient solver for linear problems associated to operator A (in fact to a finite dimensional approximation of A) will be a fundamental tool for the solution of problem (3.43) by the conjugate gradient algorithm.

3.2.2.4. Convergence of algorithm (3.49) – (3.56). A convergence analysis restricted to the finite dimensional case of our problem can be found in [63], which seems to be the oldest source where convergence is discussed. To establish a more general convergence result, we follow the lines of [34].

We introduce the concept of regular solutions of problem (3.43) by

Definition 3.16. A solution u of (3.43) is said to be regular, if the operator $S'(u)$ is an isomorphism from V onto V' .

Now we can formulate the following

Lemma 3.17. Let u be a regular solution of (3.43). If the functional J is twice continuously differentiable, then there exists a neighborhood $D \subset V$ of u , where J is strictly convex, i.e. there exist two constants $m, M \in \mathbb{R}^+$ such that

$$m\|w\|_V^2 \leq J''(v) \cdot (w, w) \leq M\|w\|_V^2 \quad \forall w \in V, \forall v \in D.$$

Proof: See Chapter IV, Theorem 6.3 in [34]. ■

REMARK 3.18. The second Fréchet-derivative of J can be defined by

$$\begin{aligned} J''(u) \cdot (v, w) \\ = \lim_{t \rightarrow 0} \frac{\langle J'(u + tw), v \rangle - \langle J'(u), v \rangle}{t}, \quad \forall u, v, w \in V. \end{aligned}$$

Theorem 3.19. Let u be a regular solution of (3.43) and the functional J twice continuously differentiable. Then, the Polak–Ribière conjugate gradient algorithm (3.49)–(3.56) converges to u , if u^0 , the initial choice in (3.49) is well chosen, i.e. $u^0 \in D$.

Proof: Combining Lemma 3.17 from above and Theorem 6.1, 6.2 from Chapter IV in [34], yields the result. ■

REMARK 3.20. In [34] the convergence result is established for a general method of descent of which the Polak–Ribière variant of the conjugate gradient algorithm is just a special case.

3.2.3. Numerical solution algorithms for the micro problems.

3.2.3.1. *The stationary Stokes system on the periodicity cell.* In this section we are concerned with the numerical solution of Stokes systems on the periodicity cell Y . We start by restating the continuous problem. For the velocity u and the pressure p it reads

$$(3.62) \quad \begin{aligned} -\mu\Delta_y u + \nabla_y p &= f && \text{in } Y_f, \\ \operatorname{div}_y u &= 0 && \text{in } Y_f, \\ u &= 0 && \text{on } \partial Y_s, \\ \{u, p\} &&& \text{is } Y\text{-periodic,} \end{aligned}$$

where $\mu \in \mathbb{R}^+$ and $f \in L^2(Y_f)^n$.

Skipping the divergence condition imposed on functions in \mathcal{W} , we define

$$\mathcal{W}^* := \{w \in H^1(Y_f)^n \mid w = 0 \text{ on } \partial Y_s, w \text{ is } Y\text{-periodic}\}.$$

Moreover, a modified pressure space is used:

$$\mathcal{R}^* := \{r \in L^2(Y_f) \mid r \text{ is } Y\text{-periodic}\}.$$

We derive a variational formulation of (3.62) by multiplying the first equation of (3.62) by test functions of \mathcal{W}^* . The second equation is multiplied by test functions of \mathcal{R}^* . Integrating over Y_f , applying Green's theorem and using the boundary conditions for u and p , we obtain the following problem

$$(3.63) \quad \begin{aligned} & \text{Find } (u, p) \in \mathcal{W}^* \times \mathcal{R}^*, \text{ such that} \\ & \mu \int_{Y_f} \nabla_y u : \nabla_y v \, dy - \int_{Y_f} p \operatorname{div}_y v \, dy = \int_{Y_f} f \cdot v \, dy, \quad \forall v \in \mathcal{W}^*, \\ & - \int_{Y_f} q \operatorname{div}_y u \, dy = 0, \quad \forall q \in \mathcal{R}^*. \end{aligned}$$

Let $\mathcal{W}_h^* \subset \mathcal{W}^*$ and $\mathcal{R}_h^* \subset \mathcal{R}^*$ be finite-dimensional subspaces of \mathcal{W}^* and \mathcal{R}^* , respectively. The index h refers to the mesh width of a finite element discretization from which the subspaces will be derived. Hence, a discrete analogon of (3.63) can be formulated:

$$(3.64) \quad \begin{aligned} & \text{Find } (u_h, p_h) \in \mathcal{W}_h^* \times \mathcal{R}_h^*, \text{ such that} \\ & \mu \int_{Y_f} \nabla_y u_h : \nabla_y v_h \, dy - \int_{Y_f} p_h \operatorname{div}_y v_h \, dy = \int_{Y_f} f \cdot v_h \, dy, \quad \forall v_h \in \mathcal{W}_h^*, \\ & - \int_{Y_f} q_h \operatorname{div}_y u_h \, dy = 0, \quad \forall q_h \in \mathcal{R}_h^*. \end{aligned}$$

As mentioned above, the spaces \mathcal{W}_h^* and \mathcal{R}_h^* are derived by finite element discretization. There exists a huge amount of literature on finite element methods and, for reference purposes, we list some classical textbooks by Braess [15], Ciarlet [17], Brezzi, Fortin [16], Girault, Raviart [34], Gunzburger [39], Roberts, Thomas [64] and Thomasset [74].

We intend to apply a conforming mixed approximation of the velocity and pressure by Taylor-Hood elements ([69], [70]) in two dimensions. The method is called *conforming*, since the resulting discrete functions are elements of the continuous spaces \mathcal{W}^* and \mathcal{R}^* . The approach is called *mixed*, since the velocity and pressure are discretized simultaneously. The periodicity cell Y is subdivided by a square mesh of width h as illustrated by Figure 2.

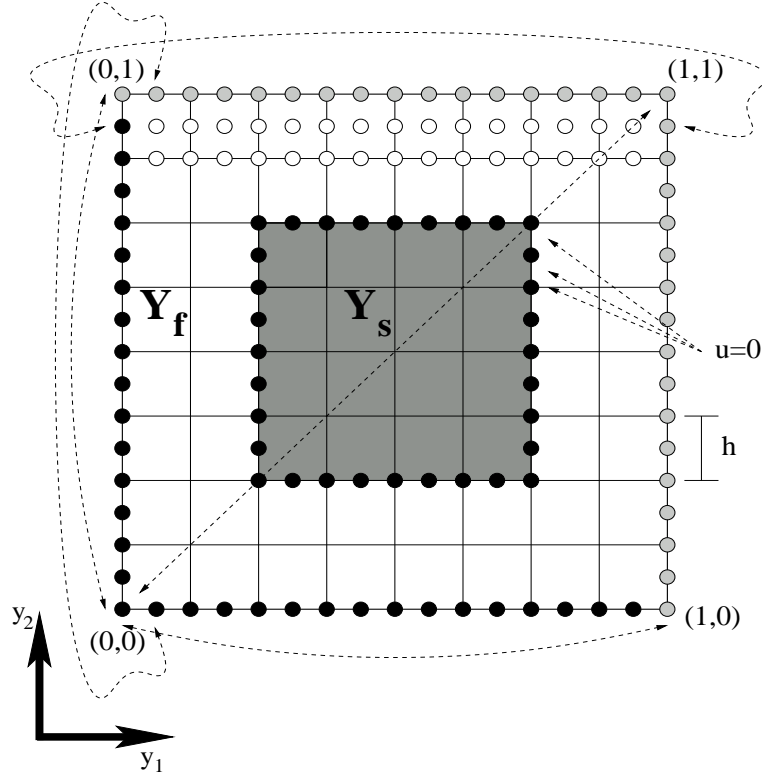


FIGURE 2. Discretization of the periodicity cell

The squares are called *elements*. We consider a reference element $T^{ref} := [-1, 1]^2$ equipped with a local coordinate system $\hat{y} = (\hat{y}_1, \hat{y}_2)$. We define bilinear and biquadratic functions recursively by linear and quadratic functions

$$\lambda_1^{lin}(t) := -\frac{1}{2}t + \frac{1}{2}, \quad \lambda_2^{lin}(t) := \frac{1}{2}t + \frac{1}{2},$$

and

$$\lambda_1^{qua}(t) := -\frac{1}{2}t(1-t), \quad \lambda_2^{qua}(t) := \frac{1}{2}t(1+t), \quad \lambda_3^{qua}(t) := (1-t)(1+t),$$

respectively.

Four bilinear functions for the approximation of the pressure are given by

$$\begin{aligned} \hat{\Phi}_1^{bilin}(\hat{y}) &:= \lambda_1^{lin}(\hat{y}_1) \cdot \lambda_1^{lin}(\hat{y}_2) = \frac{1}{4}(+\hat{y}_1\hat{y}_2 - \hat{y}_1 - \hat{y}_2 + 1), \\ \hat{\Phi}_2^{bilin}(\hat{y}) &:= \lambda_2^{lin}(\hat{y}_1) \cdot \lambda_1^{lin}(\hat{y}_2) = \frac{1}{4}(-\hat{y}_1\hat{y}_2 + \hat{y}_1 - \hat{y}_2 + 1), \\ \hat{\Phi}_3^{bilin}(\hat{y}) &:= \lambda_2^{lin}(\hat{y}_1) \cdot \lambda_2^{lin}(\hat{y}_2) = \frac{1}{4}(+\hat{y}_1\hat{y}_2 + \hat{y}_1 + \hat{y}_2 + 1), \\ \hat{\Phi}_4^{bilin}(\hat{y}) &:= \lambda_1^{lin}(\hat{y}_1) \cdot \lambda_2^{lin}(\hat{y}_2) = \frac{1}{4}(-\hat{y}_1\hat{y}_2 - \hat{y}_1 + \hat{y}_2 + 1). \end{aligned}$$

The nine biquadratic functions for the approximation of the velocity components read

$$\begin{aligned}\hat{\Phi}_1^{biqua}(\hat{y}) &= \lambda_1^{qua}(\hat{y}_1) \cdot \lambda_1^{qua}(\hat{y}_2) = \frac{1}{4}(+\hat{y}_1^2\hat{y}_2^2 - \hat{y}_1^2\hat{y}_2 - \hat{y}_1\hat{y}_2^2 + \hat{y}_1\hat{y}_2), \\ \hat{\Phi}_2^{biqua}(\hat{y}) &= \lambda_2^{qua}(\hat{y}_1) \cdot \lambda_1^{qua}(\hat{y}_2) = \frac{1}{4}(+\hat{y}_1^2\hat{y}_2^2 - \hat{y}_1^2\hat{y}_2 + \hat{y}_1\hat{y}_2^2 - \hat{y}_1\hat{y}_2), \\ \hat{\Phi}_3^{biqua}(\hat{y}) &= \lambda_2^{qua}(\hat{y}_1) \cdot \lambda_2^{qua}(\hat{y}_2) = \frac{1}{4}(+\hat{y}_1^2\hat{y}_2^2 + \hat{y}_1^2\hat{y}_2 + \hat{y}_1\hat{y}_2^2 + \hat{y}_1\hat{y}_2), \\ \hat{\Phi}_4^{biqua}(\hat{y}) &= \lambda_1^{qua}(\hat{y}_1) \cdot \lambda_2^{qua}(\hat{y}_2) = \frac{1}{4}(+\hat{y}_1^2\hat{y}_2^2 + \hat{y}_1^2\hat{y}_2 - \hat{y}_1\hat{y}_2^2 - \hat{y}_1\hat{y}_2), \\ \hat{\Phi}_5^{biqua}(\hat{y}) &= \lambda_3^{qua}(\hat{y}_1) \cdot \lambda_1^{qua}(\hat{y}_2) = \frac{1}{2}(-\hat{y}_1^2\hat{y}_2^2 - \hat{y}_1^2\hat{y}_2 + \hat{y}_2^2 - \hat{y}_2), \\ \hat{\Phi}_6^{biqua}(\hat{y}) &= \lambda_2^{qua}(\hat{y}_1) \cdot \lambda_3^{qua}(\hat{y}_2) = \frac{1}{2}(-\hat{y}_1^2\hat{y}_2^2 + \hat{y}_1^2 - \hat{y}_1\hat{y}_2^2 + \hat{y}_1), \\ \hat{\Phi}_7^{biqua}(\hat{y}) &= \lambda_3^{qua}(\hat{y}_1) \cdot \lambda_2^{qua}(\hat{y}_2) = \frac{1}{2}(-\hat{y}_1^2\hat{y}_2^2 - \hat{y}_1^2\hat{y}_2 + \hat{y}_2^2 + \hat{y}_2), \\ \hat{\Phi}_8^{biqua}(\hat{y}) &= \lambda_1^{qua}(\hat{y}_1) \cdot \lambda_3^{qua}(\hat{y}_2) = \frac{1}{2}(-\hat{y}_1^2\hat{y}_2^2 + \hat{y}_1^2 + \hat{y}_1\hat{y}_2^2 - \hat{y}_1), \\ \hat{\Phi}_9^{biqua}(\hat{y}) &= \lambda_3^{qua}(\hat{y}_1) \cdot \lambda_3^{qua}(\hat{y}_2) = \hat{y}_1^2\hat{y}_2^2 - \hat{y}_1^2 - \hat{y}_2^2 + 1.\end{aligned}$$

These functions have the property to take on the value 1 at exactly one node of the reference element and 0 at all others (see Figure 3, 4). The indices of the functions refer to the node indices where their value is equal to 1.

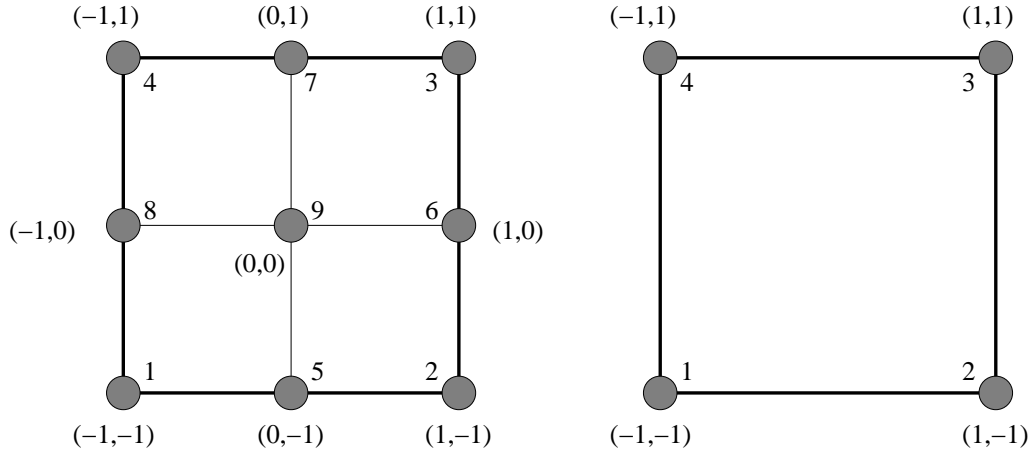


FIGURE 3. Reference element T^{ref} : Nodes in the biquadratic (left) and bilinear case (right)

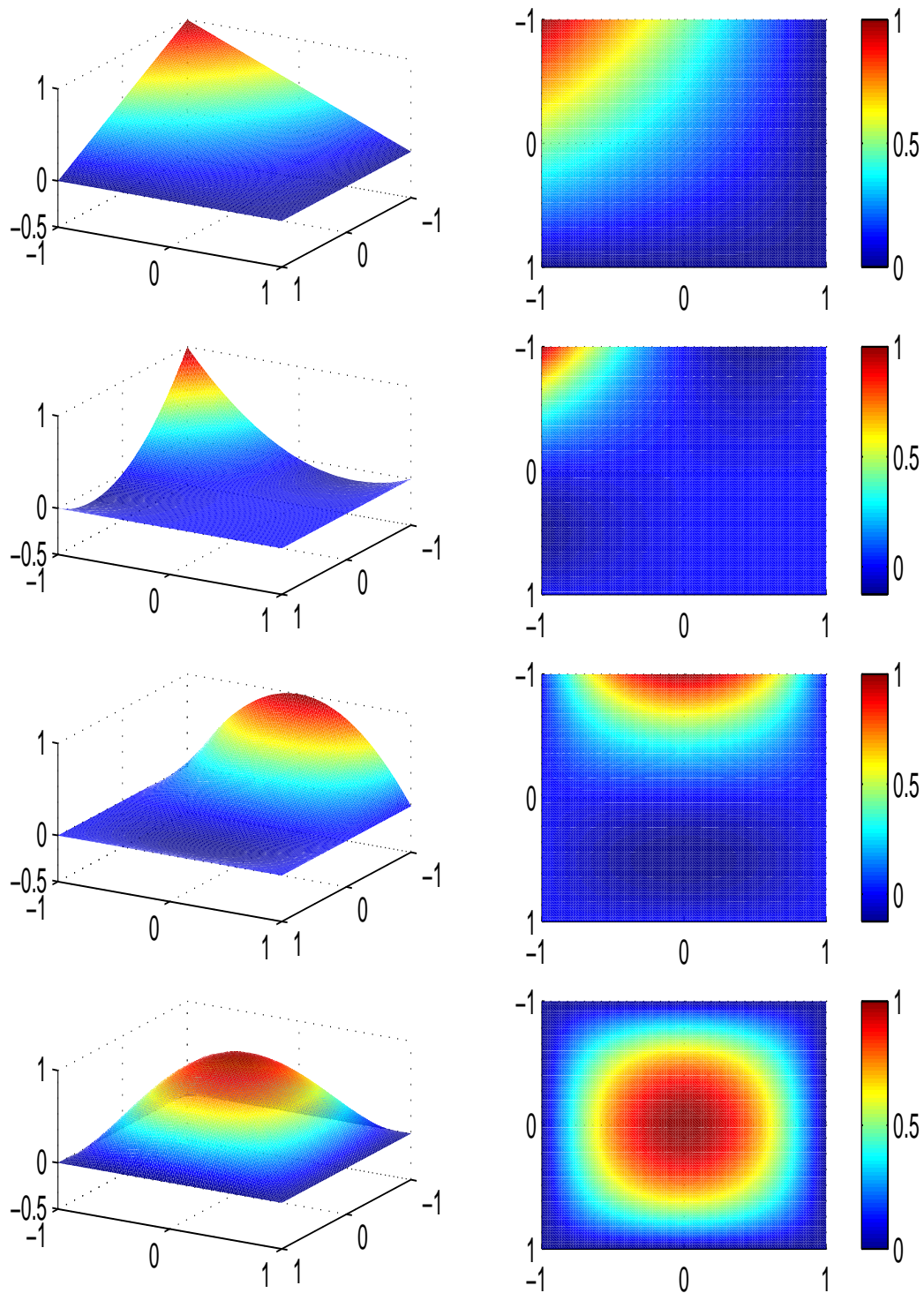


FIGURE 4. Examples of bilinear and biquadratic functions - $\hat{\Phi}_4^{bilin}$, $\hat{\Phi}_4^{biqua}$, $\hat{\Phi}_7^{biqua}$, $\hat{\Phi}_9^{biqua}$ (from top to bottom)

By means of the bilinear and biquadratic functions given on the reference element T^{ref} , one defines discrete subspaces \mathcal{W}_h^* and \mathcal{R}_h^* by constructing nodal basis functions. More precisely, by applying suitable coordinate transformations (composed of a translation and an homothety in case of square meshes) to the functions on the reference element, we obtain biquadratic and bilinear functions on each element of the mesh. Clearly, the elements also inherit the nodal structure of the reference element. Now, given one node of the square mesh, a bilinear basis function $\tilde{\Phi}_{ih}^{bilin}$ is constructed by collecting all bilinear functions on adjacent elements having value 1 on that node. In complete analogy biquadratic basis functions $\tilde{\Phi}_{ih}^{biqua}$ are derived. An example of a bilinear basis function is shown in Figure 5.

Due to the periodicity of the spaces \mathcal{W}_h^* and \mathcal{R}_h^* , we identify nodes on the outer boundary of the periodicity cell. As shown in Figure 2, all corner nodes are identified with the lower left corner node. Analogously, corresponding nodes on the left and on the right boundary, as well as on the lower and upper boundary are identified. Transferring the periodic identification to the nodal basis functions $\tilde{\Phi}_{ih}^{bilin}$ and $\tilde{\Phi}_{ih}^{biqua}$, we obtain a basis of \mathcal{R}_h^* and \mathcal{W}_h^* to be

$$(3.65) \quad \{\Phi_{ih}^{bilin} \mid 1 \leq i \leq m := \dim \mathcal{R}_h^*\},$$

and

$$\{\Phi_{ih}^{biqua} := (\Phi_{ih}^{biqua}, 0)^T, \Phi_{\frac{n}{2}+ih}^{biqua} := (0, \Phi_{ih}^{biqua})^T \mid 1 \leq i \leq \frac{n}{2}, \quad n := \dim \mathcal{W}_h^*\},$$

respectively.

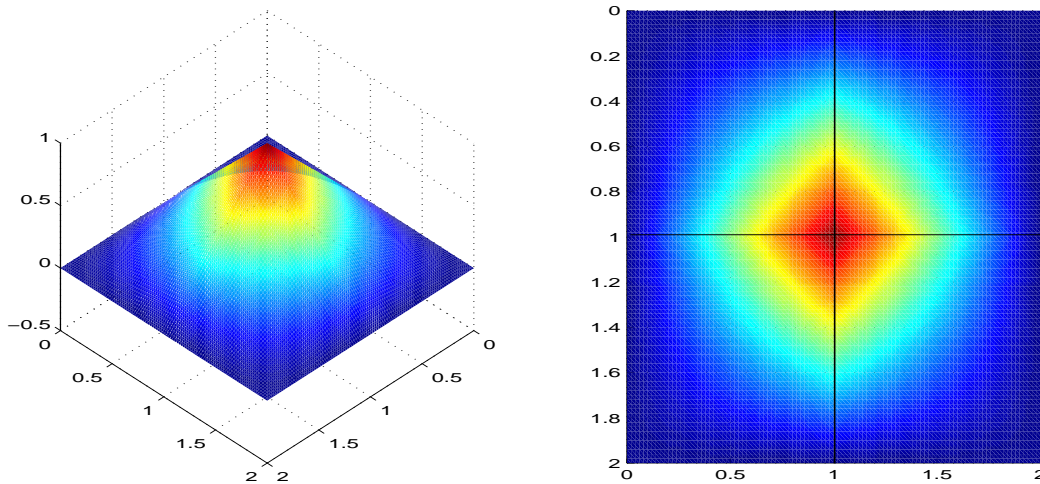


FIGURE 5. Bilinear nodal basis function

Then, the discrete velocity u_h and the discrete pressure p_h can be written in terms of the basis functions:

$$\begin{aligned} u_h &= \sum_{i=1}^n \alpha_i \Phi_{ih}^{biqua}, \\ p_h &= \sum_{i=1}^m \beta_i \Phi_{ih}^{bilin}, \end{aligned}$$

where $\alpha_i, \beta_i \in \mathbb{R}$ are unknown.

Defining $A_h \in \mathbb{R}^{n \times n}$, $B_h \in \mathbb{R}^{m \times n}$ and $b_h \in \mathbb{R}^n$ by

$$\begin{aligned} (3.66) \quad (A_h)_{ij} &:= \mu \int_{Y_f} \nabla_y \Phi_{ih}^{biqua} : \nabla_y \Phi_{jh}^{biqua} dy, \quad 1 \leq i, j \leq n, \\ (B_h)_{ij} &:= - \int_{Y_f} \Phi_{ih}^{bilin} \operatorname{div}_y \Phi_{jh}^{biqua} dy, \quad 1 \leq i \leq m, 1 \leq j \leq n, \\ b_{hi} &:= \int_{Y_f} f \cdot \Phi_{ih}^{biqua} dy \end{aligned}$$

and letting

$$\mathbf{u}_h := (\alpha_1, \dots, \alpha_n)^T \text{ and } \mathbf{p}_h := (\beta_1, \dots, \beta_m)^T,$$

the following linear system for \mathbf{u}_h and \mathbf{p}_h is obtained

$$(3.67) \quad \begin{aligned} A_h \mathbf{u}_h + B_h^T \mathbf{p}_h &= b_h, \\ B_h \mathbf{u}_h &= 0. \end{aligned}$$

Note, that A_h is symmetric and positive definite. The latter property is induced by coercivity of the bilinear form $a(v, v) := \mu \int_{Y_f} \nabla_y v : \nabla_y v dy \geq \alpha \|v\|_{\mathcal{W}^*}^2$, $\forall v \in \mathcal{W}^*$.

With only minor changes in notation in (3.67), we observe the optimality conditions mentioned in Theorem 3.9. Therefore, a saddle-point formulation of (3.67) can be derived. We apply the augmented Lagrangian Uzawa conjugate gradient method presented in Section 3.2.1. Convergence of the Uzawa method in case of the pressure is up to an additive constant.

REMARK 3.21. Integrals of (3.66) are computed by Gaussian integration formulas of third order (see [23]), which are exact for the appearing polynomials. The calculations are done on the reference element and transferred to the actual element by integral transformation.

The linear systems are solved by SuperLU 3.0 ([19]), a software package being very-well suited to solve large sparse linear systems by a direct LU decomposition. Since the matrix, which has to be inverted during the Uzawa iterations,

does not change, we have to invert it only once at the beginning. Thus making the algorithm quite efficient with respect to computation time.

Up to now, the finite element method has been introduced formally. We close this section by a convergence result relating (3.63) and (3.64).

Theorem 3.22. *Let $(u, p) \in \mathcal{W}^* \times \mathcal{R}^*$ and $(u_h, p_h) \in \mathcal{W}_h^* \times \mathcal{R}_h^*$ be unique solutions of (3.63) and (3.64), respectively, where the pressures are unique up to a constant. Let the discrete formulation be derived by Taylor-Hood elements on square meshes. Then, the inf-sup condition, which is frequently referred to as Ladyženskaja- Babuška-Brezzi condition reads*

$$(3.68) \quad \inf_{q_h \in \mathcal{R}_h^*} \sup_{v_h \in \mathcal{W}_h^*} \frac{-\int_{Y_f} q_h \operatorname{div}_y v_h \, dy}{\|v_h\|_{\mathcal{W}^*} \|q_h\|_{\mathcal{R}^*/\mathbb{R}}} \geq k_0 > 0$$

and is fulfilled, where $k_0 \in \mathbb{R}^+$ is independent of h . Assuming that $u \in W^{2,2}(Y_f) \cap \mathcal{W}^*$ and $p \in H^1(Y_f) \cap \mathcal{R}^*$, the following approximations are valid

$$(3.69) \quad \|u - u_h\|_{L^2(Y_f)^2} \leq ch^2 \text{ and } \|p - p_h\|_{\mathcal{R}^*/\mathbb{R}} \leq ch.$$

Proof: In [11], the inf-sup condition is proved for general regular triangulations including the case of square meshes. Moreover, they prove convergence in the sense of (3.69). ■

3.2.3.2. *The stationary Navier-Stokes system on the periodicity cell.* In this section we consider the stationary incompressible Navier-Stokes system on the periodicity cell. In view of its numerical solution, the least-squares conjugate gradient algorithm introduced in Section 3.2.2 is applied. The method reduces the solution of the Navier-Stokes system to the solution of a sequence of Stokes problems, which in turn are solved by the Uzawa algorithm and the discretization presented in Sections 3.2.1 and 3.2.3.1, respectively.

Formulation of the problem. Let $Y =]0, 1[^n$ be the periodicity cell and Y_s, Y_f be the solid and fluid part, respectively, as defined in Chapter 2. The stationary incompressible Navier-Stokes system is given by

$$(3.70) \quad \begin{aligned} -\mu \Delta_y u + (u \cdot \nabla_y) u + \nabla_y p &= f && \text{in } Y_f, \\ \operatorname{div}_y u &= 0 && \text{in } Y_f, \\ u &= 0 && \text{on } \partial Y_s, \\ \{u, p\} &&& \text{is } Y\text{-periodic,} \end{aligned}$$

where u and p are the unknown velocity and pressure, respectively, and $\mu \in \mathbb{R}^+$ and $f \in L^2(Y_f)^2$ are the given viscosity and force density, respectively.

We restate the definition of the Hilbert space \mathcal{W} introduced in Chapter 2:

$$\mathcal{W} := \{w \in H^1(Y_f)^n \mid \operatorname{div}_y w = 0 \text{ in } Y_f, w = 0 \text{ on } \partial Y_s, w \text{ is } Y\text{-periodic}\}.$$

\mathcal{W} is equipped with a scalar product

$$(v, w)_{\mathcal{W}} := \mu \int_{Y_f} \nabla_y v : \nabla_y w \, dy, \quad v, w \in \mathcal{W}$$

and induced norm

$$\|v\|_{\mathcal{W}} := (v, v)_{\mathcal{W}}^{\frac{1}{2}}, \quad v \in \mathcal{W}.$$

Hence, a weak formulation of (3.70) is given by:

$$(3.71) \quad \text{Find } u \in \mathcal{W}, \text{ such that} \\ \mu \int_{Y_f} \nabla_y u : \nabla_y v \, dy + \int_{Y_f} (u \cdot \nabla_y) u \cdot v \, dy - \int_{Y_f} f \cdot v \, dy = 0, \quad \forall v \in \mathcal{W}.$$

In (3.71) p is eliminated due to the solenoidal functions in \mathcal{W} . As mentioned before, unique existence of a solution of (3.71) is guaranteed, if f is sufficiently small or μ is sufficiently large.

Now, defining

$$\langle S(v), w \rangle := \\ \mu \int_{Y_f} \nabla_y v : \nabla_y w \, dy + \int_{Y_f} (v \cdot \nabla_y) v \cdot w \, dy - \int_{Y_f} f \cdot w \, dy, \quad v, w \in \mathcal{W},$$

where $\langle \cdot, \cdot \rangle$ is the duality pairing of \mathcal{W}' and \mathcal{W} , problem (3.71) is equivalent to:

$$(3.72) \quad \text{Find } u \in \mathcal{W}, \text{ such that} \\ S(u) = 0,$$

where $S(u)$ is to be understood as element of \mathcal{W}' . The linearity of $S(u)$ is obvious and the continuity follows by applying the continuity properties of the classical bilinear, trilinear and linear forms a , b , l , respectively, which are introduced later during the proof of Lemma 3.24.

Least-squares formulation. Proceeding as in the general case of Section 3.2.2, we derive a functional $J : \mathcal{W} \rightarrow \mathbb{R}$. It reads

$$(3.73) \quad J(v) = \frac{1}{2} \|S(v)\|_{\mathcal{W}'}^2 = \frac{1}{2} \mu \int_{Y_f} |\nabla_y \xi(v)|^2 \, dy, \quad v \in \mathcal{W}.$$

ξ is a nonlinear function of v determined by (3.48), which is an equation in \mathcal{W}' . The corresponding variational problem defined in \mathcal{W} reads:

$$(3.74) \quad \text{Given } v \in \mathcal{W}. \text{ Find } \xi(v) \in \mathcal{W}, \text{ such that} \\ (\xi(v), w)_{\mathcal{W}} = \langle S(v), w \rangle, \quad \forall w \in \mathcal{W}.$$

REMARK 3.23. Rewriting variational problem (3.74) as partial differential equations, we recover the following Stokes problem:

$$\begin{aligned} -\mu\Delta_y\xi(v) + \nabla_y\tilde{p} &= -\mu\Delta_yv + (v \cdot \nabla_y)v - f && \text{in } Y_f, \\ \operatorname{div}_y\xi(v) &= 0 && \text{in } Y_f, \\ \xi(v) &= 0 && \text{on } \partial Y_s, \\ \{\xi(v), \tilde{p}\} &&& \text{is } Y\text{-periodic.} \end{aligned}$$

Setting $v = u$, we observe $p = -\tilde{p}$.

Hence, we arrive at the following minimization problem, which characterizes the solution of (3.72):

$$(3.75) \quad \begin{aligned} &\text{Find } u \in \mathcal{W}, \text{ such that} \\ &J(u) \leq J(v), \quad \forall v \in \mathcal{W}. \end{aligned}$$

Solution of the least-squares problem. In order to find the minimum of the functional J , we want to apply the Polak-Ribière conjugate gradient method. We will repeat the essential steps and point out how the structural information of the Navier-Stokes system is taken into account. We have to consider the nontrivial problems of the minimization process, i.e. the computation of the gradient g^j in (3.50), (3.54) and the one-dimensional minimization problem (3.52).

In complete analogy to Remark 3.23, we observe that finding g^j requires the solution of a Stokes problem. Its variational formulation is given by

$$(3.76) \quad \begin{aligned} &\text{Find } g^j \in \mathcal{W}, \text{ such that} \\ &\mu \int_{Y_f} \nabla_y g^j : \nabla_y v \, dy = \langle J'(u^j), v \rangle, \quad \forall v \in \mathcal{W}. \end{aligned}$$

The only open question is the right hand side, which we calculate in the following

Lemma 3.24. *The Fréchet-derivative of the functional J at $v \in \mathcal{W}$ is given by*

$$\begin{aligned} \langle J'(v), w \rangle &= \mu \int_{Y_f} \nabla_y w : \nabla_y \xi(v) \, dy + \int_{Y_f} (v \cdot \nabla_y) w \cdot \xi(v) \, dy \\ &\quad + \int_{Y_f} (w \cdot \nabla_y) v \cdot \xi(v) \, dy, \quad w \in \mathcal{W}. \end{aligned}$$

Proof: We define the following classical linear, bilinear and trilinear forms to simplify notation. Let

$$\begin{aligned} l(v) &:= \int_{Y_f} f \cdot v \, dy, \quad v \in \mathcal{W}, \\ a(v, w) &:= \mu \int_{Y_f} \nabla_y v : \nabla_y w \, dy, \quad v, w \in \mathcal{W}, \\ b(v, w, z) &:= \int_{Y_f} (v \cdot \nabla_y) w \cdot z \, dy, \quad v, w, z \in \mathcal{W}. \end{aligned}$$

The following continuity properties hold. Let $v, w, z \in \mathcal{W}$, then we have

$$\begin{aligned} |l(v)| &\leq c_1 \|v\|_{\mathcal{W}}, \quad |a(v, w)| \leq c_2 \|v\|_{\mathcal{W}} \|w\|_{\mathcal{W}}, \\ |b(v, w, z)| &\leq c_3 \|v\|_{\mathcal{W}} \|w\|_{\mathcal{W}} \|z\|_{\mathcal{W}}, \end{aligned}$$

where $c_1, c_2, c_3 \in \mathbb{R}^+$ refer to certain constants. A proof of the continuity properties can be found in [24]. Now, we calculate for $v, w \in \mathcal{W}$

$$(3.77) \quad \langle J'(v), w \rangle = \lim_{t \rightarrow 0} \frac{1}{t} \{J(v + tw) - J(v)\}.$$

Therefore, we consider first

$$\begin{aligned} (3.78) \quad & 2(J(v + tw) - J(v)) = a(\xi(v + tw), \xi(v + tw)) - a(\xi(v), \xi(v)) \\ &= a(v + tw, \xi(v + tw)) + b(v + tw, v + tw, \xi(v + tw)) - l(\xi(v + tw)) \\ &\quad - a(v, \xi(v)) - b(v, v, \xi(v)) + l(\xi(v)) \\ &= a(v, \xi(v + tw)) + t a(w, \xi(v + tw)) + b(v, v, \xi(v + tw)) \\ &\quad + t b(v, w, \xi(v + tw)) + t b(w, v, \xi(v + tw)) \\ &\quad + t^2 b(w, w, \xi(v + tw)) - l(\xi(v + tw)) - a(v, \xi(v)) \\ &\quad - b(v, v, \xi(v)) + l(\xi(v)) \\ &= a(v, \xi(v + tw) - \xi(v)) + b(v, v, \xi(v + tw) - \xi(v)) \\ &\quad - l(\xi(v + tw) - \xi(v)) + t a(w, \xi(v + tw)) + t b(w, v, \xi(v + tw)) \\ &\quad + t b(v, w, \xi(v + tw)) + t^2 b(w, w, \xi(v + tw)). \end{aligned}$$

Let us now focus on the first three terms of the last expression in (3.78):

$$\begin{aligned} (3.79) \quad & a(v, \xi(v + tw) - \xi(v)) + b(v, v, \xi(v + tw) - \xi(v)) - l(\xi(v + tw) - \xi(v)) \\ &= a(\xi(v), \xi(v + tw) - \xi(v)) = a(\xi(v + tw), \xi(v)) - a(\xi(v), \xi(v)) \\ &= a(v + tw, \xi(v)) + b(v + tw, v + tw, \xi(v)) - l(\xi(v)) \\ &\quad - a(v, \xi(v)) - b(v, v, \xi(v)) + l(\xi(v)) \\ &= a(v, \xi(v)) + t a(w, \xi(v)) + b(v, v, \xi(v)) + t b(w, v, \xi(v)) + t b(v, w, \xi(v)) \\ &\quad + t^2 b(w, w, \xi(v)) - a(v, \xi(v)) - b(v, v, \xi(v)). \end{aligned}$$

In the calculations above, we used linearity with respect to each argument of the forms a , b , l , their continuity and the variational equation (3.74).

Since

$$\begin{aligned} & (\xi(v+tw) - \xi(v), z)_{\mathcal{W}} = a(\xi(v+tw) - \xi(v), z) \\ & = t a(w, z) + t b(w, v, z) + t b(v, w, z) \\ & \quad + t^2 b(w, w, z), \quad v, w, z \in V, \end{aligned}$$

choosing $z = \xi(v+tw) - \xi(v)$, applying the continuity inequalities and dividing by $\|\xi(v+tw) - \xi(v)\|_{\mathcal{W}}$, we compute

$$(3.80) \quad \lim_{t \rightarrow 0} \|\xi(v+tw) - \xi(v)\|_{\mathcal{W}} = 0, \quad v, w \in V.$$

Combining (3.78), (3.79) and using (3.80), we can go to the limit in (3.77) and obtain

$$\lim_{t \rightarrow 0} \frac{1}{t} \{J(v+tw) - J(v)\} = a(w, \xi(v)) + b(v, w, \xi(v)) + b(w, v, \xi(v)),$$

which is the desired result. ■

REMARK 3.25. To know the right hand sides of (3.50) and (3.54) in the form given by Lemma 3.24 is not at all a drawback if one intends to use finite elements for the numerical solution of the problem.

Now, we turn to the one-dimensional minimization problem (3.52). Letting $v = u^j - \rho w^j$ in (3.74), we have $\forall z \in \mathcal{W}$

$$\begin{aligned} & \mu \int_{Y_f} \nabla_y \xi^j(u^j - \rho w^j) : \nabla_y z \, dy \\ & = \mu \int_{Y_f} \nabla_y(u^j - \rho w^j) : \nabla_y z \, dy \\ & \quad + \int_{Y_f} ((u^j - \rho w^j) \cdot \nabla_y)(u^j - \rho w^j) \cdot z \, dy - \int_{Y_f} f \cdot z \, dy \\ & = \mu \int_{Y_f} \nabla_y u^j : \nabla_y z \, dy + \int_{Y_f} (u^j \cdot \nabla_y) u^j \cdot z \, dy - \int_{Y_f} f \cdot z \, dy \\ & \quad - \rho \left\{ \mu \int_{Y_f} \nabla_y w^j : \nabla_y z \, dy + \int_{Y_f} (w^j \cdot \nabla_y) w^j \cdot z \, dy + \int_{Y_f} (w^j \cdot \nabla_y) w^j \cdot z \, dy \right\} \\ & \quad + \rho^2 \int_{Y_f} (w^j \cdot \nabla_y) w^j \cdot z \, dy. \end{aligned}$$

Due to linearity of the variational problem for ξ^j , we can expand ξ^j as polynomial in ρ , i.e.

$$(3.81) \quad \xi^j = \xi_0^j + \rho \xi_1^j + \rho^2 \xi_2^j,$$

where $\xi_i^j \in \mathcal{W}$, $i = 0, 1, 2$ are determined by the following variational problems:

$$(3.82) \quad \begin{aligned} \mu \int_{Y_f} \nabla_y \xi_0^j : \nabla_y z \, dy &= \mu \int_{Y_f} \nabla_y u^j \cdot \nabla_y z \, dy \\ &+ \int_{Y_f} (u^j \cdot \nabla_y) u^j \cdot z \, dy - \int_{Y_f} f \cdot z \, dy, \quad \forall z \in \mathcal{W}, \end{aligned}$$

$$(3.83) \quad \begin{aligned} \mu \int_{Y_f} \nabla_y \xi_1^j : \nabla_y z \, dy &= -\mu \int_{Y_f} \nabla_y w^j : \nabla_y z \, dy \\ &- \int_{Y_f} (u^j \cdot \nabla_y) w^j \cdot z \, dy - \int_{Y_f} (w^j \cdot \nabla_y) u^j \cdot z \, dy, \quad \forall z \in \mathcal{W}, \end{aligned}$$

$$(3.84) \quad \mu \int_{Y_f} \nabla_y \xi_2^j : \nabla_y z \, dy = \int_{Y_f} (w^j \cdot \nabla_y) w^j \cdot z \, dy, \quad \forall z \in \mathcal{W}.$$

Due to (3.81), the minimization problem (3.52) can be formulated as

$$(3.85) \quad \begin{aligned} \rho^j &= \underset{\rho \in \mathbb{R}_0^+}{\text{ArgMin}} J(u^j - \rho w^j) \\ &= \frac{\mu}{2} (n_0 + \rho n_1 + \rho^2 n_2 + \rho^3 n_3 + \rho^4 n_4), \end{aligned}$$

where

$$\begin{aligned} n_0 &= \int_{Y_f} \nabla_y \xi_0^j : \nabla_y \xi_0^j \, dy, \\ n_1 &= 2 \cdot \int_{Y_f} \nabla_y \xi_0^j : \nabla_y \xi_1^j \, dy, \\ n_2 &= \int_{Y_f} \nabla_y \xi_1^j : \nabla_y \xi_1^j \, dy + 2 \cdot \int_{Y_f} \nabla_y \xi_0^j : \nabla_y \xi_2^j \, dy, \\ n_3 &= 2 \cdot \int_{Y_f} \nabla_y \xi_1^j : \nabla_y \xi_2^j \, dy, \\ n_4 &= \int_{Y_f} \nabla_y \xi_2^j : \nabla_y \xi_2^j \, dy. \end{aligned}$$

We have reduced the solution of the continuous Navier-Stokes system to the solution of four Stokes problems at each iteration step, namely for the gradient g^j and $\xi_0^j, \xi_1^j, \xi_2^j$ given in variational form in (3.76), (3.82)-(3.84), respectively. The minimization problem (3.85) can be solved by a classical Newton method. The overall convergence of the least-squares conjugate gradient algorithm is

shown for regular solutions u of the Navier-Stokes system (see Section 3.2.2) in [63] and [33].

Discretization. Clearly, the above derivation can immediately be transferred to the discrete case in two dimensions, where discretization is done by using the finite element method from Section 3.2.3.1. According to [11], the quadratic convergence for the velocity and the linear convergence for the pressure takes over to the nonlinear Navier-Stokes case, if the force becomes not too large or the viscosity becomes not too small.

3.2.4. Numerical solution algorithm for the macro problem. In this section, we present an algorithm, which solves the two-dimensional nonlinear macro problem (2.11) of the Navier-Stokes system with two pressures by the least-squares conjugate gradient method introduced in Section 3.2.2. Before we can solve the macro problem, we require to know the permeability function \mathcal{F} as *input from the micro scale*. In Section 3.1, we proposed two methods to calculate nonlinear filtration laws from the micro problem (2.10) of the Navier-Stokes system with two pressures. The first method uses the Taylor expansion of the permeability function \mathcal{F} and computes the expansion coefficients. The second way is based on computing the permeability function discretely and applying a least-squares fit in powers of $(f_i - \frac{\partial p_0}{\partial x_i})$, $i = 1, \dots, n$. Hence, both methods yield the same polynomial structure of \mathcal{F} . We will make use of this structure, when deriving the subproblems of the least-squares conjugate gradient method.

Simplifying notation, we set $u := \bar{u}_0(x) = \int_{Y_f} u_0(x, y) dy$, $p := p_0(x)$, $p_{x_i} := \frac{\partial p_0(x)}{\partial x_i}$, $i = 1, 2$, $\nabla := \nabla_x$ and $\operatorname{div} := \operatorname{div}_x$. The permeability function \mathcal{F} is assumed to have the following structure

$$(3.86) \quad u = \mathcal{F}(f - \nabla p) = \begin{pmatrix} \mathcal{F}_1(f - \nabla p) \\ \mathcal{F}_2(f - \nabla p) \end{pmatrix} = \begin{pmatrix} \sum_{i,j} a_{ij} (f_1 - p_{x_1})^i (f_2 - p_{x_2})^j \\ \sum_{i,j} b_{ij} (f_1 - p_{x_1})^i (f_2 - p_{x_2})^j \end{pmatrix},$$

where $i, j \in \mathbb{N}$, and $a_{ij}, b_{ij} \in \mathbb{R}$. In practice, the sums in (3.86) will be truncated finite sums.

We have seen in Section 2.5, that the permeability tensor \mathcal{K} appearing in Darcy's law is symmetric and positive definite. \mathcal{K} is also recovered up to the viscosity as first order terms of the Taylor expansion. Moreover, symmetry and positive definiteness will not be destroyed by the least-squares fit applied to the discrete values of the permeability functions in the cases, which will be

studied in the subsequent section. Therefore, we define \mathbf{K} by

$$\mathbf{K} := \begin{pmatrix} a_{10} & a_{01} \\ b_{10} & b_{01} \end{pmatrix},$$

and assume it to be symmetric and positive definite.

Formulation of the problem. We recall the macro problem for the pressure p . It reads

$$(3.87) \quad \begin{aligned} \operatorname{div} \mathcal{F}(f - \nabla p) &= 0 && \text{in } \Omega, \\ p & \text{ is } \Gamma_1\text{-periodic,} \\ \nu(x) \cdot \mathcal{F}(f - \nabla p) &= 0 && \text{on } \Gamma_2, \end{aligned}$$

where $f \in L^2(\Omega)^2$.

We consider now the Hilbert space already introduced in Section 2.3. Let

$$\mathcal{Q} := \{q \in H^1(\Omega) \mid q \text{ is } \Gamma_1\text{-periodic, } \int_{\Omega} q(x) dx = 0\},$$

where the superfix is omitted to simplify notation. We define the following scalar product

$$(q, r)_{\mathcal{Q}} := \int_{\Omega} (\mathbf{K} \cdot \nabla q) \cdot \nabla r dx, \quad q, r \in \mathcal{Q}$$

and the induced norm

$$\|q\|_{\mathcal{Q}} := (q, q)_{\mathcal{Q}}^{\frac{1}{2}}, \quad q \in \mathcal{Q}.$$

A weak formulation of (3.87) is then given by:

$$(3.88) \quad \begin{aligned} & \text{Find } p \in \mathcal{Q}, \text{ such that} \\ & \int_{\Omega} \mathcal{F}(f - \nabla p) \cdot \nabla q dx = 0, \quad \forall q \in \mathcal{Q}. \end{aligned}$$

Unique solvability of (3.88) is given by Theorem 3.5. Now we define

$$\begin{aligned} \langle S(q), r \rangle &:= \\ & \int_{\Omega} \mathcal{F}(f - \nabla q) \cdot \nabla r dx, \quad q, r \in \mathcal{Q}. \end{aligned}$$

Then (3.88) is equivalent to:

$$(3.89) \quad \begin{aligned} & \text{Find } p \in \mathcal{Q}, \text{ such that} \\ & S(p) = 0. \end{aligned}$$

$S(p)$ is an element of \mathcal{Q}' . Its linearity is obvious and continuity follows from the Cauchy-Schwarz inequality.

Least-squares formulation. We proceed as in the general case of Section 3.2.2 by defining a functional $J : \mathcal{Q} \rightarrow \mathbb{R}$. It reads

$$(3.90) \quad J(q) = \frac{1}{2} \|S(q)\|_{\mathcal{Q}'}^2 = \frac{1}{2} \int_{\Omega} (\mathbf{K} \cdot \nabla \xi(q)) \cdot \nabla \xi(q) \, dx, \quad q \in \mathcal{Q},$$

where ξ is determined by the variational problem:

$$(3.91) \quad \begin{aligned} &\text{Given } q \in \mathcal{Q}. \text{ Find } \xi(q) \in \mathcal{Q}, \text{ such that} \\ &(\xi(q), r)_{\mathcal{Q}} = \langle S(q), r \rangle, \quad \forall r \in \mathcal{Q}. \end{aligned}$$

REMARK 3.26. The partial differential equation for $\xi(q)$ corresponding to (3.91) reads

$$\begin{aligned} -\operatorname{div}(\mathbf{K} \cdot \nabla \xi(q)) &= -\operatorname{div} \mathcal{F}(f - \nabla q) && \text{in } \Omega, \\ \xi(q) & && \text{is } \Gamma_1\text{-periodic,} \\ \nu(x) \cdot \mathcal{F}(f - \nabla \xi(q)) &= \nu(x) \cdot \mathcal{F}(f - \nabla q) && \text{on } \Gamma_2. \end{aligned}$$

Note, that by construction $\mathcal{F}(f - \nabla q)$ is Γ_1 -periodic, inducing the boundary condition on $\xi(q)$.

The minimization problem, which characterizes the solution of (3.89), will be solved by a conjugate gradient algorithm and reads:

$$\begin{aligned} &\text{Find } p \in \mathcal{Q}, \text{ such that} \\ &J(p) \leq J(q), \quad \forall q \in \mathcal{Q}. \end{aligned}$$

Solution of the least-squares problem. The minimization of (3.90) by the Polak-Ribière conjugate gradient method involves two nontrivial problems: the computation of the gradient g^n (we use n instead of j for the iteration index in this section) and the one-dimensional minimization problem. Using the structural information of our problem (3.88), we will show how they can be solved.

Finding g^n , i.e. (3.50), (3.54) requires the solution of a linear elliptic partial differential equation of second order (compare Remark 3.26). The corresponding right hand side needs some further investigation. The Jacobian of \mathcal{F} at a point $\alpha \in \mathbb{R}^2$ is given by

$$D \mathcal{F}(\alpha) := \begin{pmatrix} \frac{\partial \mathcal{F}_1(\alpha)}{\partial \alpha_1} & \frac{\partial \mathcal{F}_1(\alpha)}{\partial \alpha_2} \\ \frac{\partial \mathcal{F}_2(\alpha)}{\partial \alpha_1} & \frac{\partial \mathcal{F}_2(\alpha)}{\partial \alpha_2} \end{pmatrix}.$$

The Jacobian is well-defined, since \mathcal{F} is a polynomial and it can be explicitly computed being important for the implementation of the algorithm. We have the following

Lemma 3.27.

$$\langle J'(q), r \rangle = \int_{\Omega} (\mathbf{D} \mathcal{F}(f - \nabla q) \cdot \nabla r) \cdot \nabla \xi(q) \, dx, \quad q, r \in \mathcal{Q}.$$

Proof: We calculate

$$(3.92) \quad \langle J'(q), r \rangle = \lim_{t \rightarrow 0} \frac{1}{t} \{J(q + tr) - J(q)\}, \quad q, r \in \mathcal{Q}.$$

Using the Taylor expansion of \mathcal{F} , we observe:

$$(3.93) \quad \begin{aligned} & 2(J(q + tr) - J(q)) \\ &= \int_{\Omega} (\mathbf{K} \cdot \nabla \xi(q + tr)) \cdot \nabla \xi(q + tr) - (\mathbf{K} \cdot \nabla \xi(q)) \cdot \nabla \xi(q) \, dx \\ &= \int_{\Omega} \mathcal{F}(f - \nabla(q + tr)) \cdot \nabla \xi(q + tr) - \mathcal{F}(f - \nabla q) \cdot \nabla \xi(q) \, dx \\ &= \int_{\Omega} (\mathcal{F}(f - \nabla q) - t \mathbf{D} \mathcal{F}(f - \nabla q) \cdot \nabla r + o(t)) \cdot \nabla \xi(q + tr) \\ &\quad - \mathcal{F}(f - \nabla q) \cdot \nabla \xi(q) \, dx \\ &= \int_{\Omega} \mathcal{F}(f - \nabla q) \cdot (\nabla \xi(q + tr) - \nabla \xi(q)) \, dx \\ &\quad - \int_{\Omega} (t \mathbf{D} \mathcal{F}(f - \nabla q) \cdot \nabla r + o(t)) \cdot \nabla \xi(q + tr) \, dx. \end{aligned}$$

Using the variational formulation (3.91) and again the Taylor series of \mathcal{F} , we calculate

$$(3.94) \quad \begin{aligned} & \int_{\Omega} \mathcal{F}(f - \nabla q) \cdot (\nabla \xi(q + tr) - \nabla \xi(q)) \, dx \\ &= \int_{\Omega} (\mathbf{K} \cdot \nabla \xi(q + tr)) \cdot \nabla \xi(q) - (\mathbf{K} \cdot \nabla \xi(q)) \cdot \nabla \xi(q) \, dx \\ &= \int_{\Omega} \mathcal{F}(f - \nabla(q + tr)) \cdot \nabla \xi(q) - \mathcal{F}(f - \nabla q) \cdot \nabla \xi(q) \, dx \\ &= \int_{\Omega} (\mathcal{F}(f - \nabla q) - t \mathbf{D} \mathcal{F}(f - \nabla q) \cdot \nabla r + o(t)) \cdot \nabla \xi(q) \\ &\quad - \mathcal{F}(f - \nabla q) \cdot \nabla \xi(q) \, dx \\ &= - \int_{\Omega} (t \mathbf{D} \mathcal{F}(f - \nabla q) \cdot \nabla r + o(t)) \cdot \nabla \xi(q) \, dx. \end{aligned}$$

Combining (3.92), (3.93), (3.94) and going to the limit, one obtains the desired result. ■

REMARK 3.28. A comment analogue to Remark 3.25 can be made about the structure of $\langle J'(q), r \rangle$. The required continuity arguments in the limiting process of Lemma 3.27 are trivial.

The one-dimensional minimization problem (3.52) can be handled in a way very similar to the Navier-Stokes case considered above. Letting $q = p^n - \rho w^n$ in (3.91), we obtain

$$\begin{aligned} & \int_{\Omega} (\mathbf{K} \cdot \nabla \xi(p^n - \rho w^n)) \cdot \nabla r \, dx = \int_{\Omega} \mathcal{F}(f - \nabla(p^n - \rho w^n)) \cdot \nabla r \, dx \\ &= \int_{\Omega} \left(\sum_{ij} (f_1 - p_{x_1}^n + \rho w_{x_1}^n)^i (f_2 - p_{x_2}^n + \rho w_{x_2}^n)^j \begin{pmatrix} a_{ij} \\ b_{ij} \end{pmatrix} \right) \cdot \nabla r \, dx \\ &= \int_{\Omega} \left(\sum_{ij} P_{ij} \begin{pmatrix} a_{ij} \\ b_{ij} \end{pmatrix} \right) \cdot \nabla r \, dx, \quad \forall r \in \mathcal{Q}, \end{aligned}$$

where

$$P_{ij} = \sum_{k=0}^i \sum_{l=0}^j \binom{i}{k} \binom{j}{l} \rho^{k+l} (w_{x_1}^n)^k (w_{x_2}^n)^l (f_1 - p_{x_1}^n)^{i-k} (f_2 - p_{x_2}^n)^{j-l}.$$

As mentioned in the beginning of this section, the sums will be finite, i.e. $0 \leq i \leq i_{max}$ and $0 \leq j \leq j_{max}$ and therefore the right hand side of the variational problem is a polynomial in ρ having degree $N = i_{max} \cdot j_{max}$. Due to linearity, ξ^n can also be written as a polynomial in ρ , i.e.

$$(3.95) \quad \xi^n = \sum_{m=0}^N \rho^m \xi_m^n.$$

The ξ_m^n , $m = 0, \dots, N$ are determined by the variational problems

$$\int_{\Omega} (\mathbf{K} \cdot \nabla \xi_m^n) \cdot \nabla r \, dx = \int_{\Omega} \left(\sum_{ij} P_{ij}^m \begin{pmatrix} a_{ij} \\ b_{ij} \end{pmatrix} \right) \cdot \nabla r \, dx, \quad \forall r \in \mathcal{Q}$$

with

$$P_{ij}^m = \sum_{k=0}^i \sum_{l=0}^j \begin{cases} \binom{i}{k} \binom{j}{l} (w_{x_1}^n)^k (w_{x_2}^n)^l (f_1 - p_{x_1}^n)^{i-k} (f_2 - p_{x_2}^n)^{j-l}, & \text{if } k+l = m, \\ 0, & \text{else.} \end{cases}$$

Due to (3.95) the minimization problem (3.52) reads

$$(3.96) \quad \begin{aligned} \rho_n &= \underset{\rho \in \mathbb{R}_0^+}{\text{ArgMin}} J(p^n - \rho w^n) \\ &= \sum_{m_1=0}^N \sum_{m_2=0}^N \rho^{m_1+m_2} n_{m_1 m_2}, \end{aligned}$$

where

$$n_{m_1 m_2} = \int_{\Omega} (\mathbf{K} \cdot \nabla \xi_{m_1}^n) \cdot \nabla \xi_{m_2}^n dx.$$

By the considerations from above, the solution of the macro problem is reduced to the solutions of a sequence of linear elliptic equations for the gradient g^n and ξ_m^n . Again, the minimization problem (3.96) will be solved by a simple Newton method. If one wants to avoid the use of high order quadrature formulas to evaluate \mathcal{F} in its polynomial form, it is also reasonable to use the discrete values of the permeability function and apply some kind of interpolation. Therefore, one has to use a line search algorithm, like *golden section search* (see [59]), for the minimization problem (3.96). Consequently, we need to solve some linear problems to calculate ξ at certain points.

In case of a regular solution p , the convergence of the least-squares conjugate gradient method is due to the existence of the second derivative of the functional J .

Discretization. For the numerical study in the next section, we will restrict our considerations to $\Omega =]0, 1[{}^2$. Therefore, (3.87) will be approximated by biquadratic finite elements on square grids as introduced in 3.2.3.1. The approximation is of order $O(h^2)$, if the continuous solution is sufficiently regular (see [20] and references therein). In practice, $\int_{\Omega} q dy = 0$ will be circumvented by setting the solutions of the linear problems equal to zero at exactly one node of the mesh and by projecting them a posteriori in order to have zero average. The last important point is, that during the iterative computations, one has to make sure, that the arguments of \mathcal{F} stay in the valid range. (compare Theorem 3.5 and Remark 3.6).

3.3. Numerical results

3.3.1. Convergence of the algorithms. First, we study the convergence properties of the Uzawa algorithm used to solve Stokes problems on the periodicity cell $]0, 1[{}^2$. The periodicity cell is discretized by a 80×80 square finite element mesh. The cell is equipped with a square obstacle $Y_s = [0.3, 0.7]^2$. In Figure 6 the typical convergence behavior of the norm of the residual is illustrated. The norm of the residual is defined by

$$(3.97) \quad \sqrt{\|A_h u_h^j + B_h^T p_h^j - b_h\|^2 + \|B_h u_h^j\|^2} / \|b_h\|.$$

The dependence of the convergence rate on r is in complete accordance to the results given in [28].

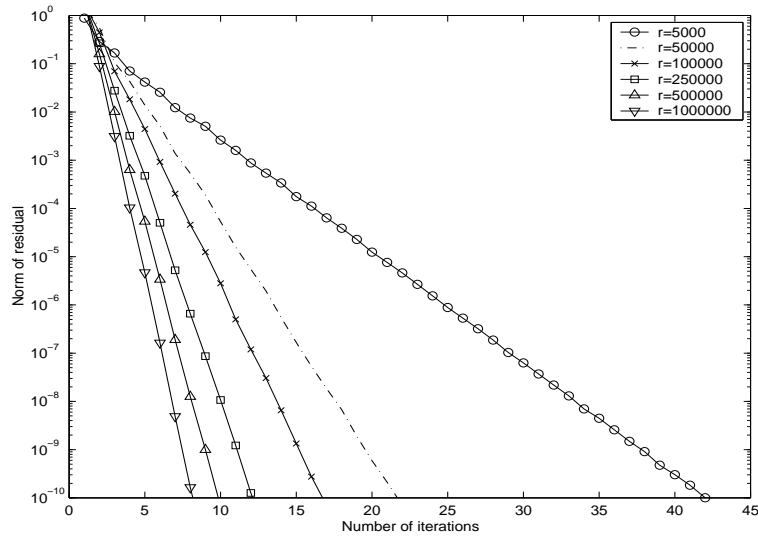


FIGURE 6. Convergence of the Stokes solver

Using the same periodicity cell as above, Figure 7 shows the convergence behavior of the least-squares conjugate gradient method, which we employ to solve the Navier-Stokes equations on the periodicity cell. Clearly, one observes the dependence of the convergence speed on the local viscosity μ , which again is a well-known fact (see [40]).

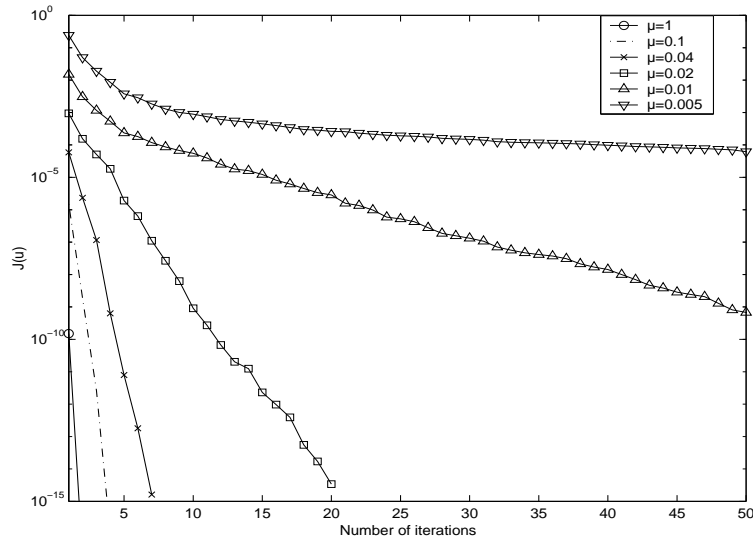


FIGURE 7. Navier-Stokes solver: Convergence of the least-squares conjugate gradient method

Now, we want to investigate the convergence of the Taylor-Hood finite element discretization used for the Navier-Stokes equations on the periodicity

cell. Therefore, we compute for a constant right hand side $f = (1, 0)^T$ at different mesh widths h and local viscosities μ the velocity and pressure solutions of the Navier-Stokes equations. To determine the convergence rate, we additionally compute reference solutions u^{ref} and p^{ref} on a 200×200 mesh and calculate for the velocity the relative L^2 and H_0^1 norms, i.e. $\frac{\|u^{ref}-u_h\|_{L^2(Y_f)^2}}{\|u^{ref}\|_{L^2(Y_f)^2}}$ and $\frac{\|u^{ref}-u_h\|_{H_0^1(Y_f)^2}}{\|u^{ref}\|_{H_0^1(Y_f)^2}}$, respectively. For the pressure, we consider the relative L^2 norm $\frac{\|p^{ref}-p_h\|_{L^2(Y_f)^2}}{\|p^{ref}\|_{L^2(Y_f)^2}}$. In each problem the Stokes residual is decreased to less than 10^{-12} . The nonlinear iteration is stopped, when $J(u) < 10^{-10}$. The data is listed in Table 1-3 and confirms the theoretical quadratic convergence of the velocity and linear convergence of the pressure. Note, that the finite element discretization error is independent of the local viscosity.

	$\mu = 1.00$	$\mu = 0.02$	$\mu = 0.01$	$\mu = 0.005$
$\frac{1}{h} = 10$	$1.48 * 10^{-1}$	$1.24 * 10^{-1}$	$1.09 * 10^{-1}$	$7.56 * 10^{-2}$
$\frac{1}{h} = 20$	$1.06 * 10^{-2}$	$8.75 * 10^{-3}$	$7.01 * 10^{-3}$	$6.40 * 10^{-3}$
$\frac{1}{h} = 40$	$4.23 * 10^{-3}$	$3.42 * 10^{-3}$	$2.59 * 10^{-3}$	$2.16 * 10^{-3}$
$\frac{1}{h} = 80$	$1.48 * 10^{-3}$	$1.20 * 10^{-3}$	$8.89 * 10^{-4}$	$7.03 * 10^{-4}$
$\frac{1}{h} = 160$	$2.42 * 10^{-4}$	$1.97 * 10^{-4}$	$1.48 * 10^{-4}$	$1.32 * 10^{-4}$

TABLE 1. Navier-Stokes solver: L^2 -convergence of the velocity

	$\mu = 1.00$	$\mu = 0.02$	$\mu = 0.01$	$\mu = 0.005$
$\frac{1}{h} = 10$	$5.29 * 10^{-1}$	$5.33 * 10^{-1}$	$5.35 * 10^{-1}$	$5.39 * 10^{-1}$
$\frac{1}{h} = 20$	$1.16 * 10^{-1}$	$1.17 * 10^{-1}$	$1.14 * 10^{-1}$	$1.17 * 10^{-1}$
$\frac{1}{h} = 40$	$7.59 * 10^{-2}$	$7.43 * 10^{-2}$	$6.90 * 10^{-2}$	$6.98 * 10^{-2}$
$\frac{1}{h} = 80$	$4.50 * 10^{-2}$	$4.35 * 10^{-2}$	$3.91 * 10^{-2}$	$3.75 * 10^{-2}$
$\frac{1}{h} = 160$	$1.48 * 10^{-2}$	$1.43 * 10^{-2}$	$1.27 * 10^{-2}$	$1.18 * 10^{-2}$

TABLE 2. Navier-Stokes solver: H_0^1 -convergence of the velocity

Analogous results for the macro solver are derived using the following setup. We consider $\Omega =]0, 1[^2 \setminus]0.3, 0.7]^2$ and put periodic boundary conditions for

	$\mu = 1.00$	$\mu = 0.02$	$\mu = 0.01$	$\mu = 0.005$
$\frac{1}{h} = 10$	$9.06 * 10^{-1}$	$7.69 * 10^{-1}$	$8.96 * 10^{-1}$	$1.32 * 10^0$
$\frac{1}{h} = 20$	$4.00 * 10^{-1}$	$3.25 * 10^{-1}$	$3.29 * 10^{-1}$	$4.30 * 10^{-1}$
$\frac{1}{h} = 40$	$2.66 * 10^{-1}$	$2.10 * 10^{-1}$	$2.04 * 10^{-1}$	$2.20 * 10^{-1}$
$\frac{1}{h} = 80$	$1.51 * 10^{-1}$	$1.17 * 10^{-1}$	$1.11 * 10^{-1}$	$1.17 * 10^{-1}$
$\frac{1}{h} = 160$	$4.07 * 10^{-2}$	$3.06 * 10^{-2}$	$2.84 * 10^{-2}$	$2.95 * 10^{-2}$

TABLE 3. Navier-Stokes solver: L^2 -convergence of the pressure

the pressure at $x_1 = 0$ and $x_1 = 1$. On the upper and lower outer boundary and on the boundary of the *macro obstacle*, the normal component of the velocity is equal to zero. The nonlinear filtration law which is used in the macro computations is presented in the next section. It is based on a square micro obstacle $Y_s = [0.27, 0.73]^2$. The right hand sides of the the Navier-Stokes solutions are discretized for $i = 1, \dots, 20$ and $j = 0, \dots, 69$ at $\alpha_{ij} = (r_i * \cos \phi_j, r_i * \sin \phi_j)^T$, $r_i = \frac{i}{20}$, $\phi_j = \frac{2\pi * i}{70}$ (compare Figure 1 of Chapter 3). The discrete data is bilinearly interpolated in polar coordinates. The mesh size of the micro problem is $h = 0.01$. Figure 8 shows the convergence of the least-squares conjugate gradient algorithm on a 80×80 mesh for $f = (0.25, 0)^T$. The convergence depends on the viscosity μ used in the computations of the filtration law.

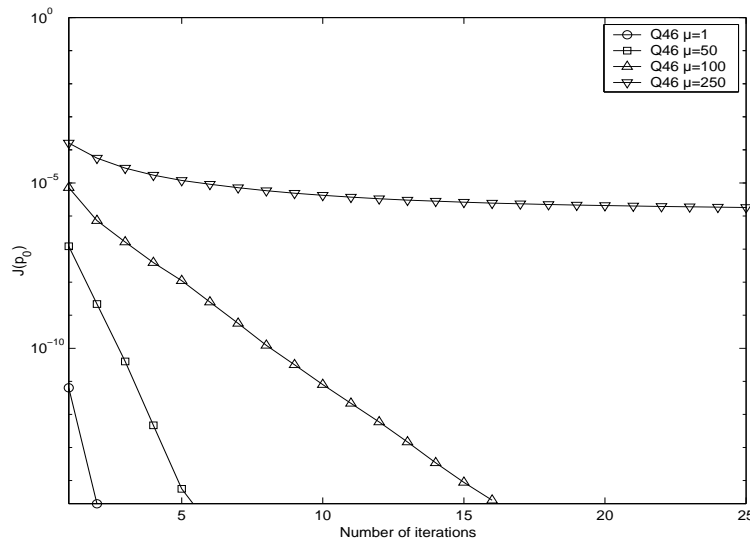


FIGURE 8. Macro solver: Convergence of the least-squares conjugate gradient method

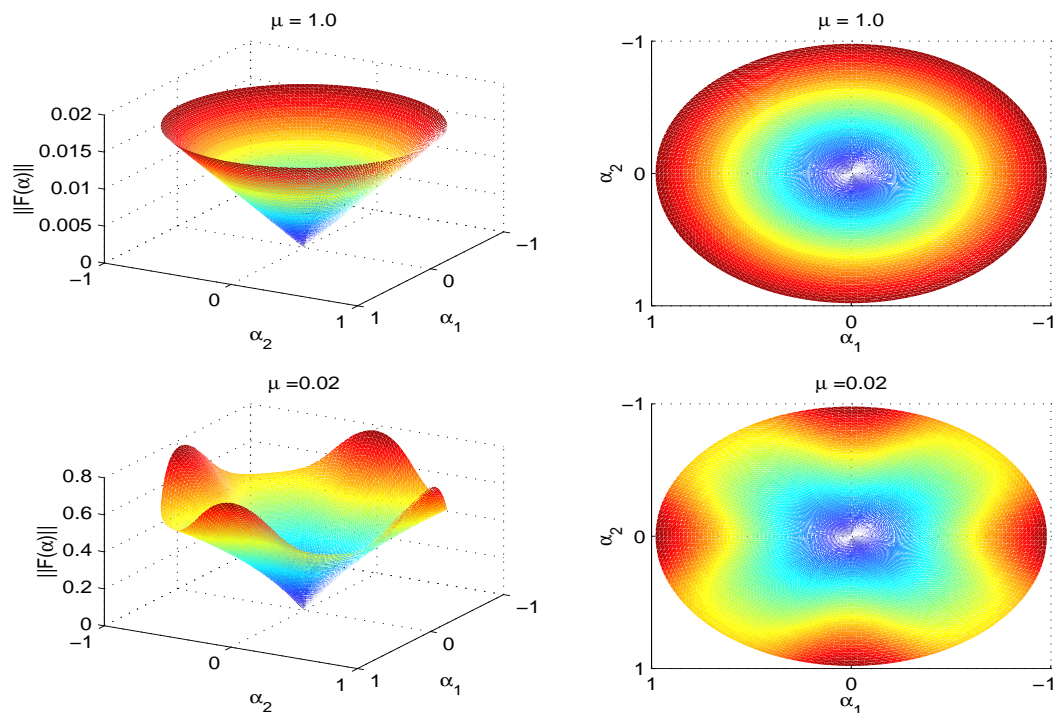
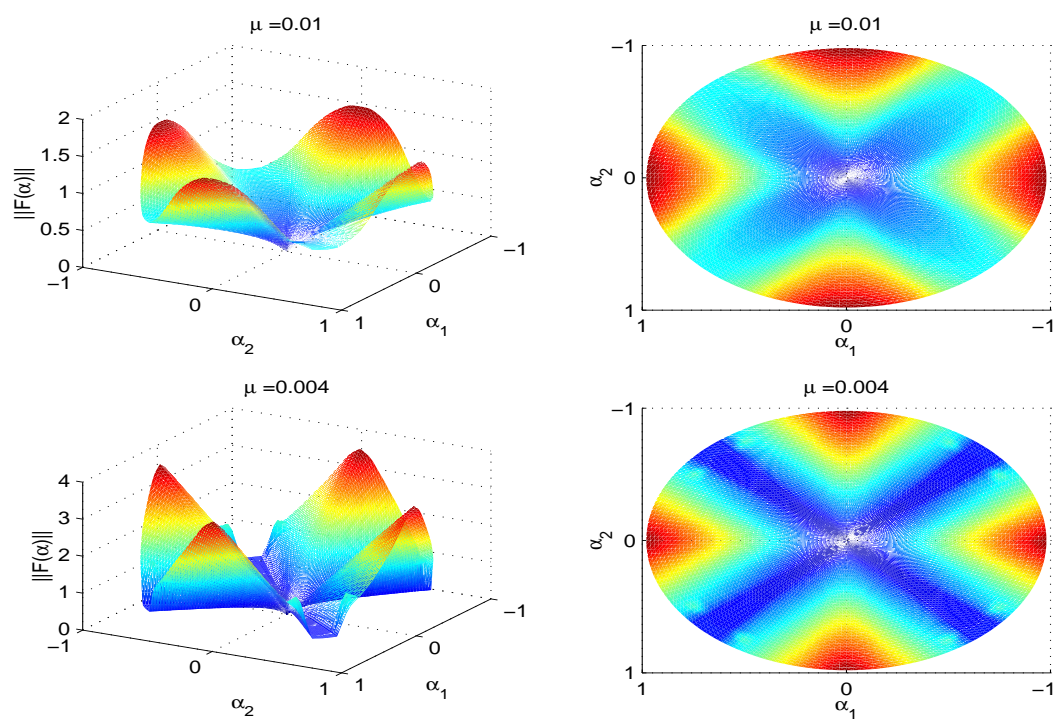
	$\frac{\ p^{ref}-p_h\ _{L^2(\Omega)^2}}{\ p^{ref}\ _{L^2(\Omega)^2}}$	$\frac{\ p^{ref}-p_h\ _{H_0^1(\Omega)^2}}{\ p^{ref}\ _{H_0^1(\Omega)^2}}$
$\frac{1}{h} = 10$	$2.03 * 10^{-1}$	$1.34 * 10^{-1}$
$\frac{1}{h} = 20$	$8.23 * 10^{-2}$	$9.93 * 10^{-2}$
$\frac{1}{h} = 40$	$3.92 * 10^{-2}$	$4.26 * 10^{-2}$
$\frac{1}{h} = 80$	$1.42 * 10^{-2}$	$2.11 * 10^{-2}$
$\frac{1}{h} = 160$	$5.28 * 10^{-3}$	$8.24 * 10^{-3}$

TABLE 4. Macro solver: Convergence of the pressure

In order to show the finite element convergence, we use the above filtration law with $\mu = 0.01$. The reference solution for the pressure is obtained on a 200×200 mesh. The data is presented in Table 4. The convergence rate is better than first order.

3.3.2. Model problems. We start our numerical investigation by computing nonlinear filtration laws for various micro obstacles. The basic setup has already been described in the previous section: We use a 100×100 mesh and compute Navier-Stokes solutions for α_{ij} . By averaging the velocities, we discretely obtain values of the permeability function (see Section 3.1). The Navier-Stokes solutions are computed to a precision of $J(u) < 10^{-10}$ in all subsequent cases.

First, we consider a square obstacle S . It is defined by two corner points $P1 = (0.27, 0.27)$ and $P2 = (0.73, 0.73)$. We use four different values for the viscosity, i.e. $\mu = 1, 0.02, 0.01$ and 0.004 . Note, that in all subsequent cases, the solution for $\mu = 1$ can always be associated with the linear Stokes solution. In Figure 9 and 10, the norm of the permeability function is plotted against the discretized *force plane* using different viscosities. For $\mu = 1$, we find an isotropic law. With decreasing viscosity, the dependence on the direction of the force becomes more and more obvious. The reason for the appearing anisotropic behavior lies in the differently developing recirculation zones as the viscosity becomes smaller. Stream function plots and vector plots of the velocity at different viscosities and forces are shown in Figure 11 and 12. The recirculation zones reduce the effective free flow domain and, hence, decrease the permeability significantly.

FIGURE 9. Obstacle S : $\|\mathcal{F}(\alpha)\|$ for $\mu = 1$ and $\mu = 0.02$ FIGURE 10. Obstacle S : $\|\mathcal{F}(\alpha)\|$ for $\mu = 0.01$ and $\mu = 0.04$

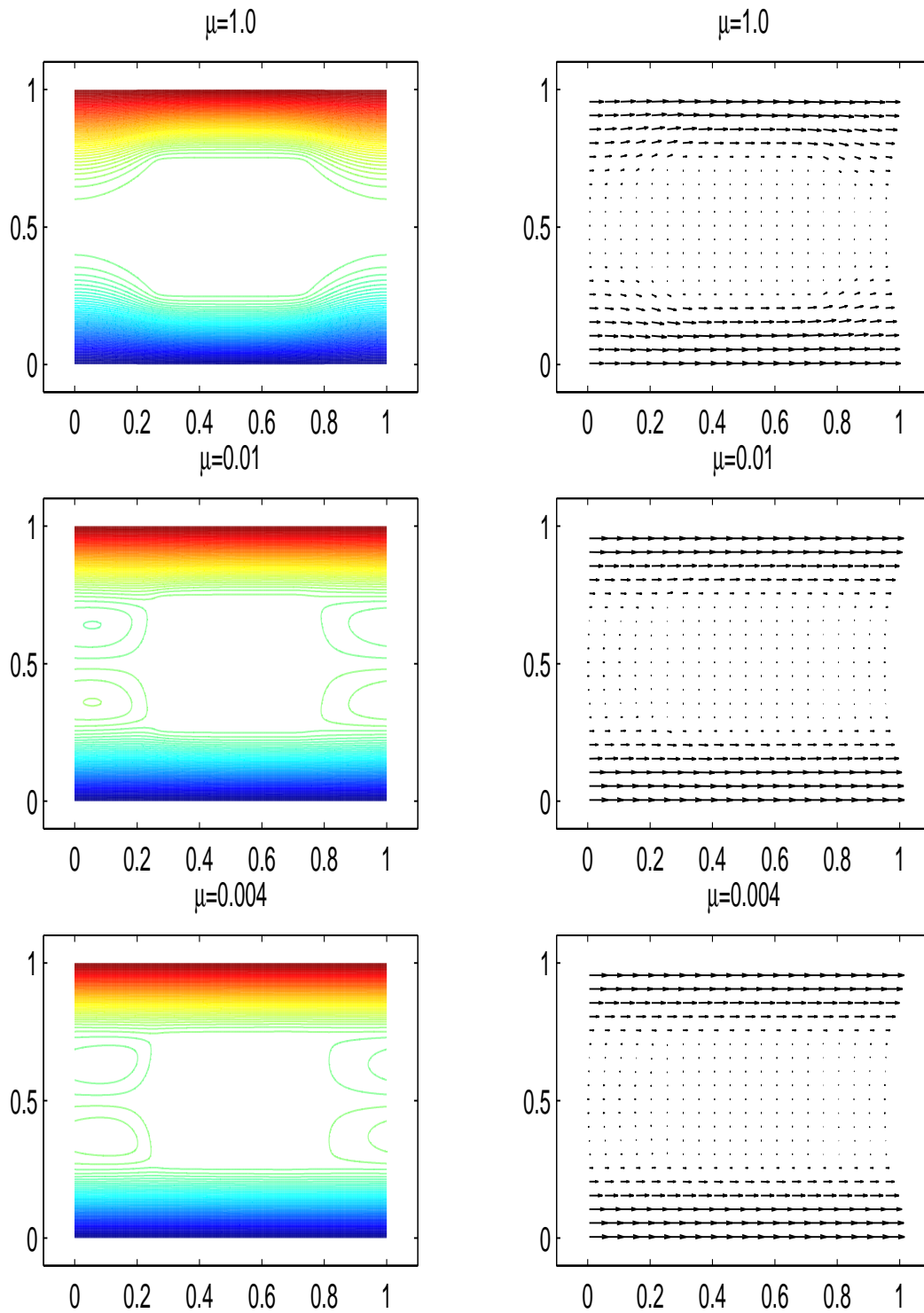


FIGURE 11. Obstacle S : Velocity for different viscosities and $\alpha = (1, 0)^T$

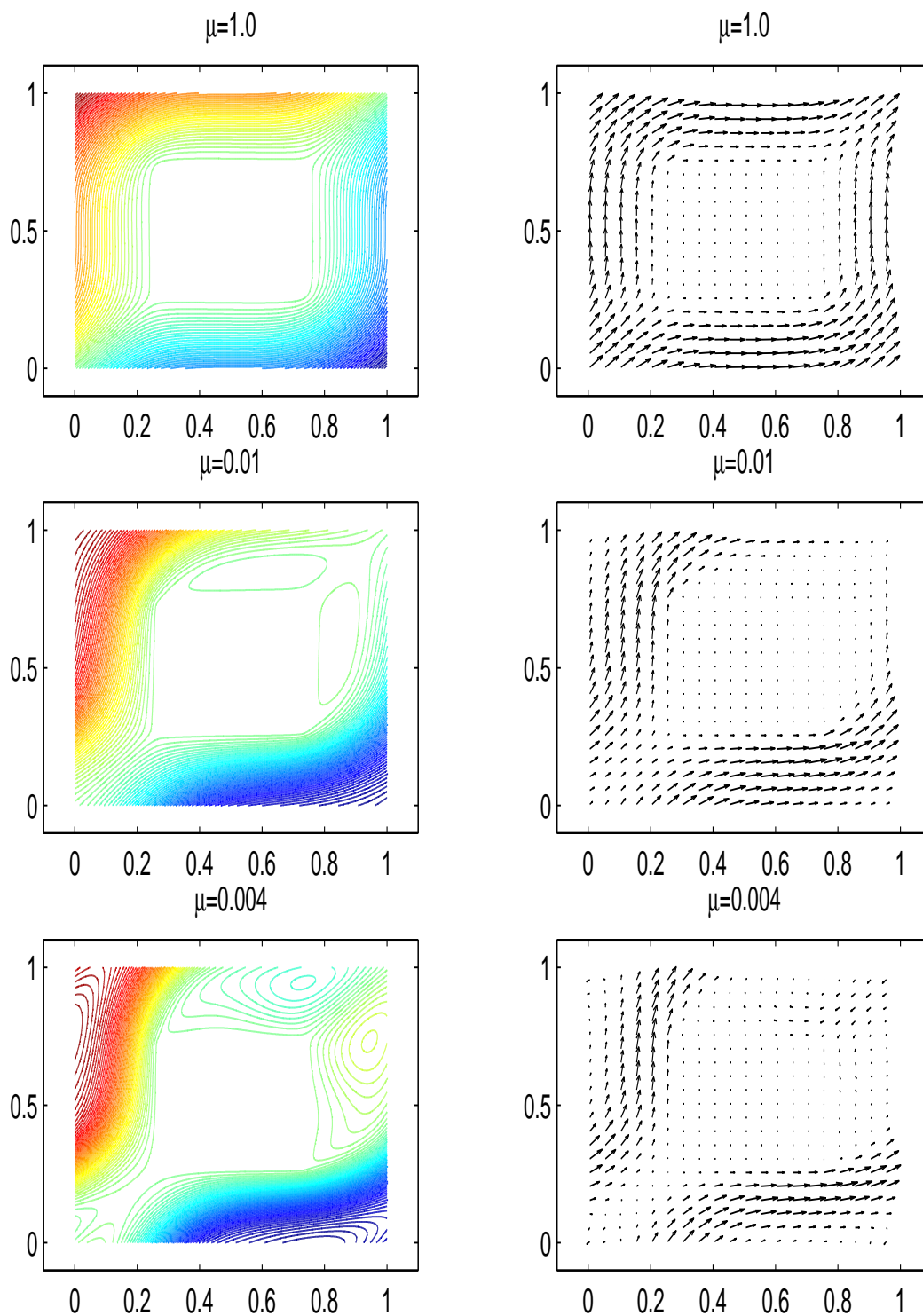


FIGURE 12. Obstacle S : Velocity for different viscosities and $\alpha = (\sqrt{2}^{-1}, \sqrt{2}^{-1})^T$

The second obstacle in consideration is defined by its corner points $P1 = (0.03, 0.47)$, $P2 = (0.91, 0.47)$, $P3 = (0.91, 0.27)$, $P4 = (0.97, 0.27)$, $P5 = (0.97, 0.73)$, $P6 = (0.91, 0.73)$, $P7 = (0.91, 0.53)$ and $P8 = (0.03, 0.53)$. It is denoted by T . The associated permeability function is strongly anisotropic even in the linear case. As illustrated in Figure 13, its anisotropic character is hardly changed when the viscosity decreases. Nevertheless, recirculation zones are created (see Figure 14 and 15), which lower the permeability relative to the linear case when using the same viscosity.

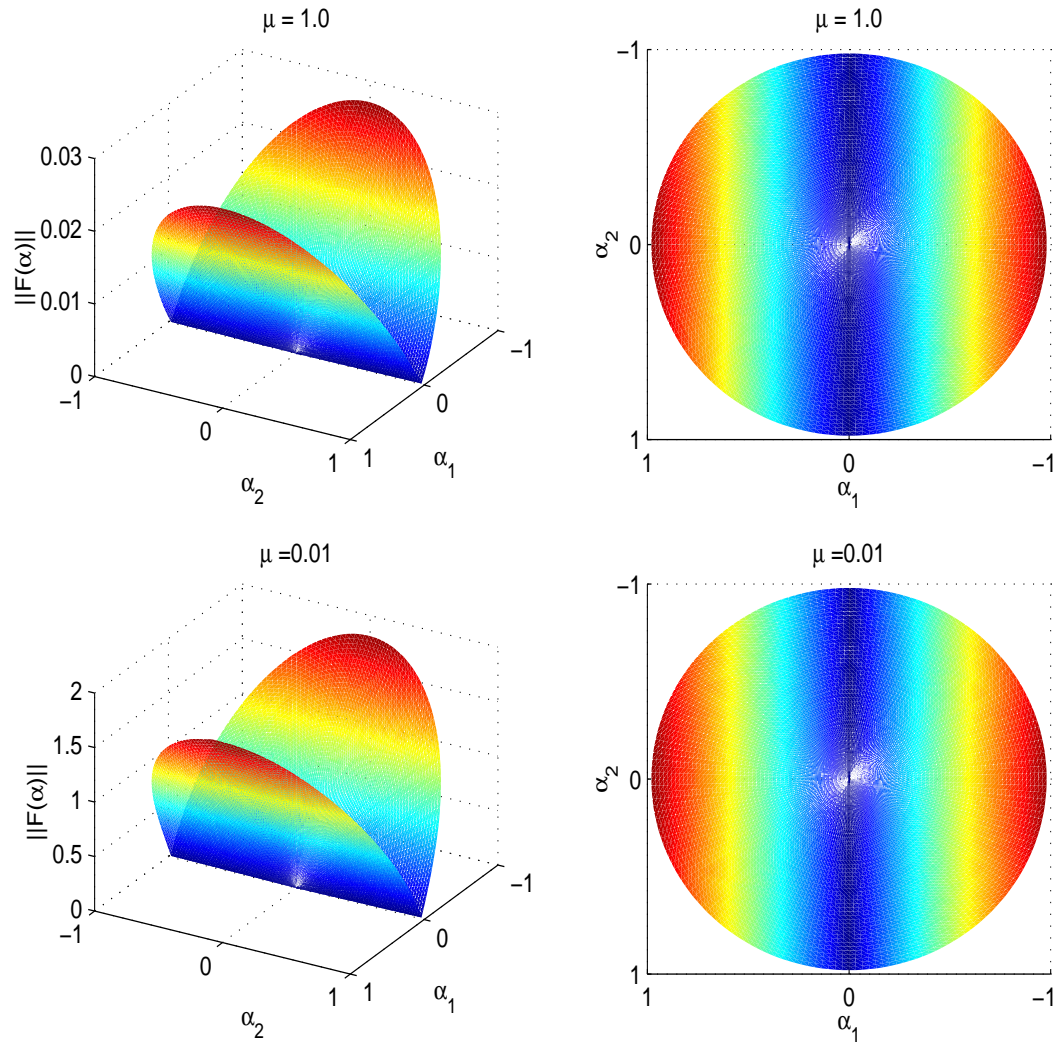


FIGURE 13. Obstacle T : $\|\mathcal{F}(\alpha)\|$ for $\mu = 1$ and $\mu = 0.01$

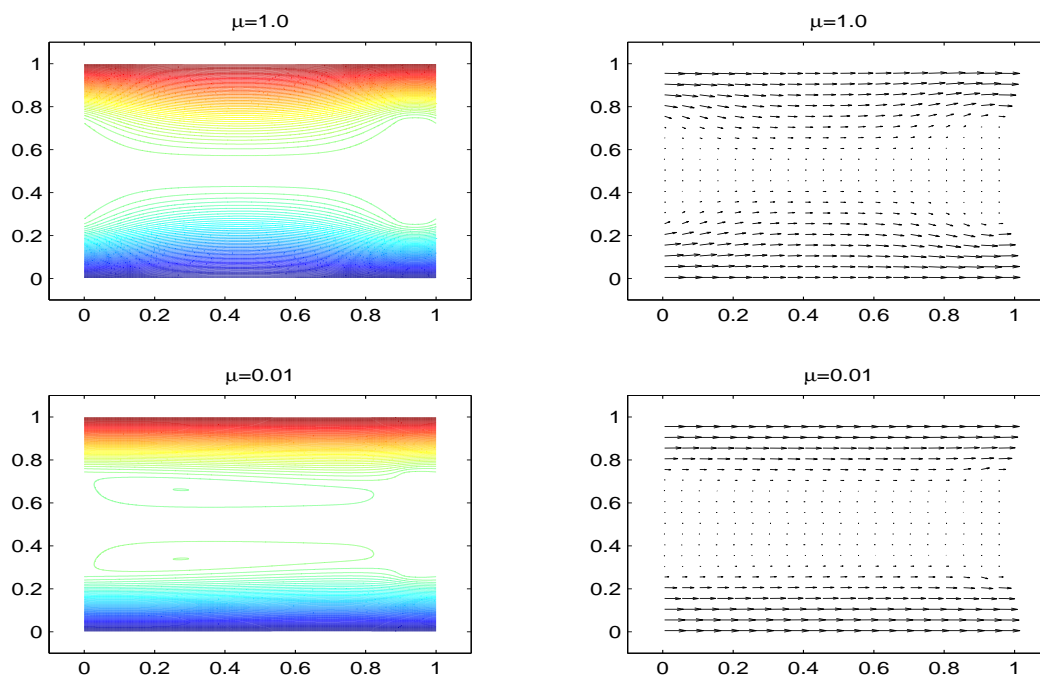


FIGURE 14. Obstacle T : Velocity for different viscosities and $\alpha = (1, 0)^T$

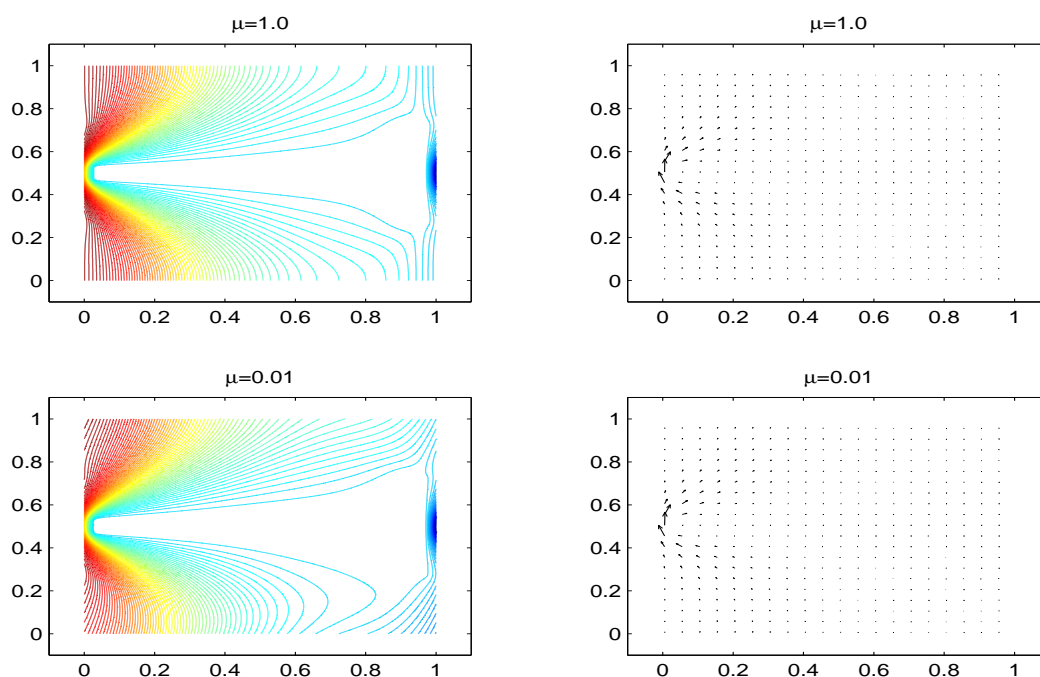


FIGURE 15. Obstacle T : Velocity for different viscosities and $\alpha = (0, 1)^T$

The third obstacle is a triangle denoted by D and defined by its corner points $P1 = (0.5, 0.5)$, $P2 = (0.95, 0.12)$ and $P3 = (0.95, 0.88)$. As for obstacle T , we obtain an anisotropic law. However, by decreasing the viscosity, its character changes as shown in Figure 16 and 17.

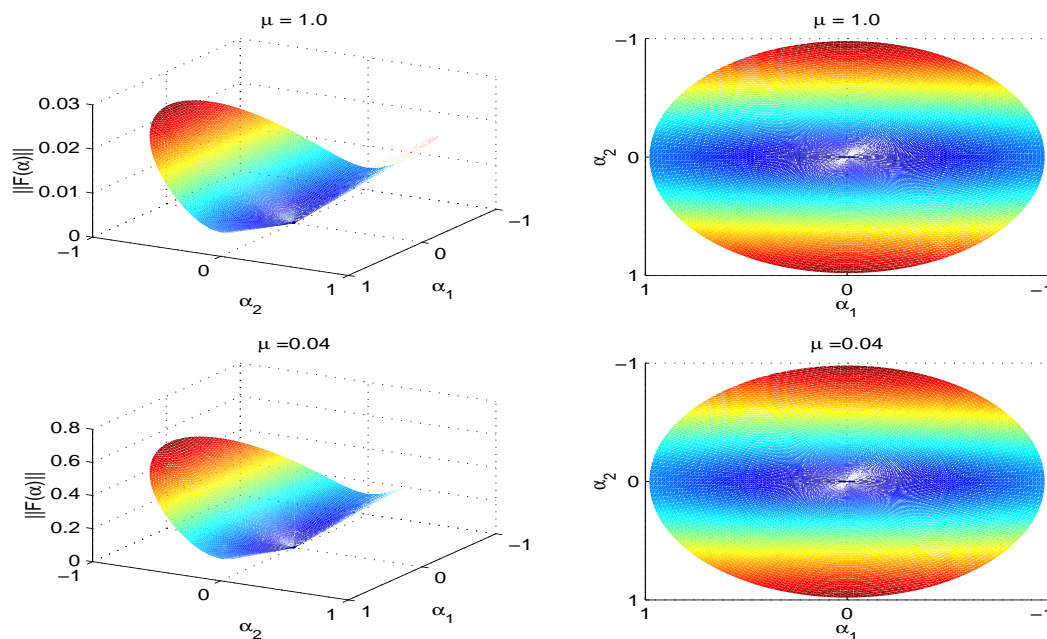


FIGURE 16. Obstacle D : $\|\mathcal{F}(\alpha)\|$ for $\mu = 1$ and $\mu = 0.04$

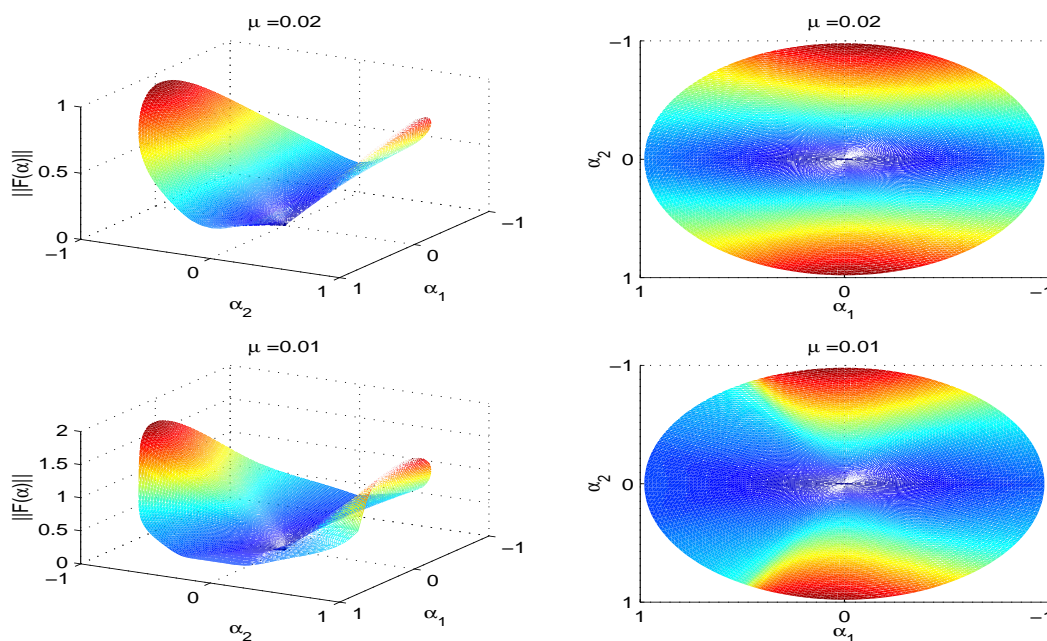


FIGURE 17. Obstacle D : $\|\mathcal{F}(\alpha)\|$ for $\mu = 0.02$ and $\mu = 0.01$

In Figure 18 and 19, velocities related to obstacle D are plotted.

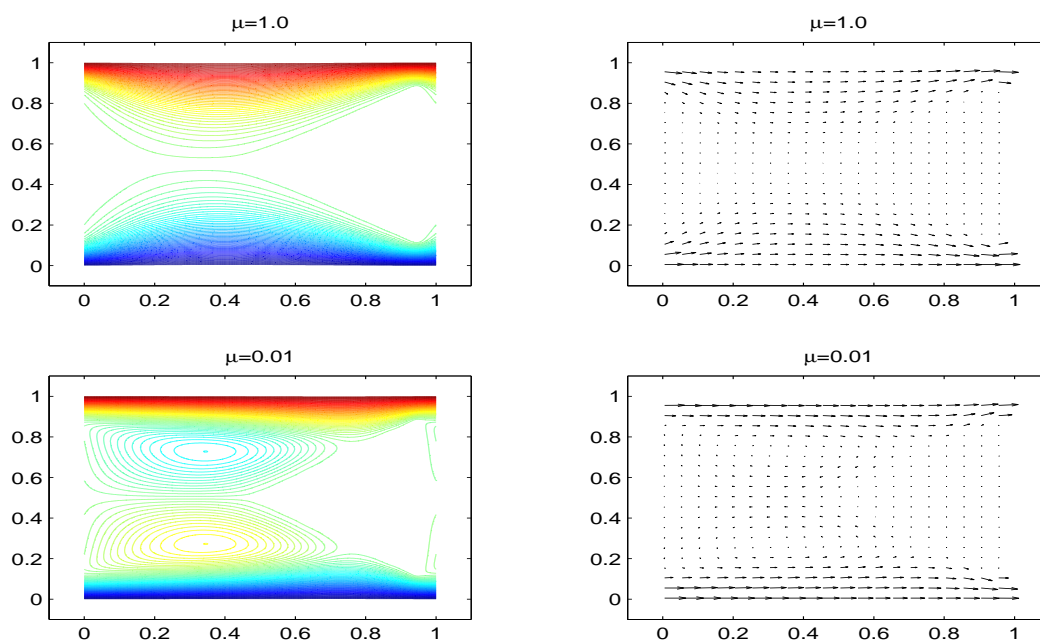


FIGURE 18. Obstacle D : Velocity for different viscosities and $\alpha = (1, 0)^T$

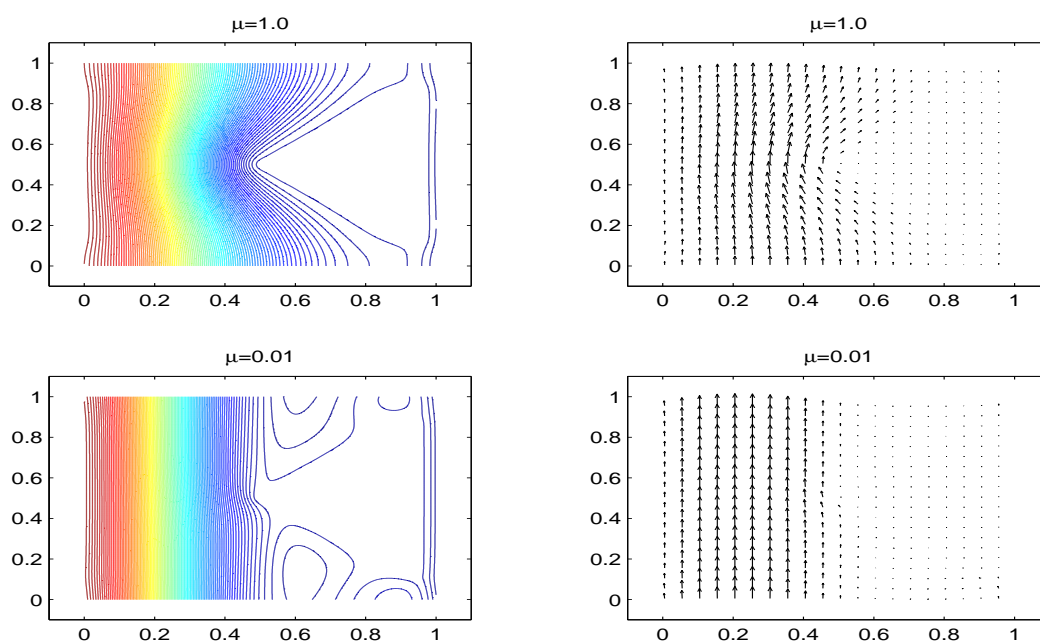


FIGURE 19. Obstacle D : Velocity for different viscosities and $\alpha = (0, 1)^T$

In Figure 20, we show filtration laws which are produced by equally distributing 25 square obstacles of edge length 0.14 over the periodicity cell. This configuration creates a strong and selective anisotropy along the main axis.

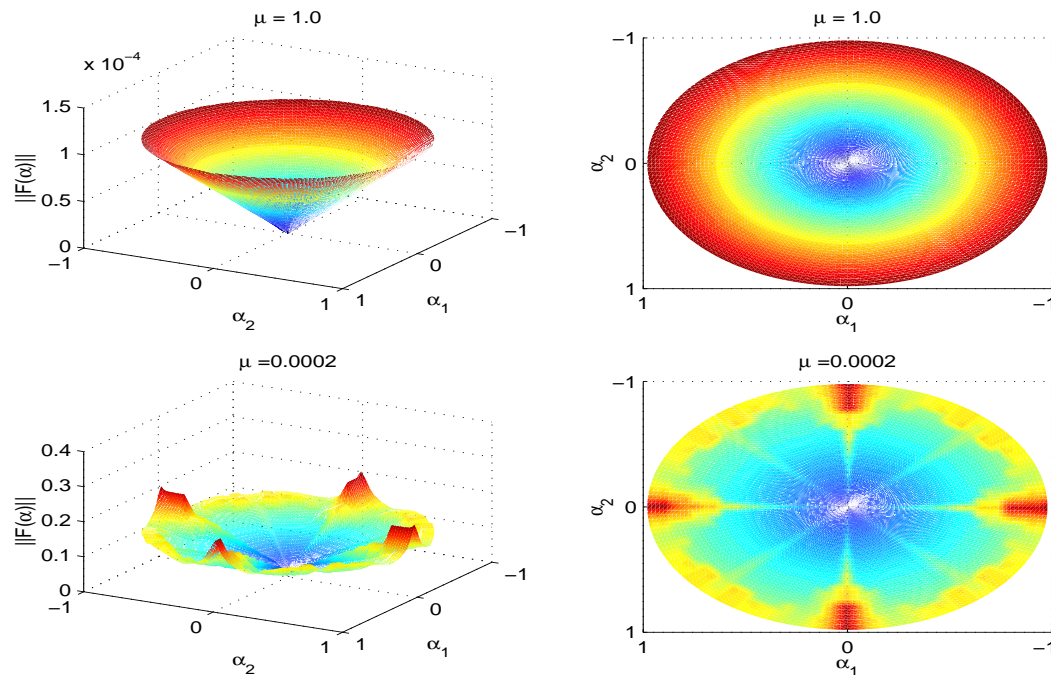


FIGURE 20. 25 square obstacles: $\|\mathcal{F}\|$ for $\mu = 1$ and $\mu = 0.0002$

The purpose of Figure 21 is to show how flow rates may deviate when passing from the linear to the nonlinear equations. A circle of radius 0.4 in the center of the periodicity cell is used. The force is aligned to the x-axis. The viscosity is set to $\mu = 0.0002$.

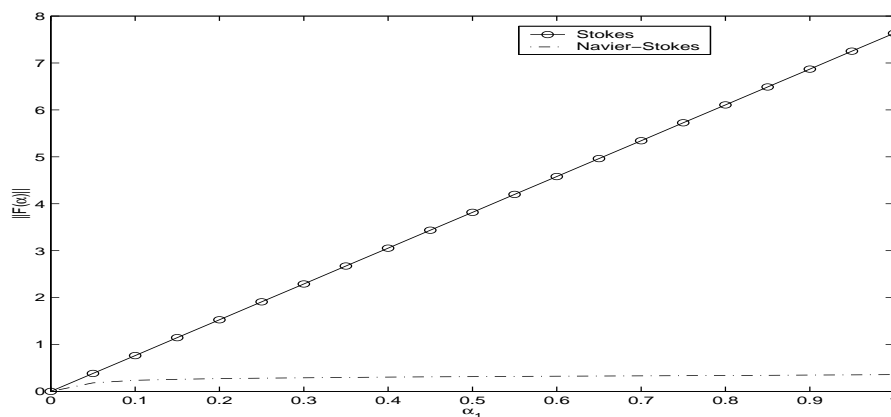


FIGURE 21. Obstacle circle: Comparison of linear and nonlinear filtration law

In Figure 21, the permeability function stays almost constant when α_1 is increased. Since the Navier-Stokes equations are not monotone, it is most probable that there exist setups of obstacles and viscosities, which lead to an decreasing permeability function if the force increases.

Now, we turn to the computation of the Taylor coefficients of the permeability function and the least-squares fits of the discrete data from above. Computing the constant σ_0 introduced in Section 3.1 for the obstacle S yields $\sigma_0 = 1.84 * 10^{-4}$. The constant σ_3 will become even smaller depending on the viscosity μ . Hence, the theoretically proved validity of the Taylor expansion is quite limited to small forces. In contrast, the discrete data is computed using a discretization of the unit circle in \mathbb{R}^2 . Therefore, it is not surprising, that the Taylor coefficients and the fitted coefficients may deviate.

In Table 5-7, we list the non-zero coefficients up to order seven which are related to the obstacle S . For $\mu = 1$, both approaches essentially yield a linear law. For $\mu = 0.02$, also higher order terms appear. Note, that only coefficients related to odd powers show up. The odd filtration law is due to the antisymmetry of the solutions of the Navier-Stokes equations, i.e. $w(\alpha) = -w(-\alpha)$, in case of the symmetric obstacle S . The antisymmetric response is also given in case of general isotropic periodicity cells. Then, without any numerical computation, one concludes by inverting the velocity-pressure relation, i.e. \mathcal{F} , that the first nonlinear term with respect to the velocity in the Forchheimer law must be cubic (see [51]).

In Table 8-10, the coefficients related to obstacle T are presented. Again, for $\mu = 1.0$, a linear filtration law is obtained. Since T is not symmetric, also even order contributions are observed. Analogously, in Table 11-13, we give the results for obstacle D .

REMARK 3.29. Finally, we want to remark, that the question for the first nonlinear term extending Darcy's law is of course interesting. It is addressed in many papers and books. However, the presented data shows, that, in general, nonlinear extensions of Darcy's law can not be accurately obtained by considering only one extra term.

	\mathcal{F}_1	\mathcal{F}_2
α_1	$1.68 * 10^{-2}$	0.0
α_2	0.0	$1.68 * 10^{-2}$

TABLE 5. Obstacle S : Taylor (=fitted) coefficients for $\mu = 1.0$

	\mathcal{F}_1	\mathcal{F}_2		\mathcal{F}_1	\mathcal{F}_2
α_1	$4.19 * 10^{-1}$	0.0	α_1	$8.14 * 10^{-1}$	0.0
α_2	0.0	$4.19 * 10^{-1}$	α_2	0.0	$8.14 * 10^{-1}$
α_1^3	$-7.02 * 10^{-3}$	0.0	α_1^3	$-1.47 * 10^{-1}$	0.0
$\alpha_1^2 \alpha_2$	0.0	$-1.27 * 10^{-1}$	$\alpha_1^2 \alpha_2$	0.0	$-1.45 * 10^0$
$\alpha_1 \alpha_2^2$	$-1.27 * 10^{-1}$	0.0	$\alpha_1 \alpha_2^2$	$-1.45 * 10^0$	0.0
α_2^3	0.0	$-7.02 * 10^{-3}$	α_2^3	0.0	$-1.47 * 10^{-1}$
α_1^5	$2.52 * 10^{-3}$	0.0	α_1^5	$2.39 * 10^{-1}$	0.0
$\alpha_1^4 \alpha_2$	0.0	$1.79 * 10^{-1}$	$\alpha_1^4 \alpha_2$	0.0	$2.72 * 10^0$
$\alpha_1^3 \alpha_2^2$	$7.61 * 10^{-4}$	0.0	$\alpha_1^3 \alpha_2^2$	$1.00 * 10^{-1}$	0.0
$\alpha_1^2 \alpha_2^3$	0.0	$7.61 * 10^{-4}$	$\alpha_1^2 \alpha_2^3$	0.0	$1.00 * 10^{-1}$
$\alpha_1 \alpha_2^4$	$1.79 * 10^{-1}$	0.0	$\alpha_1 \alpha_2^4$	$2.72 * 10^0$	0.0
α_2^5	0.0	$2.52 * 10^{-3}$	α_2^5	0.0	$2.39 * 10^{-1}$
α_1^7	$-1.19 * 10^{-3}$	0.0	α_1^7	$-1.02 * 10^{-1}$	0.0
$\alpha_1^6 \alpha_2$	0.0	$-2.95 * 10^{-1}$	$\alpha_1^6 \alpha_2$	0.0	$-1.86 * 10^{-1}$
$\alpha_1^5 \alpha_2^2$	$-3.62 * 10^{-3}$	0.0	$\alpha_1^5 \alpha_2^2$	$-3.22 * 10^{-1}$	0.0
$\alpha_1^4 \alpha_2^3$	0.0	$-4.84 * 10^{-2}$	$\alpha_1^4 \alpha_2^3$	0.0	$3.57 * 10^{-1}$
$\alpha_1^3 \alpha_2^4$	$-4.84 * 10^{-2}$	0.0	$\alpha_1^3 \alpha_2^4$	$3.57 * 10^{-1}$	0.0
$\alpha_1^2 \alpha_2^5$	0.0	$-3.62 * 10^{-3}$	$\alpha_1^2 \alpha_2^5$	0.0	$-3.22 * 10^{-1}$
$\alpha_1 \alpha_2^6$	$-2.95 * 10^{-1}$	0.0	$\alpha_1 \alpha_2^6$	$-1.86 * 10^{-1}$	0.0
α_2^7	0.0	$-1.19 * 10^{-3}$	α_2^7	0.0	$-1.02 * 10^{-1}$

TABLE 6. Obstacle S :
Taylor coefficients for
 $\mu = 0.02$ TABLE 7. Obstacle S :
Fitted coefficients for
 $\mu = 0.02$

	\mathcal{F}_1	\mathcal{F}_2
α_1	$2.78 * 10^{-2}$	0.0
α_2	0.0	$1.34 * 10^{-4}$

TABLE 8. Obstacle T : Taylor (=fitted) coefficients for $\mu = 1.0$

	\mathcal{F}_1	\mathcal{F}_2
α_1	$1.39 * 10^0$	0.0
α_2	0.0	$6.69 * 10^{-3}$
α_1^2	$7.64 * 10^{-11}$	0.0
$\alpha_1\alpha_2$	0.0	$-2.60 * 10^{-4}$
α_2^2	$2.60 * 10^{-4}$	0.0
α_1^3	$-3.76 * 10^0$	0.0
$\alpha_1^2\alpha_2$	0.0	$-6.36 * 10^{-4}$
$\alpha_1\alpha_2^2$	$-6.92 * 10^{-4}$	0.0
α_2^3	0.0	$-5.94 * 10^{-7}$
α_1^4	$-1.07 * 10^{-5}$	0.0
$\alpha_1^3\alpha_2$	0.0	$2.38 * 10^{-3}$
$\alpha_1^2\alpha_2^2$	$-3.13 * 10^{-3}$	0.0
$\alpha_1\alpha_2^3$	0.0	$1.83 * 10^{-7}$
α_2^4	$-1.46 * 10^{-7}$	0.0
α_1^5	$7.72 * 10^1$	0.0
$\alpha_1^4\alpha_2$	0.0	$2.21 * 10^{-2}$
$\alpha_1^3\alpha_2^2$	$2.74 * 10^{-5}$	0.0
$\alpha_1^2\alpha_2^3$	0.0	$1.50 * 10^{-6}$
$\alpha_1\alpha_2^4$	$3.39 * 10^{-7}$	0.0
α_2^5	0.0	$1.56 * 10^{-10}$

TABLE 9. Obstacle T :
Taylor coefficients for
 $\mu = 0.02$

	\mathcal{F}_1	\mathcal{F}_2
α_1	$2.30 * 10^0$	$5.74 * 10^{-3}$
α_2	0.0	$1.27 * 10^{-2}$
α_1^2	$-1.69 * 10^{-5}$	$2.28 * 10^{-2}$
$\alpha_1\alpha_2$	0.0	$-8.26 * 10^{-3}$
α_2^2	$1.75 * 10^{-3}$	$-7.42 * 10^{-3}$
α_1^3	$-1.86 * 10^0$	$1.34 * 10^{-2}$
$\alpha_1^2\alpha_2$	0.0	$-1.25 * 10^{-2}$
$\alpha_1\alpha_2^2$	$-1.72 * 10^{-1}$	$-5.20 * 10^{-2}$
α_2^3	0.0	$4.88 * 10^{-3}$
α_1^4	$1.94 * 10^{-5}$	$-1.12 * 10^{-2}$
$\alpha_1^3\alpha_2$	0.0	$-2.50 * 10^{-2}$
$\alpha_1^2\alpha_2^2$	$5.89 * 10^{-3}$	$-1.56 * 10^{-1}$
$\alpha_1\alpha_2^3$	0.0	$4.08 * 10^{-2}$
α_2^4	$1.88 * 10^{-4}$	$3.32 * 10^{-2}$
α_1^5	$2.86 * 10^0$	$-3.77 * 10^{-3}$
$\alpha_1^4\alpha_2$	0.0	$-4.16 * 10^{-3}$
$\alpha_1^3\alpha_2^2$	$6.83 * 10^{-1}$	$-3.46 * 10^{-2}$
$\alpha_1^2\alpha_2^3$	0.0	$3.56 * 10^{-2}$
$\alpha_1\alpha_2^4$	$2.08 * 10^{-1}$	$7.09 * 10^{-2}$
α_2^5	0.0	$-6.66 * 10^{-3}$

TABLE 10. Obstacle T :
Fitted coefficients for
 $\mu = 0.02$

	\mathcal{F}_1	\mathcal{F}_2
α_1	$5.34 * 10^{-3}$	0.0
α_2	0.0	$2.31 * 10^{-2}$

TABLE 11. Obstacle D : Taylor (=fitted) coefficients for $\mu = 1.0$

	\mathcal{F}_1	\mathcal{F}_2
α_1	$2.67 * 10^{-1}$	0.0
α_2	0.0	$1.15 * 10^0$
α_1^2	$-2.67 * 10^{-7}$	0.0
$\alpha_1\alpha_2$	0.0	$-3.16 * 10^{-1}$
α_2^2	$3.16 * 10^{-1}$	0.0
α_1^3	$-6.17 * 10^{-2}$	0.0
$\alpha_1^2\alpha_2$	0.0	$-4.73 * 10^{-1}$
$\alpha_1\alpha_2^2$	$-7.67 * 10^{-1}$	0.0
α_2^3	0.0	$-3.78 * 10^0$
α_1^4	$-1.51 * 10^{-2}$	0.0
$\alpha_1^3\alpha_2$	0.0	$8.08 * 10^{-1}$
$\alpha_1^2\alpha_2^2$	$-5.61 * 10^{-1}$	0.0
$\alpha_1\alpha_2^3$	0.0	$1.44 * 10^1$
α_2^4	$-1.33 * 10^1$	0.0
α_1^5	$4.76 * 10^{-2}$	0.0
$\alpha_1^4\alpha_2$	0.0	$1.88 * 10^0$
$\alpha_1^3\alpha_2^2$	$5.86 * 10^{-1}$	0.0
$\alpha_1^2\alpha_2^3$	0.0	$-1.70 * 10^1$
$\alpha_1\alpha_2^4$	$4.80 * 10^1$	0.0
α_2^5	0.0	$1.45 * 10^2$

TABLE 12. Obstacle D :
Taylor coefficients for
 $\mu = 0.02$

	\mathcal{F}_1	\mathcal{F}_2
α_1	$2.64 * 10^{-1}$	0.0
α_2	0.0	$1.10 * 10^0$
α_1^2	$1.21 * 10^{-2}$	0.0
$\alpha_1\alpha_2$	0.0	$-1.33 * 10^{-1}$
α_2^2	$7.38 * 10^{-2}$	0.0
α_1^3	$-5.83 * 10^{-2}$	0.0
$\alpha_1^2\alpha_2$	0.0	$-5.41 * 10^{-1}$
$\alpha_1\alpha_2^2$	$-1.66 * 10^{-1}$	0.0
α_2^3	0.0	$-5.63 * 10^{-1}$
α_1^4	$-3.56 * 10^{-2}$	0.0
$\alpha_1^3\alpha_2$	0.0	$1.44 * 10^{-1}$
$\alpha_1^2\alpha_2^2$	$6.29 * 10^{-3}$	0.0
$\alpha_1\alpha_2^3$	0.0	$1.22 * 10^{-1}$
α_2^4	$-1.74 * 10^{-1}$	0.0
α_1^5	$2.33 * 10^{-2}$	0.0
$\alpha_1^4\alpha_2$	0.0	$7.48 * 10^{-1}$
$\alpha_1^3\alpha_2^2$	$1.84 * 10^{-1}$	0.0
$\alpha_1^2\alpha_2^3$	0.0	$-1.26 * 10^{-1}$
$\alpha_1\alpha_2^4$	$1.82 * 10^{-1}$	0.0
α_2^5	0.0	$8.26 * 10^{-1}$

TABLE 13. Obstacle D :
Fitted coefficients for
 $\mu = 0.02$

We close this section by presenting numerical results concerning the macro problem. As in the previous section, we consider $\Omega =]0, 1[^2 \setminus]0.3, 0.7[^2$ and put periodic boundary conditions for the pressure at $x_1 = 0$ and $x_1 = 1$. On the upper and lower outer boundary and on the boundary of the *macro obstacle*, the normal component of the velocity is equal to zero. The filtration laws are related to obstacle S at various viscosities μ . The macro problems are solved to a precision of $J(p) < 10^{-13}$ on a mesh of size 80×80 . The force is chosen to be $f = (0.25, 0)^T$ insuring, that the solution stays in the valid range of the applied filtration laws. In Figure 22, 23, vector plots of the velocities for $\mu = 1.0, 0.02, 0.01$ and 0.004 are shown.

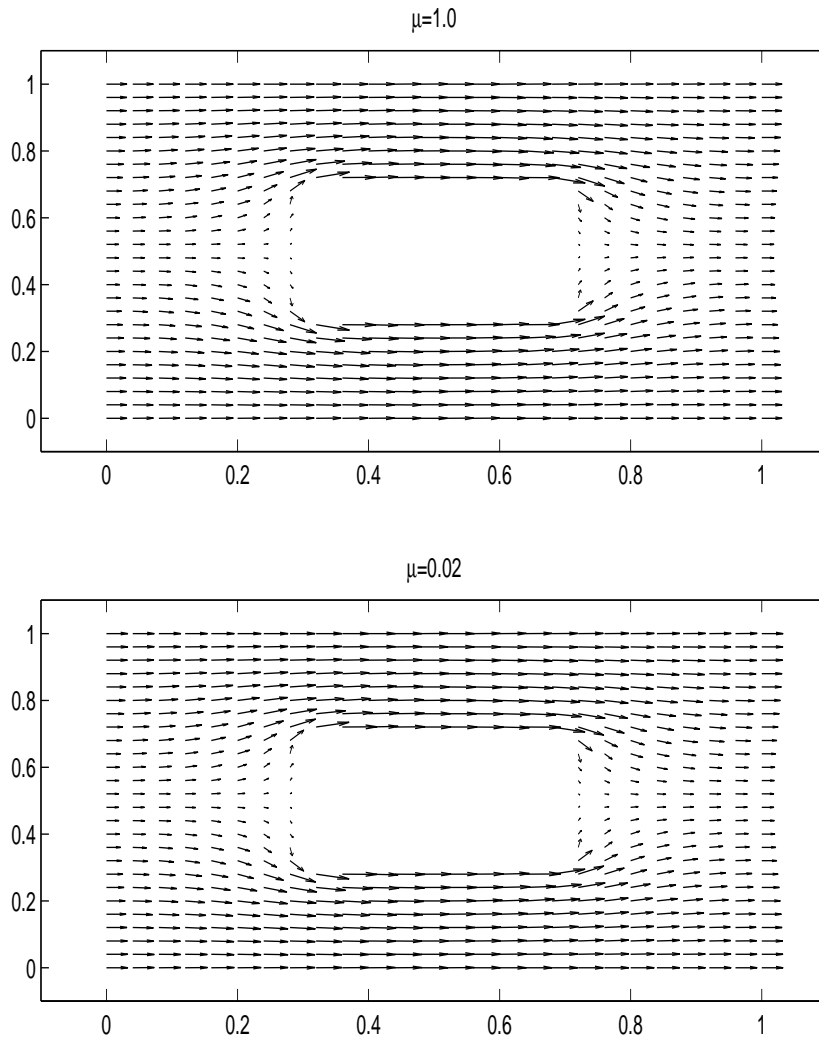
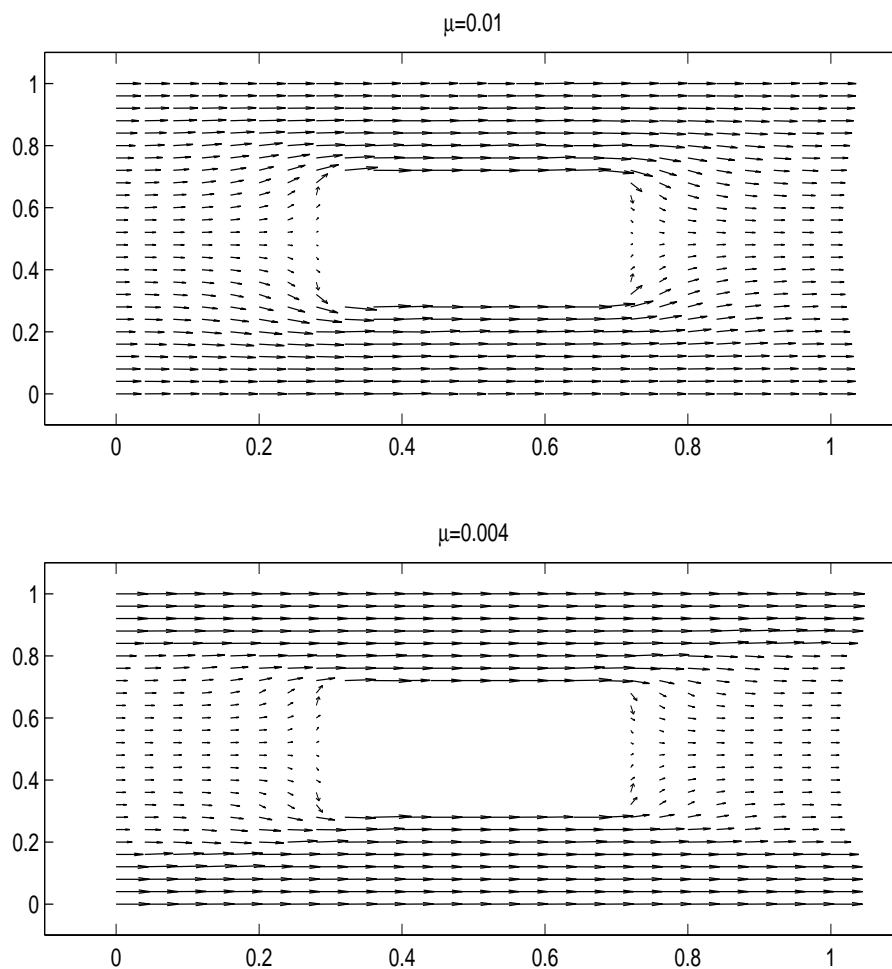


FIGURE 22. Macro problem: Velocity for $\mu = 1.0, 0.02$

FIGURE 23. Macro problem: Velocity for $\mu = 0.01, 0.004$

Since the underlying filtration becomes more and more anisotropic as μ decreases, the velocities do not only decrease relative to the linear case (see Table 14), but also the flow pattern is changed significantly.

$\int_{\Omega} u_1 dx$	Darcy	Nonlinear Law
$\mu = 1.0$	0.0035	0.0035
$\mu = 0.02$	0.1761	0.1717
$\mu = 0.01$	0.3523	0.3103
$\mu = 0.004$	0.8807	0.6619

TABLE 14. Comparison of flow rates at $f = (0.25, 0)^T$

The next picture illustrates the macroscopic pressure for $\mu = 1.0$ and $\mu = 0.004$.

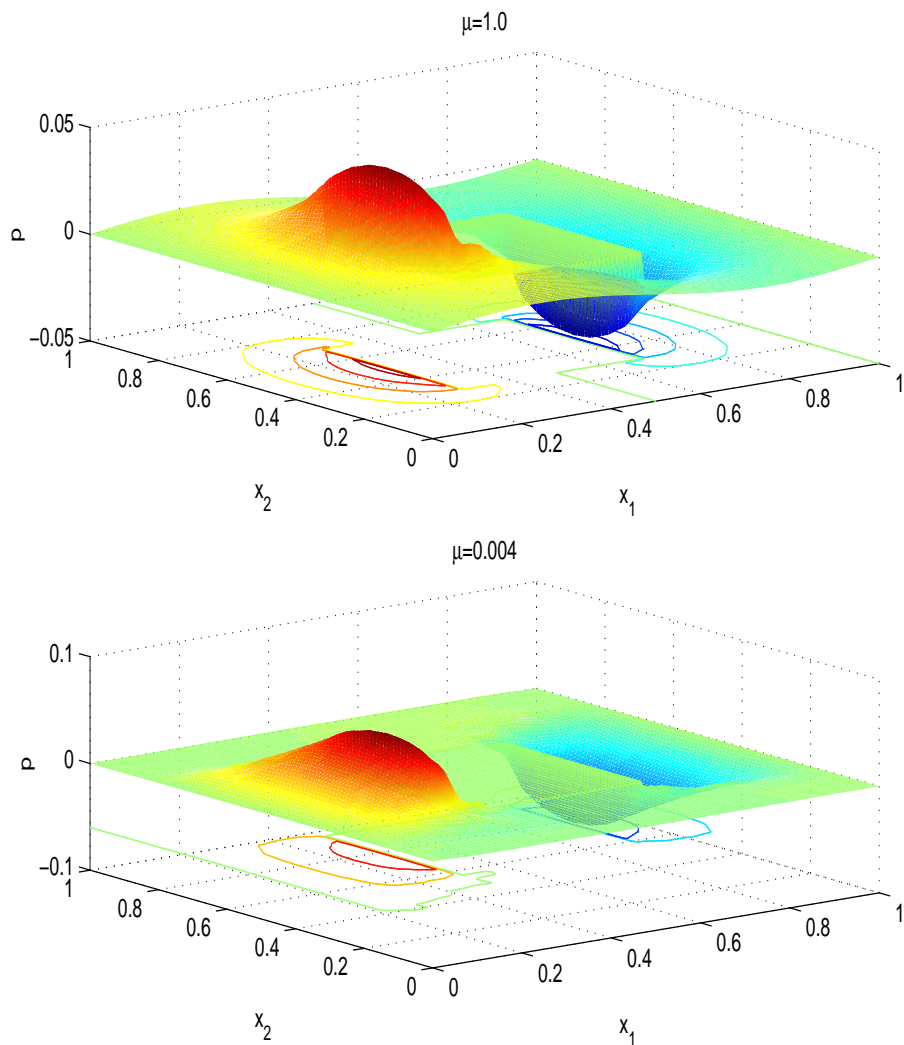


FIGURE 24. Macro problem: Pressure for $\mu = 1.0, 0.004$

CHAPTER 4

Numerical solution of the full two pressure system

In this chapter we are concerned with the numerical solution of the Navier-Stokes system with two pressures. The algorithm, that we propose, does not explicitly split the problem into micro and macro problems, but solves the full system. Starting from a two-dimensional setting of the porous medium, a four-dimensional problem in the domain $\Omega \times Y_f$ is obtained.

We will proceed as follows. First, a variational formulation of the Navier-Stokes system with two pressures is derived. The Hilbert space setting corresponds to the usual setting, in which the Stokes system with two pressures is formulated. Then, in view of the least-squares conjugate gradient algorithm introduced in Section 3.2.2, we define a functional J . Its minimization leads to a sequence of Stokes systems with two pressures. The crucial point here is, that the right hand sides depend on the variable y associated with the micro scale. Hence, computing two cell problems to obtain the permeability tensor \mathcal{K} and then solving the macro problem for the pressure p_0 is not possible. Nevertheless, we extend the idea to compute cell problems in the following way: Instead of solving two Stokes systems on the periodicity cell with constant forces aligned to the coordinate axis, we select a nodal finite element basis on Y and solve a Stokes problem for each basis function. Hence, the solution of the partial differential equation with respect to the micro scale is reduced to a simple assignment operation. To calculate the macroscopic pressure p_0 , we have to solve the usual two-dimensional linear elliptic problem.

The final section of this chapter contains a presentation of numerical results.

4.1. Numerical solution algorithm

Formulation of the problem. Let $\Omega = Y =]0, 1[^2$ be the macro domain and the periodicity cell, respectively. By Y_s and Y_f , we denote the solid part and fluid part of the periodicity cell Y , respectively. For the reader's convenience, we restate the Navier-Stokes system with two pressures. It reads

$$(4.1) \quad \left\{ \begin{array}{l} -\mu \Delta_y u_0(x, y) + (u_0(x, y) \cdot \nabla_y) u_0(x, y) \\ \quad + \nabla_y p_1(x, y) = f(x) - \nabla_x p_0(x) \quad \text{in } \Omega \times Y_f, \\ \quad \quad \quad \text{div}_y u_0(x, y) = 0 \quad \text{in } \Omega \times Y_f, \\ \quad \quad \quad u_0(x, y) = 0 \quad \text{on } \Omega \times \partial Y_s, \\ \quad \quad \quad \{u_0, p_1\} \text{ is } Y\text{-periodic,} \end{array} \right.$$

$$(4.2) \quad \left\{ \begin{array}{l} \text{div}_x \int_{Y_f} u_0(x, y) dy = 0 \quad \text{in } \Omega, \\ \quad \nu(x) \cdot \int_{Y_f} u_0(x, y) dy \quad \text{is } \Gamma_1\text{-antiperiodic,} \\ \quad \quad \quad p_0 \quad \text{is } \Gamma_1\text{-periodic,} \\ \quad \nu(x) \cdot \int_{Y_f} u_0(x, y) dy = 0 \quad \text{on } \Gamma_2, \end{array} \right.$$

where the solution (u_0, p_0, p_1) is assumed to be an element of $\mathcal{V} \times \mathcal{Q}^0 \times \mathcal{Q}^1$. The spaces \mathcal{V} , \mathcal{Q}^0 , \mathcal{Q}^1 are introduced in Section 2.3. $\mu \in \mathbb{R}^+$ and $f \in L^2(Y_f)^2$ are the given viscosity and force density, respectively.

Skipping the explicit dependence on the variable x and y , a weak formulation of (4.1), (4.2) is given by:

$$(4.3) \quad \begin{array}{l} \text{Find } u_0 \in \mathcal{V}, \text{ such that} \\ \mu \int_{\Omega} \int_{Y_f} \nabla_y u_0 : \nabla_y v dy dx + \int_{\Omega} \int_{Y_f} (u_0 \cdot \nabla_y) u_0 \cdot v dy dx \\ \quad - \int_{\Omega} \int_{Y_f} f \cdot v dy dx = 0, \quad \forall v \in \mathcal{V}. \end{array}$$

In (4.3) the pressures p_0 and p_1 are eliminated due to the divergence free functions in \mathcal{V} .

REMARK 4.1. The spaces might seem quite natural for a variational formulation indicated by the linear case, i.e. the Stokes system with two pressures. However, unique existence of solutions of (4.1), (4.2) in this Hilbert space setting has not been proved up to now. According to [56], a proof would be hard to accomplish, since the system lacks higher derivatives with respect to the macro variable x , and is therefore not easy to *control*.

Now, we define

$$\begin{aligned} \langle S(v), w \rangle &:= \mu \int_{\Omega} \int_{Y_f} \nabla_y v : \nabla_y w \, dy \, dx \\ &+ \int_{\Omega} \int_{Y_f} (v \cdot \nabla_y) v \cdot w \, dy \, dx - \int_{\Omega} \int_{Y_f} f \cdot w \, dy \, dx, \quad v, w \in \mathcal{V}, \end{aligned}$$

where $\langle \cdot, \cdot \rangle$ is the duality pairing of \mathcal{V}' and \mathcal{V} . Problem (4.3) is equivalent to:

$$(4.4) \quad \begin{aligned} &\text{Find } u_0 \in \mathcal{V}, \text{ such that} \\ &S(u_0) = 0, \end{aligned}$$

where $S(u_0)$ has to be understood as element of \mathcal{V}' . The linearity of $S(u_0)$ is obvious. Continuity for the bilinear and linear forms follows by applying the continuity properties of the classical bilinear and linear forms a and l (see Proof of Lemma 3.24 for the definition) and the Cauchy-Schwarz inequality in the space $L^2(\Omega)^2$. Showing continuity for the trilinear form is more difficult. In fact, it can not be concluded without higher regularity assumptions on the functions in \mathcal{V} . Assuming H^1 regularity with respect to the variable x , one could deduce continuity in the following way: First, one has to apply continuity of the classical trilinear form b (see again Proof of Lemma 3.24 for the definition). Then, the generalized Hölder inequality (see [29], p.22) and suitable Sobolev embedding theorems can be used to obtain the result. The latter reasoning is quite analogous to the proof of continuity of the classical trilinear form b (see [30], p. 6ff).

Least-squares formulation. Proceeding as in the general case of Section 3.2.2, we derive a functional $J : \mathcal{V} \rightarrow \mathbb{R}$. It reads

$$(4.5) \quad J(v) = \frac{1}{2} \|S(v)\|_{\mathcal{V}'}^2 = \frac{1}{2} \mu \int_{\Omega} \int_{Y_f} |\nabla_y \xi(v)|^2 \, dy \, dx, \quad v \in \mathcal{V}.$$

ξ is a nonlinear function of v determined by (3.48), which is an equation in \mathcal{V}' . The corresponding variational problem defined in \mathcal{V} reads:

$$(4.6) \quad \begin{aligned} &\text{Given } v \in \mathcal{V}. \text{ Find } \xi(v) \in \mathcal{V}, \text{ such that} \\ &(\xi(v), w)_{\mathcal{V}} = \langle S(v), w \rangle, \quad \forall w \in \mathcal{V}. \end{aligned}$$

REMARK 4.2. Rewriting variational problem (4.6) as partial differential equations, we recover the following Stokes system with two pressures:

$$\left\{ \begin{array}{l} -\mu \Delta_y \xi(v) + \nabla_y \tilde{p}_1 + \nabla_x \tilde{p}_0 = -\mu \Delta_y v \\ \quad \quad \quad + (v \cdot \nabla_y) v - f \quad \text{in } \Omega \times Y_f, \\ \operatorname{div}_y \xi(v) = 0 \quad \text{in } \Omega \times Y_f, \\ \xi(v) = 0 \quad \text{on } \Omega \times \partial Y_s, \\ \{\xi(v), \tilde{p}_1\} \text{ is } Y\text{-periodic,} \end{array} \right.$$

$$\left\{ \begin{array}{l} \operatorname{div}_x \int_{Y_f} \xi(v) dy = 0 \quad \text{in } \Omega, \\ \nu \cdot \int_{Y_f} \xi(v) dy \quad \text{is } \Gamma_1\text{-antiperiodic,} \\ \tilde{p}_0 \quad \text{is } \Gamma_1\text{-periodic,} \\ \nu \cdot \int_{Y_f} \xi(v) dy = 0 \quad \text{on } \Gamma_2. \end{array} \right.$$

Note, that setting $v = u_0$, the following relations hold: $p_0 = -\tilde{p}_0$ and $p_1 = -\tilde{p}_1$.

Finally, an equivalent minimization problem to (4.4) reads:

$$(4.7) \quad \begin{array}{l} \text{Find } u_0 \in \mathcal{V}, \text{ such that} \\ J(u_0) \leq J(v), \quad \forall v \in \mathcal{V}. \end{array}$$

Solution of the least-squares problem. Due to the structural similarity of the Navier-Stokes system with two pressures and the ordinary Navier-Stokes system, it is not surprising, that during the minimization quite similar problems have to be solved. Once we have assumed continuity of the trilinear form, the derivations can just be copied with minor changes in notation. The nontrivial problems of the minimization process are the computation of the gradient g^j in (3.50), (3.54) and the one-dimensional minimization problem (3.52).

In complete analogy to Remark 4.2, we observe that finding g^j requires the solution of a Stokes problem with two pressures. Its variational formulation is given by

$$(4.8) \quad \begin{array}{l} \text{Find } g^j \in \mathcal{V}, \text{ such that} \\ \mu \int_{\Omega} \int_{Y_f} \nabla_y g^j : \nabla_y v dy dx = \langle J'(u_0^j), v \rangle, \quad \forall v \in \mathcal{V}. \end{array}$$

The right hand side is given due to the following

Lemma 4.3. *The Fréchet-derivative of the functional J at $v \in \mathcal{V}$ is given by*

$$\begin{aligned} \langle J'(v), w \rangle &= \mu \int_{\Omega} \int_{Y_f} \nabla_y w : \nabla_y \xi(v) dy dx + \int_{\Omega} \int_{Y_f} (v \cdot \nabla_y) w \cdot \xi(v) dy dx \\ &\quad + \int_{\Omega} \int_{Y_f} (w \cdot \nabla_y) v \cdot \xi(v) dy dx, \quad w \in \mathcal{V}. \end{aligned}$$

Proof: See Proof of Lemma 3.24. ■

The one-dimensional minimization problem (3.52) is derived as in Section

3.2.3.2 by letting $v = u_0^j - \rho w^j$ in (4.6). Then, $\forall z \in \mathcal{V}$ we obtain

$$\begin{aligned}
& \mu \int_{\Omega} \int_{Y_f} \nabla_y \xi^j (u_0^j - \rho w^j) : \nabla_y z \, dy \, dx \\
= & \mu \int_{\Omega} \int_{Y_f} \nabla_y (u_0^j - \rho w^j) : \nabla_y z \, dy \, dx \\
& + \int_{\Omega} \int_{Y_f} ((u_0^j - \rho w^j) \cdot \nabla_y) (u_0^j - \rho w^j) \cdot z \, dy \, dx - \int_{\Omega} \int_{Y_f} f \cdot z \, dy \, dx \\
= & \mu \int_{\Omega} \int_{Y_f} \nabla_y u_0^j : \nabla_y z \, dy \, dx + \int_{\Omega} \int_{Y_f} (u_0^j \cdot \nabla_y) u_0^j \cdot z \, dy \, dx \\
& - \int_{\Omega} \int_{Y_f} f \cdot z \, dy \, dx \\
& - \rho \left\{ \mu \int_{\Omega} \int_{Y_f} \nabla_y w^j : \nabla_y z \, dy \, dx + \int_{\Omega} \int_{Y_f} (u_0^j \cdot \nabla_y) w^j \cdot z \, dy \, dx \right. \\
& \quad \left. + \int_{\Omega} \int_{Y_f} (w^j \cdot \nabla_y) u_0^j \cdot z \, dy \, dx \right\} \\
& + \rho^2 \int_{\Omega} \int_{Y_f} (w^j \cdot \nabla_y) w^j \cdot z \, dy \, dx.
\end{aligned}$$

Due to linearity of the variational problem for ξ^j , we can expand ξ^j as polynomial in ρ , i.e.

$$(4.9) \quad \xi^j = \xi_0^j + \rho \xi_1^j + \rho^2 \xi_2^j,$$

where $\xi_i^j \in \mathcal{V}$, $i = 0, 1, 2$ are determined by the following variational problems:

$$\begin{aligned}
(4.10) \quad & \mu \int_{\Omega} \int_{Y_f} \nabla_y \xi_0^j : \nabla_y z \, dy \, dx = \mu \int_{\Omega} \int_{Y_f} \nabla_y u_0^j \cdot \nabla_y z \, dy \, dx \\
& + \int_{\Omega} \int_{Y_f} (u_0^j \cdot \nabla_y) u_0^j \cdot z \, dy \, dx - \int_{\Omega} \int_{Y_f} f \cdot z \, dy \, dx, \quad \forall z \in \mathcal{V},
\end{aligned}$$

$$\begin{aligned}
(4.11) \quad & \mu \int_{\Omega} \int_{Y_f} \nabla_y \xi_1^j : \nabla_y z \, dy \, dx = -\mu \int_{\Omega} \int_{Y_f} \nabla_y w^j : \nabla_y z \, dy \, dx \\
& - \int_{\Omega} \int_{Y_f} (u_0^j \cdot \nabla_y) w^j \cdot z \, dy \, dx - \int_{\Omega} \int_{Y_f} (w^j \cdot \nabla_y) u_0^j \cdot z \, dy \, dx, \quad \forall z \in \mathcal{V},
\end{aligned}$$

$$(4.12) \quad \mu \int_{\Omega} \int_{Y_f} \nabla_y \xi_2^j : \nabla_y z \, dy \, dx = \int_{\Omega} \int_{Y_f} (w^j \cdot \nabla_y) w^j \cdot z \, dy \, dx, \quad \forall z \in \mathcal{V}.$$

Due to (4.9), the minimization problem (3.52) can be formulated as

$$(4.13) \quad \begin{aligned} \rho^j &= \underset{\rho \in \mathbb{R}_0^+}{\text{ArgMin}} J(u_0^j - \rho w^j) \\ &= \frac{\mu}{2} (n_0 + \rho n_1 + \rho^2 n_2 + \rho^3 n_3 + \rho^4 n_4), \end{aligned}$$

where

$$\begin{aligned} n_0 &= \int_{\Omega} \int_{Y_f} \nabla_y \xi_0^j : \nabla_y \xi_0^j dy dx, \\ n_1 &= 2 \cdot \int_{\Omega} \int_{Y_f} \nabla_y \xi_0^j : \nabla_y \xi_1^j dy dx, \\ n_2 &= \int_{\Omega} \int_{Y_f} \nabla_y \xi_1^j : \nabla_y \xi_1^j dy dx + 2 \cdot \int_{\Omega} \int_{Y_f} \nabla_y \xi_0^j : \nabla_y \xi_2^j dy dx, \\ n_3 &= 2 \cdot \int_{\Omega} \int_{Y_f} \nabla_y \xi_1^j : \nabla_y \xi_2^j dy dx, \\ n_4 &= \int_{\Omega} \int_{Y_f} \nabla_y \xi_2^j : \nabla_y \xi_2^j dy dx. \end{aligned}$$

Summarizing the above considerations, the solution of the continuous Navier-Stokes system with two pressures is reduced to the solution of four Stokes systems with two pressures at each iteration step. The problems are related to the gradient g^j and $\xi_0^j, \xi_1^j, \xi_2^j$ given in variational form in (4.8), (4.10)-(4.12), respectively. The minimization problem (4.13) can be solved by a classical Newton method. The overall convergence of the least-squares conjugate gradient algorithm can be shown by explicitly computing the second derivative of J . This will again require continuity of the trilinear form.

Discretization of Stokes systems with two pressures. As mentioned in the introduction of this chapter, the right hand sides of the Stokes systems with two pressures appearing during the least-squares conjugate gradient method depend on the micro variable y . Hence, we can not simply solve two cell problems, compute the permeability tensor \mathcal{K} and solve the macro problem for the pressure p_0 . Therefore, we have to extend the idea of a priori solving micro problems: We consider cell problems, where the right hand sides are nodal basis functions of a finite element discretization. The solutions of these cell problems can then be used to eliminate the velocity and the second pressure, respectively. As in Section (2.5), we finally arrive at a linear elliptic equation for the macro pressure. Before we detail the derivation of the macro problem, we need to modify the variational formulation (4.8) slightly.

Lemma 4.4. *Supposing, that $v, w \in \mathcal{V}$ and the solution ξ of (4.10) are sufficiently regular, respectively, the Fréchet-differential of J can be written as*

$$\langle J'(v), w \rangle = \int_{\Omega} \int_{Y_f} \mathbf{F}(\xi, v) \cdot w \, dy \, dx,$$

where

$$\mathbf{F}(\xi, v) = \begin{pmatrix} -\mu \Delta_y \xi_1 - \xi_1 \frac{\partial v_2}{\partial y_2} + \xi_2 \frac{\partial v_2}{\partial y_1} - \frac{\partial \xi_1}{\partial y_1} v_1 - \frac{\partial \xi_1}{\partial y_2} v_2 \\ -\mu \Delta_y \xi_2 + \xi_1 \frac{\partial v_1}{\partial y_2} - \xi_2 \frac{\partial v_1}{\partial y_1} - \frac{\partial \xi_2}{\partial y_1} v_1 - \frac{\partial \xi_2}{\partial y_2} v_2 \end{pmatrix}.$$

Proof: From Lemma 4.3, we know, that for $v, w \in \mathcal{V}$

$$\begin{aligned} \langle J'(v), w \rangle &= \underbrace{\mu \int_{\Omega} \int_{Y_f} \nabla_y w : \nabla_y \xi(v) \, dy \, dx}_{=: \text{INT1}} + \underbrace{\int_{\Omega} \int_{Y_f} (v \cdot \nabla_y) w \cdot \xi(v) \, dy \, dx}_{=: \text{INT2}} \\ &\quad + \underbrace{\int_{\Omega} \int_{Y_f} (w \cdot \nabla_y) v \cdot \xi(v) \, dy \, dx}_{=: \text{INT3}}. \end{aligned}$$

We have to separate w as test function. This can be achieved by applying Green's theorem and using the boundary conditions with respect to the periodicity cell. We calculate with simplified notation:

$$\begin{aligned} \text{INT1} &= \mu \int_{\Omega} \int_{Y_f} \nabla_y \xi_1 \cdot \nabla_y w_1 + \nabla_y \xi_2 \cdot \nabla_y w_2 \, dy \, dx \\ &= -\mu \int_{\Omega} \int_{Y_f} \Delta_y \xi_1 w_1 + \Delta_y \xi_2 w_2 \, dy \, dx \\ &\quad + \mu \int_{\Omega} \int_{\partial Y_f} \nu \cdot \nabla_y \xi_1 w_1 + \nu \cdot \nabla_y \xi_2 w_2 \, ds(y) \, dx \\ &= \mu \int_{\Omega} \int_{Y_f} \begin{pmatrix} -\mu \Delta_y \xi_1 \\ -\mu \Delta_y \xi_2 \end{pmatrix} \cdot w \, dy \, dx, \end{aligned}$$

$$\begin{aligned} \text{INT2} &= \int_{\Omega} \int_{Y_f} \xi_1 \left(v_1 \frac{\partial w_1}{\partial y_1} + v_2 \frac{\partial w_1}{\partial y_2} \right) + \xi_2 \left(v_1 \frac{\partial w_2}{\partial y_1} + v_2 \frac{\partial w_2}{\partial y_2} \right) \, dy \, dx \\ &= \int_{\Omega} \int_{Y_f} \begin{pmatrix} \frac{\partial w_1}{\partial y_1} \\ \frac{\partial w_1}{\partial y_2} \end{pmatrix} \cdot (\xi_1 v) + \begin{pmatrix} \frac{\partial w_2}{\partial y_1} \\ \frac{\partial w_2}{\partial y_2} \end{pmatrix} \cdot (\xi_2 v) \, dy \, dx \end{aligned}$$

$$\begin{aligned}
&= - \int_{\Omega} \int_{Y_f} w_1 \operatorname{div}_y (\xi_1 v) + w_2 \operatorname{div}_y (\xi_2 v) \, dy \, dx \\
&\quad + \int_{\Omega} \int_{\partial Y_f} \nu \cdot (\xi_1 v) w_1 + \nu \cdot (\xi_2 v) w_2 \, ds(y) \, dx \\
&= - \int_{\Omega} \int_{Y_f} \left(\begin{array}{c} \xi_1 \frac{\partial v_1}{\partial y_1} + \frac{\partial \xi_1}{\partial y_1} v_1 + \xi_1 \frac{\partial v_2}{\partial y_2} + \frac{\partial \xi_1}{\partial y_2} v_2 \\ \xi_2 \frac{\partial v_1}{\partial y_1} + \frac{\partial \xi_2}{\partial y_1} v_1 + \xi_2 \frac{\partial v_2}{\partial y_2} + \frac{\partial \xi_2}{\partial y_2} v_2 \end{array} \right) \cdot w \, dy \, dx, \\
\text{INT3} &= \int_{\Omega} \int_{Y_f} \xi_1 \left(w_1 \frac{\partial v_1}{\partial y_1} + w_2 \frac{\partial v_1}{\partial y_2} \right) + \xi_2 \left(w_1 \frac{\partial v_2}{\partial y_1} + w_2 \frac{\partial v_2}{\partial y_2} \right) \, dy \, dx \\
&= \int_{\Omega} \int_{Y_f} \left(\begin{array}{c} \xi_1 \frac{\partial v_1}{\partial y_1} + \xi_2 \frac{\partial v_2}{\partial y_1} \\ \xi_1 \frac{\partial v_1}{\partial y_2} + \xi_2 \frac{\partial v_2}{\partial y_2} \end{array} \right) \cdot w \, dy \, dx.
\end{aligned}$$

Adding the three integrals completes the proof. \blacksquare

In complete analogy, the right hand sides of the Stokes systems with two pressures (4.10) - (4.12) can be reformulated in order to have the test function separated. In fact, only the *viscous* term has to be transformed.

We consider the following Stokes system with two pressures

$$(4.14) \quad \left\{ \begin{array}{l} -\mu \Delta_y w(x, y) + \nabla_y \tilde{\pi}_1(x, y) \\ \quad = \tilde{\mathbf{F}}(x, y) - \nabla_x \tilde{\pi}_0(x) \quad \text{in } \Omega \times Y_f, \\ \quad \operatorname{div}_y w(x, y) = 0 \quad \text{in } \Omega \times Y_f, \\ \quad w(x, y) = 0 \quad \text{on } \Omega \times \partial Y_s, \\ \quad \{w, \tilde{\pi}_1\} \quad \text{is } Y\text{-periodic,} \end{array} \right.$$

$$(4.15) \quad \left\{ \begin{array}{l} \operatorname{div}_x \int_{Y_f} w(x, y) \, dy = 0 \quad \text{in } \Omega, \\ \quad \nu(x) \cdot \int_{Y_f} w(x, y) \, dy \quad \text{is } \Gamma_1\text{-antiperiodic,} \\ \quad \tilde{\pi}_0 \quad \text{is } \Gamma_1\text{-periodic,} \\ \nu(x) \cdot \int_{Y_f} w(x, y) \, dy = 0 \quad \text{on } \Gamma_2, \end{array} \right.$$

where the unknowns are w , $\tilde{\pi}_0$ and $\tilde{\pi}_1$. $\tilde{\mathbf{F}}$ denotes the general part of the right hand side covering problems (4.8), (4.10) - (4.12).

Let the periodicity cell be discretized by biquadratic finite elements on square meshes as in Section 3.2.3.1. Using the biquadratic nodal basis functions Φ_{ih}^{biqua} defined in (3.65) as right hand sides, we solve Stokes problems for the velocity

w_{ih} and the pressure π_{ih} :

$$(4.16) \quad \begin{aligned} -\Delta_y w_{ih} + \nabla_y \pi_{ih} &= \mathbf{\Phi}_{ih}^{biqua} && \text{in } Y_f, \\ \operatorname{div}_y w_{ih} &= 0 && \text{in } Y_f, \\ w_{ih} &= 0 && \text{on } \partial Y_s, \\ \{w_{ih}, \pi_{ih}\} &&& \text{is } Y\text{-periodic.} \end{aligned}$$

Due to linearity of (4.14), the following relations hold:

$$(4.17) \quad w(x, y) = \frac{1}{\mu} \sum_{i=1}^{n/2} \left(\tilde{\mathbf{F}}_1(x, y_i) w_{ih}(y) + \tilde{\mathbf{F}}_2(x, y_i) w_{(i+n/2)h}(y) \right) - \frac{1}{\mu} \sum_{i=1}^2 w_i(y) \frac{\partial \tilde{\pi}_0(x)}{\partial x_i},$$

$$(4.18) \quad \tilde{\pi}_1(x, y) = \sum_{i=1}^{n/2} \left(\tilde{\mathbf{F}}_1(x, y_i) \pi_{ih}(y) + \tilde{\mathbf{F}}_2(x, y_i) \pi_{(i+n/2)h}(y) \right) - \sum_{i=1}^2 \pi_i(y) \frac{\partial \tilde{\pi}_0(x)}{\partial x_i},$$

where $n = \dim \mathcal{W}_h^*$, y_i , $i = 1, \dots, \frac{n}{2}$ is the coordinate of the i th node on the discretized periodicity cell and $w_i = w_i(y)$, $\pi_i = \pi_i(y)$, $i = 1, 2$ are the solutions of the standard cell problems defined by (2.23).

Integrating (4.17) over Y_f , applying the divergence operator with respect to x and using the macro boundary conditions in (4.15), yields a linear elliptic problem for $\tilde{\pi}_0$:

$$(4.19) \quad \begin{aligned} -\operatorname{div}_x \left(\frac{\mathcal{K}}{\mu} \cdot \nabla_x \tilde{\pi}_0(x) \right) &= -\operatorname{div}_x \left(\frac{1}{\mu} \sum_{i=1}^{n/2} \left(\tilde{\mathbf{F}}_1(x, y_i) \int_{Y_f} w_{ih}(y) dy \right. \right. \\ &\quad \left. \left. + \tilde{\mathbf{F}}_2(x, y_i) \int_{Y_f} w_{(i+n/2)h}(y) dy \right) \right) \quad \text{in } \Omega, \\ \tilde{\pi}_0 &\text{ is } \Gamma_1\text{-periodic,} \end{aligned}$$

$$\begin{aligned} \nu(x) \cdot \left(\frac{\mathcal{K}}{\mu} \cdot \nabla_x \tilde{\pi}_0(x) \right) &= \nu(x) \cdot \left(\frac{1}{\mu} \sum_{i=1}^{n/2} \left(\tilde{\mathbf{F}}_1(x, y_i) \int_{Y_f} w_{ih}(y) dy \right. \right. \\ &\quad \left. \left. + \tilde{\mathbf{F}}_2(x, y_i) \int_{Y_f} w_{(i+n/2)h}(y) dy \right) \right) \quad \text{on } \Gamma_2. \end{aligned}$$

Note, that by construction $\tilde{\mathbf{F}}$ is Γ_1 -periodic, inducing the boundary condition on $\tilde{\pi}_0$.

For the discretization of the macro problem (4.19) biquadratic finite elements on square meshes are used leading to second order convergence, if the solution

$\tilde{\pi}_0$ is sufficiently regular.

We will draw a final remark on $\tilde{\mathbf{F}}$ which is needed to solve the macro problem. The computation of $\tilde{\mathbf{F}}$ involves calculating derivatives with respect to y of some function in \mathcal{V} . We will assume sufficient regularity of the particular function and use finite differences. Due to the biquadratic nodal structure on the periodicity cell, we use element-wise three-point approximations of the first and second derivatives. In general, a node belongs to more than one element. Therefore, the obtained derivatives are averaged. For the sake of completeness, we list the formulas for the one dimensional case (see also [4]):

$$\begin{aligned} f(P1)' &= \frac{-3f(P1) + 4f(P2) - f(P3)}{2h} + O(h^2), \\ f(P2)' &= \frac{f(P3) - f(P1)}{2h} + O(h^2), \\ f(P3)' &= \frac{3f(P3) - 4f(P2) + f(P1)}{2h} + O(h^2), \\ f(P1)'' &= \frac{f(P1) - 2f(P2) + f(P3)}{h^2} + O(h), \\ f(P2)'' &= \frac{f(P3) - 2f(P2) + f(P1)}{h^2} + O(h^2), \\ f(P3)'' &= \frac{f(P3) - 2f(P2) + f(P1)}{h^2} + O(h), \end{aligned}$$

where f , f' and f'' denotes some function and its first and second derivative, respectively. $P1$, $P2$ and $P3$ are equally spaced points with distance h .

4.2. Numerical results

4.2.1. Validation of the algorithm. To illustrate the typical convergence properties of the least-squares conjugate gradient method applied to the solution of the Navier-Stokes system with two pressures, we use the following setup: On the micro scale, a square obstacle $Y_s = [0.15, 0.85]^2$ is considered. The finite element mesh consists of 50×50 square elements. Hence, we have to compute 20402 Stokes problems for the velocity w_{ih} and pressure π_{ih} . The Uzawa algorithm is stopped when the residual is less than 10^{-12} . On the macro scale, we set $\Omega =]0, 1[^2 \setminus [0.25, 0.75]^2$ and discretize it by a 16×16 mesh. At $x_1 = 0$ and $x_1 = 1$ periodic boundary conditions on the pressure are imposed. On the remaining outer boundary and on the boundary of the macro obstacle, we impose zero normal components on the velocity. The number of grid points which have to be handled reaches 6855072. The convergence behavior for $\mu = 1.0, 0.02, 0.01$ and 0.005 is illustrated in Figure 1.

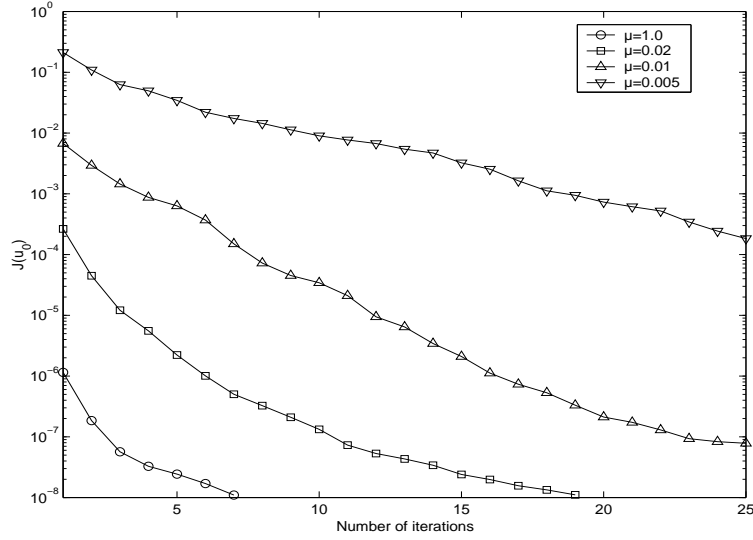


FIGURE 1. Convergence of the least-squares conjugate gradient method

Due to the computational complexity, it is not possible to perform a convergence analysis of the proposed method as for the discretizations in Chapter 3. However, we validate the method by comparing its results to semi-analytic solutions, which exist using the following macro setup. We consider $\Omega =]0, 1[^2$ (without any obstacle) and impose periodic boundary conditions on the pressure on the boundary of Ω . Using $f = (1, 0)^T$, leads to a vanishing macroscopic pressure p_0 and a constant macroscopic velocity $\bar{u}_0(\cdot) = \int_{Y_f} u_0(\cdot, y) dy$. Since we have $\alpha = f - \nabla p_0 = f$, it is possible to compare $\bar{u}_0(\cdot)$ with the value of the nonlinear filtration law at α . The results are shown in Table 1.

	\bar{u}_0	$\mathcal{F}((1, 0)^T)$
$\mu = 1.0$	$2.540 * 10^{-3}$	$2.563 * 10^{-3}$
$\mu = 0.02$	$1.256 * 10^{-1}$	$1.278 * 10^{-1}$
$\mu = 0.01$	$2.475 * 10^{-1}$	$2.513 * 10^{-1}$
$\mu = 0.005$	$4.863 * 10^{-1}$	$4.910 * 10^{-1}$

TABLE 1. Comparison of results validating the four-dimensional method

4.2.2. Model problems. In this section we are concerned with the presentation of some numerical results. In Figure 2, Stokes solutions with finite element basis functions at $y = (0, 0)$ and $y = (0.125, 0.5)$ as right hand sides are shown. The mesh is of size 50×50 and the obstacle is given by $Y_s = [0.21, 0.79]^2$.

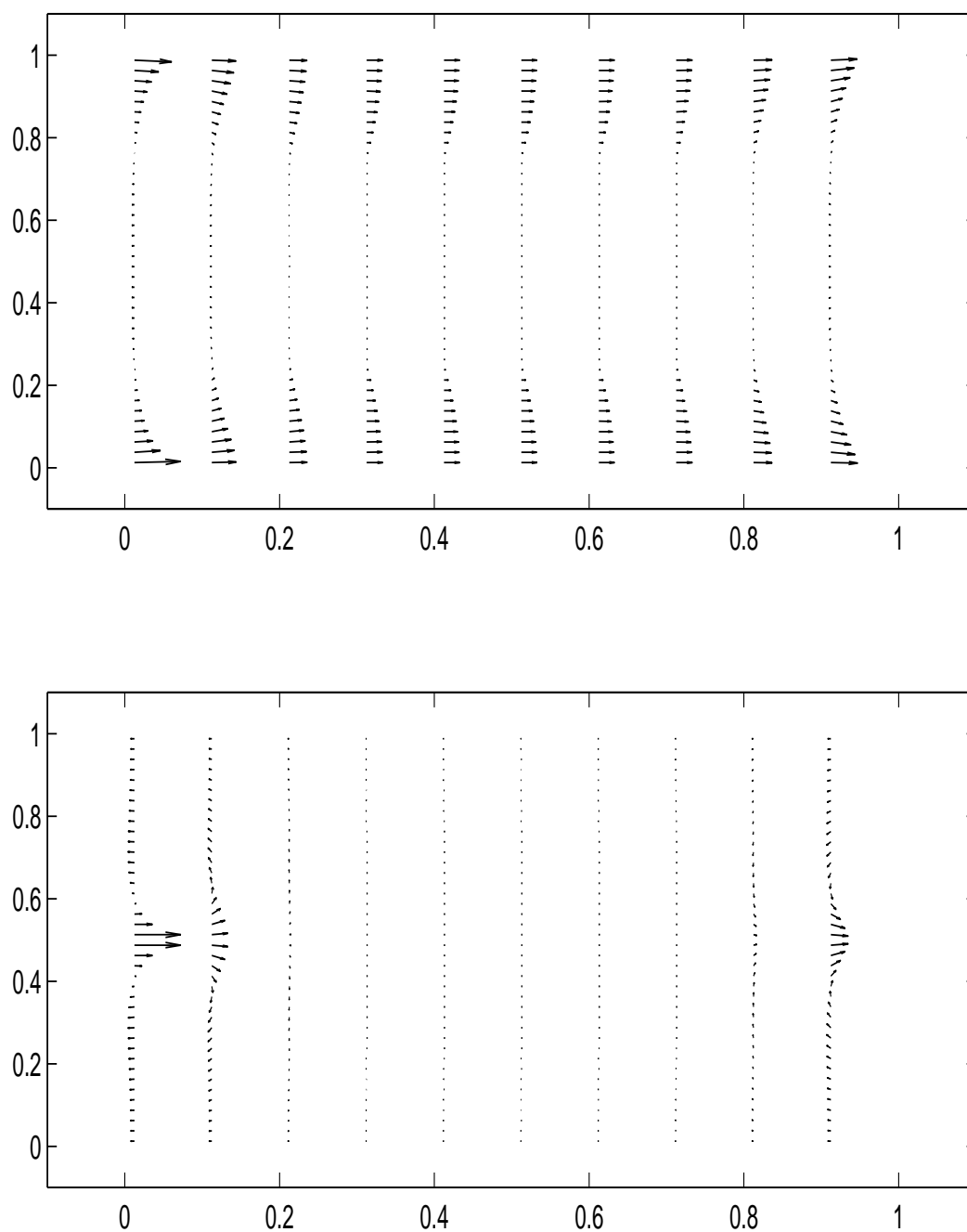


FIGURE 2. Stokes velocities using finite element basis functions at $y = (0, 0)$ (top) and $y = (0.125, 0.5)$ (bottom) as right hand side

Now, we consider $\Omega =]0, 1[^2 \setminus [0.25, 0.75]^2$. Ω is discretized by a 16×16 mesh. As before, we use periodic boundary conditions at $x_1 = 0$ and $x_1 = 1$ for the pressure and impose zero normal components of the velocity on the remaining

boundaries. The force is set to $f = (1, 0)^T$. We are interested to investigate the behavior of the term $\int_{\Omega} \bar{u}_0(x) dx$, which is some measure for the macroscopic flow rate. Clearly, in the above setting, its second component vanishes. In Table 2, the results are presented for $Y_s = [0.15, 0.85]^2$ resolved by a 50×50 grid. The second column shows the linear results in case of the Stokes system with two pressures (S2P). The third column shows slightly decreased flow rates in the case of the Navier-Stokes system with two pressures (NS2P).

	S2P	NS2P
$\mu = 1.0$	0.0015	0.0015
$\mu = 0.02$	0.0773	0.0767
$\mu = 0.01$	0.1546	0.1482
$\mu = 0.005$	0.3092	0.2762

TABLE 2. $Y_s = [0.15, 0.85]^2$: Comparison of flow rates at $f = (1.0, 0)^T$

Using a smaller micro obstacle $Y_s = [0.21, 0.79]^2$ leads to higher micro velocities and inertia effects become more important. In Table 3, we give the results, where the effect of decreasing flow rates is stronger.

	S2P	NS2P
$\mu = 1.0$	0.0045	0.0045
$\mu = 0.02$	0.2243	0.2154
$\mu = 0.01$	0.4486	0.3976
$\mu = 0.005$	0.8972	0.6659

TABLE 3. $Y_s = [0.21, 0.79]^2$: Comparison of flow rates at $f = (1.0, 0)^T$

In Figure 3, we show $\bar{u}_0(\cdot)$ for $\mu = 1.0$ and $\mu = 0.005$. Thereby, in analogy to the numerical results presented in Chapter 3, we observe how the flow pattern is changed due to microscopic inertia effects.

The advantage of the method proposed in this chapter is, that the information on the microscopic velocities is not lost by integration as in the methods presented in Chapter 3. In Figure 4, we show the associated microscopic velocities at $x = (0.125, 0.5)$ and $x = (0.25, 0.25)$. We choose these positions in order to demonstrate how significantly the velocities may change depending on the

location in the macro domain. At $x = (0.125, 0)$, we are obviously still in the linear regime, whereas at $x = (0.25, 0.25)$, the velocities are highly influenced by inertia effects.

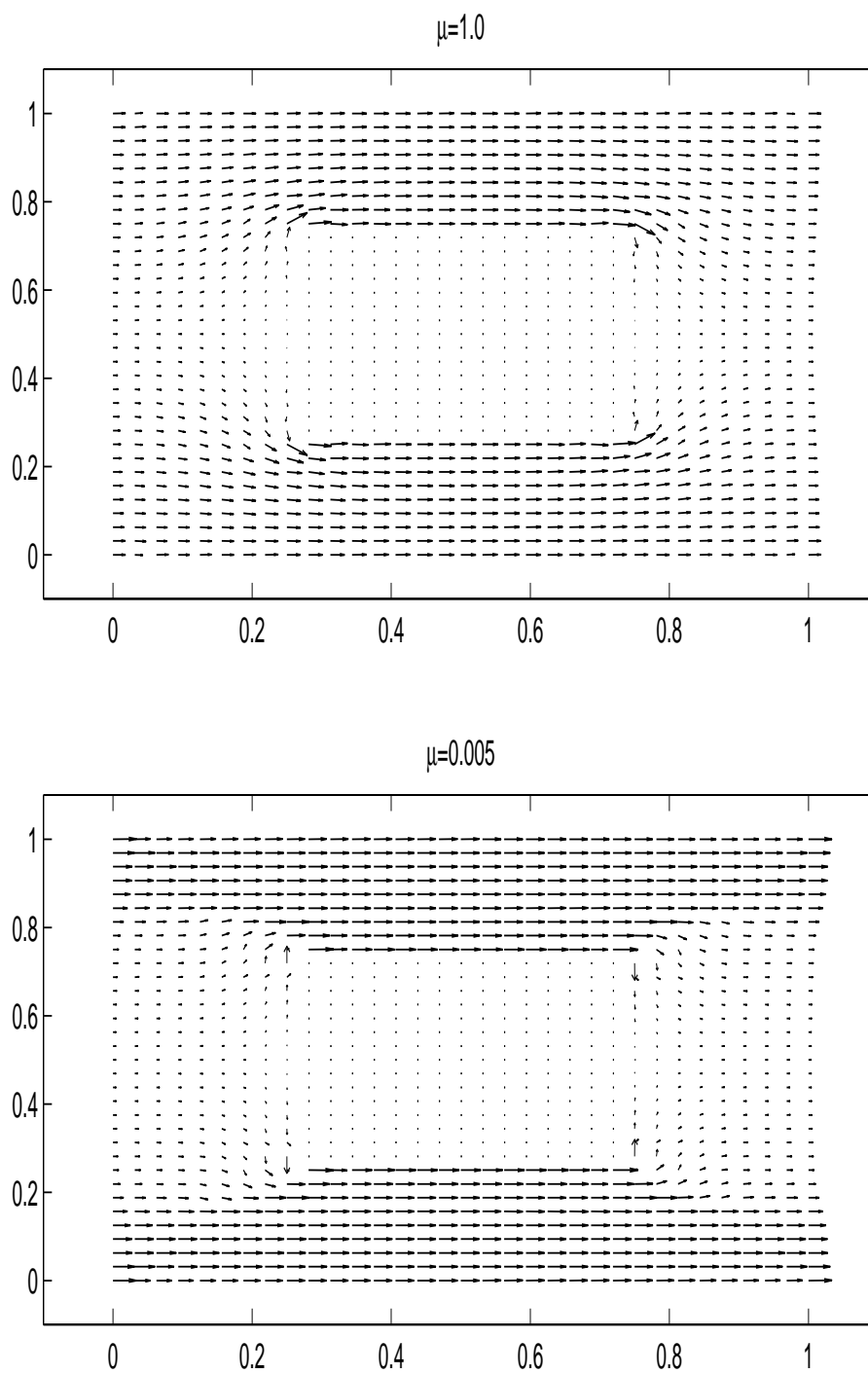


FIGURE 3. $Y_s = [0.21, 0.79]^2$: Change of flow patterns when μ increases

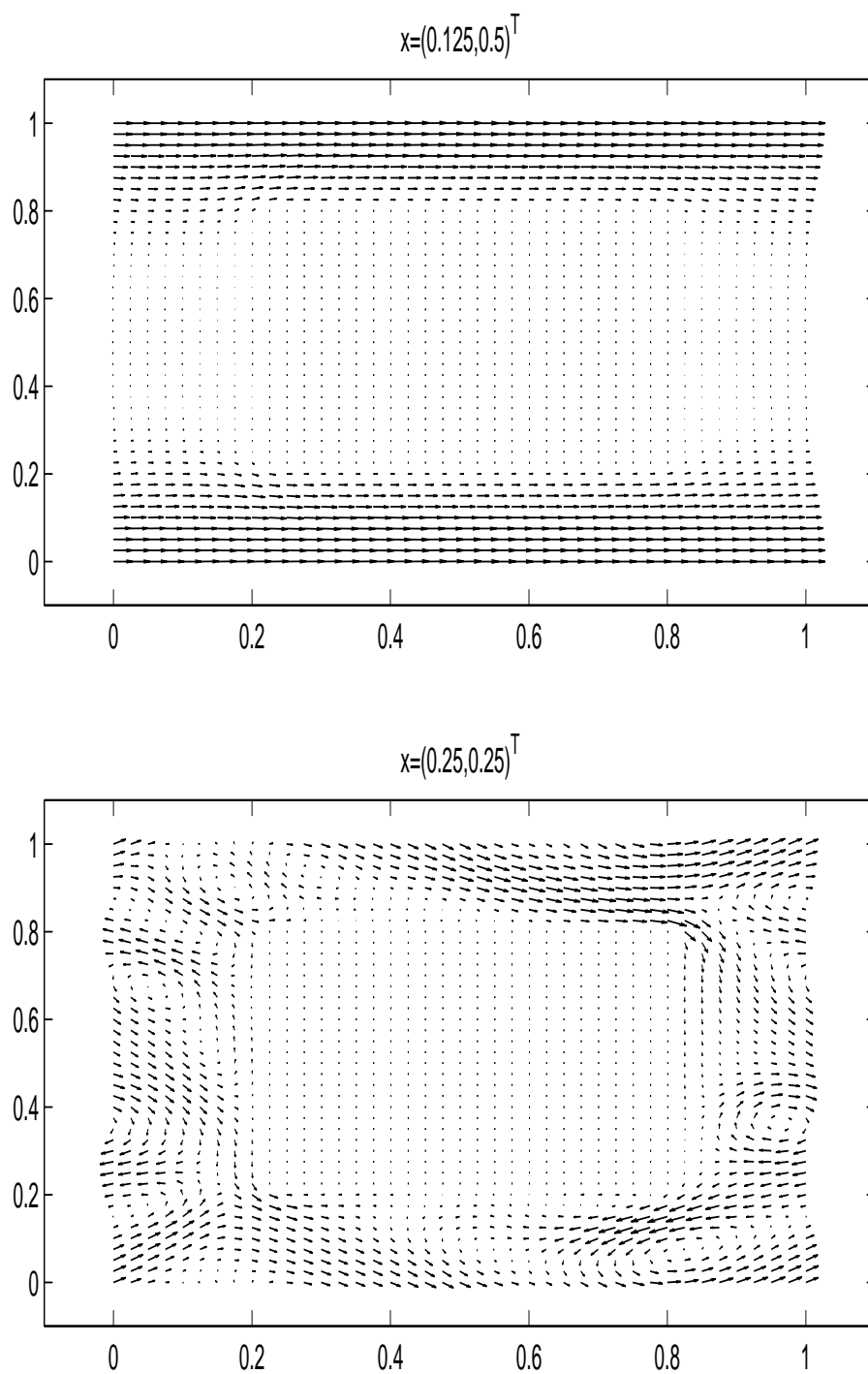


FIGURE 4. Microscopic velocities at different macro locations

CHAPTER 5

Modeling and simulation of the pressing section of a paper machine

The paper machine is a huge piece of equipment reaching width and height of 12 meters and length of up to 250 meters, respectively. Typically, it consists of four main parts: the headbox, the sheet forming section, the pressing section and the drying section (see Figure 1).

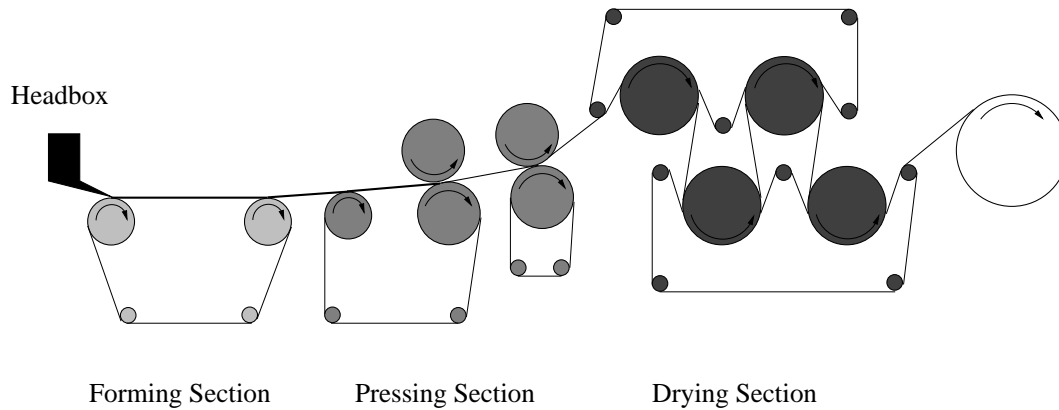


FIGURE 1. Paper machine

The headbox provides the fiber suspension having approximately 99 percent fluid content. From the headbox the suspension enters the sheet forming section at high speeds of up to $2000 \frac{m}{min}$. On a woven structure called forming fabric dewatering starts by natural filtration. Additional suction boxes may support the dewatering process, such that the fluid content is decreased to about 80 percent at the entrance of the pressing section. By means of dewatering felts the paper layer is transported through several press nips. A press nip in its simplest form consists of two rolls which compress the paper-felt sandwich (see Figure 2).

Since the felt is a porous structure providing void space, the fluid is squeezed out from the paper and enters the felt. Thereby, the fluid content is decreased to approximately 50 percent when the paper reaches the drying section. Here,

further dewatering is accomplished by evaporation. Steam-heated cylinders over which the paper layer is transported reduce the fluid content to 5 percent. In the end, the paper is stored on huge rolls ready for further processing like coating or cutting.

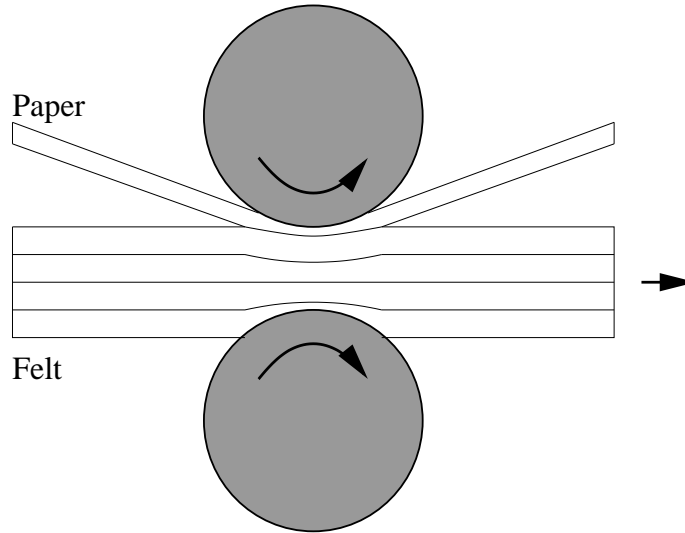


FIGURE 2. Roll press nip

In the abstract of [42], a summary of the current state of research in the paper making industry is given. It is stated, that in the paper making industry process optimization has almost always taken place by tests and measurements. Nevertheless, this trial and error approach has led to the situation that no drastic improvements can be expected in the future. But, due to the huge amount of paper being typically produced in a paper mill, even small improvements can save a lot of money and energy. To achieve progress nowadays, more detailed understanding of the dewatering processes is needed. Besides further development of experimental methods and running expensive measurement series on test paper machines, mathematical modeling and computer simulation can be the tools to support R & D in the paper making industry. One intrinsic property of modeling and simulation is that these methods are not limited to existing paper machines and clothings, but they can also be used as tools to predict the behavior of completely new designs. On the other hand, modeling and simulation will not replace measurements. They are still needed as a link to reality to provide ways for validation of the models and to give hints to empirical laws where modeling from first principles is too complicated.

We completely agree with this assessment except for the statement that no drastic improvements could be achieved. Looking at dewatering felts, we observe that the manufacturing process does not operate at the length scale of

micrometers, but merely at millimeters. Typically, a felt consists of a woven structure called base weave. It is made of yarns which may reach diameters of 0.2mm to 2mm. A needling process attaches several layers of fine fibers to the base weave. The diameters of the fine fibers are between $10\mu\text{m}$ and $80\mu\text{m}$. The needling process creates a very irregular structure which is by no means fluid dynamically or elastically optimized. Being able to manufacture at the micro scale yields great potential for future improvements and, as already mentioned above, computer simulation can play a keyrole in predicting the optimal material properties.

In this chapter we will focus on the simulation of press nips in the pressing section. Since mechanical drying is considered to be ten times cheaper than thermal drying, a lot of energy and money can be saved by improved dewatering felts and optimal press profiles. Moreover, better drying rates insure higher quality of the final product, since its elastic strength is increased. Another advantage is the fact that the paper machine may operate at higher speeds still delivering the needed heating capacity in the drying section. Hence, there is an increase in productivity of the paper machine.

In the first section of this chapter we consider the pressing section of a paper machine and establish a mathematical model describing the elastic and fluid dynamical behavior of the paper-felt sandwich when passing a press nib. In contrast to [42] and [75], the model is two-dimensional as it neglects only the cross direction of the paper machine. The paper and felt layers are considered to be porous media. Due to high pressure gradients in the nip the fluid velocities reach high levels where Darcy's law is not applicable anymore. Therefore, the model allows for the use of nonlinear filtration laws extending existing models like in [25]. In the second part of this chapter, we describe the solution algorithms of the model equations and the discretization. The third section of this chapter is devoted to model parameters, since they turn out to be a crucial part of the simulations. For example, we use the methods developed in the previous chapter and compute nonlinear macroscopic filtration laws. Therefore, we extend the methods to a three-dimensional felt structure which is generated by GeoDict, a virtual structure generator developed at Fraunhofer ITWM, Kaiserslautern. The three-dimensional flow field is then computed by ParPac which is a parallel lattice Boltzmann solver also developed at Fraunhofer ITWM. We close the chapter by a presentation of numerical results.

5.1. Model of a press nip

As mentioned in the introduction to this chapter, the pressing section of a paper machine consists of several press nips. Nowadays, there exist two different

types of press nips. In Figure 2 a sketch of a roll press nip is drawn. Figure 3 shows a modern shoe press nip. Its advantage is the enhanced press zone due to a concave-convex combination of the opposing press profiles.

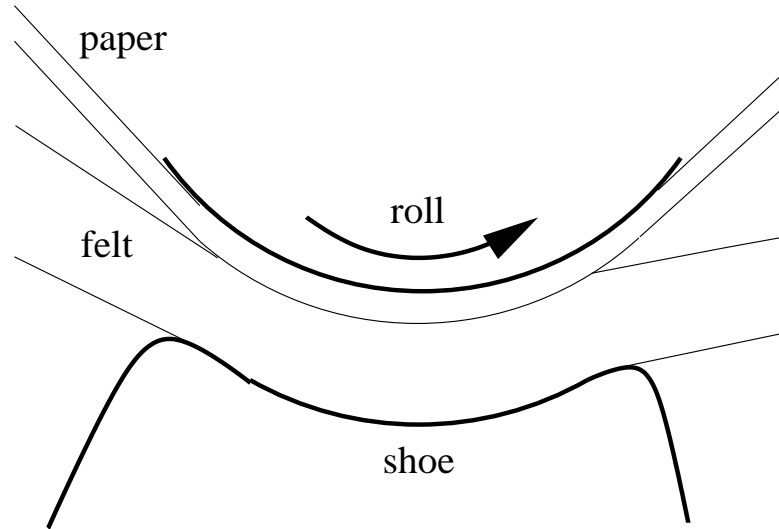


FIGURE 3. Shoe press

Typically, the press zone of a roll press nip reaches lengths between 40mm and 70mm, whereas a shoe press may reach up to 300mm. In contrast, the felt thickness is usually less than 4mm and the paper thickness may go down to 100 micrometers. The paper-felt sandwich is squeezed between the press profiles. Thereby, the fluid from the fibrous paper layer enters the porous felt structure, hence dewatering takes place. Two essential phenomena characterizing the dewatering process are elasticity and fluid dynamics.

Our model of a press nip is quite similar to the model developed in [75]. Nevertheless, it is extended to two dimensions and nonlinear filtration laws are incorporated. The derivation of the model is not entirely based on first principles and mathematically rigorous considerations. In contrast to the derivations in the previous chapters, i.e. the flow equations in a periodic porous medium in case of high velocities and full saturation, phenomenological and empirical laws are used. The reason is twofold. To the best of the author's knowledge, there does not exist a rigorous mathematical derivation of effective two-phase flow equations in porous media. In case of elasticity, a computer model on the fiber level is very complicated since contact problems including friction have to be considered. Even if a computer model were available, determining its input parameters is not easy.

As indicated in Figure 2 and Figure 3, let's assume that the felt passes the press nip from the left to the right. This direction is called *machine direction*

(MD) and will be referred to as x direction in this chapter. The y direction is aligned to the axes of the rolls and is called *cross direction* (CD). The z direction is called transversal direction (TD). Since the length of the cylindrical roll is up to 12m and, therefore, much larger than the press zone in MD and the paper-felt sandwich in ZD, the cross direction is neglected.

5.1.1. Elasticity model. To describe the elastic behavior of the felt, we follow a phenomenological approach. Due to the highly demanding process conditions, the felt is by construction very stiff in machine direction. Therefore, we consider deformation only in transversal direction. Guided by measurements, we assume that the felt behaves viscoelastically which is, indeed, a widely accepted assumption (see [75] and references therein). Motivated by [44], the paper layer is modeled quite similar to the felt layers. In contrast to the felt, the paper layer does not recover completely after the press nip. This is due to plastic deformation. It keeps a permanent compression which adds a new parameter to the model. The ordinary differential equations which describe the deformation in transversal direction when passing through the nip read:

$$(5.1) \quad \begin{aligned} \tau(t) &= E_1(\varepsilon_1(t)) + \Lambda_1 \frac{d}{dt} E_1(\varepsilon_1(t)) - K \cdot \tau_{max}(t), \\ \tau(t) &= E_i(\varepsilon_i(t)) + \Lambda_i \frac{d}{dt} E_i(\varepsilon_i(t)), \quad i = 2 \dots n. \end{aligned}$$

The preceding equations are a system of Kelvin-Voigt laws for n layers. The strain is denoted by $\varepsilon_i(t) = \frac{l_i(t) - l_{0,i}}{l_{0,i}}$, where $l_{0,i}$ is the undeformed thickness of layer i and $l_i(t)$ is the deformed thickness at time t . The stress measured in [Pa] is denoted by τ . Note, that τ is independent of the layers and just a function of t . Moreover, the functions E_i relating the elastic part of the stress and the strains ε_i might be nonlinear. Λ_i (in [s]) are viscoelastic time constants which determine the speed of relaxation. In (5.1), the first equation describes the paper layer. Therefore, we observe the additional term, which introduces a permanent deformation. This term depends linearly by the constant K on the maximum stress to which the paper has been exposed. The maximum stress is given by

$$\tau_{max}(t_0) := \max_{t \leq t_0} \tau(t).$$

By using the relation $x = c * t$, where $c = \|\mathbf{v}_s\|$, and assuming negligible rigid body motion of the layers in transversal direction, we can eliminate the time

variable and get

$$(5.2) \quad \tau(x) = E_1(\varepsilon_1(x)) + \Lambda_1 c \frac{d}{dx} E_1(\varepsilon_1(x)) - K \cdot \tau_{max}(x),$$

$$\tau(x) = E_i(\varepsilon_i(x)) + \Lambda_i c \frac{d}{dx} E_i(\varepsilon_i(x)), \quad i = 2 \dots n.$$

Clearly, we have

$$(5.3) \quad \tau_{max}(x_0) := \max_{x \leq x_0} \tau(x).$$

As indicated by Figure 4, the two press profiles are positioned by using d_{min} which is the minimum distance between the profiles. d_{min} is an input parameter of the problem. Due to the viscoelastic behavior of the porous layers, the overall thickness of the paper-felt sandwich will never exceed its initial undeformed thickness l_0 . Therefore, the function

$$(5.4) \quad f(x) := \min(l_0, \text{distance of press profiles at position } x)$$

is well-defined and, in addition to (5.2), (5.3), the following relation holds true

$$(5.5) \quad \sum_{i=1}^n \varepsilon_i(x) l_{0,i} = l_0 - f(x).$$

The deformation process can be subdivided into three phases (see Figure 4):

- *Phase 0* ($x_i \leq x \leq x_r$): no deformation; vertical position is specified by input parameter z_i ;
- *Phase 1* ($x_r \leq x \leq x_l$): viscoelastic deformation ruled by (5.2), ..., (5.5), x_l is computed by the condition $\tau(x_l) = 0$;
- *Phase 2* ($x_l \leq x \leq x_o$): as *Phase 1*, but τ is equal to zero; vertical position given by z_o (z coordinate of lower press profile at x_l).

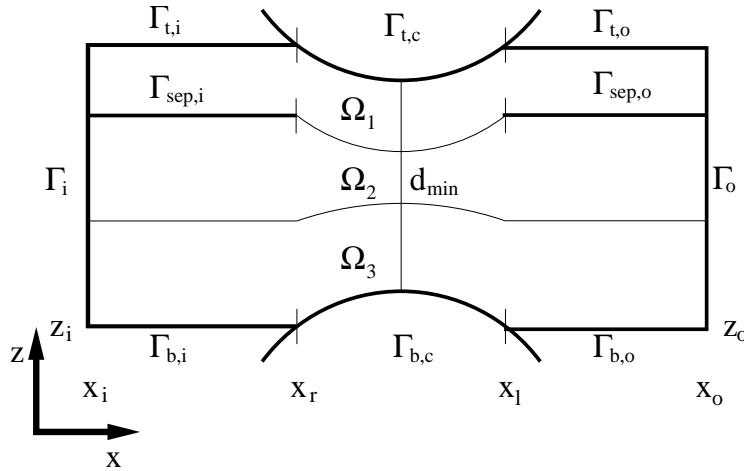


FIGURE 4. Terminology

We want to point out that there is no coupling of elasticity and fluid dynamics. For instance, we neglect the influence of the fluid pressure on the felt deformation. Furthermore, we assume that the deformation results in a temporary rearrangement of fibers rather than in a compression of fibers. Therefore, the solid phase is assumed to be incompressible. Incompressibility allows for a simple computation of the porosity, once the strain is known. Let $\Phi_{0,i}$ and Φ_i be the initial and deformed porosity of layer i , respectively. Incompressibility of the solid phase means

$$(1 - \Phi_{0,i})l_{0,i} = (1 - \Phi_i(x))l_i(x).$$

Using the definition of strain yields

$$(1 - \Phi_{0,i}) = (1 - \Phi_i(x))(1 + \varepsilon_i(x)),$$

and, finally,

$$(5.6) \quad \Phi_i(x) = \frac{\varepsilon_i(x) + \Phi_{0,i}}{1 + \varepsilon_i(x)}.$$

5.1.2. Flow model. The fibrous paper layer and the different layers of the felt, i.e. base weave and batt fiber layers consisting of fine fibers, are modeled as porous media. In the previous chapters, *fluid part* and *solid part* are used to denote the constituents of a porous medium. In the following, they will be referred to as *fluid phase* and *solid phase* indexed by 'f' and 's', respectively. Since the pore space of a felt is not entirely filled by fluid, there is an additional gaseous phase indexed by 'g'. The three phases are treated as a mixture of overlapping continua (see [3]). This approach considers the variables of each phase to be defined everywhere in the physical domain which is from a macroscopic point of view a reasonable assumption.

In the framework of overlapping continua, the momentum balance equation for the fluid phase reads

$$(5.7) \quad \Phi_f \rho_f \frac{D_f \mathbf{v}_f}{D t} - \nabla \cdot \mathbf{t}_f - \Phi_f \rho_f \mathbf{b}_f = \mathbf{m}_f,$$

where

$$\frac{D_f}{D t} = \frac{\partial}{\partial t} + \mathbf{v}_f \cdot \nabla$$

denotes the material derivative. In (5.7), the volume fraction of the fluid phase is denoted by Φ_f . ρ_f is the intrinsic fluid density in $[\frac{kg}{m^3}]$. The fluid velocity measured in $[\frac{m}{s}]$ is abbreviated by \mathbf{v}_f . \mathbf{t} is the stress tensor in $[Pa]$. The unit of the specific body force \mathbf{b}_f is $[\frac{N}{kg}]$ and the term describing the rate of momentum exchange into the fluid phase is denoted by \mathbf{m}_f and is measured in $[\frac{N}{m^3}]$.

We assume negligible gravity, a Newtonian fluid, slow flow (for the moment) and Stokes drag as model of interaction of solid and fluid phase. Then, the stationary form of equation (5.7) reads

$$(5.8) \quad \Phi_f(\mathbf{v}_f - \mathbf{v}_s) = -\frac{\mathbf{K}_f}{\mu_f} \cdot \nabla p_f.$$

μ_f is the dynamic viscosity in $[Pa\ s]$. \mathbf{K}_f denotes the permeability tensor in $[m^2]$. The hydrodynamic pressure p_f is measured in $[Pa]$. \mathbf{v}_s is the velocity of the solid phase.

Equation (5.8) is a two-phase version of Darcy's law in the case of a moving porous medium. It is supplemented by the stationary mass balance equation

$$(5.9) \quad \nabla(\Phi_f \mathbf{v}_f) = 0.$$

Although not made explicit, all model parameters may depend on the space variables x and z , since the layer properties which they describe may differ.

For the gaseous phase, we apply Richards' assumption, which states that the air has a negligible influence on the fluid and solid phases. Mathematically, this assumption is expressed by setting p_g equal to zero, i.e. p_g is set to atmospheric pressure. Richards' assumption is justified by the fact, that air has a much smaller viscosity than the fluid and is very *mobile*. In fact, to achieve even larger air mobilities in paper manufacturing, surface chemicals are added. Clearly, some phenomena like fluid enclosed air bubbles are neglected by this approach.

To close our flow model (5.8), (5.9), we introduce the notion of capillary pressure, porosity and saturation. The capillary pressure is defined by

$$p_c := p_g - p_f.$$

Since, $p_g = 0$, we simply have

$$p_c = -p_f.$$

The ratio between void and total volume of a porous medium is called porosity Φ . The saturation S indicates how much of the void volume is occupied by the fluid phase. It is defined by

$$S = \frac{\Phi_f}{\Phi}.$$

Experimental observations show, that there exists a relation between capillary pressure and saturation. In porous media theory (see [6], [9]), it is therefore quite common to use this relation as additional constitutive model equation. Influenced by steady state measurements using real dewatering felts, we choose

the following relation:

$$(5.10) \quad S(p_f) = \begin{cases} \left(\frac{1}{1-s_\infty} + \left(\frac{p_f}{a} \right)^2 \right)^{-1} + s_\infty, & \text{if } p_f \leq 0, \\ 1, & \text{if } p_f > 0, \end{cases}$$

where p_c is already substituted by $-p_f$. s_∞ is the residual saturation as p_f tends to $-\infty$. $a \in \mathbb{R}^-$ is an additional shape parameter which will be used to adjust different saturations in the felt layers at a given pressure level (see Figure 5).

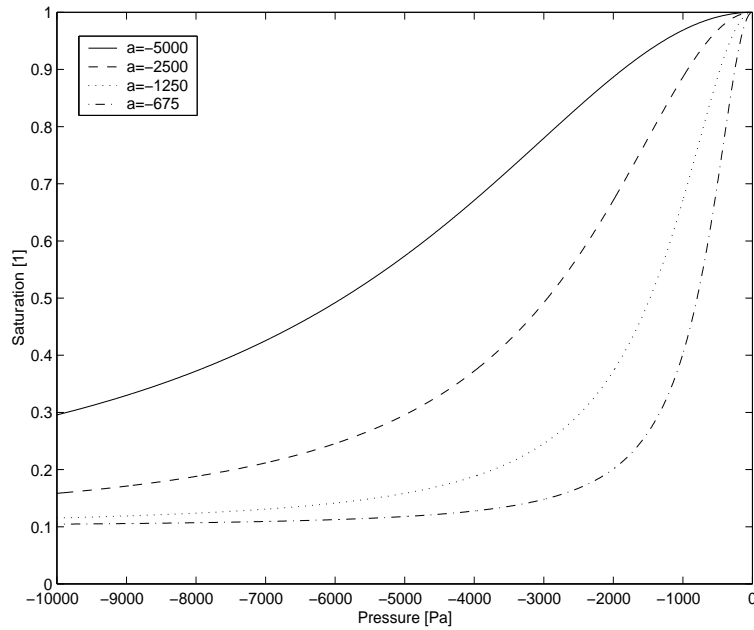


FIGURE 5. Retention curve: Variation of the parameter a ($s_\infty = 0.1$)

In (5.8), \mathbf{K}_f can not be assumed constant, since porosity and saturation will vary significantly during compression and relaxation. Therefore, we assume

$$(5.11) \quad \mathbf{K}_f(\Phi, S) = \mathbf{K}_f^0 \frac{\Phi^3}{1 - \Phi^2} S^b.$$

The factor $\Phi^3/(1 - \Phi^2)$ originates from the Kozeny-Karman relation (see [8]). $1 \leq b \in \mathbb{R}$ is a shape parameter. In (5.11) the term S^b decreases permeability as the saturation is less than 1. This is a reasonable assumption, since \mathbf{K}_f is then a relative permeability. The permeability tensor \mathbf{K}_f^0 can be interpreted as the medium's permeability when the porosity is approximately 0.775 and when the medium is fully saturated.

Let us assume that the porosity is given by the deformation model. The flow model (5.8), ..., (5.11) is then closed. Indeed, applying the divergence operator

to (5.8), using the mass balance equation (5.9) and by simple substitutions, we obtain one nonlinear partial differential equation for the fluid pressure p_f :

$$(5.12) \quad -\operatorname{div}\left(S(p_f)\Phi\mathbf{v}_s\right) = -\operatorname{div}\left(\frac{\mathbf{K}_f^0}{\mu_f}\frac{\Phi^3}{1-\Phi^2}S(p_f)^b\cdot\nabla p_f\right).$$

After computing p_f , (5.8) can be employed to calculate the fluid velocities. Now, we want to include nonlinear filtration laws in our model. The filtration laws which are derived in the previous chapters are only valid in the case of full saturation. Hence, we define

$$(5.13) \quad \mathcal{F}_0^{\text{nl}}(\nabla p_f, \Phi) := \begin{cases} \mathcal{F}^{\text{nl}}(\nabla p_f, \Phi), & \text{if } S = 1, \\ 0, & \text{if } S < 1. \end{cases}$$

The modified equation (5.8) reads

$$(5.14) \quad \Phi_f(\mathbf{v}_f - \mathbf{v}_s) = -\frac{\mathbf{K}_f}{\mu_f}\cdot\nabla p_f + \mathcal{F}_0^{\text{nl}}(\nabla p_f, \Phi).$$

Using (5.14) instead of (5.8) in the above consideration, we obtain the following partial differential equation for p_f :

$$(5.15) \quad -\operatorname{div}\left(S(p_f)\Phi\mathbf{v}_s\right) = -\operatorname{div}\left(\frac{\mathbf{K}_f^0}{\mu_f}\frac{\Phi^3}{1-\Phi^2}S(p_f)^b\cdot\nabla p_f - \mathcal{F}_0^{\text{nl}}(\nabla p_f, \Phi)\right).$$

It is a nonlinear elliptic partial differential equation if \mathbf{v}_s is sufficiently small. It has to be supplemented by suitable Dirichlet and Neumann boundary conditions. The different parts of the boundary are shown in Figure 4 in the case of a roll press nip. Nevertheless, the terminology directly applies to shoe presses. It is assumed, that Ω_1 is the paper layer. Provided that Γ_i is sufficiently far away from the center of the nip, it is reasonable to prescribe the saturation $S_{0,i}$ of each porous layer there. Using (5.10), one gets Dirichlet conditions for the pressure which are uniquely defined if the prescribed saturations are less than 1. This is always the case in real life. Moreover, we assume the system of layers to be in equilibrium, i.e. there is no fluid exchange between layers. Therefore, the Dirichlet conditions are even constant. Again, if Γ_o is sufficiently far away from the center of the nip, it is natural to assume the normal component of the relative velocity $\mathbf{v}_f - \mathbf{v}_s$ to be zero. By the aid of (5.14) one obtains a homogeneous Neumann boundary condition for p_f . Vanishing normal components of the fluid velocity are applied to all of the remaining parts of the boundary. Since the normal component of the solid velocity is zero on these parts, we have again a homogeneous Neumann boundary condition. On the parts of the boundary where the paper-felt sandwich is in contact to the press

profiles, i.e. $\Gamma_{i,c}$, $\Gamma_{b,c}$, this condition is correct since roll and shoe profiles are impervious. On $\Gamma_{t,i}$, $\Gamma_{b,i}$, $\Gamma_{t,o}$ and $\Gamma_{b,o}$ the situation may be different depending on process conditions. Observations show that fluid may escape through the top and bottom surface of the felt. In the simulations presented below, there is a very low pressure near these boundaries and, therefore, it is save to to apply homogeneous Neumann conditions. As shown in Figure 3, the paper and the felt are separated before and after the nip. We account for this fact by the introduction of $\Gamma_{sep,i}$, $\Gamma_{sep,o}$.

5.1.3. Remark on roll surfaces and belts. Besides paper and felt layers, there appear other types of layers in the press nip. We additionally find grooved roll surfaces, roll surfaces with wholes and grooved shoe press belts. These layers provide void space for the fluid, thereby decreasing the hydrodynamic pressure. The length scale of the void space structure is much coarser than the micro structure of the felt and paper fibers. Nevertheless, we model them as porous media. Their porosity is given by the ratio of void and solid space. Their permeability is set orders of magnitude higher than the respective permeabilities of felt and paper layers. The reason behind is the fact, that very small flow resistivity is to be expected due to the coarse structure. Additionally, similar to the paper layer, we introduce separating boundaries, which are determined automatically by the computed values for x_r and x_l .

5.2. Numerical solution algorithms

In this section, we present the algorithmic structure and numerical methods to solve the model equations which are derived above. The flow chart in Figure 6 shows the sequence of basic solution steps.

5.2.1. Elasticity solver. First, the press geometry is created. For that purpose, the profiles are fixed in machine direction by suitable input parameters. The lower press profile is additionally fixed in transversal direction. Then, by using d_{min} , the position of the upper press can be computed. Now, we enter *Phase 0* of the deformation simulation. z_i fixes the vertical position of the layers (see Figure 4). Starting at x_i , the x position is incremented, thereby monitoring the function f defined in (5.4). The first x position where f is smaller than l_0 determines x_r and *Phase 0* is finished. During the computation of x_r , there may be a *collision* of the porous layers and the press profiles. In that case, the horizontal fixation is done by aligning the layers to the collision press profile.

In *Phase 1*, the deformation is computed according to the model equations

(5.2), ..., (5.5). To simplify the exposition, a linear elasticity law is chosen, i.e. $E_i(\varepsilon_i) = A_i \cdot \varepsilon$. The method can be extended with minor changes to laws of type $E_i(\varepsilon_i) = A_i \cdot \varepsilon_i^r$, $r \geq 1$. Equation (5.5) allows to express ε_1 in terms of ε_i , $i = 2 \dots n$:

$$(5.16) \quad \varepsilon_1(x) = \frac{1}{l_{0,1}}(l_0 - f(x) - \sum_{i=2}^n \varepsilon_i(x)l_{0,i}).$$

Plugging (5.16) in the first equation of (5.2), yields a system in ε_i , $i = 2 \dots n$ and τ . τ is eliminated by subtracting the second equation in (5.2) from all others. Hence we have the following system of ordinary differential equations in ε_i , $i = 2 \dots n$:

$$(5.17) \quad \mathbf{A} \cdot \varepsilon' = \mathbf{B} \cdot \varepsilon + \mathbf{c}(x),$$

where \mathbf{A} and \mathbf{B} are $n - 1$ -quadratic matrices with constant entries and $\mathbf{c}(x)$ is a $n - 1$ -vector depending on x . $\varepsilon = (\varepsilon_2, \dots, \varepsilon_n)^T$. More precisely, we have:

$$\mathbf{A} = \begin{pmatrix} \Lambda_2 c A_2 + \Lambda_1 c A_1 \frac{l_{0,2}}{l_{0,1}} & \Lambda_1 c A_1 \frac{l_{0,3}}{l_{0,1}} & \Lambda_1 c A_1 \frac{l_{0,4}}{l_{0,1}} & \dots & \Lambda_1 c A_1 \frac{l_{0,n}}{l_{0,1}} \\ -\Lambda_2 c A_2 & \Lambda_3 c A_3 & 0 & \dots & 0 \\ -\Lambda_2 c A_2 & 0 & \Lambda_4 c A_4 & \dots & 0 \\ \vdots & & \dots & & \vdots \\ -\Lambda_2 c A_2 & 0 & 0 & \dots & \Lambda_n c A_n \end{pmatrix},$$

$$\mathbf{B} = \begin{pmatrix} -A_2 - A_1 \frac{l_{0,2}}{l_{0,1}} & -A_1 \frac{l_{0,3}}{l_{0,1}} & -A_1 \frac{l_{0,4}}{l_{0,1}} & \dots & -A_1 \frac{l_{0,n}}{l_{0,1}} \\ A_2 & -A_3 & 0 & \dots & 0 \\ A_2 & 0 & -A_4 & \dots & 0 \\ \vdots & & \dots & & \vdots \\ A_2 & 0 & 0 & \dots & -A_n \end{pmatrix}$$

and

$$\mathbf{c}(x) = \begin{pmatrix} \frac{A_1}{l_{0,1}}(l_0 - f(x)) - \frac{\Lambda_1 c A_1}{l_{0,1}} f'(x) - K \tau_{max}(x) \\ 0 \\ \vdots \\ 0 \end{pmatrix}.$$

The matrix \mathbf{A} is invertible, due to the fact that all parameters A_i , Λ_i , $l_{0,i}$ and c are strictly positive. Therefore, we can write (5.17) in canonical form

$$(5.18) \quad \varepsilon' = \mathbf{A}^{-1} \mathbf{B} \cdot \varepsilon + \mathbf{A}^{-1} \mathbf{c}(x).$$

This system is solved by the classical fourth-order Runge-Kutta method.

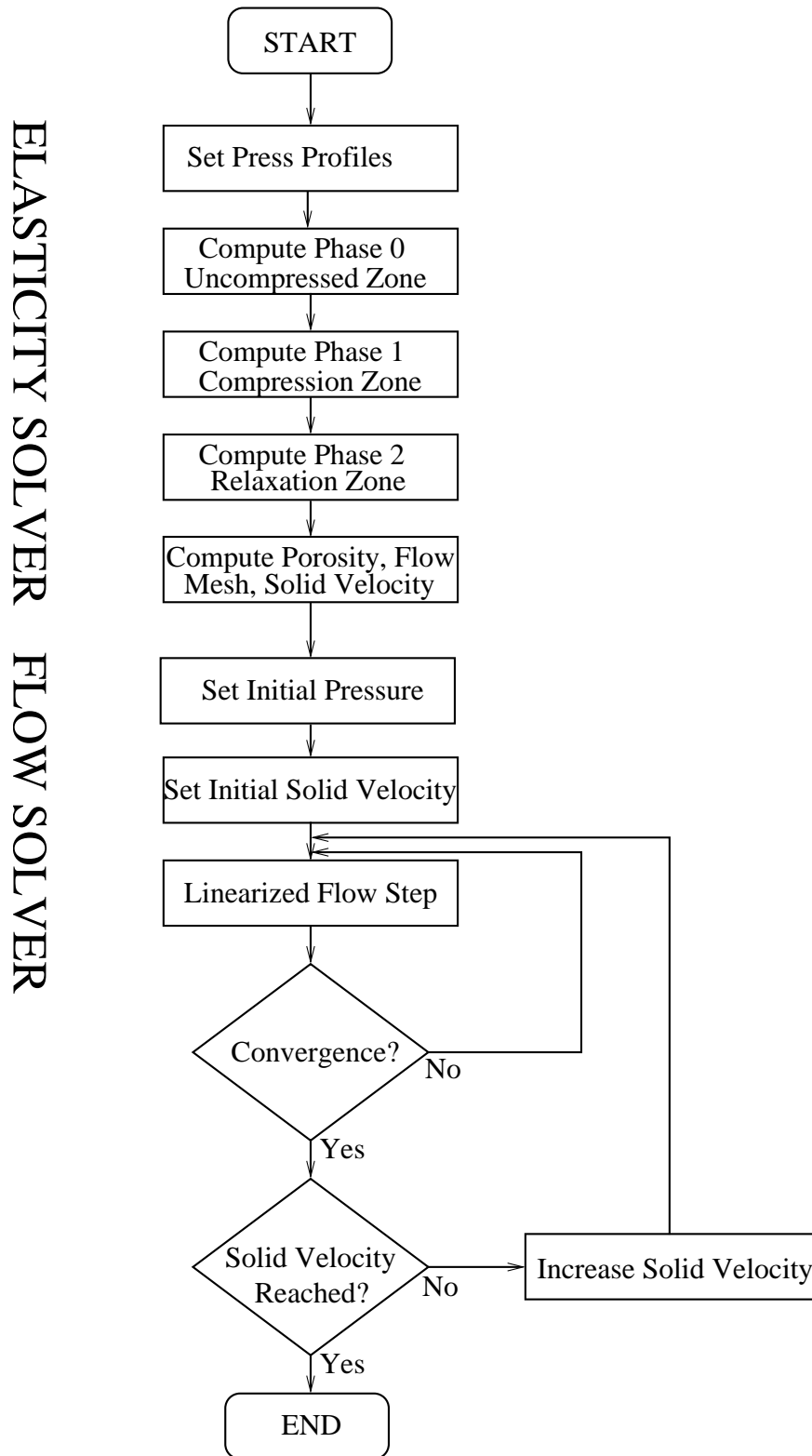


FIGURE 6. Flow chart of simulation steps

Initial conditions are given by

$$\varepsilon(x_l) = 0.$$

ε_1 and τ are computed using (5.16) and (5.2). By identifying the first zero of the function τ , we get the point x_r .

REMARK 5.1. To solve the equations of *Phase 1*, f has to be differentiable. This is no further restriction of our model. Smoothness is a technical requirement to reduce wear and guarantee paper quality and can be supposed to be given.

The system of equations describing the second phase reads:

$$(5.19) \quad \begin{aligned} E_1(\varepsilon_1) + \Lambda_1 c \frac{d}{dx} E_1(\varepsilon_1) - K\tau_{max} &= 0, \\ E_i(\varepsilon_i) + \Lambda_i c \frac{d}{dx} E_i(\varepsilon_i) &= 0 \quad i = 2 \dots n. \end{aligned}$$

The values of $\varepsilon_i(x_r)$ are used as initial conditions. Equations (5.19) are similar to previous set of equations of *Phase 1* besides the fact that τ is zero. The solution of this system is given analytically by

$$\begin{aligned} E_1(\varepsilon_1(x)) &= C_1 \cdot e^{-\frac{x-x_r}{\Lambda_1 c}} + C_2, \\ E_i(\varepsilon_i(x)) &= E_i(\varepsilon_i(x_r)) \cdot e^{-\frac{x-x_r}{\Lambda_i c}}, \quad i = 2 \dots n, \end{aligned}$$

where $C_1 = E_1(\varepsilon_1(x_r)) - K\tau_{max}(x_r)$ and $C_2 = K\tau_{max}(x_r)$. Now, we can calculate the input data needed by the flow solver. The porosity of each layer is computed by formula (5.6). The deformed grid which the flow solver needs is constructed from a regular mesh whose nodes are displaced (see Figure 7). More precisely, we store the z coordinates of points on $\Gamma_{b,i} \cup \Gamma_{b,c} \cup \Gamma_{b,o}$ during the elasticity computation. Since the step size of the Runge-Kutta method is much finer than the required mesh for the flow solver, we have precise information on the z coordinates of the flow mesh points on this boundary. Using the computed strains which are constant on each layer, the displacement of the flow mesh is immediately obtained. To obtain the solid velocities, we consider three points P_1 , P_2 and P_3 as shown in Figure 7. Since the deformed mesh is still equidistant in machine direction, the x component of the solid velocity is set to machine speed. Hence, the time and the vertical distance to move from point P_1 to P_3 is known. We use this information to compute the solid velocity at P_2 .

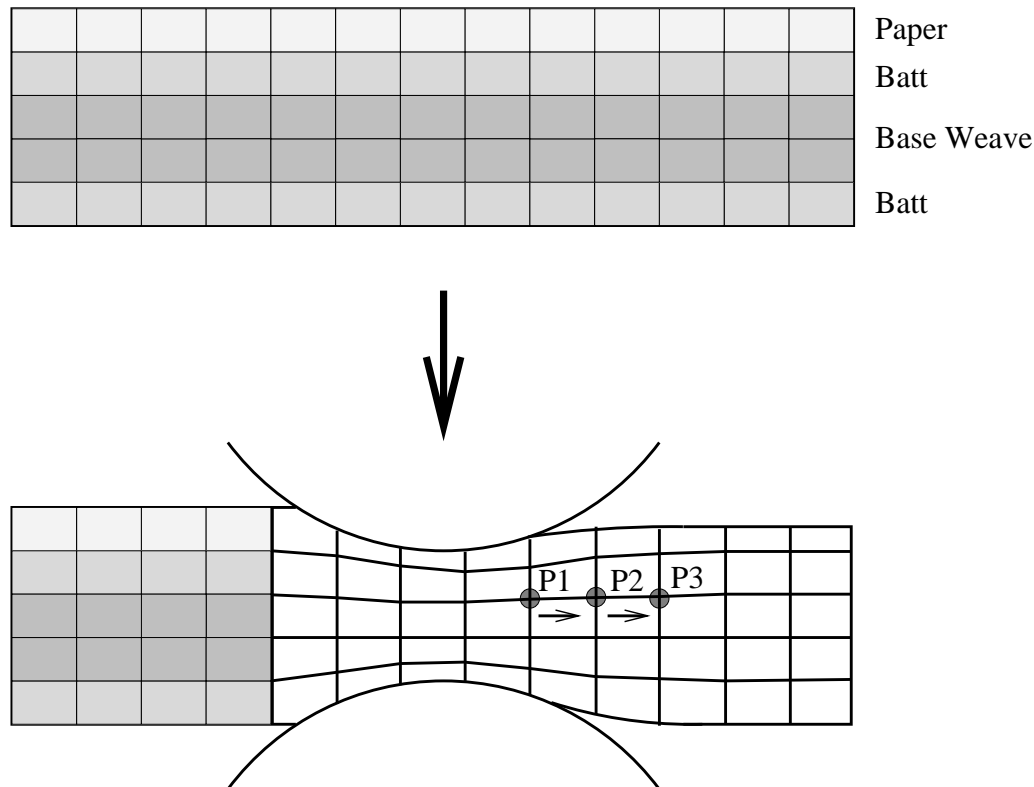


FIGURE 7. Regular and deformed mesh

5.2.2. Flow solver. The *design* of the algorithm to solve the flow problem (5.15) is guided by several observations. Since the flow problem is nonlinear, a suitable linearization has to be developed. The linearization induces some kind of iteration, whose convergence is strongly dependent on the initial choice of the solution. Remembering the boundary conditions for the pressure p_f , we immediately see, that p_f is equal to the constant Dirichlet boundary value on Γ_i , if the solid velocity is equal to zero. On the other hand, if the solid velocity increases, the pressure will rise, too. Therefore, as shown in Figure 6, a outer loop is implemented which increases the solid velocity. More precisely, starting from the known constant pressure solution, the solid velocity is scaled by a factor less than one and sufficiently small such that the nonlinear flow iteration steps (inner loop) converge. The scaling factor of the solid velocity is then increased and the inner loop is processed again. The iteration stops, when the desired final solid velocity is reached or other stopping criteria apply.

Let's have a closer look at the inner loop. We define

$$S' := \frac{\partial S(p_f)}{\partial p_f}.$$

Then, the truncated Taylor series of the retention function reads

$$(5.20) \quad S(p_f^{j+1}) \approx S(p_f^j) + S'(p_f^j)(p_f^{j+1} - p_f^j),$$

where $j \in \mathbb{N}$ is used as iteration index and p_f^{j+1} and p_f^j can be thought of two consecutive solutions of an iteration process. Plugging (5.20) into (5.15) and by further iterative linearization, we obtain

$$(5.21) \quad -\operatorname{div} \left(\left(S(p_f^j) + S'(p_f^j)(p_f^{j+1} - p_f^j) \right) \Phi \mathbf{v}_s \right) - \operatorname{div} \mathcal{F}_0^{\text{nl}}(\nabla p_f^j, \Phi) \\ = -\operatorname{div} \left(\frac{\mathbf{K}_f^0}{\mu_f} \frac{\Phi^3}{1-\Phi^2} S(p_f^j)^b \cdot \nabla p_f^{j+1} \right).$$

Reordering in terms of p_f^j and p_f^{j+1} yields

$$(5.22) \quad -\operatorname{div} \left(\left(S(p_f^j) - S'(p_f^j)p_f^j \right) \Phi \mathbf{v}_s \right) - \operatorname{div} \mathcal{F}_0^{\text{nl}}(\nabla p_f^j, \Phi) \\ = -\operatorname{div} \left(\frac{\mathbf{K}_f^0}{\mu_f} \frac{\Phi^3}{1-\Phi^2} S(p_f^j)^b \cdot \nabla p_f^{j+1} - S'(p_f^j)p_f^{j+1} \Phi \mathbf{v}_s \right).$$

REMARK 5.2. The linearization of (5.15) is motivated by Newton-type methods. Numerical experiments show that the expansion (5.20) is quite important to guaranty fast convergence.

In view of a finite element discretization of (5.22), a variational formulation is derived. Due to the Dirichlet boundary conditions on Γ_i , we define a subspace of $H^1(\Omega)$ by

$$V := \{v \in H^1(\Omega) \mid v = 0 \quad \text{on } \Gamma_i\},$$

where the domain Ω is the union of all deformed layers $\Omega_1, \dots, \Omega_n$ (see Figure 4). The pressure can be decomposed into

$$(5.23) \quad p_f^j = \hat{p}_f^j + p_0, \quad \hat{p}_f^j \in V \quad \text{and} \quad p_0 \in H^1(\Omega),$$

where the function p_0 (as extension of a constant function on Γ_i into $H^1(\Omega)$) represents the Dirichlet conditions on Γ_i .

Now, let $w \in V$ be a test function. Multiplying (5.22) by w , using (5.23),

integrating over Ω and applying Green's formula, yields

$$\begin{aligned}
(5.24) \quad & \int_{\Omega} \left(\left(S(p_f^j) - S'(p_f^j)p_f^j \right) \Phi \mathbf{v}_s + \mathcal{F}_0^{\text{nl}}(\nabla p_f^j, \Phi) \right) \cdot \nabla w \, dx \\
& - \int_{\partial\Omega} \nu(x) \cdot \left(\left(S(p_f^j) - S'(p_f^j)p_f^j \right) \Phi \mathbf{v}_s + \mathcal{F}_0^{\text{nl}}(\nabla p_f^j, \Phi) \right) w \, d\Gamma(x) \\
& - \int_{\Omega} \left(\frac{\mathbf{K}_f^0}{\mu_f} \frac{\Phi^3}{1 - \Phi^2} S(p_f^j)^b \cdot \nabla p_0 - S'(p_f^j)p_0 \Phi \mathbf{v}_s \right) \cdot \nabla w \, dx \\
& + \int_{\partial\Omega} \nu(x) \cdot \left(\frac{\mathbf{K}_f^0}{\mu_f} \frac{\Phi^3}{1 - \Phi^2} S(p_f^j)^b \cdot \nabla p_0 - S'(p_f^j)p_0 \Phi \mathbf{v}_s \right) w \, d\Gamma(x) \\
= & \int_{\Omega} \left(\frac{\mathbf{K}_f^0}{\mu_f} \frac{\Phi^3}{1 - \Phi^2} S(p_f^j)^b \cdot \nabla \hat{p}_f^{j+1} - S'(p_f^j)\hat{p}_f^{j+1} \Phi \mathbf{v}_s \right) \cdot \nabla w \, dx \\
& - \int_{\partial\Omega} \nu(x) \cdot \left(\frac{\mathbf{K}_f^0}{\mu_f} \frac{\Phi^3}{1 - \Phi^2} S(p_f^j)^b \cdot \nabla \hat{p}_f^{j+1} - S'(p_f^j)\hat{p}_f^{j+1} \Phi \mathbf{v}_s \right) w \, d\Gamma(x).
\end{aligned}$$

In (5.24), all boundary integrals vanish due to the specified boundary conditions and due to the properties of the test function. Hence, we have the following variational formulation:

$$\begin{aligned}
(5.25) \quad & \text{Find } \hat{p}_f^{j+1} \in V, \text{ such that} \\
& \int_{\Omega} \left(\left(S(p_f^j) - S'(p_f^j)p_f^j \right) \Phi \mathbf{v}_s + \mathcal{F}_0^{\text{nl}}(\nabla p_f^j, \Phi) \right) \cdot \nabla w \, dx \\
& - \int_{\Omega} \left(\frac{\mathbf{K}_f^0}{\mu_f} \frac{\Phi^3}{1 - \Phi^2} S(p_f^j)^b \cdot \nabla p_0 - S'(p_f^j)p_0 \Phi \mathbf{v}_s \right) \cdot \nabla w \, dx \\
= & \int_{\Omega} \left(\frac{\mathbf{K}_f^0}{\mu_f} \frac{\Phi^3}{1 - \Phi^2} S(p_f^j)^b \cdot \nabla \hat{p}_f^{j+1} - S'(p_f^j)\hat{p}_f^{j+1} \Phi \mathbf{v}_s \right) \cdot \nabla w \, dx, \quad \forall w \in V.
\end{aligned}$$

As already mentioned above, at least for moderate solid velocities, (5.25) is an elliptic problem. It is solved by a finite element discretization quite similar to the methods discussed in Section 3.2.3.1. The pressure is discretized by bilinear Ansatz functions on quadrilateral grids. Matrix assembly is done on a reference element using the nine-point Gaussian integration rule. Due to the deformation, we have to handle general quadrilaterals. Therefore, the simple coordinate transformation of the square case has to be extended. We used a standard method for which we refer to [57], p. 188ff. The system of linear equations is directly solved by SuperLU 3.0 (see [19]).

5.3. General model parameters

The aim of this section is to provide model parameters for the numerical studies at the end of this chapter. To determine the permeability tensor \mathbf{K}_f^0 , we create

a virtual felt made of three layers. Inspired by images like the one shown in Figure 8 and data from [73], the virtual felt has a fine fiber batt layer on top, a base weave in the middle and, finally, another batt layer.

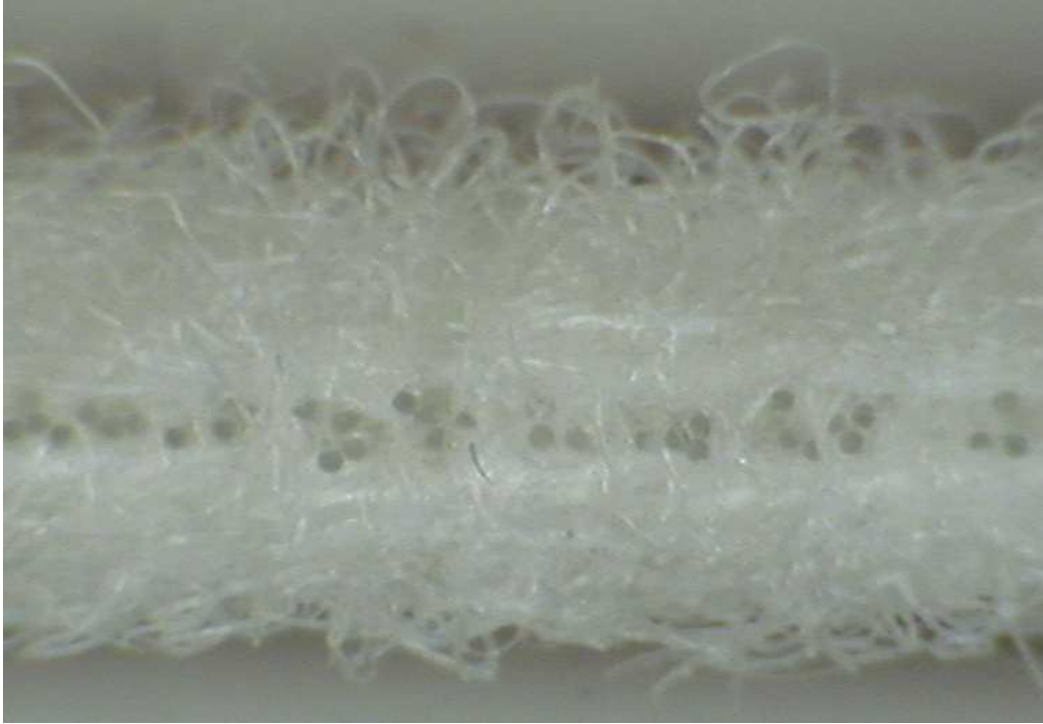


FIGURE 8. Cross section of a dewatering felt

The upper batt layer has a length of 1mm in the transversal direction and its porosity is 60%. It consists of 50% 10d tex and 50% 20d tex fibers made from polyamid 6. The unit d tex is equivalent to $\frac{1\text{g}}{10000\text{m}}$ and, hence, the actual diameter depends on the material's density. In case of polyamid 6 and round fibers, 10d tex and 20d tex correspond to $33.4\mu\text{m}$ and $47.3\mu\text{m}$, respectively. The other batt layer has a thickness of 0.5mm , 20d tex fibers only, and its porosity is 65%. The base weave has a certain arrangement of yarns. Each yarn is $350\mu\text{m}$ thick. We added a mixture of 50% 10d tex and 50% 20d tex fibers, which then results in an overall porosity of 45%. The thickness is 1.5mm . Since the fibers are usually attached to the base weave by a needling process, the fiber orientation is chosen to be transversally dominated. Figures 9, 10, 11 illustrate the generated geometries. All layers are created by GeoDict, which is a virtual structure generator developed at Fraunhofer ITWM. The resolution is chosen to be $5\mu\text{m}$. The lateral cross section of each layer is $1.8 \times 1.8\text{mm}^2$.

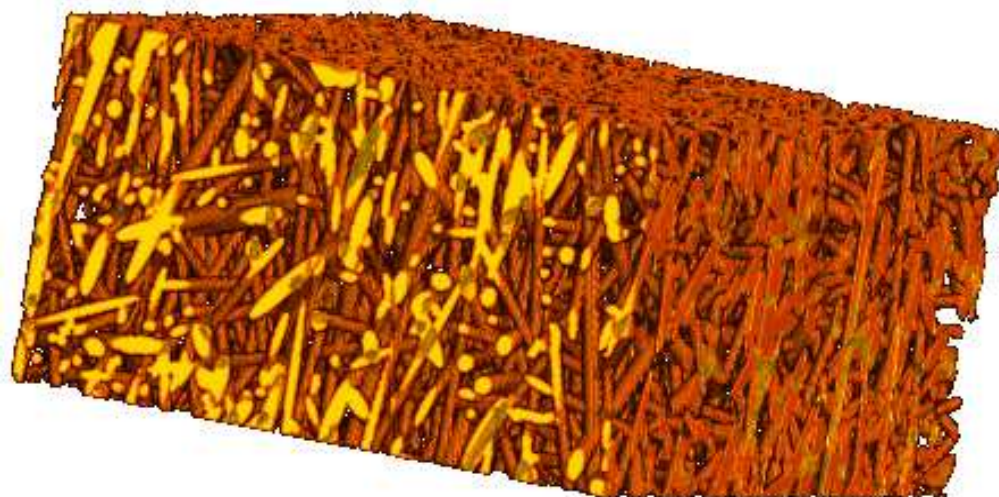


FIGURE 9. Model of the upper batt fiber layer

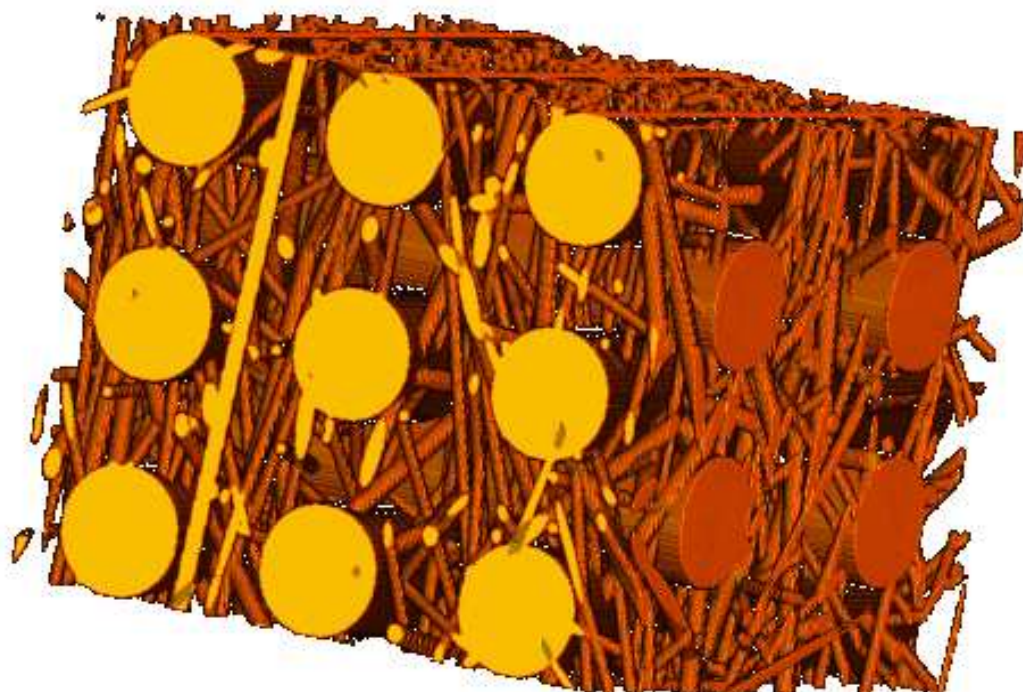


FIGURE 10. Model of the base weave layer

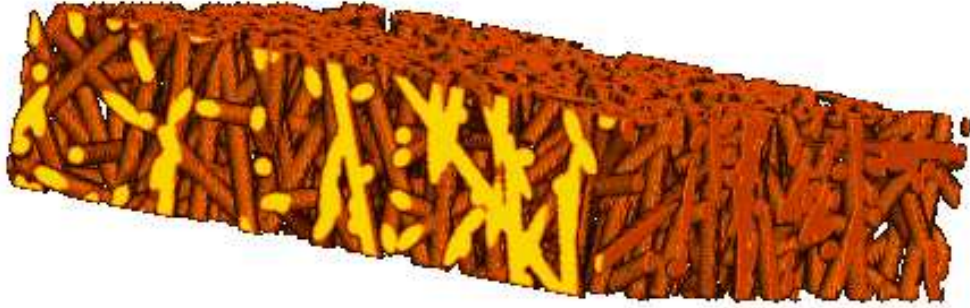


FIGURE 11. Model of the lower batt fiber layer

By the use of ParPac, which is a Lattice-Boltzmann solver by Fraunhofer ITWM, we can compute the permeability tensor \mathbf{K}_f^0 of the individual layers in three dimensions. More precisely, Stokes problems are calculated quite similar to the cell problems introduced in Chapter 2. The only difference is, that we don't homogenize the Stokes system, but calculate the effective permeability, i.e. essentially a velocity-pressure-drop relation on a sufficiently large volume element of the porous medium, i.e. of the felt. The calculated permeabilities restricted to the x- and z-direction are shown in Table 1. Due to the computational complexity, we can not compute nonlinear filtration laws as we did in Chapter 3. However, simulations indicate that nonlinear effects are important. At pressure drops of $10000 Pa/mm$ applied to the layers, one observes flow rates being significantly smaller than in the linear case. Motivated by these observations, we construct nonlinear filtration laws, which give at least qualitatively the correct behavior and allow to study the influence of inertia on paper dewatering. Based on a linear interpolation of the computed data given in Table 2, we determine \mathcal{F}_0^{nl} . For simplicity, we drop the dependence on the porosity.

Additional parameters of the elasticity and fluid dynamical model are based on data given in [75]: For each layer, we set the residual saturation to be $s_\infty = 0.1$. The shape factor b in (5.11) is chosen to be 3.4 and the fluid pressure at the inlet is $p_{f|\Gamma_i} = -5000 Pa$. For the dynamic viscosity we assume $\mu_f = 6.53 \cdot 10^{-4} Pa \cdot s$. This value corresponds to water viscosity at $\approx 40^\circ C$. The initial saturations are 0.55, 0.45 and 0.50 for upper batt, base weave and lower batt, respectively. In [75] measurements to determine the viscoelastic parameters of an entire felt are presented. The stress-strain relation is assumed nonlinear, i.e. $E(\varepsilon) = A \cdot \varepsilon^r$ and we obtain $r \approx 2$ and $A \approx 40 MPa$. The viscoelastic time constant λ is of size $0.4 ms$. It can be expected, that the

	Upper Batt	Base Weave	Lower Batt
l_0 [mm]	1.00	1.50	0.50
A [MPa]	30	70	40
r [1]	2	2	2
λ [ms] 0.4	0.4	0.4	0.4
Φ_0 [1]	0.60	0.45	0.65
S_0 [1]	0.55	0.45	0.50
$K_{f_{xx}}^0$ [m^2]	$8.77 * 10^{-11}$	$4.97 * 10^{-10}$	$1.73 * 10^{-10}$
$K_{f_{zz}}^0$ [m^2]	$1.54 * 10^{-10}$	$1.12 * 10^{-9}$	$2.50 * 10^{-10}$
$K_{f_{xz}}^0 = K_{f_{zx}}^0$ [m^2]	$1.44 * 10^{-12}$	$8.57 * 10^{-12}$	$-5.34 * 10^{-12}$

TABLE 1. Felt parameters

	Upper Batt	Base Weave	Lower Batt
MD-Ratio at $1Pa/mm$ [%]	100.0	100.0	100.0
MD-Ratio at $2000Pa/mm$ [%]	95.0	68.0	81.0
MD-Ratio at $10000Pa/mm$ [%]	72.0	40.0	51.0
CD-Ratio at $1Pa/mm$ [%]	100.0	100.0	100.0
CD-Ratio at $2000Pa/mm$ [%]	93.0	70.0	78.0
CD-Ratio at $10000Pa/mm$ [%]	70.0	40.0	48.0

TABLE 2. Computed ratios of nonlinear and linear flow rates in MD and CD

individual layers deform differently due to their different constituents. Therefore, we preserve the structure of the nonlinear law in each layer, but vary the constant A as listed in Table 1. Note, that the overall elastic response is not preserved by this heuristic choice. However, we are only interested to have qualitatively reasonable parameters, which are in the range of existing felt designs.

Now, we discuss the parameters of the paper layer, roll surface and belt. Due to the lack of measurements, the elastic parameters of the paper layer are chosen to give reasonable deformation during pressing. We want to observe a *gradual* deformation of the paper and its thickness should be decreased by not more than 50%. Due to fine cellulose fibers, which are in the range of $10\mu m$,

	Paper	Roll surface	Belt
l_0 [mm]	0.3	3	3
A [MPa]	40	10000	10000
r [1]	1.6	1	1
λ [ms]	0.4	0.4	0.4
K [1]	0.7	–	–
Φ_0 [1]	0.7	0.25	0.25
S_0 [1]	0.99	0.4 0.6	0.4 0.6
$K_{f_{xx}}^0$ [m^2]	$1.0 * 10^{-11}$	$1.0 * 10^{-8}$	$1.0 * 10^{-8}$
$K_{f_{zz}}^0$ [m^2]	$6.0 * 10^{-12}$	$1.0 * 10^{-8}$	$1.0 * 10^{-8}$
$K_{f_{xz}}^0 = K_{f_{zx}}^0$ [m^2]	0.0	0.0	0.0

TABLE 3. Parameters of paper, roll surface and belt

the paper permeability is set lower than the felt permeability. Test simulations in a micro structure made of $10\mu m$ fibers give permeabilities, which are one up to two orders smaller than the felt permeabilities. Moreover, it is well-known that the orientation of paper fibers is aligned to the machine direction due to process conditions in the forming section. We account for it by introducing an anisotropy of the permeability values in x- and z-direction. Again, the ratio is determined by simulations using the micro structure made of $10\mu m$ fibers. To account for inertia, the nonlinear filtration law of the paper layer is chosen similarly as in the case of the upper batt fiber layer. The *dry solids content* of paper is typically defined by the ratio of fiber mass to total mass. The initial saturation and initial porosity are chosen such that the dry solids content is $\approx 27.8\%$ assuming a paper weight of $80g/m^2$. In our numerical studies, the roll surfaces and belts possess wholes and a grooved structure, respectively. The dimension of the wholes and grooves are in the range of millimeters. Therefore, we chose a rather large permeability. Moreover, these layers will never be fully saturated in our simulation, which makes the use of nonlinear filtration laws obsolete. The elastic stiffness is relatively large compared to the fibrous structures. Hence, small deformations can be expected and it is reasonable to assume linear behavior. Typical values of A are in the range of $10000MPa$. The initial saturation is set to either 40% or 60%. All parameters are listed in Table 3.

Two types of press configurations are considered in the following section. The first type is a roll press nip. The rolls are $1200mm$ in diameter and positioned

at $x = 0mm$. The second type is a shoe press nip. The shoe is modeled as part of a circle with radius $1000mm$ being positioned at $x = 0mm$. The length of the shoe is chosen to be $250mm$. The opposing roll has a radius of $900mm$ and its center is positioned at $x = 3mm$. The arrangement of the layers is as follows: On top, there is the paper layer. Then, the three felt layers, i.e. upper batt, base weave and lower batt, follow. In case of the roll press nip, we find the roll surface as the lowest layer. In case of the shoe press nip, the final layer is formed by the belt.

As indicated by Figure 3, the paper layer is separated from the felt right after the press nip. Therefore, we introduce one paper separation point at $x = 40mm$ and $x = 140mm$ in case of the roll press nip and the shoe press nip, respectively. At the specific point, a boundary is introduced between the paper layer and the upper batt layer, which reaches to the right boundary of the computational domain and suppresses any fluid flow. Analogously, separating boundaries for the roll surface and the belt are introduced. They are determined by x_r and x_l (see Figure 4).

5.4. Numerical results and discussion

We use the parameters of the previous section unless otherwise stated. All numerical examples are discretized by a 1500×500 mesh. In case of the roll press, we simulate the nip for $x \in [-100, 400]$. The shoe press simulations are done in the range of $x \in [-300, 400]$. We start the computations at $\mathbf{v}_s = 250m/min$ and increase the solid velocity in steps of $250m/min$. At each velocity level, we solve the nonlinear problem until the relative accuracy of the pressure update is less than 10^{-4} . To reach this precision, typically five up to ten iterations are needed.

5.4.1. Roll press nip. In this section, we present numerical results of a roll press nip. The minimum distance d_{min} of the press profiles is automatically adjusted to match a press force of $200kN/m$. In Figure 12, 13, the porosity is shown at $\mathbf{v}_s = 750m/min$ and $\mathbf{v}_s = 1250m/min$, respectively. Higher machine speeds increase viscoelastic stresses, hence the permanent deformation of the paper layer becomes larger. Note, that the roll surface is hardly compressed in this setting.

Now, we consider results related to the flow model without nonlinear filtration laws. The degree of saturation is presented in Figure 14, 15 and 16. Figure 14 corresponds to $\mathbf{v}_s = 750m/min$ and an initial saturation of the roll surface of 40%. In Figure 15, the machine speed is increased to $\mathbf{v}_s = 1250m/min$. Additionally, in Figure 16, the initial saturation of the roll surface is set to 60%,

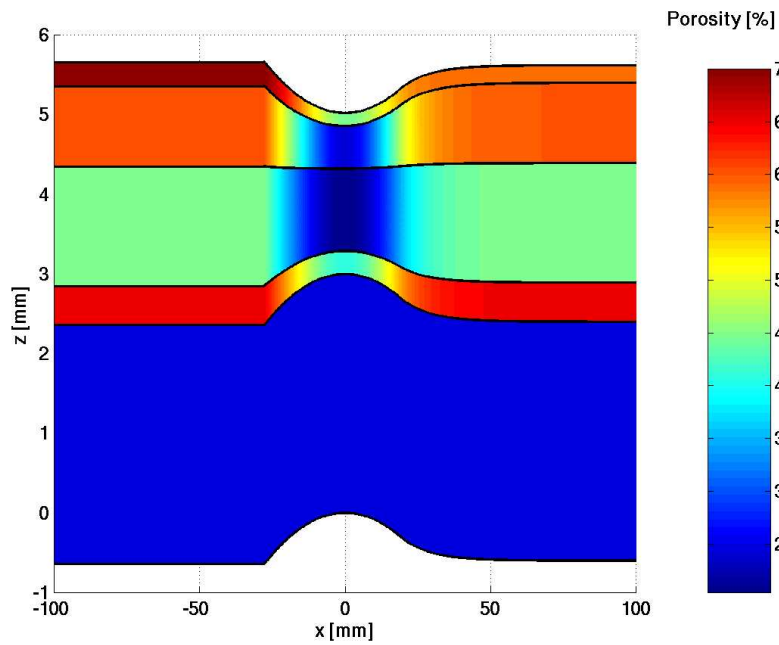
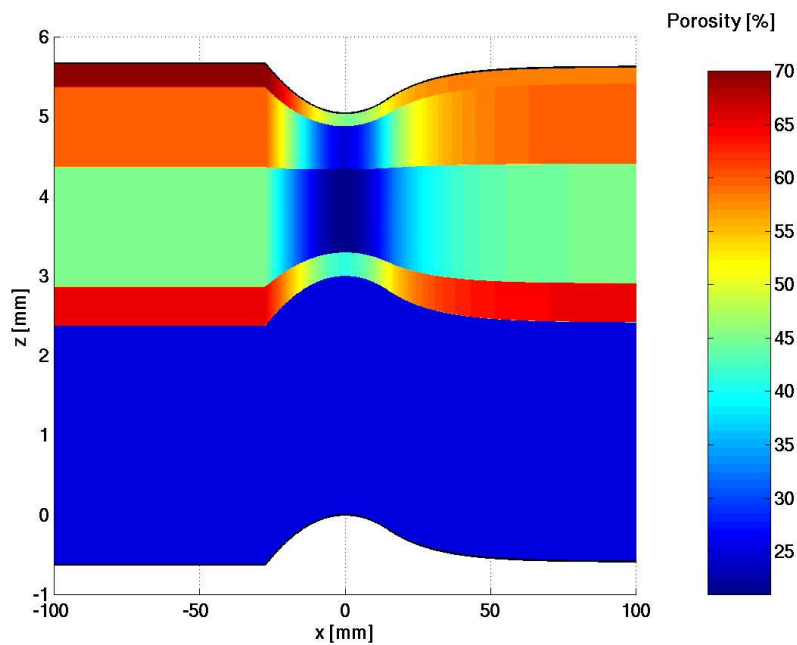
which shows a strong effect building up a fully saturated zone in transversal direction. All pictures show how the fluid is transported from the paper through the felt entering the roll surface.

For the same three setting, the hydrodynamic pressure is shown in Figure 17, 18 and 19. Due to the stronger compression especially of the paper layer, a larger amount of fluid has to be transported in shorter time and, therefore, the pressure increases as the machine speed goes up. In Figure 19, this effect becomes even stronger which is due to the increased fluid content of the roll surface.

In Figure 20, the fluid velocity is illustrated. The dewatering zone right before the center of the nip can clearly be observed. The dewatering turns into rewetting, which is less obvious, but very important in practice. Looking at Figure 21, a typical profile of the dry solids content of paper is plotted. Here, the dewatering and rewetting zones are clearly observable. The final dry solids contents of the paper layer are 41.80%, 43.11% and 41.47% for the three settings, respectively. This result is consistent with the aforementioned remarks on compression and fluid content of the overall nip.

Finally, we investigate the effect of inertia. Figure 22 corresponds to Figure 14. The saturations hardly differ. However, the underlying model included nonlinear filtration laws. The situation changes when looking at the pressures. Corresponding to Figure 17, 18 and 19, we see in Figure 23, 24 and 25 significantly increased hydrodynamic pressures.

From this observations, we draw the following conclusions: Since the saturations hardly change when incorporating nonlinear filtration laws in the flow model, the dewatering performance of the nip is hardly effected. Nevertheless, looking at Figure 26 and thinking of higher machine speeds, it might be reasonable to consider hydrodynamic pressures as additional stress in the elasticity model. This will increase d_{min} and influence the flow problem via changes in porosity.

FIGURE 12. Porosity: $v_s = 750m/min$ FIGURE 13. Porosity: $v_s = 1250m/min$

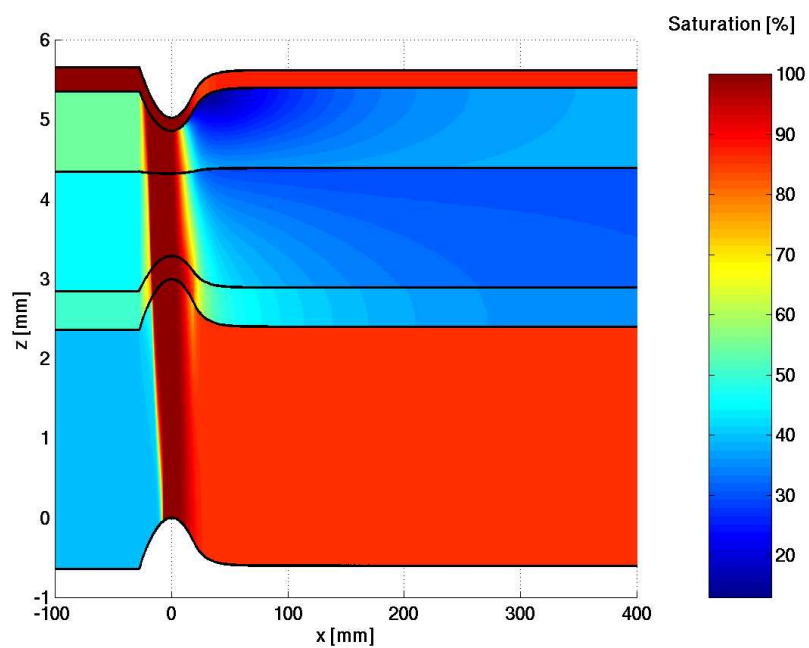


FIGURE 14. Saturation: $v_s = 750m/min$ and initial roll surface saturation $S_0 = 40\%$

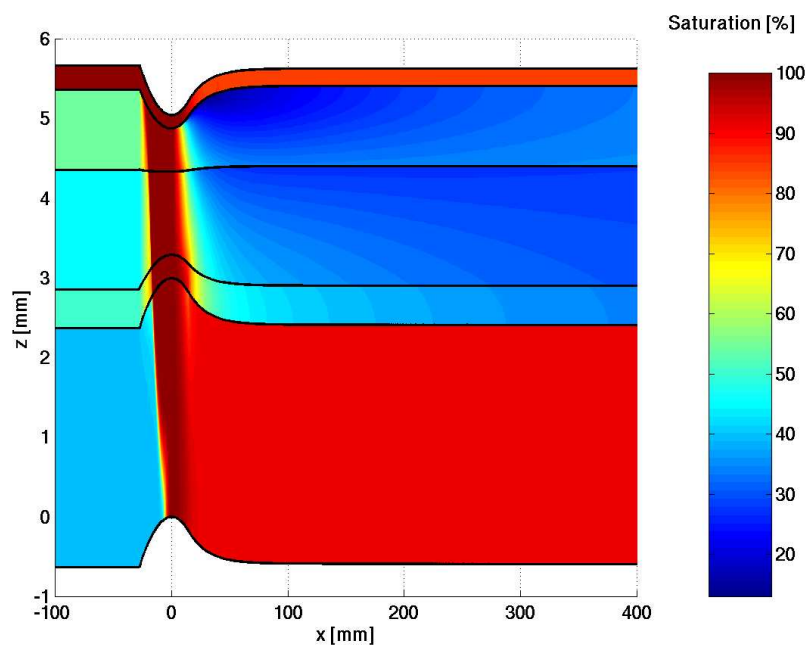


FIGURE 15. Saturation: $v_s = 1250m/min$ and initial roll surface saturation $S_0 = 40\%$

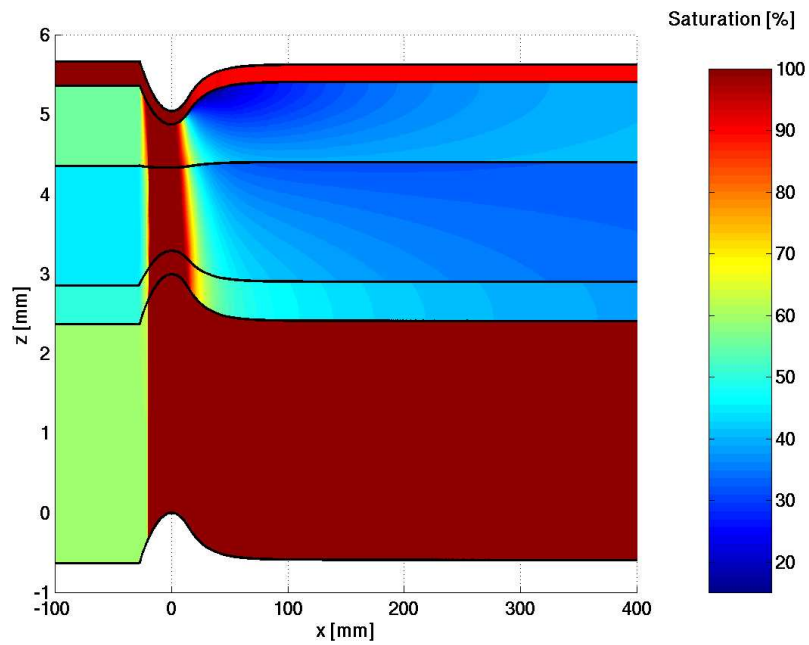


FIGURE 16. Saturation: $v_s = 1250m/min$ and initial roll surface saturation $S_0 = 60\%$

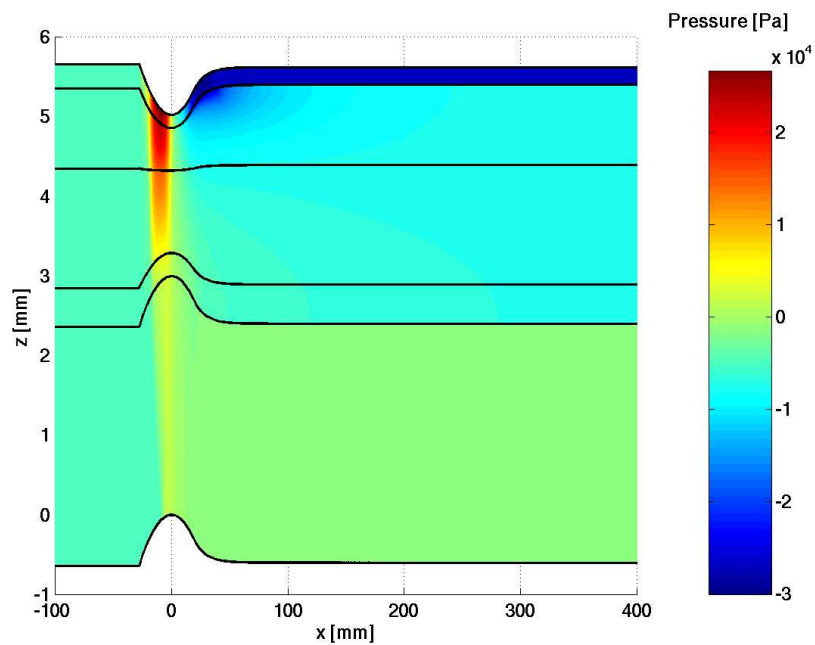


FIGURE 17. Pressure: $v_s = 750m/min$ and initial roll surface saturation $S_0 = 40\%$

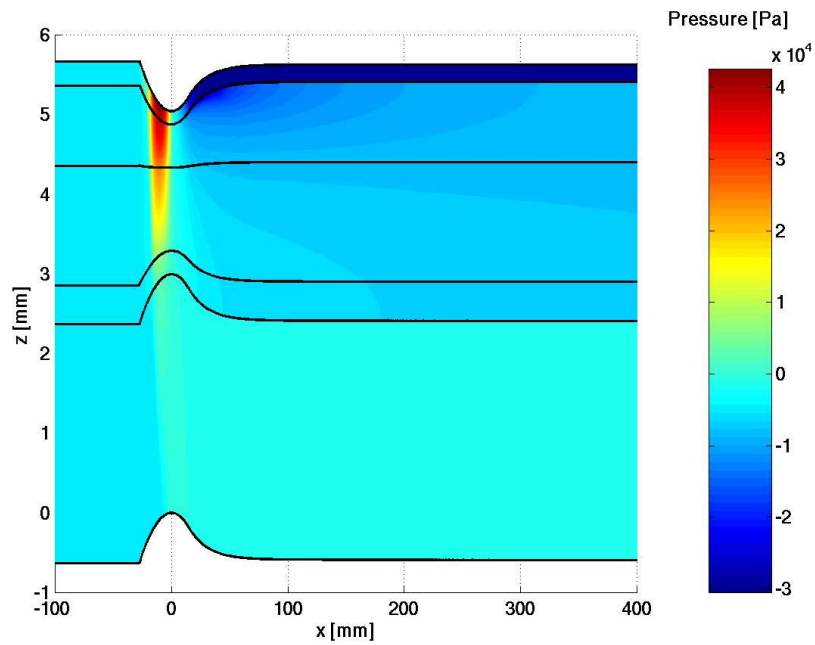


FIGURE 18. Pressure: $v_s = 1250m/min$ and initial roll surface saturation $S_0 = 40\%$

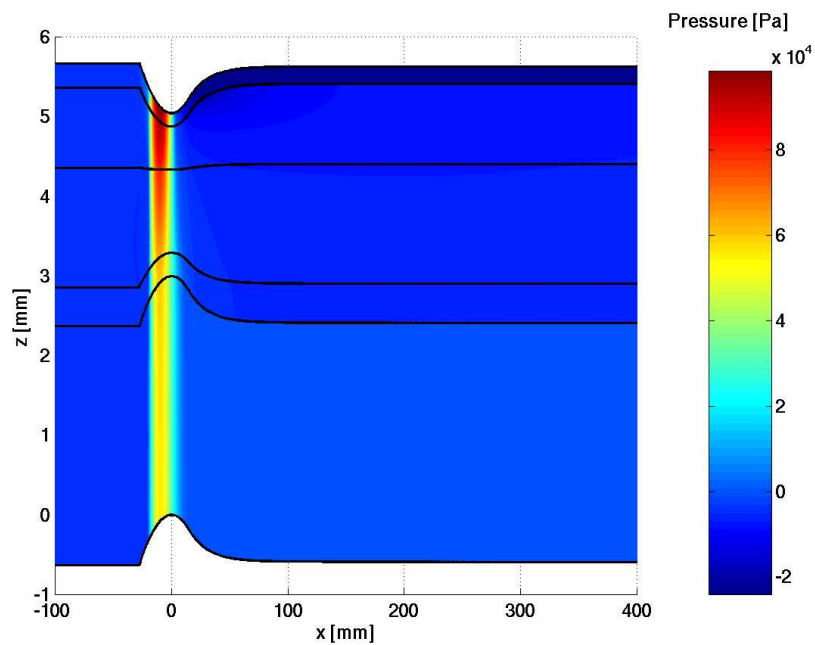


FIGURE 19. Pressure: $v_s = 1250m/min$ and initial roll surface saturation $S_0 = 60\%$

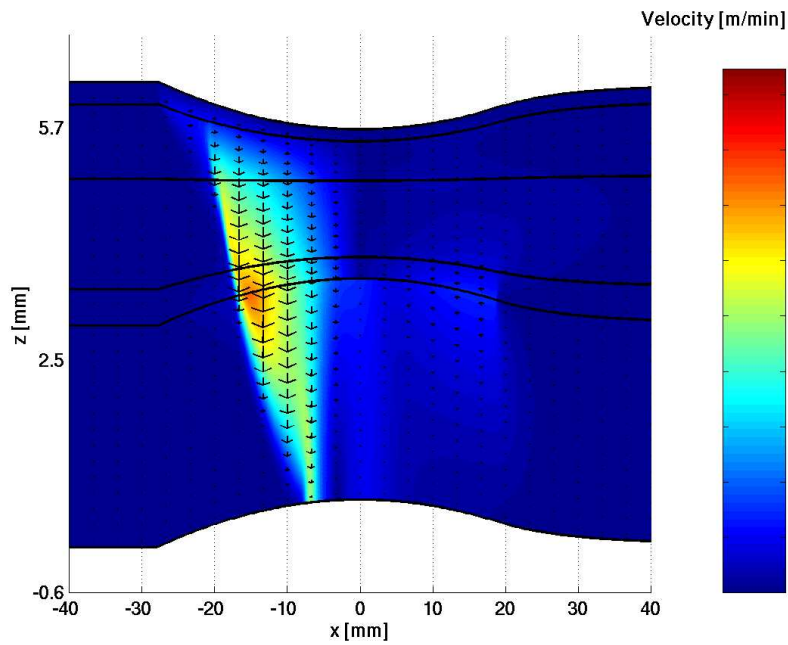


FIGURE 20. Velocity: $v_s = 750\text{m}/\text{min}$ and initial roll surface saturation $S_0 = 40\%$

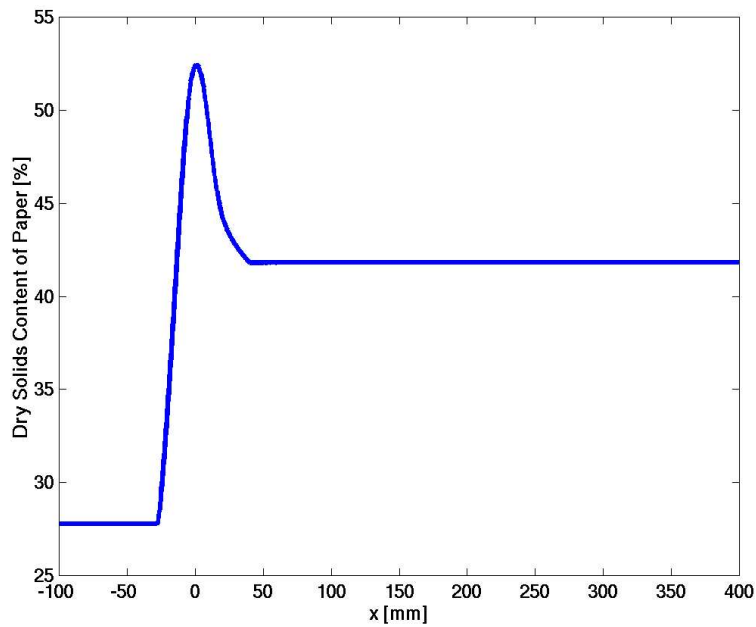


FIGURE 21. Typical profile of the dry solids content of paper

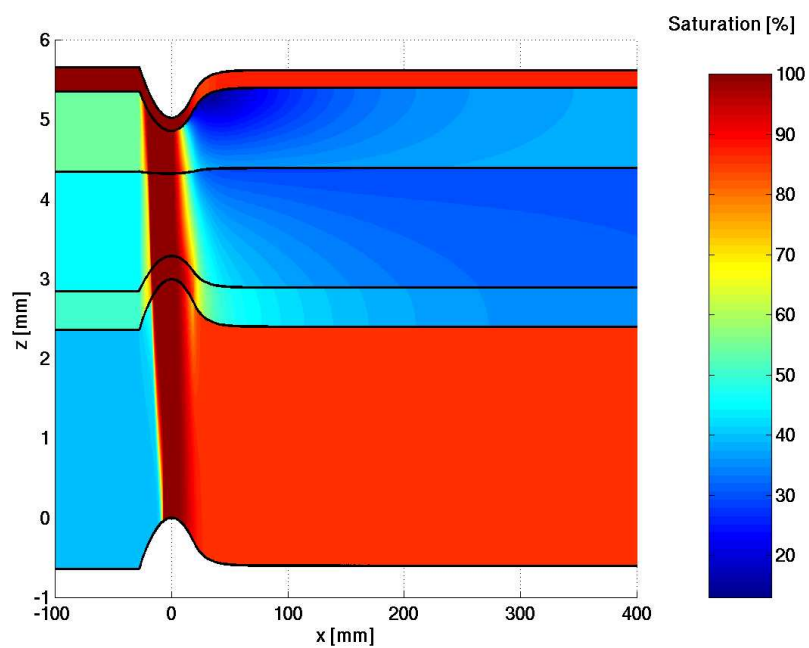


FIGURE 22. Saturation: $v_s = 750m/min$, initial roll surface saturation $S_0 = 40\%$ and with inertia

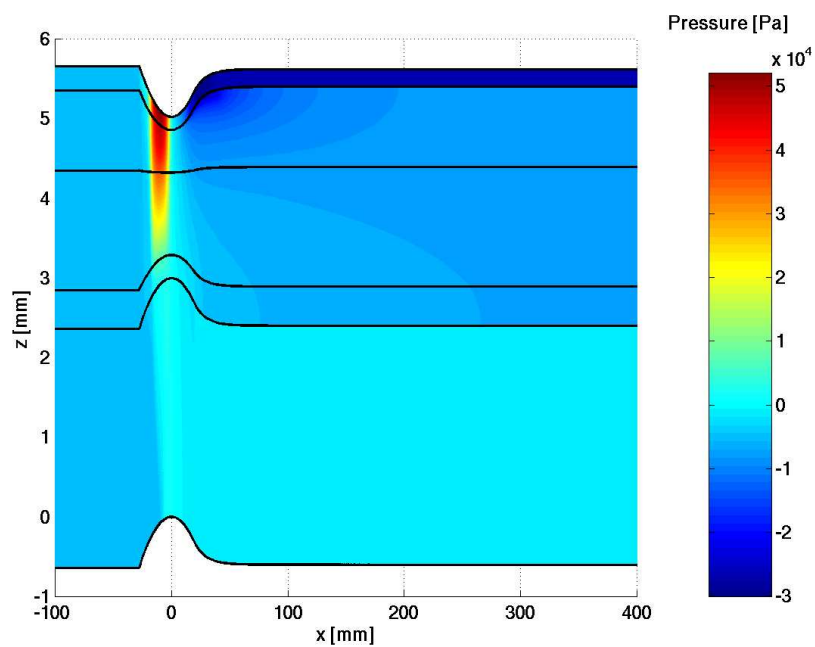


FIGURE 23. Pressure: $v_s = 750m/min$, initial roll surface saturation $S_0 = 40\%$ and with inertia

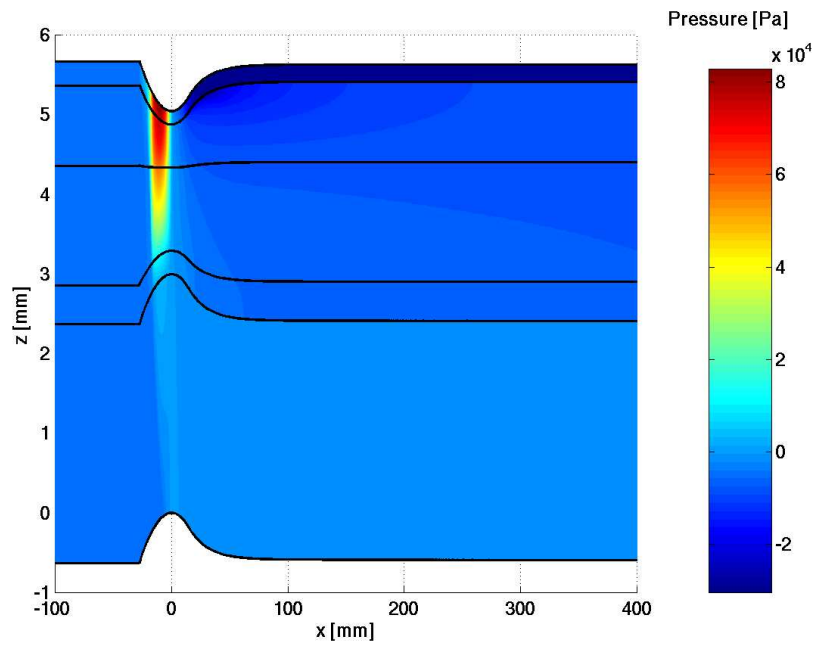


FIGURE 24. Pressure: $v_s = 1250m/min$, initial roll surface saturation $S_0 = 40\%$ and with inertia

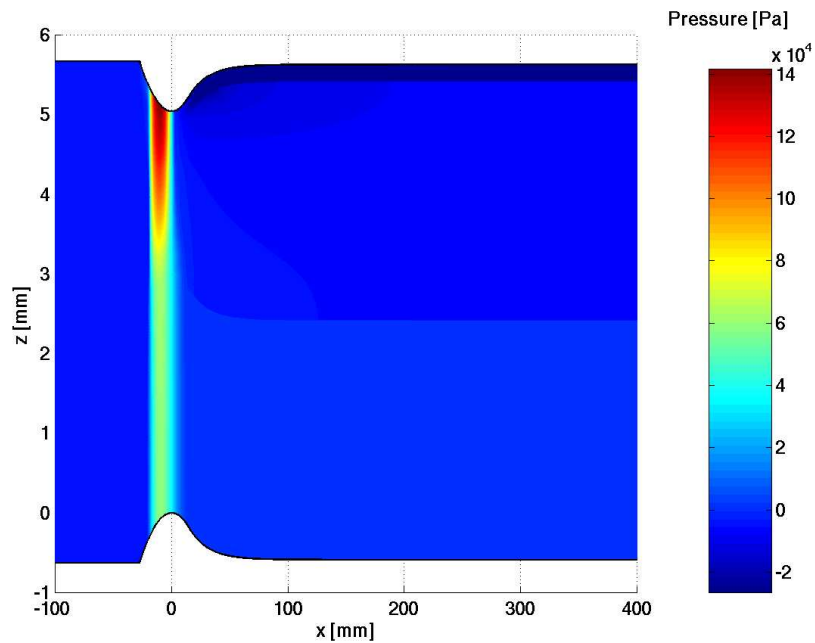


FIGURE 25. Pressure: $v_s = 1250m/min$, initial roll surface saturation $S_0 = 60\%$ and with inertia

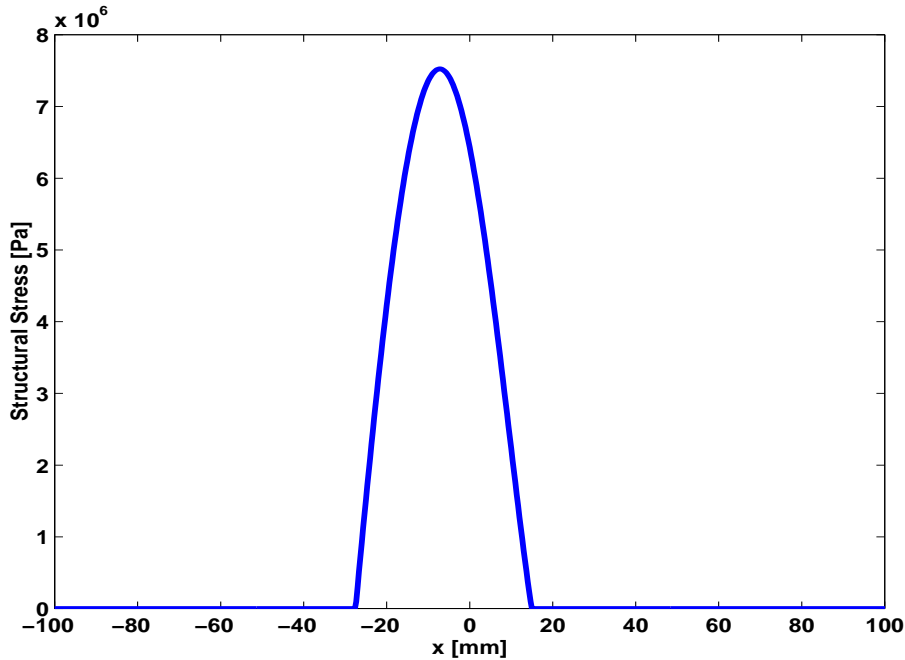
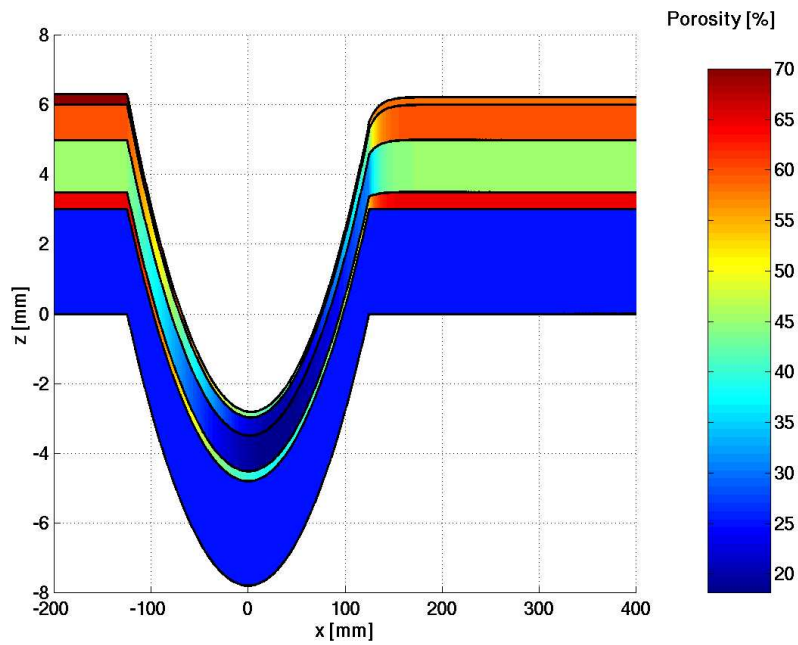
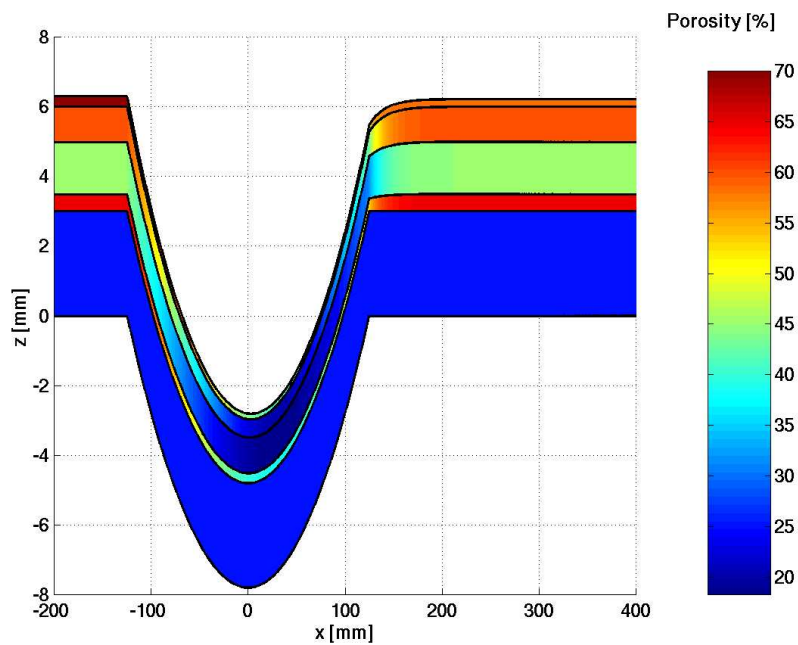


FIGURE 26. Structural stress: $v_s = 750m/min$

5.4.2. Shoe press nip. For the sake of completeness, we present simulation results of a shoe press nip. The behavior of the model is quite similar to the simulation results of the previous section. The minimum distance d_{min} of the press profiles is automatically adjusted to match a press force of $1200kN/m$. We consider three variations of the machine velocity and initial saturation of the belt, which replaced the roll surface of the roll press nip. The following sequence of figures is ordered as in the case of the roll press nip and similar comments hold. The final dry solids content at $v_s = 750m/min$ and initial belt saturation of 40% reads 39.95%. Increasing the machine speed to $v_s = 1200m/min$ yields 41.46% dry solids content. Additionally setting the initial belt saturation to 60% gives a dry solids content of 39.62%.

FIGURE 27. Porosity: $v_s = 750m/min$ FIGURE 28. Porosity: $v_s = 1250m/min$

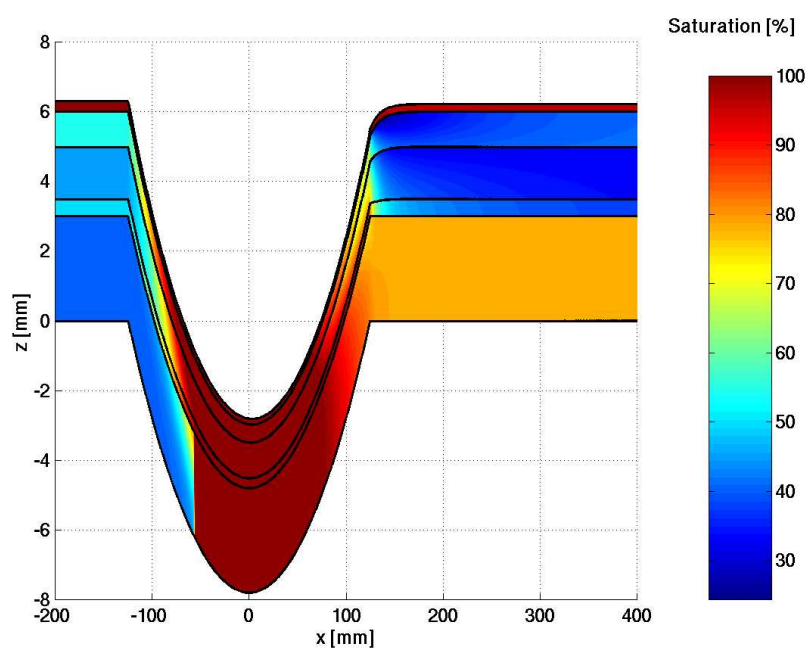


FIGURE 29. Saturation: $v_s = 750m/min$ and initial belt saturation $S_0 = 40\%$

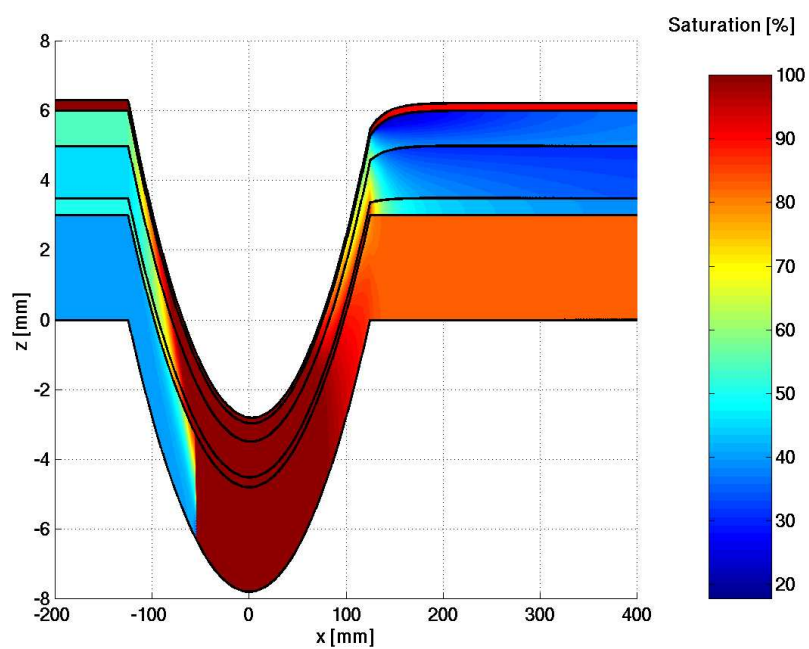


FIGURE 30. Saturation: $v_s = 1250m/min$ and initial belt saturation $S_0 = 40\%$

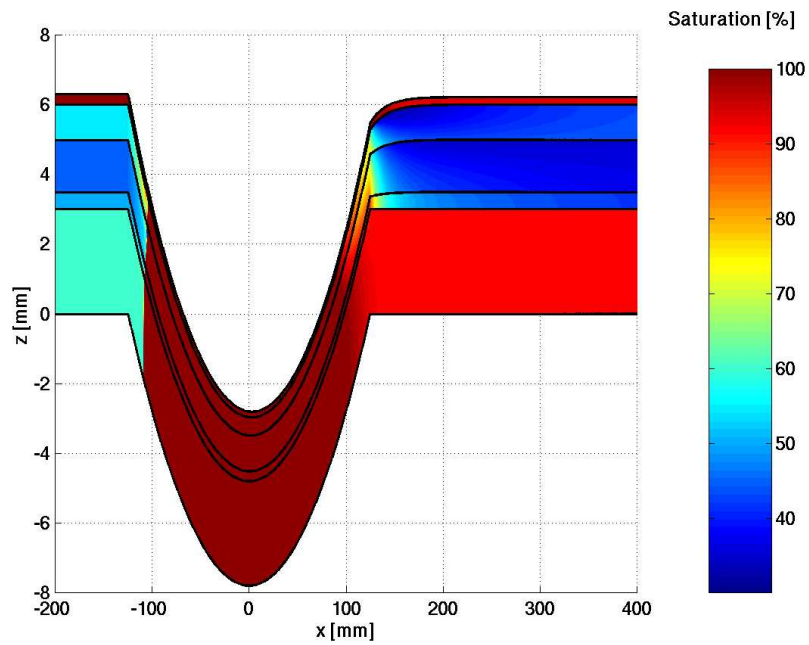


FIGURE 31. Saturation: $v_s = 1250m/min$ and initial belt saturation $S_0 = 60\%$

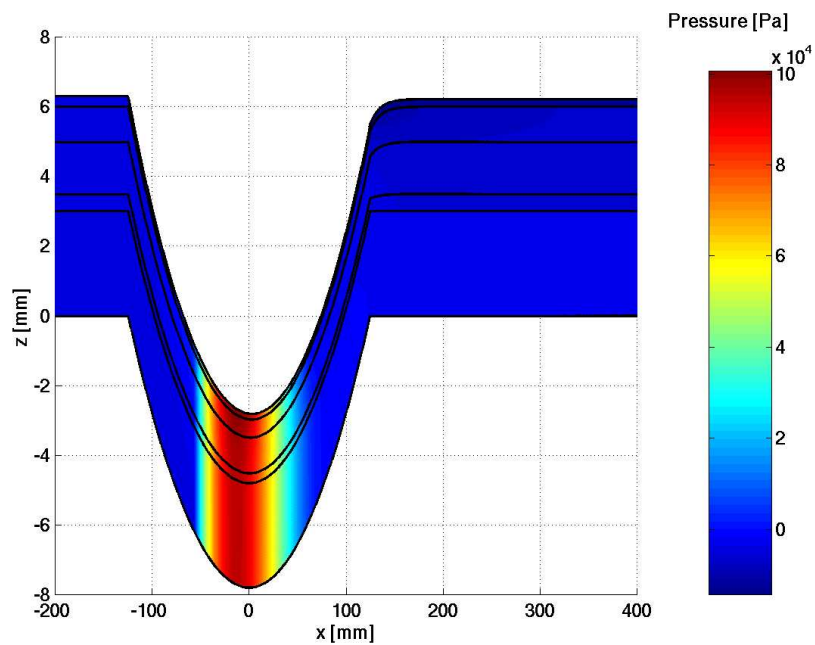


FIGURE 32. Pressure: $v_s = 750m/min$ and initial belt saturation $S_0 = 40\%$

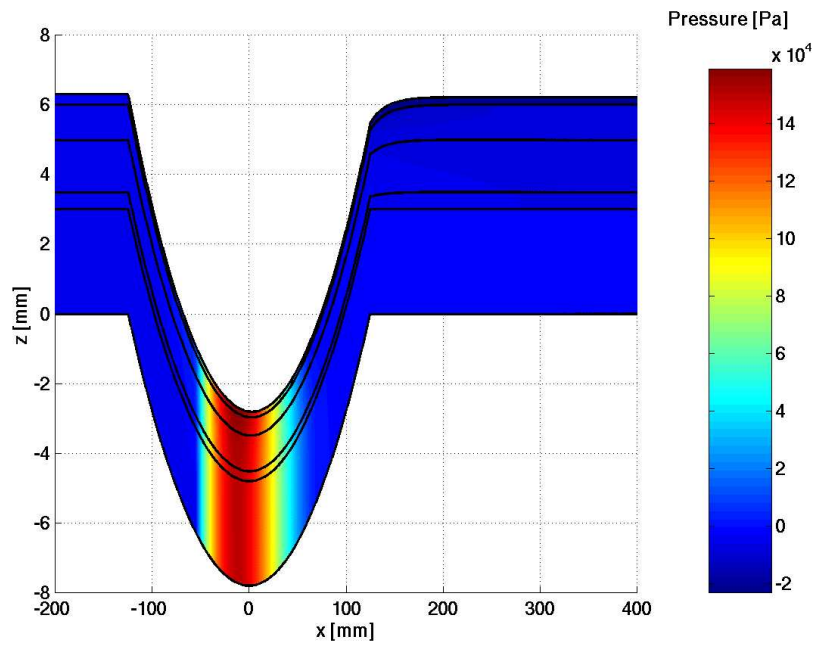


FIGURE 33. Pressure: $v_s = 1250m/min$ and initial belt saturation $S_0 = 40\%$

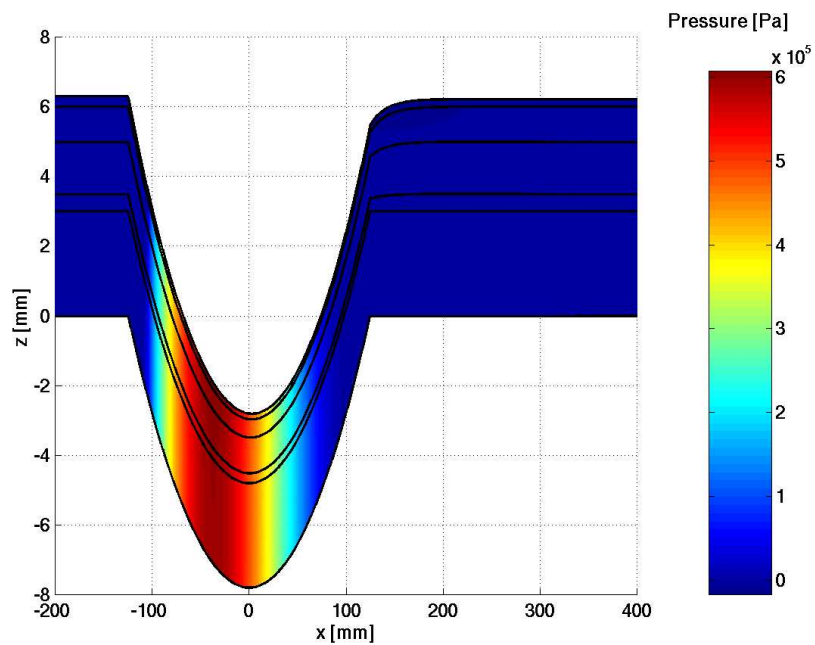


FIGURE 34. Pressure: $v_s = 1250m/min$ and initial belt saturation $S_0 = 60\%$

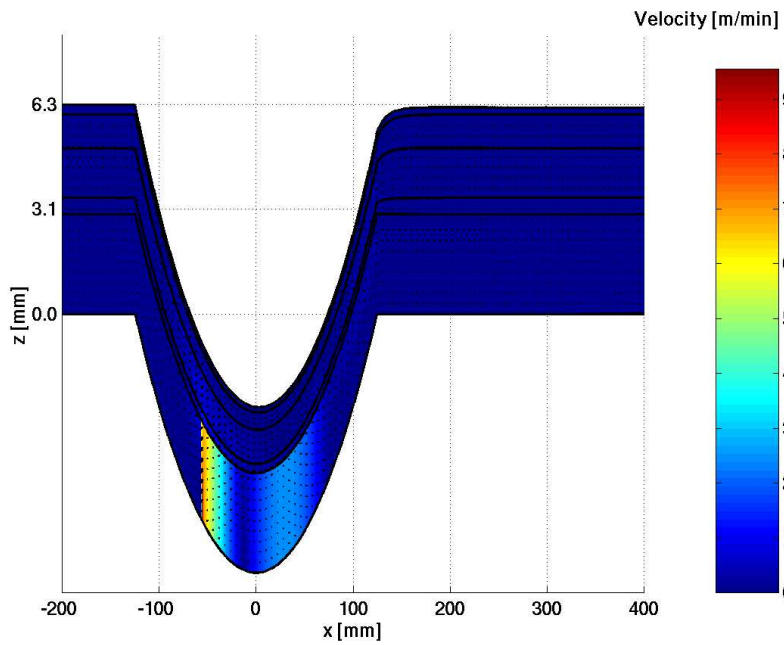


FIGURE 35. Velocity: $v_s = 750\text{m/min}$ and initial belt saturation $S_0 = 40\%$

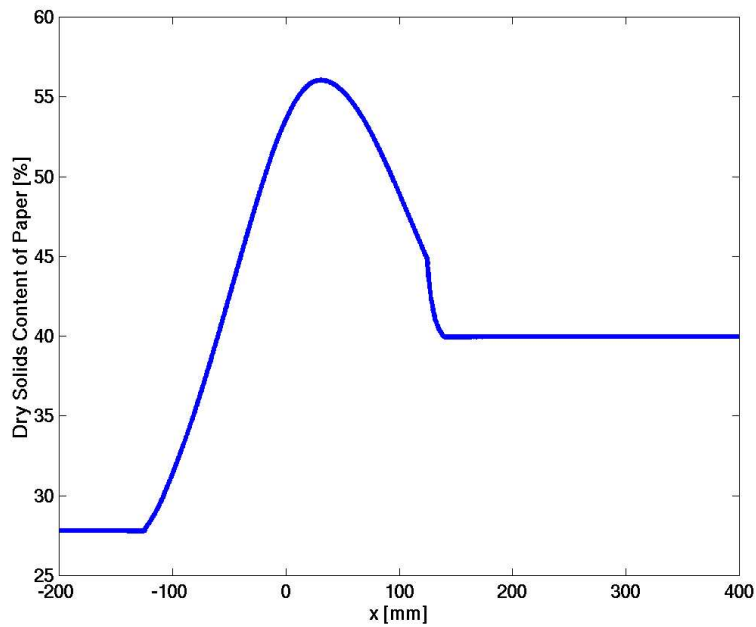


FIGURE 36. Typical profile of the dry solids content of paper

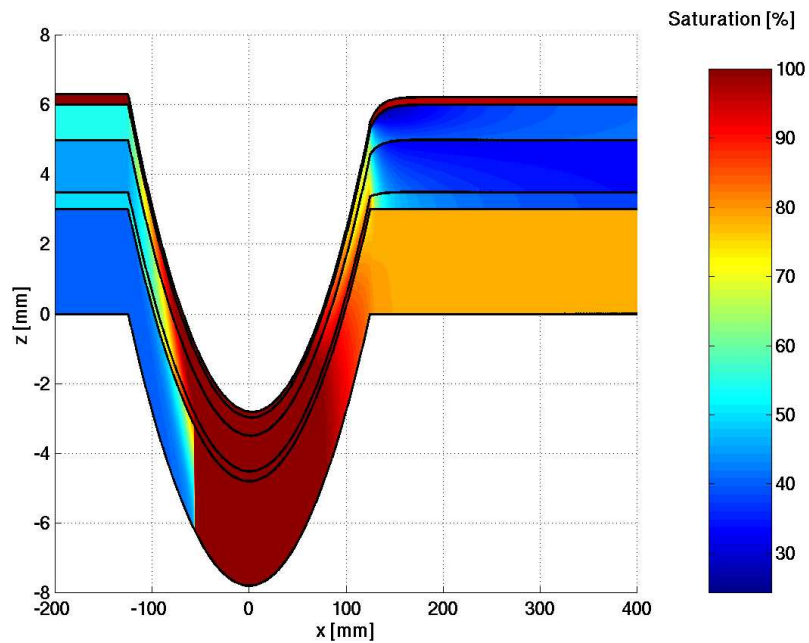


FIGURE 37. Saturation: $v_s = 750m/min$, initial belt saturation $S_0 = 40\%$ and with inertia

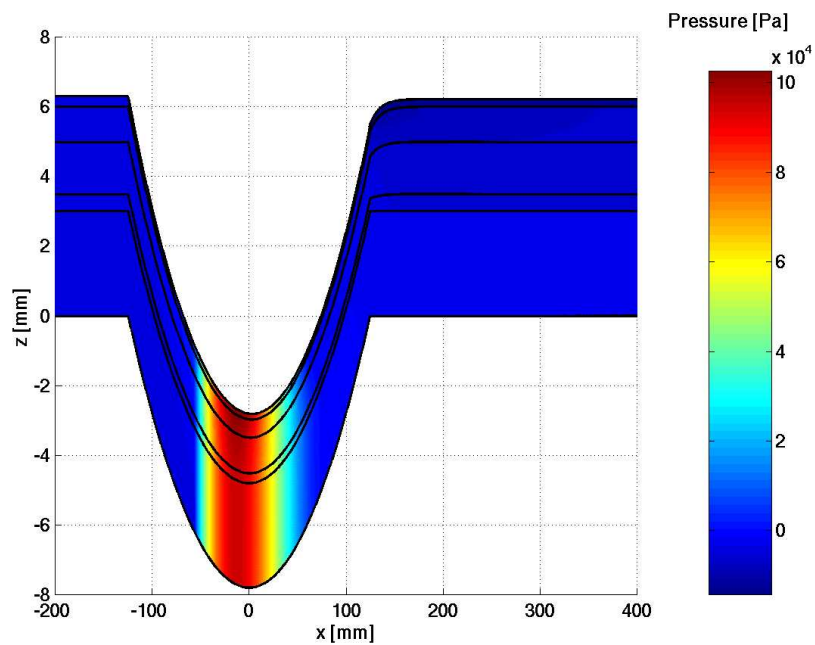


FIGURE 38. Pressure: $v_s = 750m/min$, initial belt saturation $S_0 = 40\%$ and with inertia

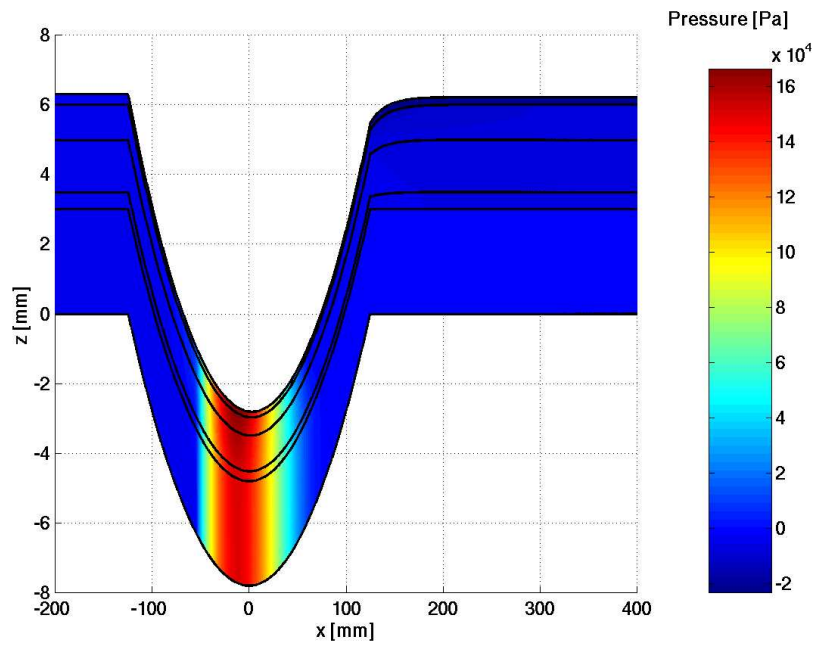


FIGURE 39. Pressure: $v_s = 1250m/min$, initial belt saturation $S_0 = 40\%$ and with inertia

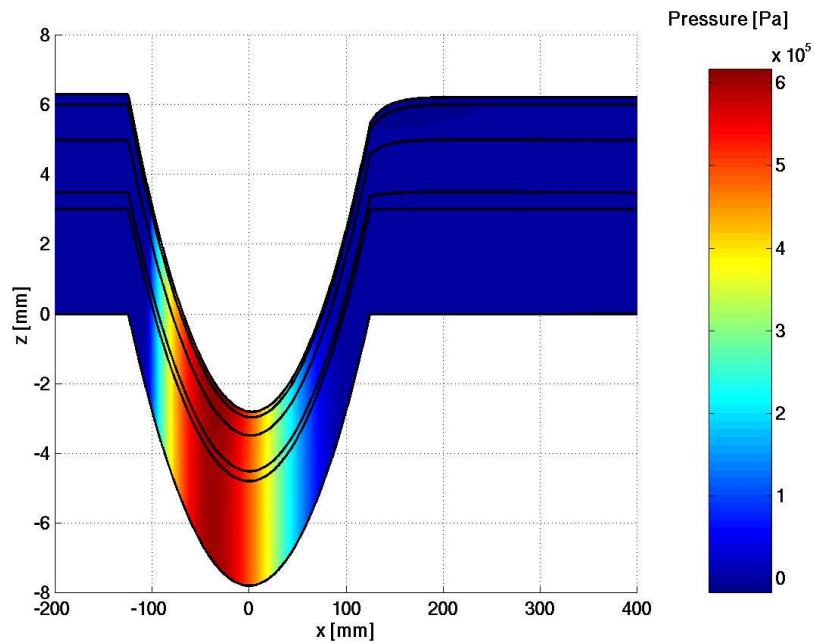


FIGURE 40. Pressure: $v_s = 1250m/min$, initial belt saturation $S_0 = 60\%$ and with inertia

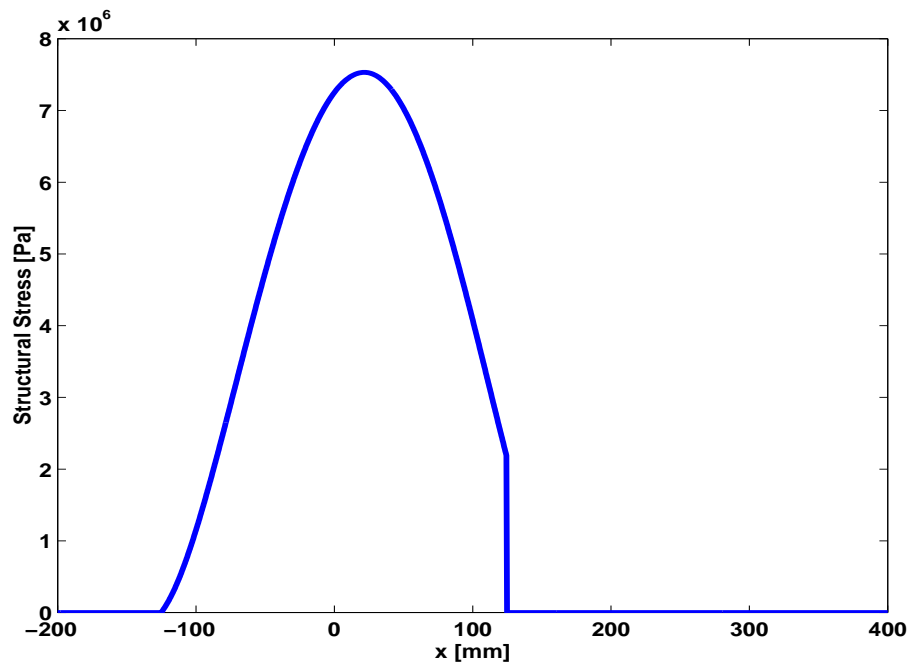


FIGURE 41. Structural stress: $v_s = 750m/min$

Conclusion

We have presented two approaches to the numerical solution of the Navier-Stokes system with two pressures. The first solution method splits the system into a micro and a macro problem. From the micro problem, one obtains nonlinear filtration laws, which are then used as parametrization of the macro problem. The second approach considers the full system and yields a four-dimensional problem when starting from a two-dimensional setting of the porous medium.

From numerical studies we draw the following conclusions: The nonlinear filtration laws extend Darcy's law to cases when inertial effects are important. The recirculation zones can be identified as reason for the observed deviations from Darcy's law. Recirculation zones reduce the effective flow domain on the micro scale. Hence, larger macroscopic pressure gradients are needed to transport the fluid through the porous medium. This is in complete consistency to experimental observations and existing literature. Moreover, the complexity of these laws shows that extensions by only one additional nonlinear term, as done in the Forchheimer law, are in general not sufficient to accurately describe the flow behavior in porous media. We showed by numerical examples that seemingly isotropic media in the Darcy regime may become strongly anisotropic when inertial effects appear. This might be an interesting point for measurements. Technical porous media are often tested in the slow flow regime, thereby neglecting the fact, that they are intended to operate in the fast flow regime. The interpretation of these measurements might be questionable. The inertial effects created on the micro scale enter the macro problem via the filtration law and, as shown by numerical simulation, may strongly influence the macroscopic velocity.

In addition, we developed a two dimensional model of the pressing section of a paper machine. The model accounts for the viscoelastic deformation of paper and felt layers and contains a macroscopic flow description including nonlinear filtration laws. Major effort went into the development of a suitable numerical solution algorithm which is based on a finite element discretization. Numerical results exhibit reasonable elastic and fluid dynamical behavior of the model in various setups. The choice of the flow parameters of the model was strongly

influenced by computations using a three-dimensional virtual felt. We determined permeabilities and the nonlinear flow regime. The application of nonlinear filtration laws shows a major impact on the hydrodynamic pressure, which increases significantly. Hence, the hydrodynamic stress contribution being small in the Darcy regime should not be neglected in the elastic model, when considering high machine speeds.

Bibliography

- [1] R. ADAMS, *Sobolev spaces*, Academic Press, New York, 1975.
- [2] G. ALLAIRE, *Homogenization of the Stokes flow in a connected porous medium*, *Asymptotic Analysis* 2 (1989), pp.203-222, North-Holland.
- [3] M. ALLEN, G. BEHIE, J. TRANGENSTEIN, *Multiphase flow in porous media*, Springer, Berlin, 1988.
- [4] D.A. ANDERSON, J.C. TANNERHILL, R.H. PLETCHER, *Computational fluid mechanics and heat transfer*, Hemisphere publ., New York, 1984.
- [5] K.J. ARROW, L. HURWICZ, H. UZAWA, *Studies in nonlinear programming*, Stanford University Press, 1958.
- [6] J. BEAR, *Dynamics of fluids in porous media*, American Elsevier, 1972.
- [7] J. BEAR, *Hydraulics of Groundwater*, McGraw Hill, 1979.
- [8] J. BEAR, A. VERRUIJT, *Modeling groundwater flow and pollution*, D. Reidel Publishing Company, 1987.
- [9] J. BEAR, Y. BACHMAT, *Introduction to modeling of transport phenomena in porous media*, Kluwer, Dordrecht, 1990.
- [10] A. BENSOUSSAN, J.L. LIONS, G. PAPANICOLAOU, *Asymptotic analysis for periodic structures*, North-Holland, 1978.
- [11] M. BERCOVIER, O. PIRONNEAU, *Error estimates for finite element method solution of the Stokes problem in the primitive variables*, *Numer. math.* 33, pp. 211-224, 1979.
- [12] A. BOURGEAT, E. MARUŠIĆ-PALOKA, *Loi d'éclouement non linéaire entre deux plaques ondulées*, *C. R. Acad. Sci. Paris*, t.321, Série I, pp. 1115-1120, 1995.
- [13] A. BOURGEAT, E. MARUŠIĆ-PALOKA, A. MIKELIĆ, *The weak non-linear corrections for Darcy's law*, *Math. Models Methods Appl. Sci.*, 8 (6), pp. 1143-1155, 1996.
- [14] A. BOURGEAT, E. MARUŠIĆ-PALOKA, *Non-linear effects for flow in periodically constricted channel caused by high injection rate*, *Math. Models Methods Appl. Sci.*, 8 (3), pp. 379-405, 1998.
- [15] D. BRAESS, *Finite Elemente*, Springer, 1992.
- [16] F. BREZZI, M. FORTIN, *Mixed and hybrid finite element methods*, Springer series in computational mathematics 15, Springer, 1991.
- [17] P.G. CIARLET, *The finite element method for elliptic problems*, North-Holland, Amsterdam, 1978.
- [18] H. DARCY, *Les fontaines publiques de la ville de Dijon*, Dalmont, Paris, 1856.
- [19] J.W. DEMMEL, S.C. EISENSTAT, J.R. GILBERT, X.S. LI, JOSEPH W.H. LIU, *A supernodal approach to sparse partial pivoting*, *SIAM J. Matrix Analysis and Applications*, Vol. 20, No. 3, pp. 720-755, 1999.
- [20] M. DOBROWOLSKI, R. RANNACHER, *Finite element methods for nonlinear elliptic systems of second order*, *Math. Nachr.* 94, pp. 155-172, 1980.

-
- [21] J. DUPUIT, *Etudes théoriques et pratiques sur le mouvement des eaux*, Dunod, Paris, 1863.
- [22] F. A. L. DULLIEN, *Porous media*, Academic Press, 1979.
- [23] H. ENGELS, *Numerical quadrature and cubature*, Academic Press, London, 1980.
- [24] M. FEISTAUER, *Mathematical methods in fluid dynamics*, Longman, 1993.
- [25] A.D. FITT, P.D. HOWELL, J.R. KING, C.P. PLEASE AND D.W. SCHWENDEMAN, *Multiphase flow in a roll press nip*, European Journal of Applied Mathematics, 13. pp. 225-259, 2002.
- [26] M. FIRDAOUSS, J.-L. GUERMOND, *Sur l'homogénéisation des équations de Navier-Stokes à faible nombre de Reynolds*, C. R. Acad. Sci. Paris, t.320, Série I, pp. 245-251, 1995.
- [27] P. FORCHHEIMER, *Wasserbewegung durch Boden*, Zeitschrift des Vereins deutscher Ingenieure, 45, pp. 1736-1741 and p. 1782-1788, 1901.
- [28] M. FORTIN, R. GLOWINSKI, *Augmented lagrangian methods: applications to the numerical solution of boundary-value problems*, North-Holland, 1983.
- [29] G.P. GALDI, *An introduction to the mathematical theory of the Navier-Stokes equations, Vol. II*, Springer, 1994.
- [30] G.P. GALDI, *An introduction to the mathematical theory of the Navier-Stokes equations, Vol. II*, Springer, 1994.
- [31] D. GILBARG, N.S. TRUDINGER, *Elliptic partial differential equations of second order*, Springer, 1983.
- [32] O. GIPOULOUX, A.-M. ZINE, *Computation of the filtration laws through porous media for a non-Newtonian fluid obeying the power law*, Computational Geosciences 1, pp. 127-153, 1997.
- [33] V. GIRAULT, P.A. RAVIART, *An analysis of a mixed finite element method for the Navier-Stokes equations*, Numer. Math. 33, pp. 235-271, 1979.
- [34] V. GIRAULT, P.A. RAVIART, *Finite element methods for Navier-Stokes equations, theory and algorithms*, Springer, 1986.
- [35] R. GLOWINSKI, H. KELLER, L. REINHART, *Continuation-conjugate gradient methods for the least squares solution of nonlinear boundary value problems*, Rapports de recherche No. 141, INRIA, 1982.
- [36] R. GLOWINSKI, *Numerical methods for nonlinear variational problems*, Springer, 1984.
- [37] R. GLOWINSKI, J.L. LIONS, R. TREMOLIERES, *Analyse numérique des inéquations variationnelles*, Vol. 1 and 2, Dunod-Bordas, Paris, 1976.
- [38] R.A. GREENKORN, *Flow phenomena in porous media*, Marcel Dekker, Inc., 1983.
- [39] M.D. GUNZBURGER, *Finite element methods for viscous incompressible flows*, Academic Press, London, 1989.
- [40] J. HARIG, *Eine robuste und effiziente Finite Elemente Methode zur Loesung der inkompressiblen 3-d Navier-Stokes-Gleichungen auf Vektorrechnern*, Interdisziplinäeres Zentrum fuer wissenschaftliches Rechnen, Preprint 91-18, Universitaet Heidelberg.
- [41] M. HESTENES, *Multiplier and gradient methods*, J. Optimization Theory and Applications, 4, pp. 303-320, 1969.
- [42] K. HILTUNEN, *Mathematical and numerical modelling of consolidation processes in paper machines*, Thesis, University of Jyvaskyla, 1995.
- [43] U. HORNUNG, *Homogenization and porous media*, Springer, 1997.

-
- [44] K. JEWETT, W. CECKLER, L. BUSKER, AND A. CO, *Computer model of a transversal flow nip*, AIChE Symposium Series 76 (200), pp. 59-70, New York, 1980.
- [45] V.V. JIKOV, S.M. KOZLOV, O.A. OLEINIK, *Homogenization of differential operators and integral functionals*, Springer, 1994.
- [46] M. KARVIANY, *Principles of heat transfer in porous media*, Springer, 1991.
- [47] O.A. LADYŽENSKAJA, N. N. URAL'CEVA, *Équations aux dérivées partielles de type elliptique*, Dunod, Paris, 1968.
- [48] O.A. LADYŽENSKAJA, *The mathematical theory of viscous incompressible flow*, Gordon and Breach, 1969.
- [49] J.L. LIONS, *Some methods in the mathematical analysis of systems and their control*, Gordon and Breach, 1981.
- [50] E. MARUŠIĆ-PALOKA, A. MIKELIĆ, *The derivation of a non-linear filtration law including the inertia effects via homogenization*, Nonlinear Analysis 42, pp. 97-137, 2000.
- [51] E. MARUŠIĆ-PALOKA, A. MIKELIĆ, *An error estimate for the correctors in the homogenization of the Stokes and Navier-Stokes equations in a porous medium*, Bollettino U.M.I. (7) 10-A (1996), pp. 661-671.
- [52] C.C. MEI, J.-L. AURIAULT, *The effect of weak inertia on flow through a porous medium*, J. Fluid Mech., Vol. 222, pp. 647-663, 1991.
- [53] A. MIKELIĆ, *Homogenization of nonstationary Navier-Stokes equations in a domain with a grained boundary*, Annali di Matematica pura ed applicata (IV), Vol. CLVIII, pp. 167-179, 1991.
- [54] A. MIKELIĆ, *Effets inertiels pour un écoulement stationnaire visqueux incompressible dans un milieu poreux*, C. R. Acad. Sci. Paris, Serie I, 320, pp. 1289-1294, 1995.
- [55] A. MIKELIĆ, *Homogenization theory and applications to filtration through porous media*, "Lecture Notes in Mathematics", Vol. 1734, Springer, 2000, p.127-214.
- [56] A. MIKELIĆ, *Private communication*, 2004.
- [57] J. TINSLEY ODEN, G.F.CAREY, *Finite Elements Volume I*, Prentice-Hall, Inc., 1984.
- [58] E. POLAK, *Computational methods in optimization*, Academic Press, 1971.
- [59] E. POLAK, *Optimization*, Applied Mathematical Sciences 124, Springer, 1997.
- [60] M.J.D. POWELL, *A method for nonlinear constraints in minimization problems*, in *Optimization*, R. Flechter ed., Academic Press, London, 1969.
- [61] M.J.D. POWELL, *Restart procedure for the conjugate gradient method*, Math. Programming 12, pp. 148-162, 1977.
- [62] M.N. RASOLOARIJAONA, J.-L. AURIAULT, *Nonlinear seepage flow through a rigid porous medium*, Eur.J. Mech.,B/Fluids, 13, No 2, pp. 177-195,1994.
- [63] L. REINHART, *Sur la résolution numérique de problèmes aux limites non linéaires par des méthodes de continuation*, Thèse de 3ème cycle, Université Pierre et Marie Curie (Paris VI), 1980.
- [64] J.E. ROBERTS, J.-M. THOMAS, *Mixed and hybrid finite element methods*, Rapports de recherche No. 737, INRIA, 1987.
- [65] E. SANCHEZ-PALENCIA, *Non-homogeneous media and vibration theory*, Lecture Notes in Physics 127, Springer, 1980.
- [66] A.E. SCHEIDEGGER, *The physics of flow through porous media*, University of Toronto Press, 1960.

-
- [67] A.E. SCHEIDEGGER, *Hydrodynamics in porous media*, Encyclopedia of Physics, Volume VIII/2 Fluid Dynamics II, S. Fluegge (editor), Springer, 1963.
- [68] L. TARTAR, *Incompressible fluid flow in a porous medium – Convergence of the homogenization process*, appendix of [65].
- [69] C. TAYLOR, P. HOOD, *A numerical solution of the Navier-Stokes equations using the finite element technique*, Computers and Fluids, Vol. 1, pp. 73-100, 1973.
- [70] C. TAYLOR, P. HOOD, *Navier-Stokes equations using mixed interpolation*, in *Finite Element Methods in Flow Problems* (J. T. Oden, ed.), UAH Press, Huntsville, Alabama, 1974.
- [71] R. TEMAM, *Navier-Stokes equations - theory and numerical analysis*, North-Holland, 1979.
- [72] R. TEMAM, *Navier-Stokes equations and nonlinear functional analysis*, SIAM, 1983.
- [73] X. THIBAUT, *Contribution à l'étude de structures tissées déformables: Application à l'évaluation du tenseur perméabilité des feutres de presses de papeterie*, Thesis, Institut National Polytechnique de Grenoble, 2001.
- [74] F. THOMASSET, *Implementation of finite element methods for Navier-Stokes equations*, Springer, 1981.
- [75] K. VELTEN, W. BEST, *Rolling of unsaturated porous materials: Evolution of a fully saturated zone*, Physical Review E, Vol. 62, No. 3, 2000.
- [76] J.-C. WODIE, T. LEVY, *Correction non linéaire de la loi de Darcy*, C. R. Acad. Sci. Paris, t. 312, Série II, pp. 157-161, 1991.
- [77] E. ZEIDLER, *Nonlinear functional analysis and its application I, II/A, II/B, III*, Springer, 1990.
- [78] A. ŽENIŠEK, *Nonlinear elliptic and evolution problems and their finite element approximation*, Academic Press, 1990.

CURRICULUM VITAE

- 24.08.1971 born in Heidelberg
- 1978 – 1981 Johann-Hoffmann-Grundschule, Mutterstadt
(primary school)
- 1981 – 1991 Staatliches Paul-von-Denis-Gymnasium, Schifferstadt
(secondary school)
- Oct. 1992 Student of Technomathematics at the University of
Kaiserslautern
- Oct. 1994 Intermediate Diploma in Technomathematics
- Jan. 1996 Student of Mathematics at the University of Grenoble,
– March 1996 France
- Dec. 1997 Diploma in Technomathematics
- Jan. 1998 Doctoral candidate at the Mathematical Department of
the University of Kaiserslautern
- since Oct. 2000 Scientific employee at the Fraunhofer Institut für Techno-
und Wirtschaftsmathematik

CURRICULUM VITAE

- 24.08.1971 geboren in Heidelberg
- 1978 – 1981 Besuch der Johann-Hoffmann-Grundschule in Mutterstadt
- 1981 – 1991 Besuch des Staatlichen Paul-von-Denis-Gymnasiums,
Schifferstadt
- Okt. 1992 Beginn des Studiums im Fach Technomathematik mit
Nebenfach Elektrotechnik an der Universität Kaisers-
lautern
- Okt. 1994 Vordiplom in Technomathematik
- Jan. 1996 Studium der Mathematik an der Universität Grenoble
– März 1996 im Rahmen des ECMI-Programms
- Dez. 1997 Diplom in Technomathematik
- Jan. 1998 Stipendiat des Graduiertenkollegs Technomathematik
an der Universität Kaiserslautern
- seit Okt. 2000 Wissenschaftlicher Mitarbeiter am Fraunhofer
Institut für Techno- und Wirtschaftsmathematik